Relative stability of metal complexes: a theoretical study

by

Paidamwoyo Noah Takawota Mangondo

Supervisor: Professor Ignacy Cukrowski

Department of Chemistry

University of Pretoria

Submitted in partial fulfilment of the requirements for the degree

Master of Science

The Faculty of Natural and Agricultural Sciences

University of Pretoria

(2015)

Declaration

I, Paidamwoyo Noah Takawota Mangondo declare that the dissertation, which I hereby submit for the degree Master of Science: Chemistry at the University of Pretoria, is my own work and has not previously been submitted by me for a degree at this or any other tertiary institution.

SIGNATURE: …….

DATE: …….

Outputs from this work

Paidamwoyo Mangondo and Ignacy Cukrowski. The true nature of H•••H interactions and their real effects on complex stability. An investigation of NTA and NTPA complexes, *Proceedings of the INORG2013 Conference*, University of Kwa Zulu Natal, July 2013. (Poster).

Paidamwoyo Mangondo and Ignacy Cukrowski. The causes of preferential complex formation: An investigation of NTA and NTPA complexes, *Proceedings from the South African Chemical Institute Young Chemists' Symposium*, University of Johannesburg, 2013. (Oral, 1st prize for best presentation).

Ignacy Cukrowski, Jurgens de Lange, Adedapo Adeyinka and Paidamwoyo Mangondo. Evaluating common QTAIM and NCI interpretations of the electron density concentration through IQA interaction energies and 1D cross-sections of the electron and deformation density distributions. *Comput. Theoret. Chem.* **2015**, *1053*, 60–76.

Abstract

It is widely known that most metal complexes will preferentially complex to form five-membered chelate rings (5m-CR) when compared to six-membered chelate rings (6m-CR) except when binding to small metal cations. A characteristic example of this phenomenon can be found in the complexes of nitrilotri-3-propionic acid (NTPA, it forms 6m-CR) and nitrilotriacetic acid (NTA, it forms 5m-CR) where the only known metal that complexes preferentially to form the 6m-CR is Be. This has largely been attributed to lone pair donor atom repulsion, steric hindrance and to a lesser extent inductive effects.

In this work the complexes of Be^{II} and Zn^{II} complexes of NTA and NTPA will be explored. Competition reactions will be used to validate the solvent optimized structures and then in depth analysis will be performed to understand the relative complex stability including: (i) geometric analysis to measure bond strength and steric repulsion based on interatomic distances, (ii) The Quantum Theory of Atoms in Molecules (QTAIM) to show the presence of atomic interaction lines (AILs) and topological properties to understand the strength and nature of coordination bonds and weak intramolecular interactions, (iii) the Non-Covalent Interactions (NCI) scheme to determine the presence of additional interactions not visualized in QTAIM, (iv) 1D cross-sections along the λ_2 eigenvector of the Hessian matrix to understand the local behaviour of the topology of electron density within an interaction, and (v) the theory of Interacting Quantum Atoms (IQA) to measure the strength of and understand the nature of interactions of interest. From this we will conclude from our data, we cannot explain the relative metal complex stability based on the local properties of interactions. In addition, we will suggest that rather than destabilize the molecule, the CH•••HC contributes to stabilizing the molecule.

Using a simplified two step model, similar to that proposed in the ETS-NOCV scheme, in which (i) the preorganization of the ligands and the preorganization of the metal fragment (in the case of Zn^{II} complexes), and (ii) binding between the preorganized fragments with the associated affinity energy will be extensively evaluated using QTAIM, NCI, IQA and the Interacting Quantum Fragments (IQF). This analysis will show that the preferential complex stability is not due to strain as a result of CH•••HC interactions, but rather due to the formation of unfavourable interactions between the lone-pair donor atoms such as oxygen and nitrogen and the resultant weaker interactions between the metal centre and water molecules (specifically when the ligands bind to a polyatomic metal fragment).

Keywords: Complex stability, NTA, NTPA, QTAIM, NCI, IQA, IQF, preorganization energy, affinity energy

Acknowledgements

Foremost I would like to express my sincere gratitude to Prof. Ignacy Cukrowski, my study leader for the supervision, the mentoring and the guidance, the financial assistance, the support and faith in me and the work that I have produced. The work here would not have been possible without his input in all facets. I would also like to thank the different members of the research group, Jurgens de Lange, Adedapo Adeyinka, Dominique Buyens, Johan van der Westhuizen, and Bryan Bulling, for their valued contributions, insights and support.

I am infinitely indebted to support that my mother has shown over the course of this degree. She has been a role model and a guide, a source of strength and advise and support, both emotional and financial over the last two and a half years. I am eternally grateful for all she has done. And I am also grateful to my father and the rest of my family for their support and belief in me.

Finally, I must thank all my friends and companions who have walked this path with me, most importantly, Phakama Botha and Jolandi Swanepoel. They reminded me that "Happiness can be found even in the darkest of times, when one only remembers to turn on the light."

Table of Contents

List of Figures

Chapter 1

Chapter 3

Chapter 4

Appendix A

Appendix B

List of Tables

Chapter 3

Chapter 4

Chapter 5

Appendix A

Appendix B

Abbreviations

QTAIM – Quantum Theory of Atoms in Molecules

NCI – Non-Covalent Interactions

IQA – Interacting Quantum Atoms

IQF – Interacting Quantum Fragments

AIL – Atomic Interaction Line

BP – Bond Path

NTA – Nitrilo-triacetic acid

NTPA – Nitrilo -3- tripropionic acid

BeNTA – $Be^{II}(NTA)$

BeNTPA – $Be^{II}(NTPA)$

ZnNTA – $Zn^{II}(NTA)(OH_2)_2$

ZnNTPA – $Zn^{II}(NTPA)(OH_2)_2$

BCP – Bond Critical Point

RCP – Ring Critical Point

HF – Hatree-Fock

DFT – Density Functional Theory

B3LYP – Becke's three parameter hybrid exchange potential combined with Lee-Yang-Parr correlational functional

PBE1PBE – The 1996 gradient-corrected correlation functional of Perdew, Burke and Ernzerhof

X3LYP – Extended three parameter hybrid exchange potential combined with Lee-Yang-Parr correlational functional

MP2 – Moller-Plesset second-order

SCF – Self-Consistent Field

PCM – Polarizable Continuum Model

UFF – Universal Force Field

CRn – Competition Reaction

LEC – Lowest Energy Conformer

ZVPE – Zero Point Vibrational Energy

SPFC – Single Point Frequency Calculation

1. Introduction

The study of chemistry involves the exploration of a complex environment of atoms, bonds, electron density and interactions. These concepts are central to understanding almost all chemistry. The fundamental problem, however, with some of these concepts is that they are often vague and unphysical. We chemists have invented a language that lacks rigorous meaning and quite often, even though the language is the same, the meaning differs from chemist to chemist. Physics is rigorous, precise, objective and mathematically sound. The eye of the physicist recognizes exact, measurable observables and hence does not have room for ambiguity. In an attempt to move from the ambiguous nature of chemistry to the real nature of physics, chemists have begun using the mathematics in order to describe their chemical reality.

Whilst there have been significant strides in the field of computational chemistry and many chemists have begun to apply computational chemistry in their experimental investigations, there are significant barriers preventing the widespread usage of theoretical techniques. These include: (i) computational chemistry is perceived as a highly specialised field, accessible to only a select few, (ii) quite often it requires the usage of expensive computers which are not affordable to all, (iii) more often than not it requires expensive software, and (iv) the vast majority of work has been done on small and/or simple molecular systems with comparatively less work on real molecular systems. This leaves many chemists in a predicament where they have numerous experimental data, but quite often use rudimentary means to explain the observed experimental trends because the perceived marginal efficacy of using computations does not outweigh the computational cost.

These issues become most notable when chemists are able to explain the behaviour of molecular systems when small, simple molecules are used, however, when larger the molecular systems are applied, the classically known chemical behaviour no longer applies or deviates. An example of such is the bimolecular nucleophilic substitution reaction (S_N2).[1] Classically the reaction occurs in polar aprotic solvents and on primary and secondary halides. [1] Excess computational resources have been dedicated to explaining simple systems, [2-8] which quite often aren't even in solvent environment; however there seems to be a vacuum in the literature when it comes to explaining larger systems theoretically.

Another problem with computational chemistry is the fact that there are so many different techniques to select, individuals who have no experience in the field can easily be overwhelmed by the numerous techniques available. Whilst the same might be said for

experimental chemistry, there at least exists a base palette that chemists can always turn to before having to explore an assortment of confusing techniques. For example, if an inorganic chemist wanted to characterize and identify a compound, they would make use of NMR, crystallography and IR. For the computational chemist, the question is not only which theoretical tool to selected from the dozens we are bombarded with (*e.g.* QTAIM, NCI, IQA(F), NBO, ETS-NOCV, MO), but also which is the best model. Hence which electronic model should be used (*e.g.* Hatree-Fock, Density Functional Theory, post-SCF methods), which level of theory should be used (*e.g.* B3LYP, X3LYP, ω-B97xD, MP2, MP4, HF) and which basis sets and polarization factors should be considered (*e.g.* 6-311++G(d,p)). What's more, some theories and techniques can be found in more than one software package and are implemented differently, *e.g.*, QTAIM is implemented in both AIMAll and ADF, or NMR is implemented in Gaussian, ADF and AIMAll. It is thus hardly surprising that computational techniques have not penetrated experimental work.

The metal ion in solution and the ability to form complexes is at the core of all inorganic chemistry. The ability to form variable oxidation states and the capacity to bind to ligands and form numerous complexes makes the usage of metal ions so appealing. It is for these reasons that metal ions have limitless applications that include biochemistry, medicine, catalysis, treatment and purification processes, and far more. However, in order to make use of the full possibilities of metal complexes one must be in tune with the nature and behaviour of metal ions in solution. The knowledge of stability (formation) constants and protonation constants plays a substantial role towards understanding the behaviour of metal ions in solution. It is for this reason that rigorous studies have been dedicated to the determination of these constants and compiled into detailed databases.[9] These physical properties are needed to generate species distribution diagrams from which one can predict the existence of specific forms at any required pH. This is of paramount important to determine the composition of a solution.

The experimental formation and protonation constants may produce interesting patterns that give some insight into the chemistry of metal ions based on metal ion selectively and factors influencing ligand design.[10] However, the fundamental understanding of the behaviour of the metal ions and the *chemistry* that controls the formation of complexes cannot be understood from the experimental data. Thus, theoretical studies on a fundamental level (atomic and molecular fragment levels) are necessary to gain deeper understanding of the chemistry behind complex stability. The development and expansion of the field of

theoretical chemistry has made it relatively simple and accessible for chemists to seek these answers using various theoretical tools.

The earliest and most prominent solution to factors influencing the stability of metal complexes is a four-part consideration: (i) steric hindrance between H-atoms, (ii) repulsion between lone-pair donor atoms, (iii) inductive effects and (iv) the size of the metal ion.[10] These considerations have become so common place that it forms part of our *chemical intuition* and we are taught this at the most basic level of chemistry. Hancock states "Where decreasing complex stability with increase in chelate ring size has not been interpreted in entropy terms, these enthalpy changes have been attributed to steric strain, or repulsion between lone pairs on donor atoms. The steric strain interpretation can be checked by molecular mechanics (MM) calculation."[10] Steric strain has become such a common and familiar chemical explanation for the stability of molecular systems that it has been used to explain a plethora of different reactions. [11-16]

Bader's Quantum Theory of Atoms in Molecules[17] is the first of many theories to provide evidence that directly refutes that CH•••HC interactions are repulsive or destabilizing in nature, by showing that atomic interaction lines (AIL – a ridge or maximally accumulated electron density typically leading to that interaction being treated as bonding in nature[18]) exist between H-atoms. [19–23] This opened the floodgates for a lengthy debate[24–41] discussing the nature of the CH•••HC interaction in numerous compounds. However, this debate often resulted in *ad hominem* attacks[32] and the tendency of chemists to be unbending on their positions meant that no compromise was reached between the two camps, one where the interaction was always repulsive and can never be attractive, and the other in which the interaction can be attractive and by extension stabilising. Unfortunately, during the debate, very few investigated other effects that might influence the relative stability of the molecular systems.

In inorganic chemistry, it is known that most metal ions will preferentially complex with ligands that form 5-membered chelate rings (5m-CR), as opposed 6-membered chelate rings (6m-CR). The classical reasoning has looked at steric repulsion in the 6m-CR. The complexes of nitrilo-triacetic acid (NTA) and nitrilo-3-tripropionic acid (NTPA) (both ligands are shown in Figure 1.1) follow such a trend – see Figure 1.2. NTA is well known for its excellent chelating properties and has numerous applications including as an alternative detergent builder[42], nuclear waste processing[43] and isotope extraction[44], and crystal

engineering[45] to name but a few examples. NTPA on the other hand finds much fewer uses in the literature. NTA forms 5m-CR with metal cations in solution, whereas NTPA forms 6m-CR due to the presence of an additional $–CH_2–$ group in each aliphatic chain, and most metal cations will preferentially complex to form 5m-CR.[9,46]

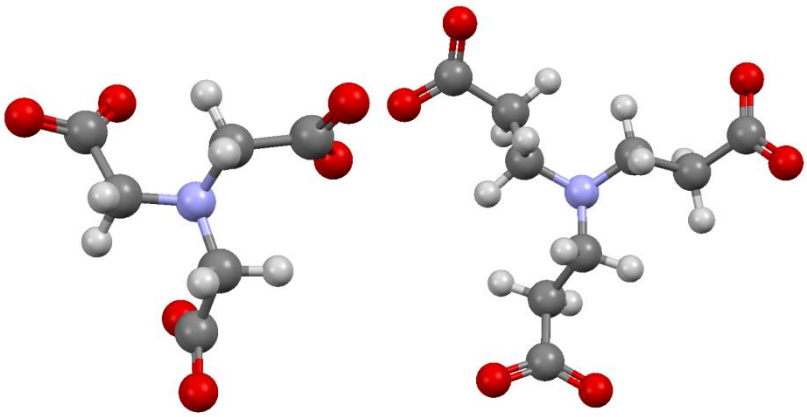

Figure 1.1. The fully deprotonated ligands of NTA and NTPA

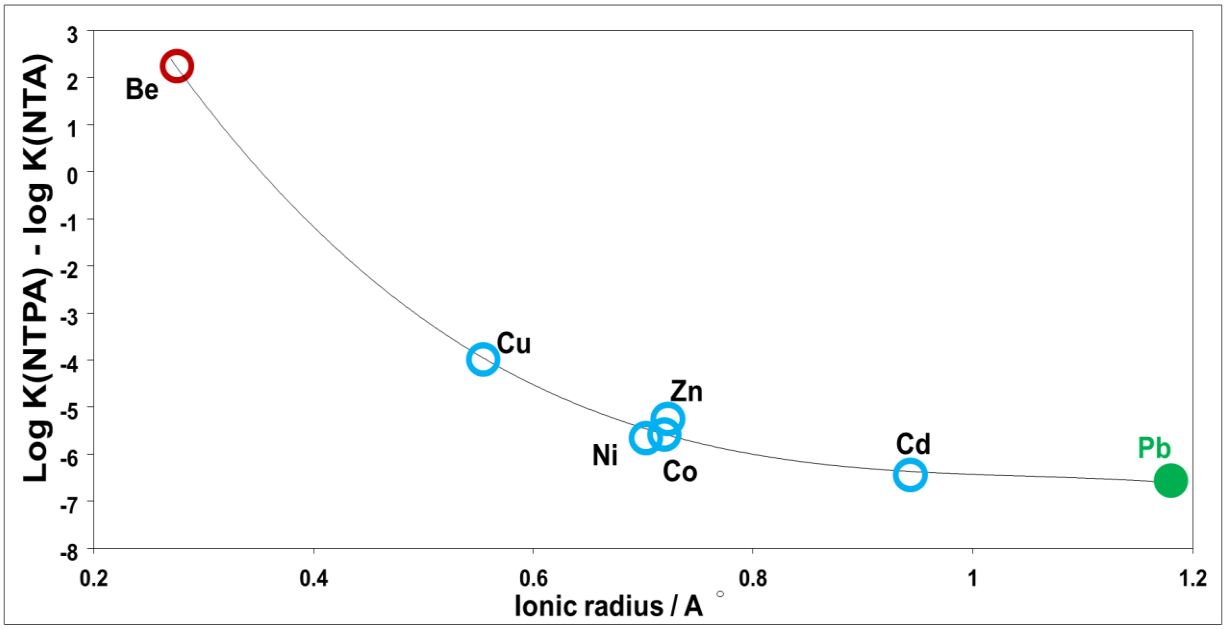

Figure 1.2. Illustration of the difference in stability constants of NTA and NTPA complexes. All complexes are obtained from the NIST database[9] except for PbNTPA which was obtained experimentally by Cukrowski.[46]

The only known example, where a metal ion preferentially complexes to NTPA, is Be^{II}. In this work, we aim to explain the known experimental trend in relative molecular stability of the complexes of NTA and NTPA. For our purposes the complexes of Be^{II} – the only known exception – and Zn^{II} have been selected. The relative stability of complexes will be explored using various theoretical tools:

(i) A competition reaction will be used to validate structures and select a level of theory suitable for further analysis.

(ii) The Quantum Theory of Atoms in Molecules (QTAIM), Non-Covalent Interactions (NCI) method, the Interacting Quantum Atoms (IQA) theory and geometric distances, will be used to analyse a variety of intramolecular interactions traditionally associated with complex stability including coordination bonds, repulsive interactions within the coordination sphere and weaker intramolecular interactions such as the CH•••HC, and CH•••O. It is important to distinguish this work from others by avoiding a disproportionate focus on the nature of the CH•••HC interactions.

(iii) The complex formation process will be decomposed into a sequence of simplified events, fragment preorganization and binding. The energetic contributions of each event will be calculated for all the complexes.

(iv) Preorganization will be analysed in depth using QTAIM, NCI and IQA to determine which fragment(s) of the molecule contributes most towards the destabilisation of this phase of the complex formation process.

(v) QTAIM, IQA and Interacting Quantum Fragments (IQF) will be used to understand the binding process and analyse interactions that drive the binding of two fragments together.

The hope is that new insight and a new protocol for understanding molecular stability can be established that shifts from sifting through hundreds of interactions and minimises the analysis whilst still be accessible to other experimental chemists. Furthermore, the protocol should easily be accessible, minimise computational cost and provide results which are intuitive.

Previously, the Ni^{II} [47] and Zn^{II} [48] complexes of NTA and NTPA have been studied extensively. The complexes of Ni^{II} revealed that NiNTPA has QTAIM atomic interaction lines (AILs) between CH•••HC and CH•••O interactions, suggesting there is no steric hindrance and that there are weak intramolecular interactions that contribute to lowering the energy of the molecule. Furthermore, the strain energy associated with the preorganization of the ligand is much greater for NTPA than NTA. Similar results were found for the Zn^{II} complexes, and in addition it was found that the CH•••HC interaction is characterized by electron flow as determined from ETS-NOCV. Furthermore, it was found that the strain from

the preorganization of the $Zn(H_2O)_2$ fragment also contributed to the weaker formation of ZnNTPA.

References

[1] Clayden, J.; Greeves, N.; Warren, S.; Wothers, P. *Organic Chemistry*, Oxford University Press In: New York, 2001.

[2] van Bachove, M.A.; Swart, M.; Bickelhaupt, F.M. *J. Am. Chem. Soc.* **2006**, *128*, 10738–10744.

[3] Wang, J.; Huang, L.; Yang, X.; Wei, H. *Organometallics* **2015**, *34*, 212−220.

[4] Tanaka, N.; Yamagishi, S.; Nishikiori, H. *Computational and Theoretical Chemistry* **2013**, *1020*, 108–112.

[5] Azofra, L.M.; Alkorta, I.; Toro-Labbe´b, A.; Elgueroa, J. *Phys. Chem. Chem. Phys*. **2013**, *15*, 14026–14036.

[6] Afzal, D.; Fountain, K.R. *Can. J. Chem.* **2011**, *89*, 1343–1354.

[7] Yang, Z.; Ding, Y.; Zhao, D. *J. Phys. Chem. A*. **2009**, *113*, 5432–5445.

[8] Grabowski, S.J. *Phys. Chem. Chem. Phys.* **2014**, *16*, 1824–1834.

[9] NIST Standard Reference Database 46. NIST Critically Selected Stability Constants of Metal Complexes Database, version 8.0; Database collected and selected by Smith, R. M., A.E.; US Department of Commerce, National Institute of Standards and Technology: Gaithersburg, MD, 2004.

[10] Martell, A. E.; Hancock, R. D. *Metal Complexes in Aqueous Solutions*, Plenum Press: New York, 1996.

[11] Etheridge, F. S.; Fernando, R. ; Golen, J. A.; Rheingold, A. L.; Sauve, G. *RSC Adv.* **2015**, *5*, 46534–46539.

[12] Foliatini; Yulizar1, Y.; Hafizah, M.A.E. *Indo. J. Chem.* **2014**, *14*, 239–245.

[13] Weisser, F.; Plebst, S.; Hohloch, S.; van der Meer, M.; Manck, S.; Führer, F.; Radtke, V.; Leichnitz, D.; and Sarkar, B. *Inorg. Chem*. **2015**, *54*, 4621−4635.

[14] Zhang, Q.; Chen, X.; Chen, J.; Wu, X.; Yu, R.; Lu, C. *Dalton Trans.* **2015**, *44*, 10022–10029.

[15] Mloston, G.; Pipiaka, P.; Lindenb, A.; Heimgartner, H. *Helvetica Chimica Acta.* **2015**, *98*, 462–473

[16] Benedetti, M.; Antonucci, D.; Girelli, G.R.; Fanizzi, F.P. *Eur. J. Inorg. Chem.* **2015**, 2308–2316.

[17] Bader, R.W.F. *Atoms in Molecules: A Quantum Theory*, Oxford University Press: Oxford, U.K., 1990.

[18] Bader, R.W.F. *J. Phys. Chem. A.* **2009**, *113*, 10391–10396.

[19] Cioslowski, J.; Mixon, S.T. *Can. J. Chem.* **1992**, *70*, 443–449.

[20] Cioslowski, J.; Mixon, S.T. *J. Am. Chem. Soc.* **1992**, *114*, 4382–4387.

[21] Jimenez-Vazquez, H.A.; Tamariz, J.; Cross, R.J. *J. Phys. Chem. A.* **2011**, *105*, 1315–1319.

[22] Jablonski, M.J. *J. Phys. Chem. A.* **2012**, *116*, 3753–3764.

[23] A.A. Popov, S.M. Avdoshenko, A.M. Pendás, L. Dunsch, *Chem. Commun.* 48 (2012) 8031–8050.

[24] Hancock, R.D. *Chem. Soc. Rev.* **2013**, *42*, 1500–1524.

[25] Bader, R. F. W. *J. Phys. Chem. A.* **2009**, *113*, 10391–10396.

[26] Poater, J.; Solà, M.; Bickelhaupt, F.M. *Chem.–Eur. J.* **2006**, *12*, 2889–2895.

[27] Poater, J.; Solà, M.; Bickelhaupt, F.M. *Chem.–Eur. J.* **2006**, *12*, 2902–2905.

[28] Poater, J.; Visser, R.; Solà, M.; Bickelhaupt, F.M. *J. Org. Chem.* **2007**, *72*, 1134–1142.

[29] Krapp, A.; Frenking, G. *Chem. Eur. J.* **2007**, *13*, 8256–8270

[30] Grimme, S.; Mück-Lichtenfeld, C.; Erker, G.; Kehr, G. Wang, H.; Beckers, H.; Willner, H. *Angew. Chem. Int. Ed.* **2009**, *48*, 2592–2595.

[31] Bader, R.W.F. *J. Phys. Chem. A.* **2011**, *115*, 12432–12435.

[32] Matta, C.F.; Hernández-Trujillo, J.; Tang, T.H.; Bader, R.F.W.; *Chem.–Eur. J.* **2003**, *9*, 1940–1951.

[33] Bader, R.F.W. *Chem.–Eur. J.* **2006**, *12*, 2896–2901.

[34] Bader, R.F.W.; Fang, D.C. *J. Chem. Theory Comput.* **2005**, *1*, 403-414.

[35] von Hopffgarten, M.; Frenking, G. *Chem.–Eur. J.* **2008**, *14*, 10227–10231.

[36] Grabowski, S.J.; Ugalde, J.M. *J. Phys. Chem. A.* **2010**, *114*, 7223–7229.

[37] Frenking, G.; Hermann, M.; *Angew. Chem.* **2013**, *125*, 6036–6039.

[38] Danovich, D.; Shaik, S.; Rzepa, H.S.; *Angew. Chem. Int. Ed.* **2013**, *52*, 5926–5928.

[39] Weinhold, F.; *J. Comp. Chem.* **2012**, *33*, 2440–2449.

[40] Cukrowski, I.; de Lange, J.H.; Mitoraj, M.; *J. Phys. Chem. A* **2014**, *118*, 623–637.

[41] Cukrowski, I.; Matta, C. *Chemical Physics Letters* **2010**, *499*, 66–69.

[42] Alder, A.C., Siegrist, H.; Gujer, W.; Giger, W. *Wat. Res.***1990**, *24*, 733-742.

[43] Vohra, M.S.; Davis, A.P. *Journal of Colloid and Interface Science* **1997**, *194*, 59–67.

[44] Toste, A. P.; Lechner-Fish, T. J. *Waste Manage.* **1937**, *13*, 237.

[45] Dey, B.; Choudhury, S.R.; Suresh, E.; Jana, A.D.; Mukhopadhyay, S.; *Journal of Molecular Structure* **2009**, *921*, 268–273.

[46] Unpublished data by Cukrowski, I.

[47] Govender, K.K.; Cukrowski, I. *Inorg. Chem.* **2010**, *49*, 6931–6941.

[48] Cukrowski, I.; Govender, K.K.; Mitoraj, M.; Srebro, M. *J. Phys. Chem. A* **2011**, *115*, 12746–12757.

2. Computational Methods

Introduction

Chemistry provides a plethora of unique and interesting problems that require solving and understanding. In an attempt to understand the chemistry behind the problem, chemists make use of models to develop an appreciation of the reality they are studying. These range from the ball and stick diagrams used to represent the molecular structure, to the reaction mechanisms used to describe chemical reactivity. Computational chemistry is thus the modelling of our chemical reality using the fundamental laws of physics. Computational chemistry has evolved in parallel to physics to include two broad approaches within the field: molecular mechanics (based on classical mechanics) and electronic structure methods (based on quantum mechanics).[1] Computational chemistry has found numerous applications including in molecular structure prediction, transition state analysis, determining chemical reactivity, identifying chemical properties, reproducing experimental spectra. That is why the use of computational techniuqes has expanded beyond physical chemistry.

In this chapter various aspects of computational chemistry will be explored, primarily focusing electronic structure methods and the implementation of these methods to develop a wavefunction, and investigation of different theoretical tools used to investigate the wavefunction of a system. The primary source of all information on electronic structure methods comes from *Exploring Chemistry with Electronic Structure Methods (2nd edition)* by Foresman and Frisch.[1]

Electronic Structure Methods

Electronic structure methods make use of quantum mechanics as the foundation for all computations. In particular, quantum mechanics focuses on solving the time-independent Schrödinger equation in order to obtain different properties of the molecule.

$$H\psi = E\psi \qquad (2.1)$$

H is the Hamiltonian operator, ψ, is the wavefunction and E is the energy of the system. The exact solutions to Schrödinger's Equation are not practical to compute for most systems and hence various mathematical approximations must be made to the solutions. The electronic structure method, in simple terms, is the means in which the approximation is made. There are three main classes of electronic structure methods: semi-empirical methods, *ab initio* methods and density functional theory.

Semi-empirical methods

Semi-empirical methods necessarily require experimental data, because parameters derived from this data are used to solve an approximate form of Schrödinger's equation. This approximation is comparatively, computationally cheap and as a result can be used for large molecular systems. Semi-empirical methods are usually used:

(i) For very large systems and it is necessary to use a quantum mechanical approach.

(ii) As pre-optimization step for large systems, that it is a large system is optimized using a semi-empirical method, and then subsequently optimized using a different electronic structure method.

(iii) For ground state molecular systems for which the semi-empirical method is well-calibrated and well-parameterized.

(iv) To obtain qualitative information about a molecule, such as its molecular orbitals, atomic charges or vibrational normal modes.

Note that the semi-empirical methods are limited to usage when parameters have been well developed. Additionally, they typically do not perform well on systems which include hydrogen bonding, transition states and poorly parameterized atoms. Examples of semi-empirical methods include AM1, PM3 and MNDO.

Ab initio methods

The *ab initio* methods make use of mathematical approximations to Schrödinger's equation without any need for experimental parameters. These methods compute using quantum mechanical laws and physical constants. The result is that *ab initio* methods produce excellent quantitative information over a number of different molecular systems. There are two broad categories of ab initio methods: (i) Hatree Fock and (ii) post SCF methods. In this work, mainly perturbation theory (specifically MP2) is used in conjunction with density functional theory. However, it is still important to discuss the Hatree Fock method.

Hatree-Fock

Hatree Fock is one of the most convenient and well-used electronic structure methods. It makes use of a number of simplifying calculations to determine the approximate solution to the Schrodinger equation. To begin, according to molecular orbital theory, the wavefunction is decomposed into a combination of molecular orbitals: ϕ_1, ϕ_2 ... ϕ_n. An orthonormal set of molecular orbitals is then selected where:

$$\iiint \phi_i * \phi_i dxdydz = 1$$

$$\iiint \phi_i * \phi_j dxdydz = 0 \quad i \neq j \tag{2.2}$$

The Hatree Product is then defined as:

$$\psi(r) = \phi_1(r_1)\phi_2(r_2)...\phi_n(r_n) \tag{2.3}$$

which is then used to form a combination of these molecular orbitals. Note that the function is not antisymmetric.

In order to have an antisymmetric function the product must be expressed as a determinant. To achieve that, electron spin is accounted. Electron spin can either be spin up (+ ½) or spin down (- ½). When considering closed shell functions, one makes use of two spin functions which are defined as:

$$\alpha(\uparrow) = 1 \qquad \alpha(\downarrow) = 0$$

$$\beta(\uparrow) = 0 \qquad \beta(\downarrow) = 1 \tag{2.4}$$

The function α has a value 1 for a spin up electron and the function β has a value 1 for a spin down electron. The product of the spin function with the molecular orbital function gives the spin orbital which results in the inclusion of electron spin in the wavefunction. The wavefunction hence takes the form:

$$\psi(r) = \frac{1}{\sqrt{n!}} \begin{vmatrix} \phi_1(r_1)\alpha(1) & \phi_1(r_1)\beta(1) & \phi_2(r_1)\alpha(1) & \phi_2(r_1)\beta(1) & \cdots & \phi_{\frac{n}{2}}(r_1)\alpha(1) & \phi_{\frac{n}{2}}(r_1)\beta(1) \\ \phi_1(r_2)\alpha(2) & \phi_1(r_2)\beta(2) & \phi_2(r_2)\alpha(2) & \phi_2(r_2)\beta(2) & \cdots & \phi_{\frac{n}{2}}(r_2)\alpha(2) & \phi_{\frac{n}{2}}(r_2)\beta(2) \\ \vdots & & & & & & \vdots \\ \phi_1(r_n)\alpha(n) & \phi_1(r_n)\beta(n) & \phi_2(r_n)\alpha(n) & \phi_2(r_n)\beta(n) & \cdots & \phi_{\frac{n}{2}}(r_n)\alpha(n) & \phi_{\frac{n}{2}}(r_n)\beta(n) \end{vmatrix} \tag{2.5}$$

The determinant takes into account the electron spin and all possible electron locations. This results in the wavefunction being antisymmetric.

Each molecular orbital is then defined as:

$$\phi_i = \sum_{\mu=1}^{N} c_{\mu i}\chi_\mu \tag{2.6}$$

$c_{\mu i}$ are the molecular orbital expansion coefficients and χ_μ are the basis functions. Given the above definition of molecular orbitals it is necessary to solve for the set of molecular orbital coefficients. The variational principle is used in this regard for Hatree Fock theory. The variational principle states that the energy of the exact wavefunction serves as a lower bound to the energies calculated by another normalised antisymmetric function. That is:

$$E(\Xi) > E(\psi) \qquad \Xi \neq \psi \tag{2.7}$$

Building up on the variational principle, Roothaan and Hall derived equations that describe the molecular orbital expansion coefficients:

$$\sum_{v=1}^{N} (F_{\mu v} - \varepsilon_i S_{\mu v}) c_{vi} = 0 \qquad \mu = 1, 2, \ldots, N \tag{2.8}$$

and the equation can be written in matrix form as:

$$\mathbf{FC} = \mathbf{SC}\varepsilon \tag{2.9}$$

Each element in the above equation is a matrix and ε represents a diagonal matrix containing orbital energies, where each element ε_i is the one-electron orbital energy of molecular orbital χ_i. The Fock matrix and the molecular orbitals are dependent on c, the molecular expansion orbital coefficients. The Self-Consistent Field (SCF) method is an iterative procedure that is used to solve for the molecular orbital expansion coefficients. In electronic structure methods, where the energy converges to a minimum, a field is generated from the orbitals and this field produces the same orbitals.

Hatree Fock has numerous advantages including that it is fast, computationally cheap and quite often reproduces experimental data with a high degree of accuracy. Unfortunately, in some instances, HF theory is unable to produce accurate results. This is because whilst Hatree Fock theory is able to determine correlation effects between electrons of the same spin (also called exchange correlation) it is however unable to correlate effects or electrons with opposite spin which often results in some form of electron-electron interaction. In order to compensate for this deficit alternative electronic structure methods are used such as density functional theory and post-SCF methods.

Post-SCF Methods.

The fundamental weakness of Hatree Fock theory comes from the inability to deal with electron correlation – the phenomenon in which there is an instantaneous interaction between electrons with opposite spins. Post-SCF methods go beyond the SCF method to deal with electron correlation effects. There are numerous methods that include electron correlation including, the Configuration Interaction energies, Coupled Cluster Methods, Bruckner Double energies and the Møller-Plesset Perturbation Theory. In this work we only use a single variant of Møller-Plesset perturbation theory and hence will focus our attention on these theories.

In Perturbation theory, the Hamiltonian is divided into two parts:

$$H = H_0 + \lambda V \tag{2.10}$$

H_0 has an exact solution and λV is a correction called the perturbation which is comparatively smaller than H_0. The perturbed wavefunction and the energy can be expressed as a power series in V.

$$\psi = \psi_{(0)} + \lambda\psi_{(1)} + \lambda^2\psi_{(2)} + \lambda^3\psi_{(3)} + \ldots$$

$$E = E_{(0)} + \lambda E_{(1)} + \lambda^2 E_{(2)} + \lambda^3 E_{(3)} + \ldots \tag{2.11}$$

The perturbed forms of the wavefunction and the energy are substituted into the Schrodinger equation:

$$(H_0 + \lambda V)(\psi_{(0)} + \lambda\psi_{(1)} + \lambda^2\psi_{(2)} + \ldots) = (E_{(0)} + \lambda E_{(1)} + \lambda^2 E_{(2)} + \ldots)(\psi_{(0)} + \lambda\psi_{(1)} + \lambda^2\psi_{(2)} + \ldots) \tag{2.12}$$

The above expression is expanded and the coefficients of each power of λ are equated which allows one to determine a series of higher order perturbations. For powers of λ corresponding to 0, 1 and 2

$$(H_0 - E_{(0)})\,\psi_{(0)} = 0$$

$$(H_0 - E_{(0)})\,\psi_{(1)} = (E_{(1)} - V)\,\psi_{(0)}$$

$$(H_0 - E_{(0)})\,\psi_{(2)} = (E_{(1)} - V)\,\psi_{(1)} + E_{(2)}\,\psi_{(0)} \tag{2.13}$$

In the particular case of Møller-Plesset perturbation theory, H_0 is defined as the sum of the one-electron Fock operators:

$$H_0 = \sum_i F_i \tag{2.14}$$

The procedure involves solving for each perturbed energy value, $E_{(0)}$, $E_{(1)}$, $E_{(2)}$ … using the expanded coefficients of the powers of λ. The sum of $E_{(0)} + E_{(1)}$ yields the Hatree Fock energy.

$$E_{HF} = E_{(0)} + E_{(1)} \tag{2.15}$$

The subsequent perturbations, $E_{(2)}$, $E_{(3)}$, $E_{(4)}$ …, can be determined and result in the lowering of the energy. In this work we will make use of the Møller-Plesset 2nd-order perturbation theory (MP2).

Density Functional Theory

Hatree Fock calculations are relatively inexpensive, and can give excellent results but quite fail to account for the electron correlation and hence fail in numerous systems. Post-SCF methods are far more accurate as they account for electron correlation but often are far more expensive. Moreover, ab initio methods make use of the wavefunction which cannot be measured experimentally. Density functional theory, which originates from the Hohenberg-Kohn theorem, uses density as the primary measure and electron correlation can be determined using general functionals of the electron density.

Current DFT methods partition the electronic energy into several components.

$$E = E_T + E_V + E_J + E_{XC} \tag{2.16}$$

E_T is the kinetic energy, E_V is the potential energy of the nuclear-electron attraction and the nuclear-nuclear repulsion, E_J is the classical component of electron-electron repulsion and E_{XC} is the exchange-correlation term which accounts for the remainder of the electron-electron interactions including electron correlation. In density functional theory, a great deal of time has been dedicated to the determination of accurate approximations of E_{XC}. This is because the exact functional is only known for free electron gas. The exchange-correlation functional is typically approximated using:

$$E_{xc}(\rho) = \int f(\rho_\alpha(r), \rho_\beta(r), \nabla\rho_\alpha(r), \nabla\rho_\beta(r)) d^3 r \tag{2.17}$$

where ρ_α refers to the α spin density, ρ_β refers to the β spin density and $\nabla\rho$ refers to the gradient of the density. To accommodate the different types of electron correlations, that is exchange (interactions between electrons with the same spin) and correlation (interactions

between electrons with opposite spin), DFT decomposes the exchange-correlation term into exchange and correlation functionals:

$$E_{XC}(\rho) = E_X(\rho) + E_C(\rho) \tag{2.18}$$

The decomposed functionals can take one of two forms: (i) local functionals – which are dependent on only the electron density, and (ii) gradient-corrected functionals – which are dependent on both the electron density and its gradient. For local exchange functionals, the definition is almost always:

$$E_X^{LDA} = -\frac{3}{2}\left(\frac{3}{4\pi}\right)^{1/3}\int \rho^{4/3} d^3\mathrm{r} \tag{2.19}$$

This reproduces exchange in a uniform electron gas, however, shows some weaknesses in describing molecular systems. In order to improve the exchange functional, the gradient corrections are often necessary such as:

$$E_X^{Becke88} = E_X^{LDA} - \gamma\int \frac{\rho^{4/3}(\rho^{-4/3}|\nabla\rho|)^2}{(1+6\gamma\sinh^{-1}(\rho^{-4/3}|\nabla\rho|))} d^3\mathrm{r} \tag{2.20}$$

In practise, there has been an increased usage of hybrid DFT schemes. These make use of weighted contributions of the exchange component that is available in the Hatree Fock theory and additional exchange and correlation functionals defined in DFT. These hybrid functionals take the form:

$$E_{XC}^{hybrid} = c^{HF}E_X^{HF} + c^{DFT}E_{XC}^{DFT} \tag{2.21}$$

where c refers to the constants which give relative weighting to the different contributions. An example of a hybrid functional is B3LYP (Becke-style three parameter functionals combined with Lee-Yang-Parr correlation) which has become fairly common place today. An extension of B3LYP, known as X3LYP (the extended three parameter functional combined with Lee-Yang-Parr correlation),[2] has been implemented and it improves upon the description of data including heat of formation and van der Waals interactions.[3–6] In this work both B3LYP and X3LYP will be utilized. Hybrid functionals have the added benefit of improving on the accuracy of Hatree Fock without requiring the massive computational resources often needed for post-SCF calculations.

Quantum Theory of Atoms in Molecules

The Quantum Theory of Atoms in Molecules (QTAIM) is a model of molecular and condensed matter electronic systems in which the principal objects in molecular structure – atoms and bonds – are natural expressions of a system's observable electron density distribution function.[6] This electron density distribution is the probability that describes the average manner in which the electronic charge is distributed throughout real space in the attractive field exerted by the nuclei. Molecular structure is revealed by stationary points of the electron density together with the gradient paths of the electron density that originate and terminate at these points. It is driven by the following assumption; since concepts of atoms and bonds have been and continue to be so ubiquitously useful in chemistry, they should have a well-defined physical basis. Chemical bonding and structure of a chemical system are defined based on the topology of the electron density. The topology is dominated by the attractive forces of the nuclei, imparting a substantial local maximum at the position of each nucleus. Certain pairs of nuclei are linked by ridges of electron density. QTAIM allows for the calculation of certain physical properties on a per-atom basis, by dividing space up into atomic volumes containing exactly one nucleus.

Nuclei act as point attractors immersed in a cloud of negative charge. The electron density is at a maximum at the nucleus and decays rapidly away from the nucleus. A gradient vector map can be generated by tracing the trajectory of $\nabla\rho$(r) (determining the gradient of electron density at each point in the field). Sets of trajectories terminate at each nucleus. This allows one to partition the molecule into basins (a region of space traversed by trajectories that terminate at a given nucleus). The QTAIM atom is hence defined as a union of an attractor and its basin and is an open system (Ω) that is bound by zero-flux surface, S(Ω;r), in the gradient vector field of electron density, $\rho(r)$:

$$\nabla\rho(r)\cdot n(r)=0 \qquad \forall r\in(\Omega;r) \tag{2.22}$$

Based on the physics of an open system, every property of the overall system (here in point a group or molecule) can be determined by the sum of the individual properties of the overall system. Atomic and group properties from QTAIM have reproduced experimentally determined group properties successfully where those contributions were transferable.

A critical point (CP) is a point where the first derivative of electron density vanishes

$$\nabla\rho = i\frac{d\rho}{dx} + j\frac{d\rho}{dy} + k\frac{d\rho}{dz} = 0 \qquad (2.23)$$

Each component is equal to zero and not just the sum. At each critical point there is a set of trajectories that start at infinity and terminate at the critical point. There is a unique pair of trajectories that each originate at the critical point and terminate at each neighbouring nucleus. These lines define a line through space along which electron density is a maximum (a ridge of maximum density) and is called an atomic interaction line (AIL) or a bond path (BP). A pair of bonded atoms is linked along this line of maximally concentrated electron density. Along an AIL there is a point of minimum electron density where the interatomic surface (which is also a zero-flux surface) defining the mutual boundary of two bonded atoms intersects the ridge of electron density. This minimum is defined as a (–3,1) critical point and is termed a bond critical point (BCP) in QTAIM. According to Bader "For a system in a stationary state, the wave function and the electron density it determines are such as to minimize the total energy." Thus, the presence of an AIL minimizes the energy associated with an interaction between two atoms.[7]

The Noncovalent Interactions Scheme

The Quantum Theory of Atoms in Molecules has a specific and rigorous definition of interactions based on the presence or absence of an atomic interaction line. The atomic interaction line necessarily means that an interaction is bonding[8] and that there is a minimization of the interaction between the two atoms. The Noncovalent Interactions (NCI) Theory, by making use of the electron density and the derivatives, enables the real-space visualization of numerous noncovalent interactions.[9–12] NCI is able to fully recover interactions found in AIM (AILs) and uncovers additional interactions.[13]

NCI originates from density functional theory. The reduced density gradient, $s(\rho)$ or RDG, is a dimensionless quantity obtained from the density and the first derivative of the density:

$$s(\rho) = \frac{1}{C_F}\frac{|\nabla\rho|}{\rho^{4/3}} \qquad (2.24)$$

where C_F is constant. The reduced density gradient identifies local deviations from homogenous electron density. The value of the reduced density gradient is large and positive far away from the molecule (i.e. in the density tails, where the density decreases exponentially) and approaches zero values where the density is large and the density gradient is small (i.e. near atoms, and regions of bonding and interactions). Plotting *s* as a function of the density allows one to visualize how bonding affects the otherwise uniform reduced density gradient. The plots of $s(\rho)$ versus ρ has the general form $s(\rho) = a\rho^{-1/3}$, where *a* is constant. When an interaction is present, there is an unavoidable deviation in electron density. This is revealed as a trough (also called peak or spike) in the plot where $s(\rho)$ tends to 0 and such troughs occur for both covalent bonding and noncovalent interactions. For covalent bonds, the trough is found at large density values whereas for noncovalent interactions, the troughs occur in the low-density, low-gradient region. The original NCI theory is not only concerned with identifying the presence of a noncovalent interaction, but also with distinguishing between different types of weak intramolecular interactions (i.e. hydrogen bonding, van der Waals and steric hindrance). This promoted further exploration of the NCI peaks.

NCI makes use of the physics of the Divergence theorem[14] to distinguish between different types of noncovalent interactions. According to the theorem, sign of the Laplacian of the electron density ($\nabla^2\rho(r)$) indicates the behaviour of the net flux gradient around a reference point. When $\nabla^2\rho(r) < 0$, the net gradient flux is entering an infinitesimal volume and hence the density is locally accumulated, or *concentrated*, and when $\nabla^2\rho(r) > 0$, the net gradient flux is leaving an infinitesimal volume, thus the density is locally depleted.[10] The Laplacian is decomposed into three eigenvalues of the electron density Hessian Matrix where $\nabla^2\rho(r) = \lambda_1 + \lambda_2 + \lambda_3$, where $\lambda_1 \leq \lambda_2 \leq \lambda_3$. According to the NCI regime, an interaction is said to be attractive when $\lambda_2 < 0$ (corresponding to a local accumulation of density in the plane perpendicular to the interaction) and an interaction is said to be repulsive when $\lambda_2 > 0$ (corresponding to a local depletion of density in the plane perpendicular to the interaction). These interpretations of the sign of the Laplacian are *mapped* onto our existing knowledge of weak, noncovalent interactions hence we have the following NCI-defined descriptors for these interactions:

(i) Bonding interactions, such as hydrogen bonds, which are classically attractive interactions, show a local accumulation of density in the plane perpendicular to the interaction, $\lambda_2 < 0$.

(ii) Van der Waals forces or dispersion interactions, which are classically described as weakly attractive interactions, show a negligible accumulation of electron density hence $\lambda_2 \leq 0$.

(iii) Nonbonded interactions, such as steric repulsion, have traditionally been interpreted as repulsive interactions and show a local depletion of electron density in the plane perpendicular to the interaction, $\lambda_2 > 0$.

Thus in order to have a plot which reveals the presence of a noncovalent interaction and indicates the types of interaction, the NCI theory plots s(ρ) versus sign(λ_2)×ρ(r). This graph is termed the NCIPlot.

The NCI theory enables the 3D visualization of these interactions in the molecule. Any deviation of the homogenous density, as determined by $s(\rho)$, is represented as an isosurface. The sign of λ_2 is represented as the colour of the isosurface implying that one can distinguish between the types of interactions. Thus, the isosurface is blue for bonding interactions, red for nonbonding interactions, and green for weakly attractive interactions.

Recently, the traditional NCI interpretations have become questionable, in particular whether or not the local density distribution is synonymous with the attractive/repulsive nature of the interaction or the stabilizing/destabilizing contribution to the molecular system.[15] In a recent study, numerous interactions in many different molecular systems were investigated. Water dimers were arranged in such a manner that O•••O and H•••H interactions were present. The classical notion would suggest that these are repulsive interactions, however a local accumulation of electron density was found. The NCI-interpretation would be that the interactions are attractive. Moreover, the interaction energy, as determined using the Interacting Quantum Atoms theory, was repulsive for these interactions (O•••O and H•••H) in the water dimers. Clearly, the physical phenomenon, the local accumulation of density, did not correspond to the NCI interpretation as an attractive interaction but rather a repulsive interaction. The results from these interactions and many others led to the conclusion that the local properties of an interaction based on the density do not correlate with the physical nature of that interaction. Hence, NCI can only be used to reveal the presence/absence of weak interactions and their local density behaviour.

One-Dimension Cross-sections

As a part of an in depth exploration of different types of interactions, a new means of analysing the topology of electron density was developed that fully recovered QTAIM and NCI results.[15] 1D cross-sections of the electron density were used to analyse numerous intermolecular and intramolecular interactions. In order to determine the 1D cross-section the geometric interaction point (GIP) is determined first. It is the point between two nuclei where the electron density between them is at a minimum. Subsequently, the eigenvector at the GIP, corresponding to the λ_2 eigenvalue of the Hessian matrix was then calculated. Two new coordinates are determined on either side of the GIP at a specific distance along the eigenvector and electron densities are recorded at these coordinates. The eigenvector is then determined for each of these coordinates and two new coordinates are determined and the density is recorded. The process of determining new coordinates, measuring the densities, determining the eigenvector and determining new coordinates is repeated until a pre-determined length is reached on either side of the GIP.

Interacting Quantum Atoms and Interacting Quantum Fragments

Quantum Chemistry has been particularly successful at the prediction of overall molecular properties including molecular geometries, energy and spectra. However, correlating the physics of quantum chemistry (molecular energy and the wavefunction) to the understanding of chemistry (atoms, bonds, functional groups etc.) remains elusive. Despite this, a number of tools and protocols have been dedicated towards understanding these chemical concepts. In order to achieve this, the energy of the molecule must be partitioned into these chemical components. Blanco and collaborators[16] propose a criteria for a good energy partition: (i) Chemically meaningful components, atoms and functional groups must be identifiable and that they retain their identity in the molecule, (ii) the partition should be able to describe the chemical bond by providing detailed definitions of interactions between chemical components (atoms, functional groups and molecules), and (iii) the partitioning scheme should be able to fully recover the energy of the system by summing up the energy of the individual components without requiring approximations.

Pendás et al proposed the Interacting Quantum Atoms (IQA)[16–18] theory which partitions the energy of the molecule in atoms. It makes use of the QTAIM definition of an atom, the

nucleus combined with the atomic basin, in order to do so. To begin, the energy of a molecule is realized as a combination of effective one-body (intra-atomic) contributions and two-body (interatomic) contributions. The intra-atomic contributions consist of the atomic kinetic energy T^{X}, the electron-nucleus attraction (the electrostatic attraction of the nucleus to the electrons within the atomic basin), and the electron-electron repulsion (the total inter-electron repulsion within the atomic basin), the sum of which gives the atomic self, sometimes called net, energy. For an atom X,

$$E_{\text{self}}^{\text{X}} = T^{\text{X}} + V_{\text{en}}^{\text{XX}} + V_{\text{ee}}^{\text{XX}} \tag{2.25}$$

The interatomic contributions are realized as the interaction energy between two atoms, X and Y, which consists of the nucleus-nucleus repulsion, the attraction between the electrons in atomic basin X to and the nucleus of atom Y, the attraction between the nucleus of atom X to the electrons of atom Y, and the electron-electron repulsion between the two atomic basins. Thus

$$E_{\text{int}}^{\text{XY}} = V_{\text{nn}}^{\text{XY}} + V_{\text{en}}^{\text{XY}} + V_{\text{ne}}^{\text{XY}} + V_{\text{ee}}^{\text{XY}} \tag{2.26}$$

Note that each term is symmetric with regards to the A ↔ B interchange (*e.g.*, $V_{\text{en}}^{\text{XY}} = V_{\text{ne}}^{\text{XY}}$). In order to decompose the interaction energy into terms that have chemical meaning, the electron-electron repulsion is decomposed into two two-electron terms, the columbic term and the exchange-correlation contributions,

$$V_{\text{ee}}^{\text{XY}} = V_{\text{C}}^{\text{XY}} + V_{\text{XC}}^{\text{XY}} \tag{2.27}$$

This allows one to define a new classical term

$$V_{\text{cl}}^{\text{XY}} = V_{\text{nn}}^{\text{XY}} + V_{\text{en}}^{\text{XY}} + V_{\text{ne}}^{\text{XY}} + V_{\text{C}}^{\text{XY}} \tag{2.28}$$

Equations (2.27) and (2.28) allow one to re-write the interactions energy as the sum of the classical term, which is the electrostatic contribution, and the exchange-correlation term, which is the quantum or electron-sharing contribution,

$$E_{\text{int}}^{\text{X,Y}} = V_{\text{cl}}^{\text{XY}} + V_{\text{XC}}^{\text{XY}} \tag{2.29}$$

The exchange-correlation can further be decomposed into an exchange term and a correlation term, however, there is no chemical meaning to the individual terms.

The total energy of the molecule is thus the sum of all intra-atomic (self energy) and interatomic contributions (interaction energy) within the system

$$E = \sum_{X} E_{self}^{X} + 0.5 \sum_{X} \sum_{Y \neq X} E_{int}^{X,Y} \tag{2.30}$$

The IQA theory additionally defines the effective energy of an atom as

$$E_{eff}^{X} = E_{self}^{X} + \sum_{Y \neq X} E_{int}^{X,Y} \tag{2.31}$$

And the additive energy of atom

$$E_{add}^{X} = E_{self}^{X} + 0.5 \sum_{Y \neq X} E_{int}^{X,Y} \tag{2.32}$$

The sum of the additive atomic energies of all atoms within the system recovers the total energy of the system

$$E = \sum_{X} E_{add}^{X} \tag{2.33}$$

The IQA theory also provides a means to explore molecular stability. The atomic self energy will remain relatively constant if the changes in the atomic environment are small. However, large changes in the environment lead to changes in the atomic basin that result in significant changes in the individual components of the self energy. Thus, the self energy of an atom carries “the atomic identity from system to system.” The deformation energy is the energy change upon the variation of the atomic density when the atom moves from the isolated (reference) state form to that in the molecule.

$$E_{def}^{X} = \Delta E_{self}^{X} = E_{self}^{X} - E_{vac}^{X} \tag{2.34}$$

The reference state is dependent on the molecular system under consideration, hence it may be isolated ions, for example, when the system is highly ionic. However, the stability of the system can be rationalized using the binding energy

$$E_{bind} = E - \sum_{X} E_{vac}^{X} = \sum_{X} E_{def}^{X} + 0.5 \sum_{X} \sum_{Y \neq X} E_{int}^{X,Y} \tag{2.35}$$

The deformation energy is typically positive (depending on the reference) and interaction energy is typically negative. Thus, during the binding process, atoms necessarily need to raise their energy and is compensated by the interaction energy.

It is incredibly important to note that because IQA calculates two-electron components, i.e. V_{ee}^{XY}, the wavefunction must be calculated using levels of theory which make use of a well-defined 2nd order density matrix. In principle DFT wavefunctions may not be used. However, the AIMAll software, developed by Todd Keith, makes use of 1st order approximation of the 2nd order density matrix for all post-Hatree Fock wavefunctions and has recently been shown to give excellent results when DFT wavefunctions are used in IQA calculations.[19]

The chemical object of interest in IQA is the atom; however, in reality we quite often deal with functional groups and molecules. Thus we need a partitioning which considers polyatomic, chemical components. Penda's et al expanded the concepts from IQA to be inclusive of groups of atoms in the Interacting Quantum Fragments (IQF) theory.[18,20] IQF, also has one-body (self energy) contributions and two-body (interaction energy) contributions. A fragment in the isolated state is composed of atoms and the interactions between those atoms. Thus, when determining the self energy of a fragment, one must sum up both the self energies of the atoms and interaction energies between the all the atoms within the fragment. Hence, the self energy of a fragment $\mathcal{G}$, is

$$E_{self}^{\mathcal{G}} = \sum_{X\in\mathcal{G}} E_{self}^{X} + 0.5\sum_{X\in\mathcal{G}}\sum_{\substack{Y\neq X\\ Y\in\mathcal{G}}} E_{int}^{X,Y} \tag{2.36}$$

The interaction energy between two fragments, $\mathcal{G}$ and $\mathcal{H}$, is the sum of the interactions of all atoms in $\mathcal{G}$ with all atoms in $\mathcal{H}$

$$E_{int}^{\mathcal{G},\mathcal{H}} = \sum_{X\in\mathcal{G}}\sum_{Y\in\mathcal{H}} E_{int}^{X,Y} \tag{2.37}$$

with corresponding classical, $V_{cl}^{\mathcal{G},\mathcal{H}} = \sum_{X\in\mathcal{G}}\sum_{Y\in\mathcal{H}} V_{cl}^{X,Y}$, and exchange-correlation, $V_{XC}^{\mathcal{G},\mathcal{H}} = \sum_{X\in\mathcal{G}}\sum_{Y\in\mathcal{H}} V_{XC}^{X,Y}$ terms.

The total energy of the system is obtained in a similar manner to that in IQA, where the self energies and the interaction energies are summed to

$$E = \sum_{\mathcal{G}} E_{self}^{\mathcal{G}} + 0.5\sum_{\mathcal{G}}\sum_{\mathcal{H}\neq\mathcal{G}} E_{int}^{\mathcal{G},\mathcal{H}} \tag{2.38}$$

Furthermore, the IQA concepts of the deformation energy, $E_{\text{def}}^{\mathcal{G}} = \Delta E_{\text{self}}^{\mathcal{G}} = E_{\text{self}}^{\mathcal{G}} - E_{\text{vac}}^{\mathcal{G}}$, and the binding energy, $E_{\text{bind}} = E - \sum_{\mathcal{G}} E_{\text{VAC}}^{\mathcal{G}} = \sum_{\mathcal{G}} E_{\text{def}}^{\mathcal{G}} + 0.5 \sum_{\mathcal{G}} \sum_{\mathcal{H} \neq \mathcal{G}} E_{\text{int}}^{\mathcal{G},\mathcal{H}}$, have been included in the IQF framework.

References

[1] Foresman, J.B.; Frisch, Æ. *Exploring Chemistry with Electronic Structure Methods*, 2nd Edition, Gaussian, Inc.: Pittsburg, 1996.

[2] Perdew, J.P.; Burke, K.; Ernzerhof, M. *Phys. Rev. Lett.* **1996**, *77*, 3865.

[3] Xu, X.; Goddard, W.A. *Proc. Natl. Acad. Sci.* USA, **2004**, *101*, 2673.

[4] Hyla-Kryspin, I.; Haufe, G.; Grimme, S. *Chem. Eur. J.* **2004**, *10*, 3411.

[5] Hammer, B.; Hansen, L.B.; Nørskov, J.K. *Phys. Rev. B.* **1999**, *59*, 7413.

[6] Bader, R.W.F. *Atoms in Molecules: A Quantum Theory*, Oxford University Press: Oxford, U.K., 1990.

[7] Bader, R.W.F.; Matta, C.F. *J. Phys. Chem. A.* **2006**, *110*, 6365–6371.

[8] Bader, R.W.F. *J. Phys. Chem. A.* **2009**, *113*, 10391–10396.

[9] Johnson, E. R.; Keinan, S.; Mori-Sánchez, P.; Contreras-García, J.; Cohen, A. J.; Yang, W. *J. Am. Chem. Soc.* **2010**, *132*, 6498−6506.

[10] Contreras-García, J.; Johnson, E. R.; Keinan, S.; Chaudret, R.; Piquemal, J. P.; Beratan, D.; Yang, W. *J. Chem. Theory Comput.* **2011**, *7*, 625−632.

[11] Gillet, N.; Chaudret, R.; Contreras-García, J.; Yang, W.; Silvi, B.; Piquemal, J. P., *J. Chem. Theory Comput.* **2012**, *8*, 3993−3997.

[12] Contreras-García, J.; Yang, W.; Johnson, E. R. *J. Phys. Chem. A* **2011**, *115*, 12983−12990.

[13] Lane, J.R.; Contreras-Garcia, J.; Piquemal, J.; Miller, B.J.; Kjaergaard. *J. Chem. Theory Comput.* **2013**, *9*, 3263−3266.

[14] Arfken, G. *Mathematical Methods for Physicists*; Academic Press: Orlando, 1985.

[15] Cukrowski, I.; de Lange, J. H.; Adeyinka, A. S.; Mangondo, P. *Comput. Theoret. Chem.* **2015**, *1053*, 60–76.

[16] Blanco, M. A.; Pendás, A. M.; Francisco, E. *J. Chem. Theory Comput.* **2005**, *1*, 1096−1109.

[17] Francisco, E.; Pendás, A. M.; Blanco, M. A. A. *J. Chem. Theory Comput.* **2006**, *2*, 90−102.

[18] Pendás, A. M.; Blanco, M. A.; Francisco, E. *J. Comput. Chem.* **2006**, *28*, 161−184.

[19] Tognetti, V.; Joubert, L.; *J. Chem. Phys.* **2013**, *138*, 024102-024108.

[20] Pendás, A. M.; Blanco, M. A.; Francisco, E. *J. Chem. Phys.* **2006**, *125*, 184112–19.

3. Exploring the Origin of Relative Stability of Molecular Systems: A Computational Investigation of Be^{II} Complexes as a Case Study Using an IQA/IQF-based Protocol

Abstract

A method designed to investigate, on a fundamental level, the origin of relative stability of molecules (or molecular systems in general) using Be^{II} complexes with NTA and NTPA as a case study (this is the only known example where a metal ion forms stronger complex with NTPA) is described. It makes use of the primary (self-atomic and diatomic interaction) and molecular fragment energy terms as defined in the IQA/IQF (Interacting Quantum Fragments) framework. An extensive classical-type investigation, focused on single descriptors (bond length, density at critical point, the size of metal ion or coordination ring, interaction energy between Be^{II} and a donor atom, etc.) showed that it is not possible to explain the experimental trend. The proposed methodology is fundamentally different in that it accounts for the total energy contributions coming from all atoms of selected molecular fragments, and monitors changes in defined energy terms (*e.g.*, fragment deformation, inter- and intra-fragment interaction) on complex formation. By decomposing combined energy terms we identified the origin of relative stability of BeNTA and BeNTPA complexes. We found that the sum of coordination bonds' strength, as measured by interaction energies between Be^{II} ion and donor atoms, favours BeNTA but the binding energy of Be^{II} ion to the entire ligand correlates well with experimental trend. Surprisingly, the origin of BeNTPA being more stable is due to less severe repulsive interactions with the backbone of NTPA (C and H-atoms). This general purpose protocol can be employed not only to investigate the origin of relative stability of any molecular system (*e.g.*, metal complexes) but, in principle, can be used as a predictive tool for, *e.g.*, explaining reaction mechanism (transitional states).

Introduction

Metal ions in solution have an almost inexhaustible list of applications which vary from catalysis, to medicine, to biological use, to extraction metallurgy. At the core of understanding the behaviour of metal ions in solution is the use and determination of formation (stability) constants.[1] Formation constants can reveal factors influencing ligand design and metal ion selectivity, which are both appealing to chemists. Extensive experimental investigations have been dedicated to the determination of protonation and formation constants resulting in detailed databases recording this data.[2] However, the experimental data do not provide sufficient insight into the nature of interactions, describe chelating effect or provide any additional insight into the factors controlling the affinity between metal ions and donor ligands.[3,4] In order to gain additional insight, the thermodynamic constants have been the subject of theoretical investigation. Attempts have been made to predict the dissociation constants of ligands[5–20] theoretically, linear free-energy relationships (LFER) have been used to predict the formation constants of metal complexes,[21,22] and the formation constants for Ni^{II} complexes of NTA and NTPA have been successfully predicted using competition reactions.[3]

While this information is insightful as it identifies (in many cases) trends in the stability of metal complexes, it still fails to provide a fundamental understanding of the relative stability of metal complexes. This is evident in the failure to explain the change in the stability of complexes when small changes are made to the ligand structure. A classic example is the preferential complex formation between five-member ring chelates and six-member ring chelates. Most metal ions will preferentially complex to form five-membered chelate rings (5m-CR) when compared to six-membered chelate rings (6m-CR) except when binding to small metal cations.[1,23] The complexes of nitrilotri-3-propionic acid (NTPA, it forms 6m-CR) and nitrilotriacetic acid (NTA, it forms 5m-CR) are characteristic examples of this phenomenon. NTA, which forms strong complexes with most metal ions, is known as an alternative detergent builder[24] and is used in Ni-NTA-gold clusters to target tagged proteins.[25] On the other hand NTPA, has very few uses because it forms weak complexes. Be^{II}, a small metal ion with ionic radius 0.27 Å,[26] is the only known example of preferential complex formation with NTPA with three 6m-CRs ($\log K_1$ = 9.23 at 25 °C, μ = 0.5 M $NaNO_3$)[2] when compared to NTA which forms three 5m-CRs ($\log K_1$ = 6.84 at 25 °C, μ = 0.5 M $NaNO_3$),[2] resulting in $\Delta \log K_1 \approx 2.4$ in favour of BeNTPA. The opposite is true for numerous larger metal ions, including Zn^{II} which has an ionic radius of 0.74 Å.[26] Zn^{II} will preferentially

complex to NTA ($\log K_1$ = 10.45 at 25 °C, μ = 0.1 M KCl)[2] rather than NTPA ($\log K_1$ = 5.3 at 25 °C, μ = 0.1 M KNO_3)[2], with $\Delta\log K_1 \approx 5.1$.

Classically, complex stability is said to be governed by repulsion between lone-pair donors (such as oxygen and nitrogen), steric repulsion between crowded atoms, the size of the metal cation, coordination bond strength as measured by its length and to a lesser extent, inductive effects.[1,27] Furthermore, the differences in the formation constants of many complexes have been attributed to repulsive H-clashes due to the presence of the CH--HC close contacts.[1,28–32] Although this is not the main focus of this work, these CH--HC close contacts are also observed in systems investigated here. This notion was challenged by Bader using the Quantum Theory of Atoms in Molecules (QTAIM).[33] QTAIM uses electron density to analyse different types of interactions, where the presence of a ridge of maximum electron density linking two atoms is defined as an atomic interaction line (AIL), which Bader interpreted as a bonding interaction, hence a bond path (BP).[34] While QTAIM has been able to recover BPs where a classical chemical bond is expected, it has also shown the presence of AILs where steric hindrance is classically expected,[35–43] thus a debate has ensued discussing the meanings and interpretations of chemical bonds, steric repulsions and the concept of bonding.[32,34,44–58] Despite this controversy, QTAIM has been widely used for the visualization and analysis of all kinds of chemical bonds in a variety of compounds, among them coordination bonds and intramolecular interactions in various metal complexes.[3,4,58–62] For the complexes of Ni^{II} and Zn^{II} with NTA and NTPA,[3,4] the following was determined: (i) BPs where found for the weak CH•••HC and CH•••O intramolecular interactions in the complexes of NTPA, (ii) the density at the ring critical point (RCP) of a chelating ring appeared to correlate with the differences in the formation constants between 5m-CR and 6m-CR complexes, and (iii) the differences in formation constants were attributed to the greater strain incurred during the preorganization of NTPA with the ratio of the strain energy of NTPA:NTA being comparable to the ratio of the formation constants.

This work presents a comprehensive study of the factors controlling the stability of metal complexes, using BeNTA and BeNTPA complexes as a case study because, to our knowledge, they have not been extensively investigated computationally. A competition reaction is used here to select an appropriate level of theory for solvent optimized complexes; our judgement is based on the quality of the prediction of experimental formation constants as well as the computed trend in molecular energies. We then examine a full battery of local, real space indices and techniques that include: (i) geometrical analysis to evaluate

coordination bond strength and steric strain, (ii) topological properties, using QTAIM,[33] in both complexes, which characterize and measure the strength of the BP-linked intramolecular interactions with the hope that it would explain the experimental trend in complex stability, (iii) NCI (Non-Covalent Interactions)[63–66] isosurfaces which visualize all intramolecular interactions with our focus on those interactions which are not recovered by QTAIM, and (iv) strength as well as physical nature and quantified (de)stabilizing energy contribution of selected interactions using the Interacting Quantum Atoms (IQA)[67–69] energy decomposition scheme. We then use an intuitive, general-purpose approach to investigate complex (or more generally molecular system) stability, where we recognize that complex formation is a process and we apply a simplified two stage model (ligand preorganization and the binding between the pre-organized ligand and metal ion) to simulate the process of complex formation. We then investigate the fundamental properties and factors controlling the two stages by using the QTAIM, NCI and IQA techniques. In the final section we will present a method, that is deeply rooted in IQA and the Interacting Quantum Fragments (IQF),[69] which gives one the ability to explore and identify the factors affecting stability of a molecular system by dividing a molecule into chemically meaningful fragments and analysing the interaction energy between them; all implemented without artificially dissecting the molecules investigated here. To our knowledge, this is the first attempt of this kind in explaining the processes of preorganization, binding and relative stability of molecular systems. In addition, we have also investigated the suitability of selected DFT techniques for the purpose of such studies using MP2 as a reference.

Computational Details

The free ligands of NTA and NTPA, as well as the Be^{II} complexes were submitted for a full conformational search in Spartan 10.[70] Geometry optimizations of the SPARTAN generated conformers (ligands and complexes) as well as of the free beryllium cation were performed in Gaussian 09 revision D,[71] at the MP2(FC) levels of theory; Cartesian coordinates for all structures obtained at indicated levels of theory are presented in Tables A1-A4 in the Appendix A. In order to have the structural benefit of the MP2-optimized structures, as well as Gibbs free energies needed to predict formation constants, but to minimize the computational expense, single point frequency calculations (SPFC) were carried out on the MP2 optimized structures at PBE1PBE, B3LYP and X3LYP. To evaluate the processes involved in complex formation, single point energy calculations were performed at

all levels of theory on the pre-organized ligand $L_{p\text{-}org}$ (ligand with the structure observed in the complexes of beryllium). All optimizations and single point calculations were performed with the 6-311++G(d,p) basis set in the PCM/UFF solvation model with water as the solvent. Selected wavefunctions were submitted for topological analysis and for the determination of IQA defined properties using the AIMAll package.[72] We must stress here that regardless of the level of theory, the change in the energy of a molecule recovered from the IQA additive atomic energies, *e.g.*, when a ligand changed from its free to pre-organized form, always followed the trend but differ somewhat in value. This is fully understandable because (i) an accurate implementation of IQA requires well-defined second order density matrix but, unfortunately, it is not implemented in AIMAll software for post HF levels of theory yet; (ii) numerous energy components contribute to the IQA-defined molecular energy, *E*, and small numerical integration errors (a numerical 'noise') are unavoidable regardless. Furthermore, because our focus is on relative trends rather than predicting energy terms on an absolute scale, we are convinced that the qualitative results and the conclusions arrived at from this work should be considered as valid. For our purposes we often made use of the X3LYP wavefunction computed on the MP2-optimized structure because (i) all DFT calculations gave good approximations of the electronic energy obtained for the competition reaction, (ii) it has been shown recently that IQA calculations on a DFT wavefunction give reasonable approximations of computationally expensive MP2 data,[73] and (iii) X3LYP is known to describe weak inter- and intra-molecular interactions[74–77] and the structure and electronic properties of molecular systems[74,77–79] in a well-defined manner. In some instances we performed MP2 computations needed to directly verify DFT results. Either NCIPlot 2.0[64] was used for the determination of isosurfaces in combination with VMD 1.9.1[80] used for their visualization, or AIMAll was employed for that purpose. One dimensional cross-sections of the electron density along the λ_2 eigenvector of the Hessian matrix were performed using in-house software according the procedure detailed previously.[81]

Results and Discussion

Selection of levels of theory

It is important to stress that our aim here is not to find an accurate prediction of formation constants, but rather to select a level of theory which confirms the experimental trend (the preferential formation of BeNTPA) and thus validates the theoretically/computationally

generated structures. To this effect, the competition reaction-based protocol proposed previously[3] to computationally predict the formation constants, was adopted in this work. For clarity, only the most important steps are presented here.

The complex formation reactions between beryllium and the ligands of interest are shown in Eqs (3.1) and (3.2) (charges have been omitted throughout for simplicity)

$$Be(H_2O)_4 + NTPA \leftrightarrow BeNTPA + 4H_2O \qquad K_1^{(a)} = \frac{[BeNTPA]}{[Be][NTPA]} \qquad (3.1)$$

$$Be(H_2O)_4 + NTA \leftrightarrow BeNTA + 4H_2O \qquad K_1^{(b)} = \frac{[BeNTA]}{[Be][NTA]} \qquad (3.2)$$

A competition reaction, CRn, between ligands NTPA and NTA for Be^{II}, can be viewed as a result of subtraction of the two complexation reactions, (3.1) – (3.2), where the participation of water is conveniently cancelled

$$BeNTA + NTPA \leftrightarrow BeNTPA + NTA \qquad K_{CRn} = \frac{[BeNTPA][NTA]}{[BeNTA][NTPA]} \qquad (3.3)$$

Because the formation constants of both complexes are known from experiment ($\log K_1^{(a)}$ = 9.23 and $\log K_1^{(b)}$ = 6.84),[2] one can determine the equilibrium constant, as $\log K_{CRn}$, for the competition reaction from

$$\log K_{CRn} = \log \frac{K_1^{(a)}}{K_1^{(b)}} = \log K_1^{(a)} - \log K_1^{(b)} = 2.4 \qquad (3.4)$$

Hence, using the well-known relationship, $\Delta G = -RT\ln K$, which correlates thermodynamic Gibbs free energy and equilibrium constant, and by converting one log unit to 1.36 kcal/mol, it is possible to determine the ΔG value expected from experiment for any reaction and, in our case, one obtains ΔG_{CRn} = –3.3 kcal/mol. This information is useful because one can attempt to reproduce this value theoretically by computing the free energy of the competition reaction (3.3) as

$$\Delta G_{CRn} = G(BeNTPA) + G(NTA) - G(BeNTA) - G(NTPA) \qquad (3.5)$$

It has been shown that the best theoretically predicted pK_a[12, 13] and $\log K$[3] values are obtained when the lowest energy conformers (LECs) of the molecules are selected for the calculation. Thus all conformers of the ligands and the complexes found from conformational search in SPARTAN have been optimized at the MP2 level of theory in water as a solvent; only the

LECs of complexes shown in Figure 3.1 (also showing notation used and numbering of atoms) and ligands shown in Figure A1 (in Appendix A) were selected for further theoretical investigations. The G values together with the $\log K_{CRn}$ values of relevant structures obtained are shown in Table 3.1.

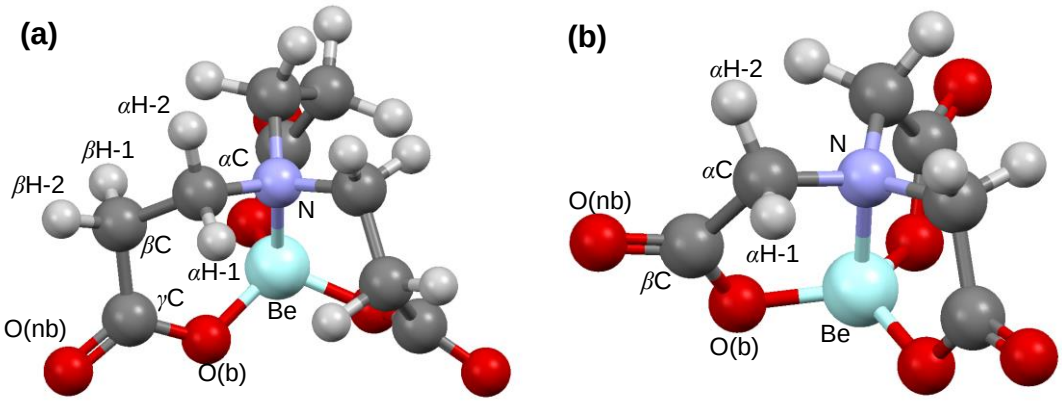

Figure 3.1. Ball-and-stick representation of the LECs of (a) BeNTPA, and (b) BeNTA, also showing notation used and numbering of atoms.

Table 3.1. Computed equilibrium constants, as $\log K_{CRn}$, for competition reaction between ligands NTPA and NTA for Be^{II}; lowest energy conformers of the ligands and complexes were used.

	G/au						
Method	BeNTA	NTPA	BeNTPA	NTA	ΔG_{CRn} [b]	$\log K_{CRn}$	$\Delta \log K$ [c]
MP2[a]	–751.7060	–854.5841	–869.2266	–737.0736	–6.4	4.7	2.3

[a] energies were obtained by optimizing the lowest energy conformer of each molecule. [b] value in kcal/mol. [c] $\Delta \log K$ = (theoretical – experimental) value.

In general, the data shown in Table 3.1 validates the structures of ligands and complexes, correlating well with the experimental trend. However, one must remember that a number of computational techniques, such as QTAIM and IQA, can only partition the electronic energy (but not the Gibbs free energy) into atomic and interatomic contributions. Hence, it was necessary to compute the change in the electronic energy for the competition reaction, Eq. (3.3), in order to select the most suitable level of theory for the quantum chemical topology techniques based analyses.

$$\Delta E_{CRn} = E(\text{BeNTPA}) + E(\text{NTA}) - E(\text{BeNTA}) - E(\text{NTPA}) \qquad (3.6)$$

Furthermore, in order to have the structural benefit of the MP2-generated conformers and avoid computationally expensive IQA calculations at this level of theory, we performed SPCs in solvent on the MP2-optimized structures at selected DFT levels of theory to compute

electronic energies and to generate the wavefunctions necessary for the QTAIM/IQA calculations. Importantly, as data included in Table A5 in the Appendix A shows, the preferential formation of BeNTPA is reproduced correctly at all levels of theory when the change in electronic energy is considered. Hence, in principle, it was possible to explore the topological properties (QTAIM, NCI and IQA) of the structures of interest at any level of theory.

Out of curiosity the SPFCs were performed on the MP2-optimized structures at the DFT levels of theory to determine *G* values; note that frequency calculations are commonly performed on fully optimized structures. Remarkably, the calculations have not produced negative frequencies and, as shown in Table A6 in the Appendix A, the prediction of $\log K_{CRn}$ improves when DFT wavefunction is used from the SPFC on the RMP2 structure; at the PBE1PBE level of the theory the value obtained is within 0.4 log units of the experimental data, a value of analytical quality.

Geometric Analysis

We will start our investigation with a brief analysis of geometric factors which are commonly used to rationalize relative trends in formation constants. The good approximation of the $\log K_{CRn}$ and ΔE_{CRn} gave us the confidence to use the MP2 optimized structure for this purpose. We performed a full geometric evaluation of the complexes based on the length of the coordination bonds, presence/absence of steric contacts and comparison of computed structures with the minimum strain geometry criteria.[1]

Coordination Bonds. Classically it has been suggested that the complex with the shorter (hence most likely stronger) coordination bonds has also stronger overall binding energy between the ligand and a metal ion. Note that NTA and NTPA have the same kind and number of donor atoms as well as binding of metal to a ligand takes place in very much the same molecular environment; hence, such a presumption should hold in this case. Data presented in Table 3.2 shows that in both complexes d(Be,O) << d(Be,N); this suggests that the coordination bonds with O-atoms are significantly stronger and results are inconclusive because $|\Delta d(Be,O)| = 0.002$ Å is only marginally in favour of BeNTPA whereas $|\Delta d(Be,N)| = 0.02$ Å is decisively in favour of BeNTA.

Table 3.2. Selected average interatomic distances in both complexes at the RMP2 level of theory.

BeNTA		BeNTPA	
Bond	d / Å	Bond	d / Å
Be–N	1.772	Be–N	1.791
Be–O13	1.612	Be–O22	1.610
Be–O15	1.612	Be–O25	1.610
Be–O19	1.612	Be–O28	1.610

Repulsive Contacts. Surprisingly, there are three severe CH--HC contacts present in the stronger BeNTPA complex (d(H,H) = 2.159±0.001 Å) whereas there are three weak contacts in BeNTA, d(H,H) = 2.331±0.002 Å (see data in Table A7 in Appendix A). The absence of steric close contacts, such as CH--HC, is quite often identified as the cause for preferential complex formation.[1,28–30] If there are short contacts between hydrogen atoms, with interatomic distance much shorter than the sum of the van der Waals radii, 2.4 Å, there is said to be an interaction which destabilizes the molecule, commonly referred to as steric hindrance. The computed difference |Δd(H,H)| = 0.172 Å between interatomic distances observed in both complexes, however, favours BeNTA which clearly contradicts experimental data in terms of a trend in relative stability. Thus, we do not have *structural* evidence to suggest that the CH--HC contacts in BeNTPA result in the steric hindrance phenomenon because this complex is more stable. Additionally, it is difficult to determine the energetic effect of the CH--HC contacts on the formation of BeNTPA because they are present in LEC NTPA where d(H,H) = 2.108±0.001 Å.

Relative complex stability has also been associated with the repulsion between lone pairs on donor atoms.[1] However, as far as we are aware, there has been no extensive investigation into the effect of the lone pair donor atoms. We assumed that the shorter the interatomic distance, the greater the repulsion and when the interatomic distance is shorter than the sum of van der Waals radii (d_{vdw}(N,O) = 3.1 Å and d_{vdw}(O,O) = 3.0 Å) then it is reasonable to consider this as a repulsive interaction. Table A7 in Appendix A shows that in both complexes the N--O and O--O contacts are much shorter than the respective sum of the van der Waals radii. Furthermore, the N--O contacts of 2.567 Å in BeNTA are much shorter, by ~0.19 Å, than those in BeNTPA which suggests that they result in greater repulsion in BeNTA. The O--O contacts of 2.653 Å, on the other hand, are shorter in BeNTPA than in BeNTA by ~0.11 Å which suggests that in this case the repulsion is more severe in BeNTPA.

Because the results produced are mixed, depending on the type of a contact, it is not possible to predict geometrically which complex is preferentially formed in a solution.

Minimum Strain Geometries. Minimum strain geometries, obtained using experimental data and molecular mechanics calculations, have been used to describe the preferential complex formation and explain the favourable complexing of small metal cations when 6m-CRs are formed while larger metal cations favourably complex to form 5m-CRs.[1] Any deviation from these minimum strain geometries would be indicative of an increase in strain, hence the greater the deviation, the greater the strain. The results of these comparisons (Table A8 in Appendix A) reveal that BeNTA consistently shows the greater deviation which is consistent with the experimental trend in log*K* values. However, when the same approach was used to compare strain induced by departure from ideal geometries in Nickel[3] and Zinc[4] complexes, it was found that the N–M–O bite angles in the NTA complexes consistently had a greater deviation from the ideal values, whereas those in NTPA were comparable to the minimum strain geometries; a trend which is exactly the same as observed for Be^{II} complexes with NTA and NTPA. This indicates that while there has been success in the instances of the beryllium complexes, this approach is not universal and may even be misleading.

Overall, it is clear that the three geometric approaches, namely (i) strength of bonding based on coordination bond length, (ii) destabilization due to steric contacts, such as CH--HC in the framework of a ligand and N--O or O--O in the coordination sphere, and (iii) deviation from the minimum strain geometry, do not provide rigorous and reliable account for the preferential complex formation. Hence, there is a need to use alternative and more advanced (computationally based) methods to fundamentally investigate relative stability of complexes and molecular systems in general.

QTAIM Analysis of Intramolecular Interactions

The molecular graphs of both LECs complexes are shown in Figure 3.2 where AILs (they represent a line of maximum electron density joining two atoms) are observed only between atoms bonded through covalent and coordination bonds; hence, these interactions can be seen in this case as real bond paths which fully correlate with chemists' understanding of chemical bonding. Because the topological properties at the bond critical points (BCPs) of the bond paths were successfully used to characterize and classify many chemical bonds, we will

compare the nature and strength of bonding in the coordination sphere of both complexes with an attempt to rationalize the preferential complex formation. Furthermore, we will attempt to evaluate properties of 5- and 6-membered chelate rings using topological properties at the ring critical points (RCPs).

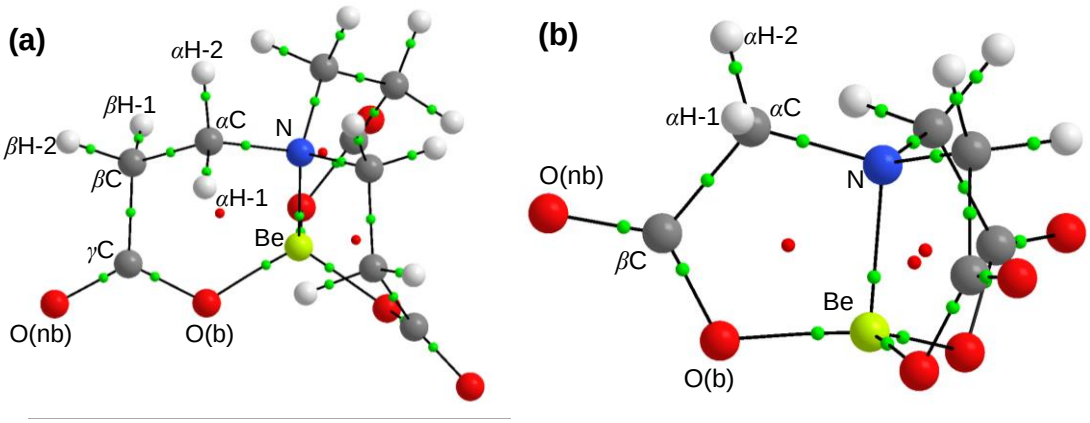

Figure 3.2. The QTAIM molecular graphs of the lowest energy conformers of (a) BeNTPA, and (b) BeNTA.

Coordination bonds. Table 3.3 shows the topological properties of the coordination bonds at the BCPs. The values of $\rho(\boldsymbol{r})$ and Laplacian, $\nabla^2\rho(\boldsymbol{r})$, at the BCPs in both complexes, are consistent with those expected to be for closed-shell, non-covalent interactions.[82] The ratio of the local potential energy density $V(\boldsymbol{r})$ to the local kinetic energy density $G(\boldsymbol{r})$ has also been frequently and successfully used[58,83,84] as a descriptor of the nature of the bonding between two atoms. When $|V(\boldsymbol{r})|/G(\boldsymbol{r}) < 1$, this is typical of a classical ionic (or closed shell) interaction and when $|V(\boldsymbol{r})|/G(\boldsymbol{r}) > 2$, it is indicative of a classical covalent bond.

Based on the characteristics of the electron density at the BCPs, all coordination bonds show borderline behaviour of classical ionic character with the $|V(\boldsymbol{r})|/G(\boldsymbol{r})$ ratio very close to 1; the Be–N bonds show some degree of covalency. The electron density at BCP has been used[3,4,60] to measure the bond strength between two atoms. For both complexes, ρ_{BCP}(Be–O) > ρ_{BCP}(Be–N) and this is consistent with results found for the Zn complexes.[4] However, by comparing the ρ_{BCP} values of the coordination bonds in BeNTA and BeNTPA, it is clear that the electron density is somewhat greater in all coordination bonds of BeNTA which suggests that the binding of NTA to beryllium is stronger; this is in accord with a chemist's intuition because the more chemical glue, *i.e.* electron density between atoms, the stronger bond is expected to be.

Table 3.3. QTAIM-defined topological data at BCPs of the coordination bonds in BeNTA and BeNTPA at the RMP2[a] level of theory.

Bonds	$\rho(r)$	$\nabla^2\rho(r)$	$G(r)$	$V(r)$	$\lvert V(r)\rvert/G(r)$	DI(A|B)
			BeNTA			
Be–N	0.0636	0.3775	0.1019	–0.1095	1.07	0.11
Be–O13	0.0771	0.5655	0.1418	–0.1423	1.00	0.14
Be–O15	0.0771	0.5656	0.1419	–0.1423	1.00	0.14
Be–O19	0.0771	0.5655	0.1418	–0.1423	1.00	0.14
			BeNTPA			
Be–N	0.0598	0.3453	0.0917	–0.0971	1.06	0.11
Be–O22	0.0755	0.5660	0.1402	–0.1389	0.99	0.14
Be–O25	0.0755	0.5659	0.1402	–0.1388	0.99	0.14
Be–O28	0.0755	0.5660	0.1402	–0.1389	0.99	0.14

[a] all values are in au except $\lvert V(r)\rvert/G(r)$ and DI(A|B).

It is now well established that an exponential decrease should be observed for ρ_{BCP} plotted against an interatomic distance when an interaction of interest takes place in similar (comparable) molecular environment. In an attempt to reconcile the geometric (shorter bond length) and the QTAIM (larger ρ_{BCP}) notions of coordination bond strength we correlated the ρ_{BCP} with the corresponding interatomic distances (note that, due to molecular symmetry of ligands, there are not sufficient data points to generate a meaningful graph). Considering Be–N coordination bonds, as expected, the shorter bonds have larger ρ_{BCP}. However, this trend does not hold for Be–O coordination bonds. This clearly indicates that some other physical properties, most likely related to differences in highly crowded environment of the coordination spheres, must have contributed to the reverse trend in density at these critical points. Following the classical notion of chemical bonding and using accumulated density in the bonding region, ρ_{BCP}, as a measure of the strength of the coordination bonds one might reason that BeNTA should be the preferentially formed complex, again a misleading prediction. This leads us to the conclusion that one cannot use a coordination bond length or ρ_{BCP} of the coordination bonds as a rigorous, universal and reliable tool in predicting relative complex strength as measured by log$K$ values.

Ring Critical Points. In previous works[3,4] a good correlation was found between the electron density at the RCPs of the chelating 5- and 6-membered ring and the formation constant, as log$K$ value, of the NTA and NTPA complexes with Ni^{II} and Zn^{II}. Table A9 in

Appendix A shows the electron densities as well as the value of the Laplacian at the ring critical points found for the Be^{II} complexes with NTA and NTPA. This data reveals that the trends in ρ_{RCP} are the same in these complexes, namely ρ_{RCP}(MNTPA) < ρ_{RCP}(MNTA) and the ratio ρ_{RCP}(MNTA): ρ_{RCP}(MNTPA) is approximately two, regardless of the identity of the metal ion (here M = Be^{II}, Ni^{II}, Zn^{II}) and regardless of which complex (here ligand = L = NTA, NTPA) is formed preferentially (similar observations fully apply to the Laplacian at RCPs). It would be of great interest and fundamental importance in the ligand design strategies to find out whether such relationship is of general nature, *i.e.* does it also hold for (i) other metal ions for which formation constants with NTA and NTPA are known, and (ii) for other ligands which form 5m- and 6m-CRs.

Based on the additional findings of this work and noting that coordination rings differ only by the presence of an additional $–CH_2-$ fragment we suggest that the topological properties at the ring critical point depend predominantly on the size of the ring under consideration. One might reason that the larger the ring, the more room there is for electron density to decrease from the bond paths' critical points to the ring critical point; hence, consistently one observes ρ_{RCP}(6m-CR) << ρ_{RCP}(5m-CR) but one does not know yet whether the ratio, ρ_{RCP}(5m-CR)/ ρ_{RCP}(6m-CR) depends on a central metal ion and to what extent. To conclude this section, it is clear that the value of ρ_{RCP} cannot be used to confidently predict the relative strength of metal complexes involving the NTA and NTPA ligands.

NCI Analysis

The inconclusive results of the above analyses strongly suggest that, besides geometric and topological parameters (the latter generated from the QTAIM analysis), there must be some other factors controlling or influencing the relative stability of molecular systems. It is important to note that although there are numerous, geometrically-detected, close interatomic contacts in both complexes, they are not characterised by the presence of AILs. This is not entirely surprising because BPs were shown to represent the privileged exchange-correlation channels;[85] hence, often one (i) does not observe a BP-linked atoms for which a geometrical criterion is met, as is the case in this work, or (ii) see a BP linking atoms being further apart even though other and shorter analogous contact(s) exist in the same molecular environment – an example of that is shown in Figure A3 in Appendix A.

To address shortcomings of the QTAIM-based analysis of intramolecular interactions, we turned our attention to the recently developed NCI method, which enables the real space visualization of non-covalent interactions in molecular systems[63–66]. An attractive feature of this technique lies in the ability to recover non-covalent weak interactions as defined in the QTAIM regime as well as other interactions not visualized in QTAIM and this produces the full picture of intramolecular interactions. This technique, using the reduced density gradient, *s*, and the sign of the second eigenvalue, λ_2, of the Hessian Matrix, has been used to distinguish between attractive and repulsive interactions. The colour-coded isosurfaces in Figure 3.3 indicate a local (i) accumulation of electron density as a blue region when $\lambda_2 < 0$ (then a negative trough in the NCIPlot is observed), a typical NCI index used to identify stabilizing interactions, and (ii) depletion of electron density as a red region when $\lambda_2 > 0$, a NCI index for destabilizing or non-bonded interactions (a positive trough in the NCIPlot is then observed) often interpreted as steric repulsion.[63–66,86]

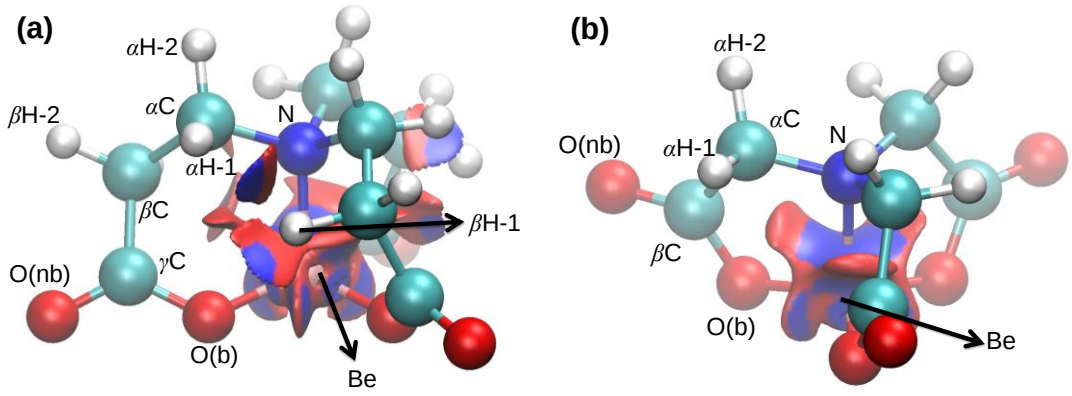

Figure 3.3. The NCI isosurfaces of the LECs of (a) BeNTPA, and (b) BeNTA complexes with a RDG isovalue of 0.5 au and isosurfaces coloured from blue to red using –0.07 au ≤ sign(λ_2)×$\rho(r)$ ≤ +0.03 au.

Let us first focus on the coordination spheres of complexes. The NCI isosurfaces in Figure 3.3 show that all coordination bonds are characterized by large blue regions in the bonding region, indicative of electron density accumulation. Thus the NCI-based interpretation as stabilizing interaction fully recovers a general notion of coordination bonds. These blue regions appear to be immersed in sheet-like extended surfaces, the results of multi-centric interactions taking place in this crowded environment. This extended multi-surface NCI plot is coloured in red and this might be interpreted as revealing strain in the coordination sphere. Interestingly and importantly, a similar phenomenon of density accumulation is also observed between the lone pairs of the donor atoms in the coordination sphere. Notice that the O•••O interactions have blue surfaces in the interatomic region which,

as also observed for the coordination bonds, are part of the extended red surface in the coordination sphere which supports our interpretation of the coordination sphere being strained. A similar phenomenon was found in the case of non-equilibrium water and ammonia dimer conformations, where a large blue disk was found between water dimers[81] and nitrogen atoms[86] in a repulsive arrangement. One must realize, however, that (i) any density accumulation might be a result of either a bonding interaction or unavoidable output of an "excess" of electron density, such as a free pair of electrons in a crowded environment, and (ii) a density accumulation must be accompanied by an adjacent region from which density was depleted. Hence, even though a red region of electron density depletion in crowded environments was interpreted as the presence of steric repulsion,[58,66] each case, in our opinion, must be analysed separately and interpreted with outmost care. What is unquestionable, however, is the physical meaning of the blue/red regions which simply uncovers locally increased/decreased density which directly points at non-covalently interacting atoms. Furthermore, one observes a blue area in the interatomic region between O(b) and βH1 in BeNTPA and this can be interpreted as the result of attractive interaction occurring just at the edge of coordination sphere, hence this constitutes a part of the extended polycentric isosurface.

Figure 3.3 also reveals that there are no interactions outside of the coordination sphere in the BeNTA complex. This finding is important because it implies that there are no additional (whether attractive or repulsive) interactions within a ligand framework, hence the short CH--HC contacts identified from the geometrical analysis do not play any role on complex stability (they neither de- nor stabilize BeNTA).

Conversely, the NCI-analysis uncovers the presence of many additional intramolecular interactions outside the coordination sphere of the BeNTPA complex which were 'missed' by the QTAIM-based interpretation. For all CH•••O and CH•••HC interactions (they are distributed uniformly around the molecule) we observe in Figure 3.3 classical in the NCI-interpretations bi-centric in nature and bi-coloured pill-like isosurfaces with blue region being placed in the interatomic region and red end pointing at a location of a potential ring critical point, where lowest density is observed within a ring. The work of Lane *et al.*[86] found numerous interactions (CH•••O, CH•••N, NH•••H, NH•••OC) which they described as ring closure, which are similar to our CH•••O and CH•••HC interactions. Their work[86] revealed the presence of classical OH•••O interactions in (a) 1,2-ethanediol, even though a bond path and associated BCP and RCP were absent, and (b) 1,3-propanediol and 1,4-butanediol, where

AILs were present. The interactions were qualitatively indistinguishable and the only significant difference was in the minimum values of the reduced density gradient, s_{min}. In principle, very much the same picture was found for the CH•••O and CH•••HC interactions in BeNTPA – see NCI plots in Figure 3.4(a) where the CH•••HC interaction is characterized by negative trough (corresponding to an attractive interaction and the blue isosurface) being placed at more negative value of sign(λ_2)×ρ and s_{min} closer to 0 when compared with the NCI plot obtained for the CH•••O interaction. The shape and placement of troughs in Figure 3.4(a) might indicate, besides larger density at NCI-defined critical point, that the density accumulation in the bonding region of the CH•••HC interaction is better defined in terms of a special shape.

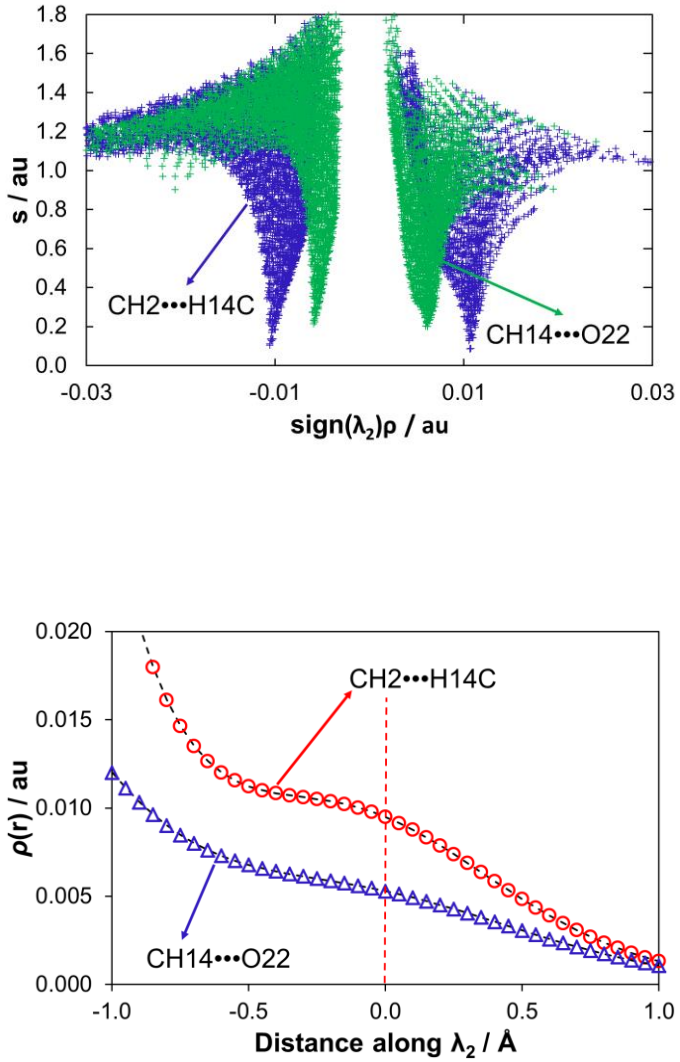

Figure 3.4. (a) The 2D NCI plots for selected CH•••HC and CH•••O interactions in the BeNTPA complex. (b) The corresponding cross-sections of the electron density along the λ_2 eigenvector where the red line indicates the GIP.

In search for qualitative differences between the CH•••O and CH•••HC intramolecular interactions in BeNTPA and to gain further insight on density distribution in their bonding regions we decided to employ recently reported 1D cross-section along the λ_2 eigenvector of the Hessian matrix.[81] This methodology was also shown to be able to explain the presence/absence of an AIL between atoms being at an interatomic distance shorter than the sum of the van der Waals radii. Results obtained from cross-sections, shown in Figure 3.4(b), lead to the following observations: (i) in both cases, locally concentrated density at any point of the cross-section is lower when compared with the preceding point which fully explains the absence of an AIL,[81] (ii) the density at the geometric critical point (placed in the middle between the interacting atoms) is indeed significantly larger in the case of the CH•••HC interaction as also found from the NCI plots, (iii) the shape of the cross-section obtained for the CH•••HC interaction (in Figure 3.4(b)) is by far better defined in terms of density accumulation represented by clearly visible hump, and finally (iv) qualitatively, there appears to be no difference in the density distribution in the bonding regions of these two interactions; a steady decrease in accumulated density is observed.

The following commonly accepted classical interpretations might be considered, namely (i) the intramolecular OH•••O interaction (a classical intramolecular H-bond) adds to the molecule's stability and (ii) the blue NCI-defined region of density accumulation is synonymous with stabilizing interaction. In view of these interpretations, in conjunction with the observation that there is no qualitative difference in the results obtained from the NCI and cross-section methodologies when applied to these two intramolecular interaction, one might tentatively conclude that since these features hold for the stabilizing CH•••O interaction, then there is no obvious reason to interpret the CH•••HC interaction differently, both in the BeNTPA complex. If this is so, then one might also postulate that maybe the preferential complexation of BeNTPA is due to the additional stabilization of the complex by CH•••O and CH•••HC. However, as also strongly advocated in a recent report[81] these suppositions must be supported by additional physical properties and we turn our attention to IQA for further insight.

IQA-based Analysis of Diatomic Interactions in the Complexes

The IQA method partitions the molecular energy, *E*, into one-body (atoms of a molecule) and two-body (interatomic) interaction energy components.[67–69] In the simplest way, *E* can be partitioned into additive atomic energy for each atom X, $E_{\mathrm{add}}^{\mathrm{X}}$, such that

$$E = \sum_{\mathrm{X}} E_{\mathrm{add}}^{\mathrm{X}} \tag{3.7}$$

The additive atomic energy is defined as the sum of the self-energy of an atom and halved sum of interaction energies with remaining atoms in a molecule as described by Eq. 3.8

$$E_{\mathrm{add}}^{\mathrm{X}} = E_{\mathrm{self}}^{\mathrm{X}} + \sum_{\mathrm{Y}\neq\mathrm{X}} 0.5 E_{\mathrm{int}}^{\mathrm{X,Y}} \tag{3.8}$$

Hence, as shown in Eq. 3.9, the energy of a molecule can be recovered by summing up all self-atomic energies and all unique diatomic interaction energies,

$$E = \sum_{\mathrm{X}} E_{\mathrm{self}}^{\mathrm{X}} + 0.5 \sum_{\mathrm{X}} \sum_{\mathrm{Y}\neq\mathrm{X}} E_{\mathrm{int}}^{\mathrm{X,Y}} \tag{3.9}$$

One of the attractive features of IQA is the information one can gain about the strength of any diatomic interaction (from $E_{\mathrm{int}}^{\mathrm{X,Y}}$) regardless if atoms are covalently or QTAIM-bonded via an AIL. Furthermore, one can also determine the nature of the interaction, *e.g.* when $E_{\mathrm{int}}^{\mathrm{X,Y}} < 0$ then interaction is attractive. Additional insight on the physical character of an interaction can also be gained because $E_{\mathrm{int}}^{\mathrm{X,Y}}$ can be decomposed further into a classical (electrostatic) contribution, $V_{\mathrm{cl}}^{\mathrm{X,Y}}$, and exchange-correlation, XC, energy term, $V_{\mathrm{XC}}^{\mathrm{X,Y}}$ (which loosely might be interpreted as a classical covalent contribution). These energy components are of great importance as one can use them to quantify and characterize, in principle, all interactions of interest in any molecular system, hence also in the complexes investigated here.

In the following sections, in search of additional insight on parameters controlling relative stability of molecules, we will investigate the interactions between atoms (i) which are traditionally viewed as chemically bonded, (ii) where there is likely to be lone pair repulsion, and (iii) where there has been contention with regards to the nature of certain interactions, all of which are present in the BeNTPA complex.

Interactions within the Coordination Sphere of the Complexes. Table 3.4 shows the interaction energies between all atoms (Be, N and O) in the coordination spheres in BeNTA

and BeNTPA – selected MP2 interaction energies are shown in brackets. Although the data using the X3LYP does not recover exact values at the RMP2 level of theory, the trends are identical giving confidence to the X3LYP data.

All the Be–O and Be–N coordination bonds are dominated by a classical contribution, $V_{\mathrm{cl}}^{\mathrm{X,Y}}$, which is an order of magnitude larger than the exchange-correlation term, $V_{\mathrm{XC}}^{\mathrm{X,Y}}$. This contradicts the general notion of the mechanism of the coordination bonds formation which classically is interpreted as sharing of a donated electron pair between a donor atom (here N and O) and the central metal ion, as also found for other molecular systems.[58]

Table 3.4. IQA partitioning of two-bodied interaction energies in BeNTA and BeNTPA for selected interactions of interest using the RXL3YP wavefunction on the MP2 structures. Selected MP2 data are shown in brackets.

BeNTA				BeNTPA			
Interaction	$V_{\mathrm{cl}}^{\mathrm{X,Y}}$	$V_{\mathrm{XC}}^{\mathrm{X,Y}}$	$E_{\mathrm{int}}^{\mathrm{X,Y}}$	Interaction	$V_{\mathrm{cl}}^{\mathrm{X,Y}}$	$V_{\mathrm{XC}}^{\mathrm{X,Y}}$	$E_{\mathrm{int}}^{\mathrm{X,Y}}$
Be–N	–417.8 (–443.0)	–19.4 (–19.7)	–437.2 (462.6)	Be–N	–403.8 (–423.8)	–20.5 (–20.5)	–424.3 (–444.3)
Be–O13	–457.6 (–472.2)	–26.7 (–26.6)	–484.4 (–498.8)	Be–O22	–459.0 (–473.9)	–25.9 (–25.8)	–484.9 (–499.6)
Be–O15	–457.6	–26.7	–484.3	Be–O25	–458.9	–26.0	–484.9
Be–O19	–457.6	–26.8	–484.3	Be–O28	–459.0	–25.9	–484.9
Sum:	–1790.6	–99.6	–1890.2	Sum:	–1780.7	–98.3	–1879.0
N•••O13	210.4 (226.1)	–13.4 (–14.5)	196.9 (211.6)	N•••O22	193.7 (205.5)	–10.5 (–11.5)	183.2 (194.1)
N•••O15	210.3	–13.4	196.9	N•••O25	193.7	–10.5	183.2
N•••O19	210.5	–13.5	197.0	N•••O28	193.7	–10.5	183.2
O13•••O15	207.0 (215.8)	–9.7 (–10.3)	197.3 (205.5)	O22•••O25	215.9 (225.1)	–11.7 (–12.5)	204.1 (212.7)
O15•••O19	207.0	–9.6	197.3	O25•••O28	216.0	–11.7	204.3
O13•••O19	206.9	–9.6	197.3	O22•••O28	216.0	–11.7	204.3
Sum:	1252.0	–69.3	1182.7	Sum:	1228.9	–66.8	1162.2
Total:	–538.5	–168.8	–707.5	Total:	–551.7	–164.9	–716.9

Focusing on the coordination bonds, we note that $E_{\mathrm{int}}^{\mathrm{X,Y}}$ is larger (more negative by about 40-50 kcal/mol) for the Be–O than the Be–N bonds in both complexes, indicating that the Be–O are significantly stronger. This correlates well with the general trends, for interatomic distances d(Be,O) < d(Be,N) and density at BCPs ρ_{BCP}(Be–O) > ρ_{BCP}(Be–N), found for these complexes. Interestingly, even though the strength of the Be–O coordination bonds might be considered as comparable between the two complexes, the somewhat weaker Be–O in

BeNTA (by about 0.5 kcal/mol) are characterised by slightly higher density at the BCPs, by about 0.002 au. This also correlates with the reverse trend in the ρ_{BCP} *vs.* d(Be,O) relationship and reveals that the larger density accumulation in the interatomic bonding region is not synonymous with stronger interaction in a complex, multi-atomic and congested molecular environment. This implies that, although ρ_{BCP} appears to be mainly controlled by the properties of interacting atoms, the surrounding atoms might add/remove some density; hence, a diatomic interaction might not necessarily imply an entirely localized event. On the other hand, the slightly more covalent character of the Be–O in BeNTA, as measured by the $|V(r)|/G(r)$ ratio, is fully recovered by smaller classical term $V_{cl}^{X,Y}$ and, on average, slightly larger $V_{XC}^{X,Y}$ contribution. Furthermore, the Be–N bond of BeNTA is stronger than that in BeNTPA because $E_{int}^{Be,N}$ is significantly more negative by –14 kcal/mol. Hence, if one were to limit themselves to the properties of the coordination bonds, BeNTA would be predicted as the preferentially formed complex, a contradiction to what is known experimentally.

The repulsive interactions within the coordination spheres (N--O and O--O) of the BeNTA and BeNTPA complexes are dominated almost entirely by the electrostatic component (the XC-term contributes only ~5%). These interactions show two opposite trends; on average, $E_{int}^{N,O}$ is larger in BeNTA by ~16.7 kcal/mol whereas $E_{int}^{O,O}$ is larger in BeNTPA by ~9 kcal/mol. This correlates well with the observed interatomic distances, d(N,O) is shorter in BeNTA by ~0.2 Å and d(O,O) is longer by ~0.1 Å. Clearly, a mixed picture emerges from the analyses of $E_{int}^{X,Y}$ as well as interatomic distances. To gain deeper understanding, we summed up all the interaction energies between Be, N and O atoms. The sum of these interaction energies is –707.5 and –716.9 kcal/mol for BeNTA and BeNTPA respectively suggesting that there is a net stabilization in the coordination sphere in favour of BeNTPA. This can be seen as the first quantitative and conclusive finding in support of preferential formation of BeNTPA relative to BeNTA.

Furthermore, it is now possible to quantify specific energy contributions and we found that (i) four coordination bonds have a more stabilizing contribution (–1890 and –1879 kcal/mol in BeNTA and BeNTPA, respectively) than six steric clashes in the coordination sphere, N--O and O--O, which contributed 1183 and 1162 kcal/mol in BeNTA and BeNTPA, respectively, which explains why these complexes are formed, (ii) the total energy contribution made by coordination bonds in BeNTA is larger (more stabilizing) by ~–11 kcal/mol, and (iii) the total

destabilizing contribution made by steric contacts (N--O and O--O) is smaller in BeNTPA by ~20 kcal/mol. Importantly, the difference of the $\Sigma E_{\text{int}}^{\text{X,Y}}$ values seen in Table 3.4 (BeNTPA – BeNTA) of –9.4 kcal/mol correlates well with the electronic energy for the competition reaction (–3.4 kcal/mol at X3LYP, which is comparable with experimentally observed $\Delta\log K_1$) and, at the same time, points at coordination sphere as the main contributor to the relative stability of these complexes. However, this contribution must be partly compensated by some other unfavourable sources of energy which most likely should be located outside the coordination sphere.

Interactions Outside the Coordination Sphere of the Complexes. Recalling that the NCI isosurfaces revealed the presence of additional interactions, CH•••HC and CH•••O, but only in the BeNTPA complex, it was of importance to explore their natures and quantify their contributions to the overall energy of this complex – relevant data are shown in Table 3.5. Looking at CH•••O, we found that the interaction energy $E_{\text{int}}^{\text{H,O}}$ is –5.0 kcal/mol; hence these three attractive interactions contribute about –15 kcal/mol in a stabilizing manner. Furthermore, as one would expect, this interaction is dominated by the classical term, $V_{\text{cl}}^{\text{H,O}}$ = –3.7 kcal/mol - see Table 3.5. Considering the CH•••HC interactions, because $V_{\text{cl}}^{\text{H,O}}$ 0.1 kcal/mol and $V_{\text{XC}}^{\text{H,H}}$ term of –2.3 kcal/mol dominates, they also appear to be of an overall stabilizing nature.

Table 3.5. IQA partitioning of two-bodied interaction energies in BeNTPA for intramolecular interactions identified by NCI isosurfaces using the RXL3YP wavefunction on the MP2 structures.

Interaction	kcal/mol		
	$V_{\text{cl}}^{\text{X,Y}}$	$V_{\text{XC}}^{\text{X,Y}}$	$E_{\text{int}}^{\text{X,Y}}$
H6 ••• H12	0.1	–2.3	–2.2
H2 ••• H14	0.1	–2.3	–2.2
H10 ••• H16	0.1	–2.3	–2.2
H14 ••• O22	–3.7	–1.4	–5.0
H16 ••• O25	–3.7	–1.4	–5.0
H12 ••• O28	–3.7	–1.4	–5.0
Total:	–10.8	–11.1	–21.6

In order to insure that we had a correct qualitative description of these weak intramolecular interactions, some of them were analysed at the RMP2 level of theory.

Interestingly, the results predicted both interactions to contribute to the complex stability even more in stabilizing manner. Although we obtained $V_{cl}^{H,H}$ marginally larger (by ~0.1 kcal/mol) for the CH2•••H14C interaction, a significant increase in the $V_{XC}^{H,H}$ term resulted in an increase of an overall stabilizing contribution made, in absolute term by 0.3 kcal/mol. In case of the CH14•••O22 interaction, $V_{cl}^{H,O}$ and $V_{XC}^{H,O}$ of –4.4 and –1.6 kcal/mol, respectively, were found at MP2. This analysis not only shows that the CH•••HC interaction is only slightly repulsive and does appear to add to molecular stability, but also and importantly validates the usage of the X3LYP functional on the MP2-optimized structure. For both CH•••HC and CH•••O interactions in the BeNTPA complex, it is important to note that: (i) there are no AILs present, (ii) both show a blue region of concentration, an NCI indicator of stabilizing interaction due to density accumulation, (iii) an adjacent red isosurface, indicative of density depletion within a pseudo ring formed due to density accumulation between interacting atoms, (iv) electron density which consistently decreases along the cross-section (Figure 3.5(b)), and finally (v) these interactions are characterized by the overall negative interaction energy. Thus, from the IQA perspectives, there is no evidence which suggests that firstly, the CH•••HC interaction is locally destabilizing (note that this would provide an additional reason for preferential BeNTA complex formation) and secondly, that the CH•••O and CH•••HC intramolecular interaction differ qualitatively in nature. The most significant difference between the two interactions arises in the relative contributions made by the classical term, where it is almost negligible (but repulsive) for the CH•••HC interaction and attractive for the CH•••O interaction; in this respect, the IQA analysis recovered the common notion of these interactions' nature.

When the values of the interaction energy of the CH--HC and CH--O contacts are compared to those of (i) classically repulsive contacts in the coordination sphere (N--O and O--O), and (ii) coordination bonds, it is clear that the impact they have on the molecules' (in)stability is orders of magnitude smaller. On the other hand, the two intramolecular interactions, CH•••O and CH•••HC, contribute significantly to the overall stability of a molecule. When their total interaction energy contributions of –21.6 kcal kcal/mol is combined with that found from coordination spheres, –9.4 kcal/mol, the formation constant of BeNTPA would be expected to be much larger, by about 28 log units, which clearly is not the case (the experimental difference is about 2.4 log units only). This is another strong indication that there must be other and destabilizing energy components which must totally compensate contributions coming from the intramolecular CH•••HC and CH•••O interactions.

Table 3.6. Comprehensive overview of the properties investigated and an indication of which complex formation is favoured by a specified single property.[a]

Complex	d(Be,N)	d(Be,O)	d(H,H)	$\rho_{BCP}^{Be\text{-}N(O)}$	ρ_{RCP}	$E_{int}^{Be,N}$	$E_{int}^{Be,O}$	Sum-1	$E_{int}^{N,O}$	$E_{int}^{O,O}$	Sum-2
	Å			au		kcal/mol					
BeNTPA	1.791	1.610	2.159	0.060 (0.075)	0.018	–424.3	–484.9	–1781	183.2	204.3	1229
BeNTA	1.772	1.612	2.331	0.064 (0.077)	0.034	–437.2	–484.3	–1791	196.9	197.3	1252
In favour of:	NTA	NTPA	NTA	NTA	NTA	NTA	NTPA	NTA	NTPA	NTA	NTPA

[a] Sum-1 stands for summed interaction energies of all coordination bonds, Sum-2 stands for summed interaction energies between O and N atoms of the coordination spheres.

Finally, Table 3.6 gives a comprehensive summary of numerous analyses performed from which we hoped to find factors controlling relative stability of these two molecular systems. Unfortunately, neither geometric parameters, QTAIM- and NCI-based analyses nor IQA-based interpretation of diatomic interactions in both complexes were able to provide a conclusive answer. A common feature of all analyses discussed above is that they provided one-sided pictures as they quantified each descriptor individually hence the spread in pointing at either NTPA or NTA complex being favourably formed. Thus we came to the conclusion that further analyses of local indices most likely will be as fruitless and we decided to develop a protocol which should account for the combined effect of many components and this is the subject of sections that follow.

Evaluating Processes Involved in Complex Formation

A formation of a complex in aqueous environment can be schematically seen as the sum of two simplified or imaginary separate processes as shown in Scheme 3.1.

Scheme 3.1. A simplified decomposition of the complex formation process.

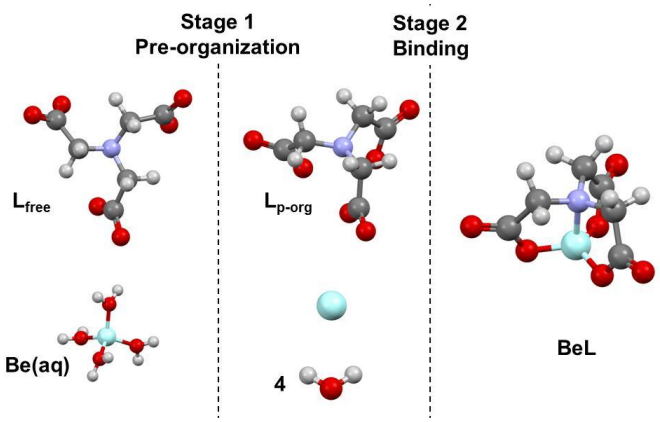

We assumed that the large hydration spheres of all components involved (a real environment with many water molecules must be very much the same for the ligands and complexes) can be neglected in gaining an insight on relative stability from the comparative studies. Moreover, dissociation of $Be(H_2O)_n$ is the same process for both complexes, thus dissociation energy E_{diss} cancels off, hence our focus is on two processes:

a) Stage 1 in Scheme 3.1 represents preorganization of a ligand, a necessary structural change leading from a free ligand structure L_{free} to that observed in a complex; it is expected that the related penalty energy, called here a preorganization energy, $E^{L}_{p\text{-}org}$, should be different for both complexes, $E^{NTA}_{p\text{-}org}$ and $E^{NTPA}_{p\text{-}org}$. Moreover, our hope is to gain an understanding of and an insight on the origin(s) of strain in structures of pre-organized ligands, $L_{p\text{-}org}$.

b) Stage 2 in Scheme 3.1 represents binding between $L_{p\text{-}org}$ and Be, which leads to complex formation; this step will be used to uncover processes and the related energy components. The energy released on binding, E_{bind}, can also be seen as a measure of affinity between a bear metal ion and $L_{p\text{-}org}$.

There is an additional advantage of this protocol, namely one can also compare changes occurring when $L_{p\text{-}org}$ changes its fundamental physical properties to those when in a complex (L_{comp}); this should tell us, *e.g.* whether and how much and where a ligand is gaining/losing energy when coordination bonds are formed. Note that even though structurally $L_{p\text{-}org}$ and L_{comp} are identical, the atomic energies as well as intramolecular interactions must be totally different because only interactions within the ligand framework are taking place in $L_{p\text{-}org}$ whereas the presence of Be will add many interactions as well as modify those within the framework of L_{comp} relative to $L_{p\text{-}org}$. Importantly, because the IQA-defined one- and two-

body components will be accounted for, this should provide us with a total description of changes taking place and we hope that this will explain relative stability of the complexes as well as point at major energy contributions (the origin) controlling the relative stability of molecular systems examined in this work. Furthermore, the geometry of atoms not involved in the coordination bond formation can also change when a ligand changes from the L_{free} to $L_{p\text{-}org}$ states and this might result in somewhat different (i) density distribution within atomic basins as well as (ii) net charge of these atoms. These two changes in the atoms' physical properties, in addition to their different 3D placement in the L_{free} to $L_{p\text{-}org}$ states, will also contribute to the computed change in the interaction energy terms; hence, the geometric deformation energy of atoms not involved in the intramolecular interaction should be, although indirectly, accounted for to some extent.

The preorganization energy, $E_{p\text{-}org}$, related to the first stage in Scheme 3.1 can be written as

$$E_{p\text{-}org} = E(L_{p\text{-}org}) - E(L_{free}) \tag{3.10}$$

and binding energy, E_{bind}, related to the second stage can be expressed as

$$E_{bind} = E(BeL) - E(L_{p\text{-}org}) - E(Be) \tag{3.11}$$

Notice that the sum of the two processes, $E_{p\text{-}org} + E_{bind}$, should amount to the resultant complex formation energy, $E_{ML} = E(BeL) - E(L_{free}) - E(Be)$, related to the reaction of the metal ion with the free ligand L_{free}. The nuance in this approach is that rather than defining complex stability based on selected properties of the final ML structure, we recognize complex formation is a process and expect that the combined changes in physical properties on the complex formation are likely to bear more weight on the relative stability of complexes formed. In principle, this decomposition scheme is similar to that utilized previously[4] when the ETS-NOCV method[87-89] was used. By making use of a preparation/distortion energy (equivalent to preorganization) and an interaction energy (equivalent to binding), this technique has successfully investigated several molecular systems. While ETS-NOCV has been useful in understanding overall changes in the molecular system, it does not provide an insight on the origin (down to atomic and interatomic level) of these contributions. Our approach expands on this technique by (i) using real chemical fragments and not radicals obtained from artificial dissections, and (ii) utilizing the molecular partitioning provided in QTAIM and IQA to pinpoint the atomic and interatomic contributions to the global molecular changes.

Table 3.7. Computed preorganization (strain) energies and affinity energies (all in kcal/mol) using relevant energy terms obtained for L_{free} of NTA and NTPA, the complexes BeNTA and BeNTPA, and the respective $L_{p\text{-}org}$.

Level of Theory	$E_{p\text{-}org}$				E_{bind}				ΔE_{ML} [a]
	NTA	NTPA	$\Delta E_{p\text{-}org}$ [b]	Ratio[c]	BeNTA	BeNTPA	ΔE_{bind} [d]	Ratio[c]	
MP2[e]	52.0	61.2	9.2	1.2	–266.5	–284.5	–18.0	1.1	–8.8
PBE1PBE[f]	53.7	67.7	14.0	1.3	–264.4	–283.0	–18.6	1.1	–4.7
B3LYP[f]	53.5	69.5	16.0	1.3	–268.8	–287.4	–18.6	1.1	–2.7
X3LYP[f]	53.2	68.6	15.4	1.3	–270.5	–289.2	–18.7	1.1	–3.4

[a] $\Delta E_{ML} = E_{BeNTPA} - E_{BeNTA}$; [b] $\Delta E_{p\text{-}org} = E_{p\text{-}org}(NTPA) - E_{p\text{-}org}(NTA)$; [c] Ratio = (NTPA/NTA) value; [d] $\Delta E_{bind} = E_{bind}(BeNTPA) - E_{bind}(BeNTA)$; [e] energies were obtained by optimizing the lowest energy conformer of each molecule; [f] electronic energy obtained by performing a single point calculation on the MP2 structure at the indicated level of theory.

The results in Table 3.7 (corresponding *G* values are shown in Table A10 in Appendix A) show that both ligands needed additional and significant energy (*e.g.*, 52 kcal/mol in case of NTA at MP2) to attain the required geometry (as observed in complexes). We found that $\Delta E_{p\text{-}org}$ is ~9 kcal/mol at MP2 in favour of NTA, probably because there are more atoms present in NTPA. Importantly, this trend is consistent with the strain energies found for the same ligands forming zinc and nickel complexes.[3,4] As one would expect, the affinity of the metal ion to the pre-organized ligand is such that the energy released overrides the energy penalty incurred to pre-organize the ligand in both cases, with ΔE_{bind} ~–18 kcal/mol in favour of BeNTPA. Importantly, the difference between the overall energy needed to form the complexes, *i.e.*, $\Delta E_{ML} = (E_{p\text{-}org}(NTPA) + E_{aff}(BeNTPA)) - (E_{p\text{-}org}(NTA) + E_{aff}(BeNTA)) = -8.8$ kcal/mol at MP2, corresponds with the experimental trend.

As a matter of fact, the relative complex formation energy, ΔE_{ML}, which was obtained from Scheme 3.1 by partitioning the complex formation reaction into two processes, is equal to the E_{CRn} value, *i.e.*, $\Delta E_{p\text{-}org} + \Delta E_{bind} = E_{ML} = E_{CRn}$, obtained at each level of theory, thus reinforcing the employed protocol. Because of that and the fact that the DFT data qualitatively agreed with the MP2 ones we were able to explore the origins of energy changes related to each separate stage in Scheme 3.1 using most suitable theory level for a particular purpose.

Exploring first stage of complex formation – toward understanding the pre-organization (strain) energy of a ligand

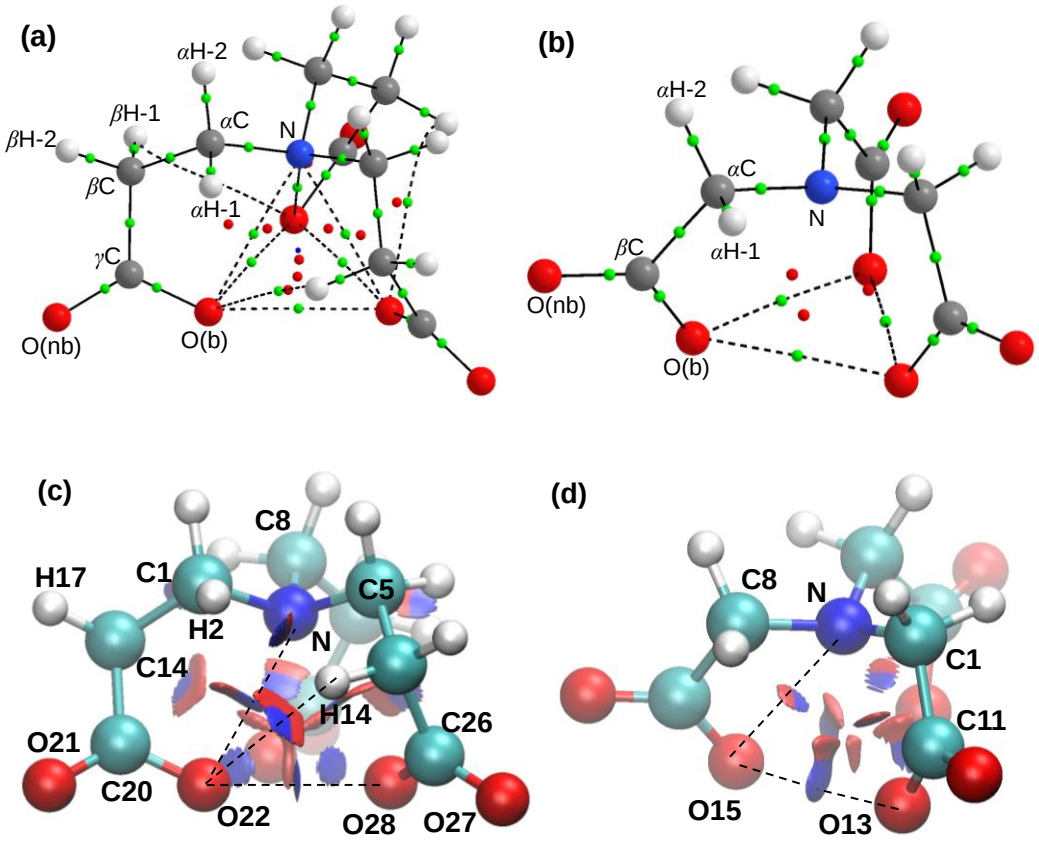

Figure 3.5. The QTAIM molecular graphs of ligands as found in (a) $L_{p\text{-}org}$(NTPA), and (b) $L_{p\text{-}org}$(NTA), as well as the NCI isosurfaces of (c) $L_{p\text{-}org}$(NTPA), and (d) $L_{p\text{-}org}$(NTA), with a RDG isovalue of 0.5 au and isosurfaces coloured from blue to red using -0.07 au $\leq$ sign(λ_2)×$\rho(r) \leq$ +0.03 au.

In the previous section, we decomposed the process of complex formation into the preorganization (strain) energy and the binding energy between a metal ion and $L_{p\text{-}org}$. We will now look at the changes which occurred in the ligand molecules on the preorganization step from the QTAIM and IQA perspectives - Figure 3.5(a,b) shows the molecular graphs of the $L_{p\text{-}org}$ structures of NTPA and NTA.

Let us begin with QTAIM-based interpretation of the pre-organized ligands. Surprisingly, despite the presence of the highly repulsive environment within the coordination spheres, there are atomic interaction lines present between donor atoms; we found ρ_{BCP}(O--O) of 0.0139 and 0.0153 au in NTA and NTPA, respectively. It is thus rather difficult to interpret the AILs according to the classical meaning of QTAIM-defined bond paths. However, one might attempt to rationalize the appearance of these AILs as a way of decreasing repulsive forces between atoms involved by specific dissipation of electron density. Recall that the

appearance of any AILs implies the presence of new XC-term which is always negative; hence, this must partly minimize intramolecular strain. Also, due to density dissipation throughout the coordination sphere in the form of AILs, the electron population on atoms involved in steric clashes must decrease which should lead to a decrease in the repulsive interaction energy.

Furthermore, we note that (i) there are no AILs present in the case of the N--O contacts in the pre-organized structure of NTA but there are three in NTPA with ρ_{BCP}(N--O) = 0.0163 au and (ii) there are additional AILs in the pre-organized form of NTPA which represent typical hydrogen bonds between O(b)-atoms and the βH atoms with ρ_{BCP}(O--H) = 0.0050 au, therefore they might be seen as an orthodox bond paths. In general, molecular graphs in Figure 3.6 can be seen as an excellent example showing how a molecular system responds to the structural change from fully relaxed (lowest energy state) to highly crowded 3D atoms distribution. It appears that an AIL is formed not only when well-known classical bond is formed (then it is appropriate to call such AILs bond paths) but also might be formed to minimize energy penalty due to the highly repulsive environment; regardless, in both cases AILs must minimize the instability of a molecular environment; otherwise they would not be present. This observation not only correlates well with Bader's view that "For a system in a stationary state, the wave function and the electron density it determines are such as to minimize the total energy."[90] but it also extends his interpretation to a transitional state. The NCI isosurfaces shown in Figure 3.5(c,d), fully recover the QTAIM molecular graphs, indicating blue regions of electron density accumulation where AILs were present and red cigar-shaped isosurfaces (elongated along directions of increasing density) with the thickest middle part coinciding with RCPs on molecular graphs. Very intriguing isosurfaces are observed between O-atoms involved in the steric clash in NTPA; blue-coloured discs are observed (without a trace of red surrounding area, which is synonymous with stabilizing interaction in classical NCI interpretations, *e.g.*, this is exactly the picture which one observes for classical intramolecular H-bond (see Figure A4 in Appendix A). To rationalize this observation one might speculate that this simply represents an overlap of orbitals with free pairs of electrons and this does not require a density re-arrangement which explains why we do not see red coloured isosurfaces. There are only three AILs in the pre-organized NTA but the NCI revealed the presence of additional bi-centric isosurfaces; a red area directly between N- and O(b)-atoms with an adjacent blue region placed outside the ring. Because density was removed from the interatomic region (thus NCI-interpreted repulsion), this might suggest that

there was an 'excess' of density within the ring and as a result an adjacent blue region was formed which signifies the output of the redistributed excess electron density in the highly crowded environment.

There are many, complex features observed in both, the NCI isosurfaces and molecular graphs, but their interpretation is far from trivial and intrinsically would be highly speculative. Because of that, we decided to trace the origin of preorganization energies from the IQA-perspectives using NCI isosurfaces as a useful guide. Furthermore, because the energy of a molecule is the sum of the additive energies of each atom, this allows identifying atoms that have made the greatest (de)stabilizing contribution to the change of the molecule's energy when L_{free} changes to $L_{p\text{-}org}$, *e.g.*, atoms which are involved in highly repulsive environment (hence the classically interpreted steric strain) should experience a large increase in the additive atomic energy, E^{X}_{add}, and become highly destabilized.

Data shown in Table 3.8 reveals that order(s) of magnitude larger changes in ΔE^{X}_{add} (they affect the $E_{p\text{-}org}$ value) occurred on the nitrogen atoms and all atoms of the carboxylate groups. Furthermore, the variation in the additive atomic energies, ΔE^{X}_{add} (when a ligand changed from the L_{free} to $L_{p\text{-}org}$ state) shows that by far more significant changes took place in NTPA. However, regardless of the magnitude of changes, there appear to be a consistent pattern in both ligands: the highly negatively charged atoms, N, O(b) and O(nb), experienced a large increase in atomic additive energies whereas the highly positively charged C-atoms of the carboxylate groups became stabilized the most. The analysis of energy components, an intra-atomic contribution (E^{X}_{self}) and interatomic contributions ($\sum_{Y\neq X} 0.5E^{X,Y}_{int}$) which, when summed up results in E^{X}_{add} as shown in Eq. (3.8), in combination with additional physical properties shown in Table 8, lead to the following conclusions:

(i) For the negatively charged atoms involved in contacts in $L_{p\text{-}org}$, O(b) and N, the energy penalty is driven by unfavourable, hence destabilizing change in interactions with all remaining atoms in a ligand which is much greater in value than the change in their self-atomic energies; $\Delta\sum_{Y\neq X} 0.5E^{X,Y}_{int} >> |\Delta E^{X}_{self}|$. The process of preorganization forced a large outflow of electron density from the negatively charged atoms, *e.g.*, ΔN^{N} = –0.207 and –0.093*e* for NTPA and NTA, respectively, which is accompanied by the most significant among all atoms contraction in atomic volume, *e.g.*, ΔVol^{N} = –25.4 and –17.5 bohr^3 for

NTPA and NTA, respectively; note that these changes are more significant for NTPA. Because of that, a reduction in the electron-electron repulsion, $\Delta V_{ee}^{XX} < 0$, and the electron-neutron attraction, $\Delta V_{ne}^{XX} > 0$, within atomic basins is observed (note that one always observes $\Delta V_{ne}^{XX} > \left|\Delta V_{ee}^{XX}\right|$ for the O(b) and N atoms in both ligands). These two changes, in combination with $\Delta T^{X} < 0$, explain the observed decrease in these atoms self-energy, $\Delta E_{self}^{X} < 0$; recall that $E_{self}^{X} = T^{X} + V_{ne}^{XX} + V_{ee}^{XX}$.

(ii) For the non-bonded to the central metal ion oxygen, O(nb) atoms of the carboxylate groups, the opposite is noted: the origin of the observed increase of these atoms additive atomic energies can be traced to unfavourable increase in their self-atomic energies resulting in $|\Delta\sum_{Y\neq X} 0.5E_{int}^{X,Y}| << \Delta E_{self}^{X}$. It is also clear that to accommodate the dissipation of electron density from the crowded coordination sphere region in $L_{p\text{-}org}$, a large inflow of electron density into negatively charged O(nb) atoms took place, $\Delta N^{X} = 0.077e$, and this increased these atoms volume, $\Delta Vol^{X} = 3.8$ bor^3. Interestingly, this was accompanied by a small decrease in the average electron density per unit volume, $\Delta d_{e}^{X} < 0$. As a consequence, the electron-electron repulsion, $\Delta V_{ee}^{XX} > 0$, as well as electron-neutron attraction, $\Delta V_{ne}^{XX} < 0$, increased in these atoms basins. Here, despite $\left|\Delta V_{ne}^{XX}\right| > \left|\Delta V_{ee}^{XX}\right|$, we see that $\Delta T^{X} > \left|\Delta V_{ne}^{XX} + \Delta V_{ee}^{XX}\right|$ and this fully explains the observed large increase in self-atomic energies found for O(nb).

(iii) Considering the highly, positively charged C-atoms of the carboxylate groups, the preorganization process resulted in increased stability of these atoms, $\Delta E_{add}^{X} << 0$, mainly due to a decrease in their self-atomic energies, $\Delta E_{self}^{X} < 0$. Interestingly, the γC-atoms of NTPA found themselves in more attractive molecular environment as judged from the highly stabilizing change in these atoms interactions with remaining atoms of the ligand, $\Delta\sum_{Y\neq X} 0.5E_{int}^{X,Y} = -24.6$ kcal/mol, but only a small, although unfavourable, change in diatomic interactions with remaining atoms is observed for the βC-atoms of NTA. From the observed $\Delta N^{X} > 0$ (the charge decreases from 1.619 to 1.578), it also follows that electron population increased not only in highly negatively charged atoms, which are not directly involved in the steric contacts in the $L_{p\text{-}org}$ form of the ligands, but also for highly and positively charged C-atoms of the carboxylic groups. This means that all highly charged (negatively and positively) atoms which are in close proximity to the centre of

Table 3.8. Relative to L_{free} structures, changes in the selected QTAIM (at the MP2 level of theory) and IQA (at the RX3LYP level of theory on the MP2 structure) energy terms (in kcal/mol) and additional properties of atoms in the pre-organized NTPA and NTA ligand

Atom X	ΔE^X_{add}	$\Delta\sum_{Y\neq X}0.5E^{X,Y}_{int}$	ΔE^X_{self}	ΔT^X	ΔV^{XX}_{ne}	ΔV^{XX}_{ee}	q^X_{free}	$q^X_{L_{p-org}}$	ΔE^X	ΔN^X	ΔVol^X	$\Delta d_e{}^X$
					NTPA							
αC	–3.5	0.1	–3.6	–2.2	–16.1	14.7	0.343	0.332	7.4	0.011	0.43	–0.0008
αH–1	0.2	1.2	–1.0	6.2	–13.3	6.0	–0.002	–0.029	–6.2	0.027	2.02	–0.0004
αH–2	0.3	0.7	–0.5	7.8	–15.4	7.1	–0.014	–0.044	–8.0	0.030	1.99	–0.0003
βC	–1.4	–0.3	–1.1	–3.9	9.4	–6.6	0.006	0.007	10.2	–0.002	0.86	–0.0015
βH-1	1.1	–1.1	2.2	–2.1	4.4	0.0	–0.005	0.002	2.5	–0.007	–2.89	0.0011
βH-2	–0.2	2.1	–2.3	3.5	–9.7	3.9	–0.010	–0.032	–2.8	0.022	4.49	–0.0015
γC	–46.1	–24.6	–21.5	21.5	–107.9	64.9	1.619	1.578	–18.3	0.041	1.56	–0.0036
O(nb)	38.3	0.7	37.7	75.5	–298.9	261.1	–1.298	–1.375	–64.6	0.077	3.82	–0.0009
O(b)	56.1	73.8	–17.8	–58.7	380.7	–339.7	–1.298	–1.169	76.1	–0.129	–21.24	0.0084
N	20.8	50.5	–29.7	–56.3	465.2	–438.6	–1.020	–0.813	72.0	–0.207	–25.45	0.0363
					NTA							
αC	–1.5	2.1	–3.6	–16.1	38.3	–25.8	0.313	0.322	23.0	–0.009	2.67	–0.0056
αH-1	0.2	2.8	–2.6	3.8	–11.0	4.5	0.019	–0.006	–3.6	0.025	4.22	–0.0014
αH-2	–0.3	0.6	–0.9	4.8	–7.3	1.7	–0.027	–0.034	–5.0	0.007	0.70	–0.0002
βC	–17.0	2.0	–19.0	23.9	–105.5	62.7	1.630	1.588	–21.7	0.042	2.04	–0.0049
O(nb)	18.7	–19.7	38.4	81.4	–291.7	248.7	–1.305	–1.369	–73.1	0.064	2.44	–0.0005
O(b)	29.2	56.7	–27.5	–72.5	362.3	–317.3	–1.291	–1.193	87.3	–0.098	–9.13	0.0032
N	5.0	9.9	–4.9	–21.4	181.9	–165.4	–1.019	–0.926	31.2	–0.093	–17.55	0.0268

[a] $E^X_{self} = T^X + V^{XX}_{ne} + V^{XX}_{ee}$, by definition; T^X - the electronic kinetic energy of an atom (a Hamiltonian form); V^{XX}_{ne} - attraction energy between electron density distribution of atom X and nucleus of Atom X; V^{XX}_{ee} - two-electron interaction energy of atom X with itself; E^X - approximation to a virial-based total energy of atom X; N^X - average No of electrons in atom X (atomic electron population); Vol^X – atomic volume in bohr^3 (volume bounded by interatomic surfaces of atom X and by isosurface of the electron density distribution (0.001au isodensity surface was used); $d_e{}^X = N(Vol^X)/Vol^X$ - average electron density in Vol^X where $N(Vol^X)$ is average number of electrons in Vol^X.

the coordination sphere experienced an increase in the electron density which clearly facilitates the charge dissipation and must have resulted in somewhat smaller repulsive nature of diatomic interactions between atoms in the coordination sphere.

In general, except for a difference in the sign and value of the interaction energies with remaining atoms, all other physical properties of the C-atoms of the carboxylic groups are characterized by comparable in value and of the same sign changes observed when going from the L_{free} to $L_{p\text{-}org}$ state of the ligands.

Another striking observation can be made, namely the additive atomic energies of all H-atoms, regardless whether they were/are involved in close contacts (αH-1 and βH-1) in $L_{free}/L_{p\text{-}org}$ have not changed significantly, typically by a fraction of kcal/mol. Also, their self-atomic energies changed marginally. This observation contradicts again the common notion that H-atoms involved in a steric clash become highly strained; clearly this is not the case for these two ligands.

In summary, the energy penalty experienced on preorganization is due to a global unfavourable change in all diatomic interactions with interactions between coordinating atoms (O(b) and N) playing the most significant role. Additionally, in order to compensate for this, electron density is dissipated into to the surrounding regions, resulting in the destabilization of the O(nb) atoms and stabilization of the C-atoms in the carboxylate groups. The difference in the preorganization strain energy, between NTPA and NTA, is largely due to the formation of far more repulsive interactions in NTPA as measured by $\Delta\sum_{Y\neq X}0.5E_{int}^{X,Y}$. Contrary to classical suggestions, our findings show that the H-atoms involved in short contacts (and the same applies to all H-atoms of the ligands) play a negligible role when they contribution to the preorganization energy is considered.

Exploring Second Stage of Complex Formation – towards understanding relative stability of complexes

Knowledge of binding energy points directly at the more stable complex but does not provide any insight on mechanisms or origin of energetic changes leading to the preferential complex formation. To gain further insight, we decided to decompose the computed E_{bind} by making use of the primary and molecular fragment energy terms as defined in the IQA and Interacting Quantum Fragments (IQF) methods (IQF is an expansion of IQA). The concept of

fragment energies can be traced back to ideas coming from the theory of electronic separability of McWeeny,[91] but they were not used extensively within the IQA/IQF framework and what follows is a new implementation of these ideas to investigate relative stability of molecules (in general, molecular systems). Because the proposed protocol is of general purpose and can be applied to any molecular system (here containing a metal ion) we will replace Be in all expressions by M. Furthermore, for the purpose of analysis in the fragment notation, we will treat our complexes as made of two fragments, a mono-atomic $\mathcal{M}$ = M and polyatomic $\mathcal{L}$ = L. Because binding is the process involving a free metal ion M_{free} and the pre-organized ligand, we will use $\mathcal{M}_f = M_{free}$ and $\mathcal{L}_p = L_{p\text{-}org}$ in the fragment notation to describe their properties. Similarly, we will use $\mathcal{M}_c = M_{comp}$ and $\mathcal{L}_c = L_{comp}$ to distinguish these fragments' properties from those of $\mathcal{M}_f$ and $\mathcal{L}_p$. Let us first express the components of the binding energy, as shown in Eq. 3.11, in terms of additive atomic energies,

$$E_{bind} = \sum_{X \in ML} E_{add}^{X} - \sum_{X \in \mathcal{L}_p} E_{add}^{X} - E_{add}^{M_f} \tag{3.12}$$

Next, to gain further insight, one can decompose the additive atomic energies in Eq. 3.12 which results in

$$E_{bind} = \sum_{X \in ML} E_{self}^{X} + 0.5 \sum_{X \in ML} \sum_{\substack{Y \neq X \\ Y \in ML}} E_{int}^{X,Y} - \sum_{X \in \mathcal{L}_p} E_{self}^{X} - 0.5 \sum_{X \in \mathcal{L}_p} \sum_{\substack{Y \neq X \\ Y \in \mathcal{L}_p}} E_{int}^{X,Y} - E_{self}^{M_f} \tag{3.13}$$

where: first two terms on the right-hand site of Eq. 3.13 represent the energy of a complex expressed in terms of IQA primary energy terms; the third term accounts for self-energies of all atoms the pre-organized ligand is made of and in the fragment notation can be written as $E_{self}^{\mathcal{L}_p}$, a self-energy of a fragment $\mathcal{L}_p$; the fourth term accounts for all unique diatomic interaction energies between atoms constituting a polyatomic molecular fragment, here $\mathcal{L}_p$, and in fragment notation stands for the intra-fragment interaction energy term, $E_{int}^{\mathcal{L}_p}$. Note that the free metal ion in Stage 2 in Scheme 3.1 is assumed to share no interactions with any other atom, hence $E_{add}^{M_f} = E_{self}^{M_f}$ and in our case also $E_{self}^{M_f} = E_{self}^{\mathcal{M}_f}$ applies. From this follows that Eq. 3.13 can be written in the fragment notation as

$$E_{bind} = \sum_{X \in ML} E_{self}^{X} + 0.5 \sum_{X \in ML} \sum_{\substack{Y \neq X \\ Y \in ML}} E_{int}^{X,Y} - E_{self}^{\mathcal{L}_p} - E_{int}^{\mathcal{L}_p} - E_{self}^{\mathcal{M}_f}. \tag{3.14}$$

Upon final complex formation, all intra-fragment interactions in $\mathcal{I}_p$ must change to those present in $\mathcal{I}_c$ which now interacts with M_{comp}. As a matter of fact, because of a large density redistribution taking place on complex formation, not only the diatomic interaction energies, but also the self-atomic and additive atomic energies in the ligand framework must have changed too. To understand all the changes taking place in the ligand, it was necessary to further decompose the interaction energy term applicable to the ML complex (second term in Eq. 3.14) into separate contributions coming from (i) interactions between atoms within a ligand framework when in complex and (ii) all new diatomic interactions in the complex between M_{comp} and all atoms of L_{comp}, the first and second term in Eq. 3.15, respectively

$$0.5\sum_{X\in ML}\sum_{\substack{Y\neq X\\ Y\in ML}}E_{int}^{X,Y} = 0.5\sum_{X\in \mathcal{I}_c}\sum_{\substack{Y\neq X\\ Y\in \mathcal{I}_c}}E_{int}^{X,Y} + \sum_{\substack{X\neq M_{comp}\\ X\in ML}}E_{int}^{M_{comp},X}. \qquad (3.15)$$

where the last term can be seen as an inter-fragment interaction energy term, hence in the fragment notation we obtain

$$0.5\sum_{X\in ML}\sum_{\substack{Y\neq X\\ Y\in ML}}E_{int}^{X,Y} = E_{int}^{\mathcal{I}_c} + E_{int}^{\mathcal{M}_c,\mathcal{I}_c} \qquad (3.16)$$

It is important to note that this step expands our analysis from a focus on just coordination bonds to scrutinizing all possible interactions involving M_{comp}. This step also allows us to define a term that estimates an energy gain/loss caused just by the changes in the diatomic intra-fragment interaction energies, as

$$\Delta E_{int}^{\mathcal{I}} = 0.5\sum_{X\in \mathcal{I}_c}\sum_{\substack{Y\neq X\\ Y\in \mathcal{I}_c}}E_{int}^{X,Y} - 0.5\sum_{X\in \mathcal{I}_p}\sum_{\substack{Y\neq X\\ Y\in \mathcal{I}_p}}E_{int}^{X,Y} \qquad (3.17)$$

Hence, it provides an estimate of energy related to the rearrangement of diatomic intramolecular interactions within a ligand framework, $\mathcal{I}$, when the $\mathcal{I}_p$ state changes to the $\mathcal{I}_c$ state. In the fragment notation we can express Eq. 3.17 as

$$\Delta E_{int}^{\mathcal{I}} = E_{int}^{\mathcal{I}_c} - E_{int}^{\mathcal{I}_p} \qquad (3.18)$$

By making use of expression 3.16 and 3.18 and combining contributions coming from self-atomic energies one can re-write Eq. 3.14 as

$$E_{bind} = \sum_{X\in ML}\Delta E_{self}^{X} + \Delta E_{int}^{\mathcal{I}} + E_{int}^{\mathcal{M}_c,\mathcal{I}_c} \qquad (3.19)$$

where

$$\sum_{X\in ML}\Delta E^{X}_{self} = \sum_{X\in ML}E^{X}_{self} - \sum_{X\in L_{p\text{-}org}}E^{X}_{self} - E^{M_f}_{self} \tag{3.20}$$

which, for brevity can be written as

$$\Delta E^{ML}_{self} = E^{M_f}_{self} - E^{\mathcal{I}_p}_{self} - E^{\mathcal{M}_f}_{self} \tag{3.21}$$

The term $\sum_{X\in ML}\Delta E^{X}_{self} = \Delta E^{ML}_{self}$ defined in Eq. 3.20 accounts for the total energy contribution coming from the self-atomic energies of all atoms of the molecular system when the pre-organized ligand and a free metal ion bind to form a final complex ML; ΔE^{ML}_{self} stands for a change in the molecular system self-energy.

To learn about the nature of changes observed in diatomic interactions with the ligand framework, one can make use of a classical (electrostatic) contribution, $V^{X,Y}_{cl}$, and exchange-correlation, XC energy term, $V^{X,Y}_{XC}$, which are obtained from the decomposition of a diatomic energy term, $E^{X,Y}_{int} = V^{X,Y}_{cl} + V^{X,Y}_{XC}$. Thus we can isolate the interaction energy rearrangements in the ligand framework as being of the classical electrostatic and exchange-correlation origin,

$$\Delta E^{\mathcal{I}}_{int} = \Delta V^{\mathcal{I}}_{cl} + \Delta V^{\mathcal{I}}_{XC} \tag{3.22}$$

where

$$\Delta V^{\mathcal{I}}_{cl} = 0.5\sum_{X\in\mathcal{I}_c}\sum_{\substack{Y\neq X\\ Y\in\mathcal{I}_c}}V^{X,Y}_{cl} - 0.5\sum_{X\in\mathcal{I}_p}\sum_{\substack{Y\neq X\\ Y\in\mathcal{I}_p}}V^{X,Y}_{cl} \tag{3.23}$$

and

$$\Delta V^{\mathcal{I}}_{XC} = 0.5\sum_{X\in\mathcal{I}_c}\sum_{\substack{Y\neq X\\ Y\in\mathcal{I}_c}}V^{X,Y}_{XC} - 0.5\sum_{X\in\mathcal{I}_p}\sum_{\substack{Y\neq X\\ Y\in\mathcal{I}_p}}V^{X,Y}_{XC} \tag{3.24}$$

Equally important is the insight one can gain from classical and XC contributions making up the inter-fragment interaction energy $E^{\mathcal{M}_c,\mathcal{I}_c}_{int}$ term and this can be easily computed from

$$E^{\mathcal{M}_c,\mathcal{I}_c}_{int} = V^{\mathcal{M}_c,\mathcal{I}_c}_{cl} + V^{\mathcal{M}_c,\mathcal{I}_c}_{XC} = \sum_{\substack{X\neq M\\ X\in ML}}V^{M_{comp},X}_{cl} + \sum_{\substack{X\neq M\\ X\in ML}}V^{M_{comp},X}_{XC} \tag{3.25}$$

All the above is of great importance as it allows to trace changes in the IQA/IQF-defined fragment energy terms and their components which we hope will be of great help in tracking the origin and nature of factors controlling preferential affinity between two fragments, $\mathcal{M}$

and $\mathcal{I}$, in both complexes, hence also should explain relative stability of molecular systems under investigation.

Finally, it is also of interest and importance to recover additional terms defined in the IQF approach.[69,92] To achieve that, let us first recall that in the IQA framework, the deformation energy of an atom is defined as the change in the self-energy of an atom X, $E_{\mathrm{def}}^{\mathrm{X}} = \Delta E_{\mathrm{self}}^{\mathrm{X}} = E_{\mathrm{self}}^{\mathrm{X}} - E_{\mathrm{vac}}^{\mathrm{X}}$, where the last term typically represents the energy of an atom *in vacuo*. Because there are two fragments in the molecular system investigated here, a polyatomic $\mathcal{I}$ and monoatomic $\mathcal{M}$, the energy contribution due to the combined change in self-energies of all atoms in a complex, $\Delta E_{\mathrm{self}}^{\mathrm{ML}}$, can be conveniently divided into those for each atom of the ligand, $\Delta E_{\mathrm{self}}^{\mathcal{I}}$, when it changes from the $\mathcal{I}_{\mathrm{p}}$ to $\mathcal{I}_{\mathrm{c}}$ state and $\Delta E_{\mathrm{self}}^{\mathcal{M}}$ when the free metal ion, $\mathcal{M}_{\mathrm{f}}$, changes to its state in the complex, $\mathcal{M}_{\mathrm{c}}$,

$$\Delta E_{\mathrm{self}}^{\mathrm{ML}} = \Delta E_{\mathrm{self}}^{\mathcal{M}} + \Delta E_{\mathrm{self}}^{\mathcal{I}} \tag{3.26}$$

where

$$\Delta E_{\mathrm{self}}^{\mathcal{M}} = E_{\mathrm{self}}^{\mathcal{M}_{\mathrm{c}}} - E_{\mathrm{self}}^{\mathcal{M}_{\mathrm{f}}} \tag{3.27}$$

and

$$\Delta E_{\mathrm{self}}^{\mathcal{I}} = \sum_{\mathrm{X}\in\mathcal{I}_{\mathrm{c}}} E_{\mathrm{self}}^{\mathrm{X}} - \sum_{\mathrm{X}\in\mathcal{I}_{\mathrm{p}}} E_{\mathrm{self}}^{\mathrm{X}} = E_{\mathrm{self}}^{\mathcal{I}_{\mathrm{c}}} - E_{\mathrm{self}}^{\mathcal{I}_{\mathrm{p}}} \tag{3.28}$$

According to the IQF framework, the deformation energy of a fragment is defined as the sum of the atomic deformation energies within a fragment and the sum of all unique interaction energies within the fragment when separated atoms form a molecule. Because in our case free atoms are not used as a reference state to monitor changes in $\mathcal{I}$, we express the deformation energy of $\mathcal{I}$ as a difference in the net energies of fragments $\mathcal{I}_{\mathrm{c}}$ and $\mathcal{I}_{\mathrm{p}}$,

$$E_{\mathrm{def}}^{\mathcal{I}} = E_{\mathrm{net}}^{\mathcal{I}_{\mathrm{c}}} - E_{\mathrm{net}}^{\mathcal{I}_{\mathrm{p}}} = \left(E_{\mathrm{self}}^{\mathcal{I}_{\mathrm{c}}} + E_{\mathrm{int}}^{\mathcal{I}_{\mathrm{c}}}\right) - \left(E_{\mathrm{self}}^{\mathcal{I}_{\mathrm{p}}} + E_{\mathrm{int}}^{\mathcal{I}_{\mathrm{p}}}\right) = \Delta E_{\mathrm{self}}^{\mathcal{I}} + \Delta E_{\mathrm{int}}^{\mathcal{I}} \tag{3.29}$$

Eq. 3.29 describes deformation energy of the fragment $\mathcal{I}$ in terms of changes in the fragment's self and intra-fragment interaction energy change when $\mathcal{I}_{\mathrm{p}}$ changes to the $\mathcal{I}_{\mathrm{c}}$ state. Furthermore, because the $\mathcal{M}$ fragment is monoatomic (there are no diatomic interactions within this fragment), then we can write $\Delta E_{\mathrm{self}}^{\mathcal{M}} = E_{\mathrm{def}}^{\mathcal{M}}$.

Thus, the binding energy for a metal complex can be expressed within the IQF framework as the sum of the deformation energies of the individual fragments and the interaction energy between the two fragments (intra-fragment interaction energy term) and by substituting Eq. 3.25 and 3.28 into Eq. 3.19 we obtain

$$E_{\text{bind}} = \Delta E_{\text{self}}^{\mathscr{M}} + \Delta E_{\text{self}}^{\mathscr{I}} + \Delta E_{\text{int}}^{\mathscr{I}} + E_{\text{int}}^{\mathscr{M}_c,\mathscr{I}_c} = E_{\text{def}}^{\mathscr{M}} + E_{\text{def}}^{\mathscr{I}} + E_{\text{int}}^{\mathscr{M}_c,\mathscr{I}_c} \tag{3.30}$$

Comparing Eq. 3.30 and 3.19, the decomposition of the E_{bind} in Eq. 3.30 refocuses the IQA-defined components into IQF related components; the contribution of intra-atomic energies, $\Delta E_{\text{self}}^{\text{ML}}$, and the contribution of diatomic interactions within a particular fragment, $\Delta E_{\text{int}}^{\mathscr{I}}$, are expressed in terms of relevant deformation energy terms, which, as will be seen from discussion that follows, makes the interpretation of relevant stability of molecular systems much easier and convincing.

A set of energy terms used to interpret relative stability of the two complexes, BeNTA and BeNTPA, is included in Table 3.9 and it conclusively points at BeNTPA as preferentially formed because ΔE_{bind} = –8.5 kcal/mol is in favour of BeNTPA. As expected, due to the limitations of the AIMAll software, we have not obtained the exact value of ΔE_{bind} determined form electronic energies, but we have recovered the trend and it is clear that it is driven by the inter-fragment interaction energy term, $E_{\text{int}}^{\mathscr{M}_c,\mathscr{I}_c}$. This exemplifies the importance and significance of the protocol proposed in this work. Note that using just the sum of interaction energies of all coordination bonds (hence their strength) as a predictive tool points at BeNTA as more stable because this contribution is in favour of this complex by about 10 kcal/mol. However, through making use of the combined energy terms (molecular fragments' energies which account for all possible intra- and inter-fragment energy components) makes it clear that the additional interactions (excluding coordination bonds) contributed to the $E_{\text{int}}^{\mathscr{M}_c,\mathscr{I}_c}$ energy term which was found here to be responsible for higher stability of the BeNTPA complex. Furthermore, these results clearly demonstrate that formation of a chemical bond (here coordination bonds) in a multi-atomic environment is not an affair localized to M—L interatomic region but it must be viewed as a global, on a molecular scale, event. Importantly, the computed binding energies also agree with chemists' intuition as the recovered trend - the larger interaction energy between free metal ion and an incoming ligand (and the resultant binding energy) - the stronger complex is formed, is exactly what one would expect.

Table 3.9. The indicated energy components (in kcal/mol), computed within a IQA/IQF framework, which were used in the interpretation of relative stability of BeNTA and BeNTPA complexes. Selected MP2 data is shown in brackets.

Energy term	BeNTA	BeNTPA	ΔE[a]
Energy components of E_{bind}			
$E_{\text{def}}^{\mathscr{M}}$	–123.4 (–134.1)	–122.6 (–133.3)	0.8 (0.8)
$E_{\text{def}}^{\mathscr{L}}$	119.7	132.3	12.5
$E_{\text{int}}^{\mathscr{M}_c,\mathscr{L}_c}$	–1043.5 (–1064.9)	–1065.4 (–1088.5)	–21.9 (–23.6)
E_{bind}	–1047.2	–1055.7	–8.5
Additional energy terms			
$\Delta E_{\text{self}}^{\text{ML}}$	112.5	126.2	13.7
$\Delta E_{\text{int}}^{\mathscr{L}}$	–116.2	–116.5	–0.3
$\Delta V_{\text{cl}}^{\mathscr{L}}$	–174.6	–190.4	–15.8
$\Delta V_{\text{XC}}^{\mathscr{L}}$	58.4	73.9	15.5
$V_{\text{cl}}^{\mathscr{M}_c,\mathscr{L}_c}$	–941.41	–964.4	–23.0
$V_{\text{XC}}^{\mathscr{M}_c,\mathscr{L}_c}$	–102.1	–101.0	1.1

a) $\Delta E = E(\text{NTPA}) - E(\text{NTA})$

Both ligands show large affinity to beryllium ion, as measured by the binding energy which is in absolute value above one thousand kcal/mol. The change from the free to the complexed metal ion stabilized Be. As a result, $E_{\text{def}}^{\mathscr{M}}$ is also stabilizing in both complexes with no significant difference between the two complexes; thus from this perspective the metal ion does not show a preference toward a 5- or 6-membered coordination rings. Looking now from the ligand perspective we note that the deformation energy, $E_{\text{def}}^{\mathscr{L}}$, of NTPA is larger by about 12 kcal/mol even though BeNTA consistently shows more significant deviations from the minimum strain energy geometries (Table A8 in Appendix A).

From the analysis of additional energy terms shown in Table 3.9 it follows that a significant increase in the self-energy of the atoms is observed on both complex formation even though the pre-organized ligands were used as an initial state. Furthermore, the total change in self-energy of molecular systems (here beryllium complexes) $\Delta E_{\text{self}}^{\text{ML}}$, is larger by about 13.7 kcal/mol for BeNTPA (most likely because there are more atoms in BeNTPA). However, $\Delta E_{\text{self}}^{\text{ML}}$ is compensated over by highly favourable change in the interaction energies between Be and the remaining atoms of $\mathscr{L}$. These inter-fragment interactions are highly

dominated by classical (electrostatic) term and we observe $V_{\mathrm{cl}}^{\mathcal{M}_{\mathrm{c}},\mathcal{I}_{\mathrm{c}}}$ (i) an order of magnitude larger than the $V_{\mathrm{XC}}^{\mathcal{M}_{\mathrm{c}},\mathcal{I}_{\mathrm{c}}}$ term for both complexes, and (ii) more significant, by –23 kcal/mol, in BeNTPA. Furthermore, it is clear that the classical term of inter-fragment interaction energy has contributed the most to higher stability of BeNTPA because the exchange-correlation terms in both complexes are very much of the same value, about –100 kcal/mol, which still should be seen as significant contribution of covalent nature. As one would expect, the overall change in the interaction energies between atoms of a ligand, the intra-fragment interaction energy term, $\Delta E_{\mathrm{int}}^{\mathcal{I}}$, is of highly stabilizing, dominated by the classical term, $\Delta V_{\mathrm{cl}}^{\mathcal{I}}$, nature and almost of the same value in both complexes (~–116 kcal/mol). We also observe that both terms ($\Delta V_{\mathrm{cl}}^{\mathcal{I}} < 0$ and $\Delta V_{\mathrm{XC}}^{\mathcal{I}} > 0$ in both complexes) are more significant in the case of BeNTPA and this is again most likely due to larger number of atoms in NTPA.

The above fragment-based analysis allowed us to identify the main source of higher BeNTPA stability, the inter-fragment interaction energy. Hence, we decided to analyse individual components of $E_{\mathrm{int}}^{\mathcal{M},\mathcal{I}}$ with an aim of finding the origin of the resultant effect - see relevant data in Table 3.10. The analysis of data shown in Table 3.10 leads to a number of interesting and important observation:

(a) The XC term is only significant in the case of coordination bonds which is in agreement with common sense and chemists' intuition,
(b) Interactions of Be with electronegative atoms (oxygen and nitrogen) are attractive whereas all other interactions are electrostatically repulsive,
(c) There is a clear trend in the repulsive energies involving C-atoms and Be in both complexes; interactions involving C-atoms of carboxylate groups are about 4.5 times larger when compared with α-carbons. Note also that interactions with β-carbons in BeNTPA are order(s) of magnitude smaller.
(d) Interactions between Be and O(nb)- and N-atoms are more attractive, by about –4 and –14 kcal/mol, in BeNTA (the interaction energies with O(b) are comparable in both complexes).
(e) The sum of all attractive Be-X interactions (where X = N, O(nb) and O(b)) accounts for –2473.6 and -2451.8 kcal/mol in BeNTA and BeNTPA, respectively (a difference of about 22 kcal/mol in favour of BeNTA).

(f) The sum of all repulsive interactions, however, is greater in BeNTA than in BeNTPA (1430.1 and 1386.5 kcal/mol, respectively); a difference of about 44 kcal/mol in favour of BeNTPA despite the presence of additional atoms with which the beryllium has repulsive interactions in this complex.

Table 3.10. IQA partitioning of two-bodied interaction energies of all interactions with the Be atom in BeNTPA and BeNTA using the RXL3YP wavefunction on the MP2 structures.

BeNTPA					BeNTA				
Atoms		$V_{cl}^{X,Y}$	$V_{XC}^{X,Y}$	$E_{int}^{X,Y}$	Atoms		$V_{cl}^{X,Y}$	$V_{XC}^{X,Y}$	$E_{int}^{X,Y}$
X	Y				X	Y			
Be	C1	79.0	–0.2	78.8	Be	C1	83.0	–0.2	82.8
Be	H2	7.6	0.0	7.6	Be	H2	14.6	0.0	14.6
Be	H3	7.7	–0.1	7.6	Be	H3	13.1	0.0	13.1
Be	N4	–403.8	–20.5	–424.3	Be	N4	–417.8	–19.4	-437.2
Be	C5	79.1	–0.2	78.9	Be	C5	83.2	–0.2	83.0
Be	H6	7.5	0.0	7.5	Be	H6	14.6	0.0	14.6
Be	H7	7.7	–0.1	7.6	Be	H7	13.1	0.0	13.1
Be	C8	79.1	–0.2	78.9	Be	C8	83.2	–0.2	83.0
Be	H9	7.7	–0.1	7.6	Be	H9	13.2	0.0	13.1
Be	H10	7.6	0.0	7.6	Be	H10	14.6	0.0	14.6
Be	C11	3.6	–0.1	3.5	Be	C11	366.5	–0.3	366.1
Be	H12	7.2	0.0	7.2	Be	O12	–194.3	–0.2	-194.5
Be	C13	3.6	–0.1	3.5	Be	O13	–457.6	–26.7	-484.4
Be	H14	7.2	0.0	7.2	Be	C14	366.5	–0.3	366.2
Be	C15	3.6	–0.1	3.5	Be	O15	–457.6	–26.7	-484.3
Be	H16	7.3	0.0	7.2	Be	O16	–194.3	–0.2	-194.5
Be	H17	8.4	0.0	8.4	Be	C17	366.3	–0.3	366.0
Be	H18	8.4	0.0	8.4	Be	O18	–194.2	–0.2	-194.4
Be	H19	8.4	0.0	8.4	Be	O19	–457.6	–26.8	-484.3
Be	C20	349.3	–0.3	349.0	Sum (kcal/mol):		**–941.4**	**–102.1**	**–1043.5**
Be	O21	–190.7	–0.2	–190.9					
Be	O22	–459.0	–25.9	–484.9					
Be	C23	349.2	–0.3	348.9					
Be	O24	–190.7	–0.2	–190.9					
Be	O25	–458.9	–26.0	–484.9					
Be	C26	349.3	–0.3	349.1					
Be	O27	–190.7	–0.2	–190.9					
Be	O28	–459.0	–25.9	–484.9					
Sum (kcal/mol):		**–964.4**	**–101.0**	**–1065.4**					

The above analysis leads to quite an unexpected conclusion that, in terms of interaction energies, this is not the strength of coordination bonds that controls the relative stability of these complexes but the unfavourable interactions which are significantly less severe in the case of BeNTPA.

Finally, the presence of the inductive effect can also be deduced here; the repulsion between the beryllium ion and the α-carbon atoms is approximately 4.0 kcal/mol greater in BeNTA than in BeNTPA and the repulsion with the carboxylate carbon atoms is ~17 kcal/mol greater. It is also interesting to note that there is significant and measurable repulsion with α-hydrogens which is almost twice as large in BeNTA.

Conclusions

The theoretical prediction of the relative stability of compounds (not only metal-containing species) is of paramount importance and a great effort has been made in, *e.g.*, predicting parameters controlling preferential formation of metal complexes in aqueous solutions.[1] This lead to a number of different simple and semi-empirical rules which were of great help in the ligand design strategies. The aim of this work was to fundamentally understand why beryllium forms a stronger complex with NTPA relative to NTA, whereas all other metal ions have larger formation constants with NTA. It is important to realize that our undertaking was not trivial and could be seen as ambitious because relative energy difference between the two complexes amounts to just 3.3 kcal/mol.

Following commonly used methodologies, we have examined numerous individual local indices (structural and topological) and a very mixed picture emerged; seven pointed at NTA and only four at NTPA as forming the stronger complex with Be. Furthermore, none of them were decisively in favour of a particular complex or large enough to override the significance of others. Those in favour of NTA were: (i) a shorter coordination Be–N bond, (ii) longer distance between 'clashing' H-atoms which then were found as not interacting by the NCI analysis (three such contacts were found in BeNTPA), (iii) on average larger density at BCPs of coordination bonds, (iv) larger density at RCPs, (v) larger (more negative) interaction energy between Be and N-atom, (vi) smaller repulsive interaction energy between O-atoms in the coordination sphere, and finally (vii) the sum of interaction energy of all coordination bonds. Considering descriptors pointing at BeNTPA: (i) slightly shorter (by 0.002 Å) Be–O coordination bonds and associated with that larger, by 0.004 a.u., density at BCPs, (ii) marginally more stabilizing, by –0.6 kcal/mol, interaction energy between Be and O-atoms of the coordination bonds, (iii) less repulsive interaction between N and O atoms of the coordination sphere, and also (iv) the sum of all repulsive interaction energies between donor atoms of the coordination sphere was smaller in the BeNTPA complex.

Although geometrical (structural), QTAIM-, IQA- or NCI-defined properties provided lots of information and interesting insights on numerous physical and fundamental properties of these complexes, none of the techniques was able to provide the sought after answer. It became very clear that a different approach was required. This inspired us to develop a methodology based on the concept of molecular fragments and their properties, rather than pursuing a classical approach focused on individual (or paired) atoms and their properties. We have also realized that much more information might be gained when changes in properties rather than properties in the final product (here a metal complex) are analysed on a fundamental level. To this effect we have implemented a simplified, two-stage process of complex formation; Stage 1 involved pre-organization of a ligand from the lowest energy structure to that observed in the complex whereas Stage 2 involved binding between free metal ion and the pre-organized ligand. Furthermore, two fragments were used in Stage 2, namely a monoatomic, $\mathcal{M}$, consisting of the central metal ion, here Be, and polyatomic $\mathcal{L}$ (a ligand) needed for fragment-based analyses.

An in depth QTAIM-and IQA-based analysis allowed us to uncover the origin and physical nature of larger strain computed for NTPA when it attained a pre-organized structure. In general, the larger penalty energy in NTPA was mainly due to the contribution made by all possible interactions between N- and O-donor atoms. Density was dissipated into the surrounding atoms upon preorganization which resulted in the large destabilization of O(b)- and O(nb)-atoms and stabilization of C-atoms of carboxylic groups. Importantly, we have also found that all H-atoms of the ligands (this also includes those involved in steric contacts) play a negligible role when the contribution to the preorganization energy is considered; typically, their additive energies changed by a fraction of kcal/mol, hence they were not (de)stabilized to any significant degree. To summarize this part, the computed difference in the pre-organization energy for both ligands showed that, as it was found also for larger metal ions, NTPA is more strained than NTA (hence there must be some other energy sources to reverse this trend and make BeNTPA more stable) but, importantly, we could point at the origin of the intramolecular strain in both ligands and this allowed us to find the main contributor on one hand and eliminate a major classic suspect, steric CH--HC contacts, on the other.

For the purpose of Stage 2 of complex formation (binding process between Be and pre-organized ligand) we derived an expression for the binding energy, $E_{\text{bind}} = E_{\text{def}}^{\mathcal{M}} + E_{\text{def}}^{\mathcal{L}} + E_{\text{int}}^{\mathcal{M}_c,\mathcal{L}_c}$,

which is expressed in molecular fragments energy terms, deformation energies of metal and ligand fragments and inter-fragment interaction energy. The computed difference, ΔE_{bind}, fully recovered the experimentally observed relative stability of these two complexes. Furthermore, it became obvious that the energy source of higher stability of BeNTPA (i) is not related to coordination bonds (they were found stronger in BeNTA) but (ii) it comes from the overall more stabilizing contribution made by all possible interactions Be is involved in with all atoms of NTPA, the inter-fragment interaction energy term, $E_{\text{int}}^{\mathcal{M},\mathcal{L}}$. The deformation energy, $E_{\text{def}}^{\mathcal{M}} = \Delta E_{\text{self}}^{\mathcal{M}}$, for a metal ion (it accounts for the change in self-atomic energy of Be on transition from the free to complexed state) has almost identical values in both complexes (the difference being within one kcal/mol). Deformation energy $E_{\text{def}}^{\mathcal{L}} = \Delta E_{\text{self}}^{\mathcal{L}} + \Delta E_{\text{int}}^{\mathcal{L}}$ for the ligands accounts for changes in all atoms self-energies and intra-fragment diatomic interactions of the ligand fragment $\mathcal{L}$; for both ligands we found $E_{\text{def}}^{\mathcal{L}} \geq +120$ kcal/mol with that for NTPA being ~12 kcal more significant. However, it was fully compensated over by the difference in the $E_{\text{int}}^{\mathcal{M},\mathcal{L}}$ term which was found to be ~–22 kcal/mol more in favour of BeNTPA. Having established main source of higher BeNTPA stability we decided to search for its origin. The inspection of all intramolecular interactions Be is involved in both complexes revealed that all negatively charged atoms (N- and both O-atoms of carboxylic group) are involved in highly stabilizing interactions with Be whereas all remaining atoms are involved in repulsive interactions with Be, but overall they are by far less significant. Interestingly and somewhat unexpectedly, the total contribution made by attractive interactions was more significant in BeNTA by ~–22 kcal/mol. However, the sum of repulsive interaction was significantly smaller for BeNTPA by ~44 kcal/mol. Hence, the following picture emerged. The large attractive interactions between donor atoms and Be (they are in the range between –420 and –485 kcal/mol) can be seen as driving the complex formation to completion. Moreover, they are strongly assisted by interactions between Be and remaining O-atoms of carboxylic groups which are in the range between –190 and –195 kcal/mol in both complexes. The large energy released, more than –2500 kcal/mol, is partly compensated by positive (destabilizing) interactions and the larger compensation observed in BeNTA resulted in the more stable BeNTPA. This is an entirely unexpected, but highly informative, result as the relative stability of molecular systems does not have to be controlled by the strongest interactions (here coordination bonds). These results indicate a combined

effect of other and much smaller in value energy sources which might decide on preferential formation of a system.

This is the first and, in our opinion, highly successful implementation of fragment-based interpretation of metal complexes relative stability, which must be seen as of general purpose. It is easy to imagine that the same protocol can be used in the study of, *e.g.*, preferential reaction path to predict most likely product of either organic or inorganic reaction, or preferential protonation site from which a protonation sequence could be predicted. An added value of the proposed protocol is gaining an invaluable insight (on a fundamental level) on the nature and origin of parameters controlling preferred formation of a compound.

References

[1] Martell, A. E.; Hancock, R. D. *Metal Complexes in Aqueous Solutions*, Plenum Press: New York, 1996.

[2] NIST Standard Reference Database 46. NIST Critically Selected Stability Constants of Metal Complexes Database, version 8.0; Database collected and selected by Smith, R. M., A.E.; US Department of Commerce, National Institute of Standards and Technology: Gaithersburg, MD, 2004.

[3] Govender, K.K.; Cukrowski, I. *Inorg. Chem.* **2010**, *49*, 6931–6941.

[4] Cukrowski, I.; Govender, K.K.; Mitoraj, M.; Srebro, M. *J. Phys. Chem. A.* **2011**, *115*, 12746–12757.

[5] da Silva, C. O.; da Silva, E. C., Nascimento, M.A.C. *J. Phys. Chem. A.* **1999,** *103*, 11194-11199.

[6] Sarcino, G. A. A.; Improta, R.; Barone, V. *Chemical Physics Letters* **2003**, *373*, 411–415.

[7] Liptak, M. D.; Gross, K. C.; Seybold, P.G.; Feldgus, S.; Shields, G.C. *J. Am. Chem. Soc.* **2002**, *124*, 6421-6427.

[8] Namazian, M.; Zakery, M.; Noorbala, M.R.; Coote, M.L. *Chemical Physics Letters* **2008**, *451*, 163–168.

[9] Liton, M.A.K.; Ali, M.I.; Hossain, M.T. *Computational and Theoretical Chemistry*, **2012**, *999*, 1–6.

[10] Kelly, C.P.; Cramer, C.J.; Truhlar, D.G. *J. Phys. Chem. A.* **2006,** *110*, 2493-2499.

[11] Jorgensen, W.L.; Briggs, J.M. *J. Am. Chem. Soc.* **1989,** *111*, 4190-4197.

[12] Govender, K.K.; Cukrowski, I. *J. Phys. Chem. A.* **2010**, *114*, 1868–1878.

[13] Govender, K.K.; Cukrowski, I. *J. Phys. Chem. A.* **2009,** *113*, 3639–3647.

[14] Namazian, M.; Halvani, S.; Noorbala, M.R. *Journal of Molecular Structure: THEOCHEM* 2004, *711*, 13–18.

[15] Sanf-Aroon, W.; Ruangpornvisuti, V. *International Journal of Quantum Chemistry* **2008**, *108*, 1181–1188.

[16] Benson, M.T.; Moser, M.L.; Peterman, D.R.; Dinescu, A. *Journal of Molecular Structure: THEOCHEM* 2008, *867*, 71–77.

[17] Liptak, M.D.; Shields, G.C. *International Journal of Quantum Chemistry* **2001**, *85*, 727–741.

[18] Harding, A.P.; Wedge, D.C.; Popelier, P.L.A. *J. Chem. Inf. Model.* **2009,** *49*, 1914–1924.

[19] Bodnarchuck, M.S.; Heyes, D.M.; Dini, D.; Chahine, S.; Edwards, S. *J. Chem. Theory Comput.* **2014**, *10*, 2537−2545.

[20] Pliego, J.R., Riveros, J.M. *J. Phys. Chem. A* **2002,** *106*, 7434-7439.

[21] Hancock, R.D.; Bartolotti L.J. *Inorganica Chimica Acta* **2013**, *396*, 101–107.

[22] Hancock, R.D.; Bartolotti L.J. *Inorg. Chem.* **2005**, *44*, 7175-7183.

[23] Hancock, R.D. ***Acc. Chem. Res.*** **1990**, *23*, 253-257.

[24] Alder, A.C., Siegrist, H.; Gujer, W.; Giger, W. *Wat. Res.***1990**, *24*, 733-742.

[25] Hainfield, J.F.; Liu, W. Halsey, C.M.R., Freimuth, P.; Powell, R.D. *Journal of Structural Biology* **1999**, *127*, 185–198.

[26] Shannon, R. D. *Acta Crystallogr Sect. A* **1976**, *A32*, 751–767.

[27] Hancock, R. D. *Acc. Chem. Res.* **1990**, *23*, 253–257

[28] Hancock, R. D.; de Sousa, A. S.; Walton, G. B.; Reibenspies, J. H. *Inorg. Chem.* **2007**, *46*, 4749–4757.

[29] Thom, V. J.; Fox, C. C.; Boeyens, J. C. A.; Hancock, R. D. *J. Am. Chem. Soc.* **1984**, *106*, 5947–5955.

[30] Hambley, T. W. *J. Chem. Soc., Dalton Trans.* **1986**, 565–569.

[31] Hancock, R.D.; Nikolayenko, I.V. *J. Phys. Chem. A.* **2012**, *116*, 8572−8583

[32] Hancock, R.D. *Chem. Soc. Rev.* **2013**, *42*, 1500–1524.

[33] Bader, R.W.F. *Atoms in Molecules: A Quantum Theory*, Oxford University Press: Oxford, U.K., 1990.

[34] Bader, R. F. W. *J. Phys. Chem. A* **2009**, *113*, 10391–10396.

[35] Cioslowski, J.; Mixon, S.T.; *Can. J. Chem.* **1992**, *70*, 443-449.

[36] Cioslowski, J.; Mixon S.T. *J. Am. Chem. Soc.***1992**, *114*, 4382–4387.

[37] Jimenez-Vazquez, H.A.; Tamariz, J.; Cross, R.J. *J. Phys. Chem. A.* **2001**, *105*, 1315–1319.

[38] Kobayashi, K.; Nagase, S. *Chem. Phys. Lett*. **2002**, *362*, 373–379.

[39] Haaland, A.; Shorokhov, D.J.; Tverdova, N.V. *Chem.–Eur. J.* **2004**, *10*, 4416–4421.

[40] Jablonski, M.J.; *Phys. Chem. A.* **2012**, *116*, 3753–3764.

[41] Cerpa, E.; Krapp, A.; Flores-Moreno, R.; Donald, K.J.; Merino, G. *Chem.–Eur. J.* **2009**, *15*, 1985–1990.

[42] Popov, A.A.; Dunsch, L. *Chem.–Eur. J.* **2009**, *15*, 9707–9729.

[43] Dem'yanov, P.; Polestshuk, P. *Chem.–Eur. J.* **2012**, *18*, 4982–4993.

[44] Poater, J.; Solà, M.; Bickelhaupt, F.M. *Chem.–Eur. J.* **2006**, *12*, 2889–2895.

[45] Poater, J.; Solà, M.; Bickelhaupt, F.M. *Chem.–Eur. J.* **2006**, *12*, 2902–2905.

[46] Poater, J.; Visser, R.; Solà, M.; Bickelhaupt, F.M. *J. Org. Chem.* **2007**, *72*, 1134–1142.

[47] Krapp, A.; Frenking, G. *Chem. Eur. J.* **2007**,*13*, 8256–8270

[48] Grimme, S.; Mück-Lichtenfeld, C.; Erker, G.; Kehr, G. Wang, H.; Beckers, H.; Willner, H. *Angew. Chem. Int. Ed.* **2009**, *48*, 2592–2595.

[49] Bader, R.W.F. *J. Phys. Chem. A* **2011**, *115*, 12432–12435.

[50] Matta, C.F.; Hernández-Trujillo, J.; Tang, T.H.; Bader, R.F.W.; *Chem.–Eur. J.* **2003**, *9*, 1940–1951.

[51] Bader, R.F.W. *Chem.–Eur. J.* **2006**, *12*, 2896–2901.

[52] Bader, R.F.W.; Fang, D.C. *J. Chem. Theory Comput.* **2005**, *1*, 403-414.

[53] von Hopffgarten, M.; Frenking, G. *Chem.–Eur. J.* **2008**, *14*, 10227–10231.

[54] Grabowski, S.J.; Ugalde, J.M. *J. Phys. Chem. A.* **2010**, *114*, 7223–7229.

[55] Frenking, G.; Hermann, M.; *Angew. Chem.* **2013**, *125*, 6036–6039.

[56] Danovich, D.; Shaik, S.; Rzepa, H.S.; *Angew. Chem. Int. Ed.* **2013**, *52*, 5926–5928.

[57] Weinhold, F.; *J. Comp. Chem.* **2012**, *33*, 2440–2449.

[58] Cukrowski, I.; de Lange, J.H.; Mitoraj, M.; *J. Phys. Chem. A.* **2014**, *118*, 623–637

[59] Cukrowski, I.; Matta, C. *Chemical Physics Letters* **2010**, *499*, 66–69.

[60] Varadwaj, P.R.; Cukrowski, I.; Perry, C.B.; Marques, H.M. *J. Phys. Chem. A* **2011**, *115*, 6629–6640

[61] Varadwaj, P.R., Cukrowski, I., Marques, H.M., *J. Phys. Chem. A* **2008,** *112*, 10657–10666

[62] Varadwaj, P.R., Cukrowski, I., Marques, H.M., *Journal of Molecular Structure: THEOCHEM* **2009**, *902*, 21–32

[63] Johnson, E. R.; Keinan, S.; Mori-Sánchez, P.; Contreras-García, J.; Cohen, A. J.; Yang, W. *J. Am. Chem. Soc.* **2010**, *132*, 6498−6506.

[64] Contreras-García, J.; Johnson, E. R.; Keinan, S.; Chaudret, R.; Piquemal, J. P.; Beratan, D.; Yang, W. *J. Chem. Theory Comput.* **2011**, *7*, 625−632.

[65] Gillet, N.; Chaudret, R.; Contreras-García, J.; Yang, W.; Silvi, B.; Piquemal, J. P., *J. Chem. Theory Comput.* **2012**, *8*, 3993−3997.

[66] Contreras-García, J.; Yang, W.; Johnson, E. R. *J. Phys. Chem. A* **2011**, *115*, 12983−12990.

[67] Blanco, M. A.; Pendás, A. M.; Francisco, E. *J. Chem. Theory Comput.* **2005**, *1*, 1096−1109.

[68] Francisco, E.; Pendás, A. M.; Blanco, M. A. A. *J. Chem. Theory Comput.* **2006**, *2*, 90−102.

[69] Pendás, A. M.; Blanco, M. A.; Francisco, E. *J. Comput. Chem.* **2006**, *28*, 161−184.

[70] (2010) *Spartan 10, Wavefunction Inc.*.Irvine, CA 92612, USA.

[71] M. J. Frisch, G. W. Trucks, H. B. Schlegel, G. E. Scuseria, M. A. Robb, J. R. Cheeseman, G. Scalmani, V. Barone, B. Mennucci, G. A. Petersson, H. Nakatsuji, M. Caricato, X. Li, H. P. Hratchian, A. F. Izmaylov, J. Bloino, G. Zheng, J. L. Sonnenberg, M. Hada, M. Ehara, K. Toyota, R. Fukuda, J. Hasegawa, M. Ishida, T. Nakajima, Y. Honda, O. Kitao, H. Nakai, T. Vreven, J. A. Montgomery, Jr., J. E. Peralta, F. Ogliaro, M. Bearpark, J. J. Heyd, E. Brothers, K. N. Kudin, V. N. Staroverov, R. Kobayashi, J. Normand, K. Raghavachari, A. Rendell, J. C. Burant, S. S. Iyengar, J. Tomasi, M. Cossi, N. Rega, J. M. Millam, M. Klene, J. E. Knox, J. B. Cross, V. Bakken, C. Adamo, J. Jaramillo, R. Gomperts, R. E. Stratmann, O. Yazyev, A. J. Austin, R. Cammi, C. Pomelli, J. W. Ochterski, R. L. Martin, K. Morokuma, V. G. Zakrzewski, G. A. Voth, P. Salvador, J. J. Dannenberg, S. Dapprich, A. D. Daniels, Ö. Farkas, J. B. Foresman, J. V. Ortiz, J. Cioslowski, and D. J. Fox, Gaussian 09, Revision D.1, Gaussian, Inc., Wallingford CT, 2009.

[72] A. Keith, AIMAll (Version 13.11.04), TK Gristmill Software, Overland Parks KS, USA, 2013 (aim.tkgristmill.com).

[73] Tognetti, V.; Joubert, L.; *J. Chem. Phys.* **2013**, *138*, 024102-024108.

[74] Xu, X.; Goddard, W.A. *Proc. Natl. Acad. Sci.* USA, **2004**, *101*, 2673.

[75] Perdew, J.P.; Burke, K.; Ernzerhof, M. *Phys. Rev. Lett.* **1996**, *77*, 3865.

[76] Hyla-Kryspin, I.; Haufe, G.; Grimme, S. *Chem. Eur. J.* **2004**, *10*, 3411.

[77] Hammer, B.; Hansen, L.B.; Nørskov, J.K. *Phys. Rev. B.* **1999**, *59*, 7413.

[78] Zhang, Y.; Yang, W. *Phys. Rev. Lett.* **1998**, *80*, 890.

[79] Maximoff, S.N.; Peralta, J.E.; Barone, V.; Scuseria, G.E. *J. Chem. Theory Comput.* **2005,** *1*, 541.

[80] Humphrey, W.; Dalke, A.; Schulten, K. *J. Molec. Graphics* **1996**, *14*, 33–38.

[81] Cukrowski, I.; de Lange, J. H.; Adeyinka, A. S.; Mangondo, P. *Comput. Theoret. Chem.* **2015**, *1053*, 60–76.

[82] Bader, R. F. W.; Essen, H. *J. Chem. Phys.* **1984**, *80*, 1943–1960

[83] Espinosa, E.; Alkorta, I.; Elguero, J.; Molins, E. *J. Chem. Phys.* **2002**, *117*, 5529−5542

[84] Flaig, R.; Koritsanszky, Dittrich, B.; Wagner, A.; Luger, P. *J. Am. Chem. Soc.* **2002**, *124*, 3407-3417

[85] Pendás, A.M.; Francisco, E.; Blanco, M.A.; Gatti, C.; *Chem.–Eur. J.* **2007**, *13*, 9362–9371.

[86] Lane, J.R.; Contreras-Garcia, J.; Piquemal, J.; Miller, B.J.; Kjaergaard. *J. Chem. Theory Comput.* **2013**, *9*, 3263−3266

[87] Mitoraj, M. P.; Michalak, A.; Ziegler, T. *J. Chem. Theory Comput.* **2009**, *5*, 962-975.

[88] Mitoraj, M. P.; Michalak, A.; Ziegler, T. *Organometallics* **2009**, *28*, 3727–3733.

[89] Mitoraj, M. P. *J. Phys. Chem. A.* **2011**, *115*, 1470814716.

[90] Bader, R.W.F.; Matta, C.F. *J. Phys. Chem. A.* **2006**, *110*, 6365–6371.

[91] McWeeny, R. *Methods of Molecular Quantum Mechanics*, 2nd ed., Academic Press, London, 1992.

[92] Pendás, A. M.; Blanco, M. A.; Francisco, E. *J. Chem. Phys.* **2006**, *125*, 184112-19.

4. The Introduction of a Holistic Model to the Complex Formation Process. A Computational Investigation of Zn^{II} Complexes as a Case Study Using an IQA/IQF-based Protocol

Abstract

Classically, as chemists we have become heavily reliant on describing molecular stability by analysing individual interactions and inferring a global molecular effect. Whilst that approach excellently explains the behaviour of simple systems, it often fails for more complex systems. In this work the Zn^{II} complexes of NTA and NTPA are thoroughly investigated to explain the preferential formation of ZnNTA in solution. Analysis of individual interactions using a battery of local indices shows that such an approach is often cumbersome and produces a clatter of numerical values which provide little insight. Proposed here is a nuanced approach which recognises that complex formation is a process and hence should be analysed as a sequence of events. As such, a simplified two stage process is used to decompose the formation of the complex where in the first stage the fragments of the complex must preorganise and in the second stage preorganised fragments must bind together. IQA- and IQF-based analysis of the stages reveals that preorganization of the ligand fragment is destabilising due to the formation of unfavourable interactions between the coordinating atoms. On the other hand, in order to accommodate the ligand around the metal centre, the Zn–O(w) bonds (where O(w) points at O-atom of a coordinated water molecule) must elongate; as a result they become somewhat destabilized (weaker). This work shows that the preferential formation of ZnNTA is not due to the size of a coordination 5-membered ring as commonly considered but almost entirely due to the fact that the ligand NTA is smaller hence occupying less space around the metal centre and thus the Zn–O(w) interactions (or coordination bonds) are less destabilised. As a result, the Zn–O(w) coordination bonds are shorter in ZnNTA than in ZnNTPA making the former more stable.

Introduction

Molecular stability is both a necessary and puzzling chemical phenomenon: necessary because it is the central focus of most, if not all, chemistry and it is puzzling because there are numerous and, at times, contradictory accounts explaining molecular stability. With the development and progression of chemical techniques, there has been significant improvement in the measurement of molecular stability, quite often using thermodynamic constants such as the enthalpy of formation, formation (stability) constants and protonation constants. There is one important caveat associated with this information: whilst one identifies trends and patterns in the molecular stability, this cannot provide the fundamental understanding of why one molecular system is more stable than the other. The direct implication is that there is no chemical meaning and understanding of the phenomenon.

This does not imply that there have been no attempts at explaining these experimental trends. In fact, there have been numerous attempts at explaining molecular stability, which have gradually grown into two general approaches. The first approach interprets molecular stability by understanding the properties in the final structure of molecule, primarily focusing on the individual interactions or properties. Considering trends in complex stability,[1] they have primarily been accounted for by: (i) lone-pair repulsion between electron rich atoms such as oxygen and nitrogen, (ii) steric repulsion in crowded environments, (iii) coordination bond strength, (iv) the size of the central metal cation, and (v) inductive effects to a lesser degree.[2–6] The influence of some of these factors has become contentious, *e.g.*, steric repulsion between H-atoms in crowded environments, particularly due to the Quantum Theory of Atoms in Molecules (QTAIM).[7] QTAIM defines molecular structure by obtained ridges of maximum electron density between atoms called atomic interaction lines (AILs) or bond paths (BPs). These AILs where considered bonding and hence have a stabilizing effect on molecules.[8] The discovery of AILs between atoms in crowded steric environments contradicted the classical interpretation of the CH•••HC interaction.[9-17] This resulted in a lengthy and intensive discussion around the nature of these interactions, and the meaning and interpretations of QTAIM.[5,8,17-33] Two camps have emerged from this debate: (i) one which staunchly believes that the presence of the AIL leads to a lowering of the overall energy of the molecule, even when present in traditionally steric environments, and (ii) the other camp which states that the CH•••HC interactions are always repulsive and hence destabilizing regardless of local chemical environment. Whilst this debate has been valuable by forcing

chemists to deepen their understanding of fundamental chemical concepts it is still inconclusive as there have been no concessions from either party. Moreover, the disproportionate focus on CH•••HC interactions meant that the other factors were largely ignored or unanalysed. Considering that the nature of one of the most prevelant factors (the CH•••HC interaction) is now questionable, is there any way to explain the relative trends in complex stability?

The second approach to understanding molecular stability attempts to understand the relative stability of molecular systems by analysing the energetic changes as the molecular system changes from one to another.[34-37] This has been done in a variety of methods including reaction mechanisms, and decomposition schemes. Decomposition schemes involve breaking the molecule into either real or artificial fragments. The value of these schemes lies in the ability to recover experimental trends as determined by thermodynamic constants. Additionally, the energetic effect of the structural changes that occur when a molecule goes from the lowest energy form to a higher energy form can be measured. While these approaches are meaningful and successfully recover the experimental trends of relative stability (especially when used together), they aggregate effects into global changes and lack resolution at an atomic and interatomic level.

In order to explore the complex question of molecular stability we have selected the following chemical phenomenon: it is known that most metal cations will selectively bind to ligands to which five-membered chelate rings (5m-CR) rather than to six-membered chelate rings (6m-CR) except when the metal cation is very small. The complexes of NTA (nitrilotriacetic acid) and NTPA (nitrilotri-3-propionic acid) have been selected for this investigation. Most metal complexes will selectively complex to NTA, which forms three 5m-CR, as opposed to the NTPA, which forms three 6m-CR, *e.g.*, Cd^{II}NTA with $\log K_1 = 9.76$ and Cd^{II}NTPA with $\log K_1 = 3.4$.[38] The Be^{II} complexes are the only known example where NTPA is the preferentially formed complex *i.e.*, for BeNTPA, $\log K_1 = 9.23$ and for BeNTA, $\log K_1 = 6.84$.[38]

Ni^{II} [39] and Zn^{II} complexes of NTA and NTPA were the subjects of prior investigations.[33,40] It was concluded that the most likely cause of preferential complex stability of NTA over NTPA is due to the strain incurred when the ligand framework is preorganized. Additionally, it was shown that analysing individual interactions (such as coordination bonds) regardless of the technique (structural, QTAIM) could not fully explain the experimental trend. Moreover,

using the Electronic Transition State with the Natural Orbital for Chemical Valence (ETS-NOCV)[34-36] scheme, it was determined that for the Zn^{II} complexes (i) the distortion or preparation energy (energy required to preorganize the Zn^{II} fragments and the ligand fragments) was strongly destabilizing and in favour of ZnNTA, (ii) the interaction energy (the energy released when the two preorganized fragments bond to form the complex) is strongly stabilizing and in favour of ZnNTPA, and (iii) the bonding or binding energy related to the combination of the distortion and the interaction energies was firmly in favour of ZnNTA, reaffirming that the differences in formation constants is largely due to the greater strain not only in the ligand but also in the hydrated Zn^{II} fragment of ZnNTPA.

The focus of this work is on the Zn^{II} complexes of NTA ($\log K_1$ = 10.45 at 25 °C, μ = 0.1 M KCl) and NTPA ($\log K_1$ = 5.3 at 25 °C, μ = 0.1 M KNO_3) where ZnNTA is preferentially formed with a difference in the formation constants of about 5.7.[38] In order to ensure that the most suitable solvent-optimized complexes are selected for analysis, a competition reaction is used and based on the prediction of the experimental trend; from that a level of theory will be selected for all subsequent analysis. The study is then dedicated to understanding the relative stability of the complexes from the perspective of individual interactions by analysing (i) geometric properties of the coordination bonds, steric contacts and chelating rings, (ii) QTAIM[7] topological properties, to characterize and measure the strength of intramolecular interactions linked by AILs, (iii) intramolecular interactions decovered by NCI (Non-Covalent Interactions)[41-44] isosurfaces, particularly those not revealed in QTAIM, and (iv) the interaction energies, using the Interacting Quantum Atoms (IQA) method,[45-47] will be used to determine the strength and the nature of selected interactions. Following these analyses, will be a detailed discussion of the factors influencing relative complex formation based on simplified two stage model in which (i) fragments containing metal ion and ligands are preorganized, and (ii) the preorganized fragments bind together to form the complex. QTAIM, NCI and IQA will be used to monitor the changes in the molecular system, for each step of the complex formation. Finally, the binding energy between the two fragments will be investigated using IQA and the Interacting Quantum Fragments technique.[47]

Computational Details

The free ligands of NTA and NTPA were submitted for a full conformational search in Spartan 10.[48] Geometry optimizations of the SPARTAN generated ligand conformers and the lowest energy conformers of Zn^{II} complexes obtained from previous studies[40] were performed in Gaussian 09 revision D,[49] at the PBE1PBE, B3LYP, X3LYP and MP2(FC) levels of theory. Only the MP2 optimized Zn^{II} complexes generated the expected octahedral complex and hence they were selected for further computations and studies. In order to have the structural benefit of the MP2-optimized structures but to minimize the computational expense and obtain free energies necessary to compute formation constants, single point frequency calculations (SPFC) were carried out on the MP2 optimized structures at PBE1PBE, B3LYP and X3LYP. To compute the preorganization and binding energies for each complex, single point energy calculations were performed at all levels of theory on the pre-organized ligands, $\mathcal{L}_p$, the pre-organized metal-containing fragment for each complex, $\{Zn(H_2O)_2\}_p = (\mathcal{M}_w)_p$ and the free metal-containing fragment, $(\mathcal{M}_w)_f$ – an example of the fragments selected for ZnNTA is shown Figure 4.1a. To obtain the $(\mathcal{M}_w)_f$ fragment, the fully hydrated zinc complex,

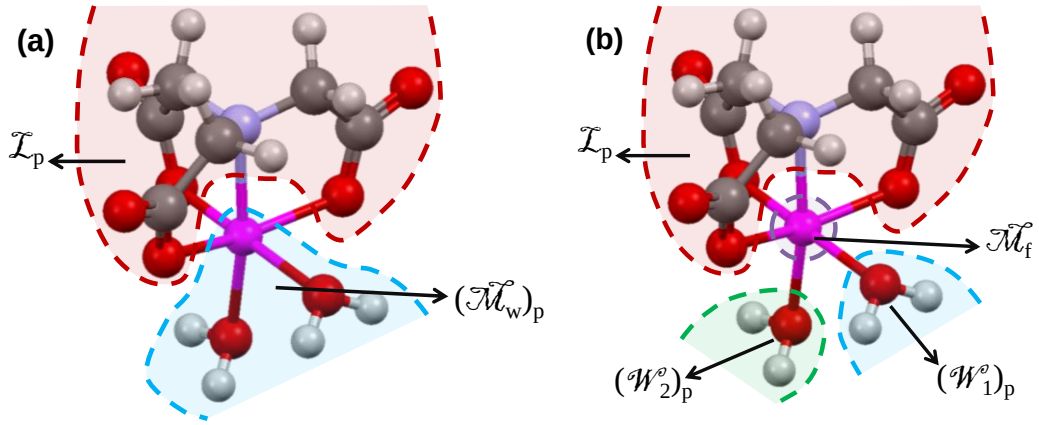

Figure 4.1. The fragments selected for the computation of the binding energy of metal complexes (a) a 2-component partitioning and (b) a 4-component partitioning.

$[Zn(H_2O)_6]^{2+}$, was optimized in solvent at the MP2 level of theory. Different diaqua fragments $[Zn(H_2O)_2]^{2+}$ were generated and single point calculations were performed. The lowest energy fragment was selected for computation of the preorganization energy of the metal-containing fragment. To verify the selection of the $[Zn(H_2O)_2]^{2+}$ fragment ($\mathcal{M}_w$), a higher energy fragment was used to determine relative IQA energies for the preorganization of the metal-

containing fragments; the preorganization energies of the highest and lowest energy $\mathcal{M}_w$ fragments were found to be identical to the first decimal place in kcal/mol. Alternatively, the binding energy was determined as the energy released when the ligand $\mathcal{L}_p$, metal centre, $\mathcal{M}_f$, and two water molecules, $(\mathcal{W}_1^o)_p$ and $(\mathcal{W}_2^o)_p$, form the complex. In this instance single point calculations were required of the preorganized water molecules and the free Zn^{2+} ion. The individual fragments are shown in Figure 4.1b.

The electronic structure calculations were performed with the 6-311++G(d,p) basis set modelled with implicit solvation (PCM/UFF) and water as the solvent. Selected wavefunctions were submitted for topological analysis and for the determination of IQA defined properties using the AIMAll package.[50] IQA energy terms contain two-electron components and hence require a level of theory with a well-defined 2nd order density matrix. However, these energy terms also make the calculation computationally expensive. In the AIMAll package, all post-HF wavefunctions, including DFT, make use of a Müller approximation of the 2nd order density matrix to minimize the expense of the computation. Given that there is a reasonable approximation of the 2nd order density matrix and that previously,[51] reasonable approximations of IQA energies have been obtained using DFT wavefunctions, we used an X3LYP wavefunction to determine the IQA-related energy components. Furthermore, because our focus is on relative trends rather than predicting energy terms on an absolute scale, we are convinced that qualitative results and the conclusions arrived at from this work should be considered as valid. NCI-isosurfaces were determined using NCIPlot 2.0[42] and these isosurfaces were visualized using VMD 1.9.1. One-dimensional cross-sections of the electron density along the λ_2 eigenvector of the Hessian matrix were performed using in-house software according the procedure detailed in a previous work.[52]

Results and Discussion

Preliminary Investigations

Selection of Suitable Theory Level

A protocol based on competition reaction, CRn (see Eq. 4.1), described for Be^{II} complexes, (for convenience details are shown as PART 1 in the Appendix B) was used to

validate optimized structures and select the most economic and suitable level of theory for further

$$\text{ZnNTA} + \text{NTPA} \leftrightarrow \text{ZnNTPA} + \text{NTA} \quad K_{\text{CRn}} = \frac{[\text{ZnNTA}][\text{NTPA}]}{[\text{ZnNTPA}][\text{NTA}]} \qquad (4.1)$$

computations. The equilibrium constant for such a competition reaction can be determined by the difference of the formation constants of the competing complexes, here logK_{CRn} of 5.15. This can be converted into the free energy of the competition reaction using the well-known relationship, $\Delta G = -RT\ln K$, and a conversion factor of 1.36 kcal/mol. In this instance, ΔG_{CRn} = –7.0 kcal/mol. In this section we will validate the lowest energy conformers[39,53-54] used in computations by obtaining reasonable predictions of the experimental trend in formation constants. The structures of ligands and complexes for which ΔG_{CRn} and ΔE_{CRn} have been computed are shown in Figures B1 and B2 in the Appendix B. Data obtained are shown in Tables 4.1. and 4.2.

Table 4.1. Computed equilibrium constants, as logK_{CRn}, for the competition reaction (4.1) using the lowest energy conformers of the ligands and complexes.

	G(aq)/au						
Method	ZnNTPA	NTA	ZnNTA	NTPA	ΔG_{CRn} [b]	logK_{CRn}	$\Delta\log K$ [c]
PBE1PBE[a]	–2787.4999	–738.1393	–2669.7634	–855.8834	–4.8	3.5	–1.7
B3LYP[a]	–2788.9152	–738.9579	–2671.0350	–856.8529	–9.3	6.8	1.7
X3LYP[a]	–2788.4192	–738.6723	–2670.6029	–856.5015	–8.1	6.0	0.8

[a]free energy obtained by performing a single point frequency calculation on the RMP2 structure. [b]Value in kcal/mol. [c]$\Delta\log K$ = (theoretical – experimental) value.

Table 4.2. Computed ΔE_{CRn}, for the competition reaction for zinc ion using the lowest energy conformers of the ligands and complexes of NTA and NTPA.

	E(aq)/au				
Method	ZnNTPA	NTA	ZnNTA	NTPA	ΔE_{CRn} [b]
PBE1PBE[a]	–2787.7180	–738.2275	–2669.8990	–856.0522	–3.6
B3LYP[a]	–2789.1318	–739.0440	–2671.1665	–857.0189	–6.0
X3LYP[a]	–2788.6367	–738.7590	–2670.7357	–856.6684	–5.2

[a] electronic energy obtained by performing a single point frequency calculation on the RMP2 structure at the level of theory of interest in solvent (PCM/UFF) using the 6-311++G(d,p) basis set. [b] value in kcal/mol.

It is clear that the predictions using SPFCs worked well, as was the case with Be^{II} complexes, predicting, in this case, the preferential formation of ZnNTA. At the X3LYP level of theory, a logK_{CRn} prediction of analytical quality ($\Delta \log K$ = 0.8) was obtained. Considering that a molecule's energy is hundreds of thousands or even millions kcal/mol (*e.g.*, for ZnNTPA we obtained ~1.75 million kcal/mol at X3LYP), a small deviation of 1.1 kcal/mol from the experimental ΔG_{CRn} value must be seen as an excellent result. While thermodynamic data is typically computed using energy minimized structures, the excellent prediction of the experimental trend and the absence of negative frequencies, seems to suggest that the structures are close enough to energy minima to be considered valid. Recall that ΔE_{CRn} is necessary as all quantum topological techniques, such as QTAIM and IQA, decompose the electronic energy and not the Gibbs Free Energy. Once again and importantly, ΔE_{CRn} excellently reproduces the experimental trend which favours the formation of ZnNTA. Thus, even if the thermodynamic data is assumed to be not valid (note that G values will not and cannot be used in tracking the origin of relative stability of chemical compunds), the electronic energies validate these structures. These results gave us the confidence to explore the full array of interactions using various geometrical, topological, and energetic properties.

Analysis of Coordination Bonds

In order to understand the factors contributing to complex stability, we also analysed selected properties that have been commonly used to interpret the relative stability of metal complexes. This section focuses on analysing coordination bonds using geometrical, topological, and IQA approaches – relevant data is shown in Table 4.3 and full sets of data at the critical points are shown in Tables B2 to B5 in the Appendix B. To distinguish between the different O-atoms, O(b) will represent a carboxylic oxygen atom in the ligand which is bonded to the Zn centre, O(nb) will represent a carboxylic O-atom which is not bonded to the zinc metal centre and O(w) will be used to represent the donor O-atoms in water molecules.

Analysis of the various coordination bonds reveals that the geometric trend d(Zn–O^-) < d(Zn–N) < d(Zn–O(w)) follows the trend in interaction energies, $E_{int}^{Zn,O^-} < E_{int}^{Zn,N} < E_{int}^{Zn,O(w)}$, and the shorter bonds had stronger (most negative) interaction energies in both complexes. Furthermore, all coordination bonds showed some mixed (covalent and ionic) character based on the $|V(r)|/G(r)$ ratio (recall that for covalent bonds $|V(r)|/G(r) > 2$ applies and $|V(r)|/G(r) <$ 1 suggests an ionic bond), but with no correlation to the bond length nor the interaction

energy. The Zn–N bond in both complexes shows the most covalent contribution as also found in Be^{II} complexes with NTA and NTPA. Similarly, there is no consistent trend between d(X,Y) and $\rho(r)$ at a bond critical point, and hence $E_{int}^{X,Y}$; note, that the Zn–N bond in ZnNTPA is shorter and less attractive (based on $E_{int}^{X,Y}$) however $\rho(r)$ is larger than in the ZnNTA. Classically, the inductive effect suggests that with the presence of additional carbon

Table 4.3. QTAIM-defined topological data at BCPs of the coordination bonds in ZnNTA and ZnNTPA at the X3LYP level of theory on the MP2 optimized structure.[a]

Bond (X–Y)	d(X,Y)	$\rho(r)$	$\nabla^2\rho(r)$	$\lvert V(r)\rvert/G(r)$	DI(A|B)	$E_{int}^{X,Y}$
			ZnNTA			
Zn–N	2.130	0.0688	0.2384	1.21	0.31	–273.2
Zn–O13(b)	2.060	0.0676	0.3092	1.11	0.33	–300.2
Zn–O15(b)	2.058	0.0677	0.3120	1.10	0.33	–300.8
Zn–O19(b)	2.057	0.0679	0.3142	1.10	0.32	–301.9
					Sum:	**–1176.1**
Zn–O21(w1)	2.222	0.0446	0.1826	1.12	0.19	–250.2
Zn–O22(w2)	2.139	0.0537	0.2389	1.10	0.23	–268.3
					Sum:	**–518.5**
					Total:	**–1697.6**
			ZnNTPA			
Zn–N	2.127	0.0692	0.2425	1.21	0.34	–272.0
Zn–O22(b)	2.019	0.0724	0.3567	1.09	0.35	–311.1
Zn–O25(b)	2.029	0.0699	0.3445	1.09	0.34	–306.8
Zn–O28(b)	2.037	0.0699	0.3374	1.09	0.34	–307.9
					Sum:	**–1197.8**
Zn–O30(w1)	2.356	0.0327	0.1238	1.11	0.15	–229.7
Zn–O31(w2)	2.242	0.0441	0.1682	1.14	0.21	–255.4
					Sum:	**–485.1**
					Total:	**–1682.9**

[a] d(X,Y) is the bond length measured in Å; $\rho(r)$ is the electron density at the bond critical point in au; $\nabla^2\rho(r)$ is the Laplacian of the electron density at the bond critical point in au; $\lvert V(r)\rvert/G(r)$ is the ratio of the kinetic energy density to the potential energy density at the bond critical point; DI(A|B) is the delocalization index between the two atoms in au, and $E_{int}^{X,Y}$ is the IQA interaction energy between the two atoms in the bond, in kcal/mol.

atoms in the chelating ring, there will be increased electron density in the surrounding regions. Noticeably, the Zn–N and Zn–O^- bonds have larger $\rho(r)$ at the critical points and this is indicative of the inductive effect in ZnNTPA and furthermore coincides with the comments of Hancock[1] which suggests that despite the presence of the inductive effect, the 6m-CR is

less favourable. *DI*(A,B) are comparable for the coordination bonds of Zn to the donor atoms of NTA and NTPA, and the coordination bonds with the water molecules consistently show less delocalization (note that $d(Zn–OH_2)_{ZnNTPA} > d(Zn–O^-)_{ZnNTA}$).

If one where to limit themselves to the coordination bonds between the metal cation and ligand of interest (Zn–N and Zn–O$^-$), then ZnNTPA would be predicted as the preferentially formed complex (the sum of the interaction energies is –1176.1 and –1197.8 kcal/mol in ZnTPA and ZnNTA, respectively) a contradiction of the experimental trend. Interestingly, the sum of the interaction energies to the water molecules is far more stabilizing in ZnNTA (–518.5 and –485.1 kcal/mol in ZnNTA and ZnNTPA, respectively). As a result, the total of these two sums favours ZnNTA by ~–15 kcal/mol. It is also important to note that the bonds to water molecules are consistently stronger in ZnNTA than in ZnNTPA, as these interactions have shorter inter atomic distances and larger, $\rho(r)$ and $\nabla^2\rho(r)$, *DI*(A|B) and $E_{int}^{X,Y}$ values. These findings strongly point at the coordinated water molecules as most likely responsible for relative stability of these complexes.

Analysis of Repulsion in the Coordination Sphere

Classically, complex stability has been associated with the repulsion between lone-pair donor atoms coordinating to the central metal cation. Figure 4.2 shows the molecular graphs and Figure 4.3 shows the NCI-isosurfaces for the ZnNTA and ZnNTPA complexes – relevant data is available in Table 4.4. The coordination bonds result in the three chelating rings in

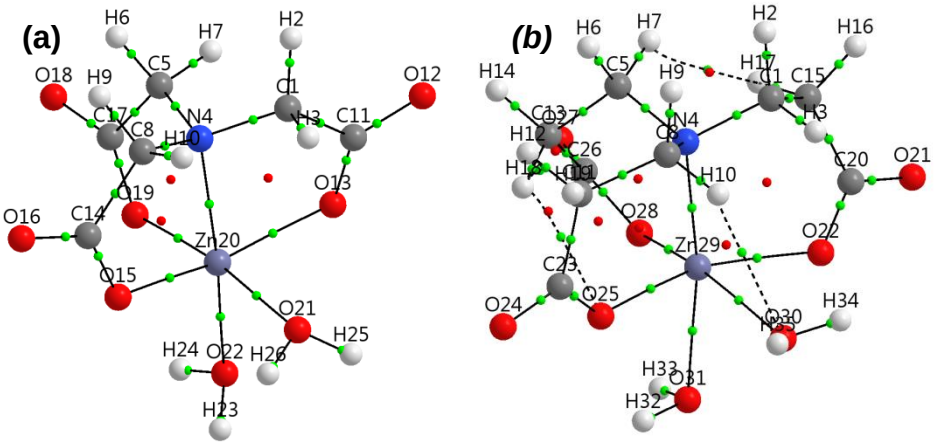

Figure 4.2. The QTAIM molecular graphs of the lowest energy conformers of (a) ZnNTA, and (b) ZnNTPA.

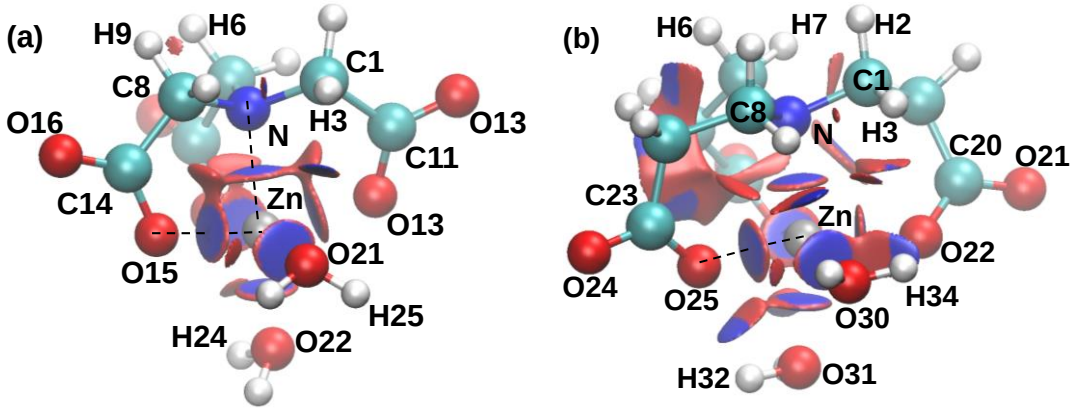

Figure 4.3. The NCI isosurfaces of the LECs of (a) ZnNTA, and (b) ZnNTPA with a RDG isovalue of 0.5 au and isosurfaces coloured from blue to red using –0.07 au ≤ sign(λ_2)×$\rho(r)$ ≤ +0.03 au.

Table 4.4. Geometric, NCI and IQA properties of repulsive interactions in the coordination spheres of ZnNTA and ZnNTPA at the X3LYP[a] level of theory on the MP2 optimized structure. Only data for atoms with d(X,Y) < sum of vdW radii is included.

Interaction (X•••Y)	d(X,Y)	*NCI*	$E_{int}^{X,Y}$
ZnNTA			
N•••O13	2.709	red-RCP	148.9
N•••O15	2.772	red-RCP	147.5
N•••O19	2.812	red-RCP	146.1
O19•••O15	3.001	None	155.3
O21•••O13	2.886	None	147.3
O21•••O15	2.823	Red	149.5
O22•••O19	2.813	Red	148.4
ZnNTPA			
N•••O22	3.087	red-RCP	130.4
N•••O25	3.016	red-RCP	133.6
N•••O28	3.050	red-RCP	133.0
O30•••O22	2.667	Red	154.2
O30•••O25	2.881	Red	148.8
O31•••O25	2.749	Red	153.7
O31•••O28	2.820	Red	152.1

[a]d(X,Y) is the interatomic distance measured in Å, and $E_{int}^{X,Y}$ is the IQA interaction energy between the two atoms, in kcal/mol.

both complexes, thus the associated ring critical points in the molecular graphs and the corresponding NCI-defined red isosurfaces. Table 4.4 only shows the interactions where the atomic distances were shorter than the sum of the van der Waals radii. In general, the O•••O interactions are more repulsive in ZnNTPA and all have the NCI-defined red isosurface in the interatomic region, which is indicative of electron density depletion – this is synonymous with strain within interatomic region. In contrast, only two O•••O interactions show such density depletion in ZnNTA, thus the other interactions are not strained as a result of deformation in the uniform density distribution despite an overall repulsive interaction energy. Considering deformation in the density distribution as a measure of strain in the molecule, it can be concluded that ZnNTPA is significantly more strained in the coordination sphere. Note that the largest value of $E_{\text{int}}^{\text{O,O}}$ is in ZnNTA, where $E_{\text{int}}^{\text{O19,O15}}$ is the most repulsive even though the interatomic distance is the largest and no NCI isosurface is observed. The data clearly shows that these descriptors (d(X,Y), NCI-coloured isosurface and E_{int}) do not have to correlate with each other. All the above can be used as an excellent textbook example illustrating the fact that a repulsive interaction (as computed from IQA) is not sinonimous with intramolecular strain as uncoverd by NCI in the form of red isosurfaces, regions with depleted density, a response of a crowded molecular environment to mimimize strain.

The mechanism for responding to crowded coordination environment is different between the Be^{II} and the Zn^{II} complexes. The interatomic distances between O(b)-atoms in Be^{II} complexes are significantly shorter than those in Zn^{II} complexes. The more closely crowded atoms in the coordination environment of Be^{II} complexes result in an unavoidable output of an excess of electron density, such as a free pair of electrons. This results in the local accumulation of electron density (blue isosurfaces) to minimize the large electrostatic repulsion between these atoms. The larger interatomic distances between N- and O(b)-atoms in Zn^{II} complexes, prevents free pairs of electrons overlapping in the interatomic region and hence depletion of electron density is the preferred mechanism. Furthermore, the excess in electron density is shared with H-atoms of the water molecule as shown by the blue isosurfaces in the interatomic region, resulting in bonding H-interactions in ZnNTPA.

Table B6 in the Appendix B contains the interaction energies for all repulsive interactions in the coordination sphere of ZnNTA and ZnNTPA. Note that the presence/absence of a short contact, or the presence/absence of an NCI-isosurface, is not indicative of the relative strength of an interaction. In fact, there are numerous interactions which are unaccounted for by the

interatomic distances and the NCI isosurfaces which have significant energetic contributions, *e.g.* for O25(b)•••O28(b) in ZnNTPA the interatomic distance is 3.217 Å, and $E_{int}^{X,Y}$ is 149.9 kcal/mol. The repulsive interactions of the coordination region (N•••O(b), N•••O(w), O(b)•••O(b), O(b)•••O(w), and O(w)•••O(w)) do not show a consistent trend and it is almost impossible to relate these interactions to the preferential complex stability. To gain further insight, the summed energy contributions show that (i) all coordination bonds including those to water molecules (–1694.7 and –1682.9 kcal/mol for ZnNTA and ZnNTPA, respectively) contribute towards the overall stability of the molecule but cannot override the overwhelming number of repulsive interactions which contribute 2019.3 and 1994.9 kcal/mol for ZnNTA and ZnNTPA, respectively, (ii) the total energy contribution made by the coordination bonds is more stabilizing in ZnNTA by ~–12 kcal/mol, (iii) the total destabilizing contribution made by repulsive interactions is smaller in ZnNTPA by 22 kcal/mol. The sum of all these diatomic interactions *in the coordinating region* is 324.6 and 312.0 kcal/mol for ZnNTA and ZnNTPA respectively, suggesting that there is a net destabilization which is significantly smaller in the instance of ZnNTPA. Whilst summing the interaction energies in the coordination sphere worked well in the instance of Be^{II} complexes in identifying the preferentially formed complex, this is not the case of Zn^{II} complexes. The reason for that is simple if one recalls that Be complexes do not have coordinated water molecules.

Steric Contacts and Weak Intramolecular Interactions

We wanted to investigate the nature and significance of numerous weak intramolecular interactions. These interactions were selected based on either (i) the presence of a short contact with interatomic distance smaller than the sum of the van der Waals radii, (ii) the presence of an NCI-isosurface in the interatomic region, or (iii) the strength of the interaction energy – the selected interactions are shown in Table 4.5 and a full set of topological properties are shown in Tables B7 and B8 in Appendix B.

All CH•••HC interactions have small classical contributions, regardless of the interatomic distance, the nature of the NCI-isosurface and the overall strength of the interaction energy between the H-atoms. Furthermore, there is an attractive exchange-correlation component for these interactions which overrides the classical repulsive component, except for the H2•••H9 interaction in ZnNTPA. There is no correlation between (i) distance and the NCI-coloured isosurfaces between atoms, (ii) the distance and $E_{int}^{X,Y}$, and (iii) the NCI-coloured isosurface

and the $E_{int}^{X,Y}$. Note that the red isosurfaces can only be found between αH-atoms and according to NCI theory, the interactions between these atoms are strained. All H•••O interactions have both attractive classical and exchange correlation components, regardless of the presence/absence of an AIL or the presence/absence of an NCI-isosurface.

Table 4.5. IQA partitioning of two-bodied interaction energies in ZnNTA and ZnNTPA for interactions of interest (the XL3YP wavefunction on the MP2 structures was used).

Interaction (X•••Y)	d / Å	$\rho(r)$ / au	NCI	q^X / e	q^Y / e	kcal/mol		
						$V_{cl}^{X,Y}$	$V_{XC}^{X,Y}$	$E_{int}^{X,Y}$
ZnNTA								
H2•••H7	2.378		Red	+0.0300	+0.0441	0.3	–0.8	–0.5
H6•••H9	2.160		Red	+0.0352	+0.0333	0.3	–2.2	–1.8
H3•••H10	2.123		Red	+0.0455	+0.0455	0.4	–2.2	–1.8
ZnNTPA								
H2•••H7	2.371		Red	+0.0100	+0.0223	0.1	–0.8	–0.7
H6•••H9	2.295		Red	+0.0191	+0.0085	0.2	–1.4	–1.2
H2•••H9	2.396		None	+0.0100	+0.0085	0.2	0.0	+0.2
H3•••H10	2.207		Red	+0.0253	+0.0222	0.2	–1.7	–1.5
H6•••H12	2.255		Blue	+0.0191	+0.0236	0.1	–1.6	–1.5
H7•••H17	2.031	0.0134	Blue	+0.0223	+0.0251	0.1	–3.2	–3.1
H12•••H18	2.274	0.0092	Blue	+0.0236	+0.0248	0.1	–1.6	–1.5
CH10•••O30(w1)	2.673	0.0078	Blue	+0.0222	–1.1516	–1.5	–3.3	–4.8
CH18•••O25(b)	2.563	0.0096	Blue	+0.0248	–1.2289	–2.5	–3.6	–6.1
OH32•••O25(b)	2.274		Blue	+0.6010	–1.2289	–101.0	–3.2	–104.1
OH34•••O22(b)	2.355		Blue	+0.5971	–1.2227	–98.9	–2.0	–100.8
OH35•••O25(b)	3.110		None	+0.5881	–1.2289	–78.5	–0.1	–78.6

Interestingly, the OH•••O interactions have interaction energies which are at least an order of magnitude more attractive than the CH•••O interactions. The differences in the interaction energy between the O•••H interactions can be rationalized by the local environment. H18 is attached to a less electronegative carbon atom whereas H32 is attached to the highly electronegative oxygen atom. The charge on the H32-atom is significantly more positive than that on H18 (q^{H18} = +0.025 au and q^{H32} = +0.601 au) resulting in a larger difference in charge between the interacting atoms, which significantly increases the $V_{ne}^{H,O}$ attraction and reduces $V_{ee}^{H,O}$ for the OH32•••O such that the overall classical term is 40 times more attractive. This reinforces the conclusion that the presence or absence of an AIL cannot be used as a measure of strength of these interactions.

In order to determine if there are distinguishable qualitative differences between interactions where the QTAIM and NCI indicators are identical, in particular CH•••O and

CH•••HC with AILs, it was necessary to analyse the 1D cross-section of the electron density for each interaction along the λ_2 eigenvector of the Hessian matrix.[52] The value of this method comes from the ability to explain the presence/absence of AILs.

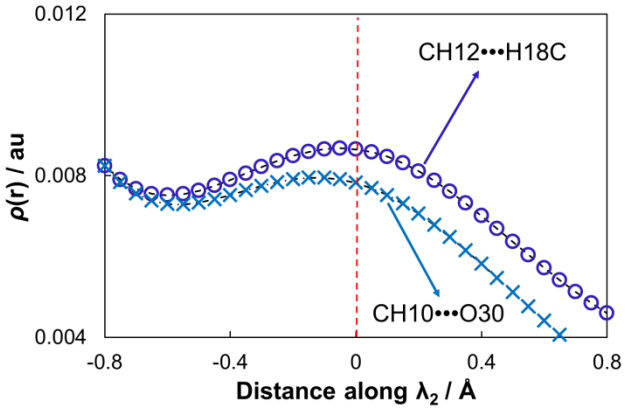

Figure 4.4. The cross-sections of the ρ(r) along the λ_2 eigenvector where the red line indicates the GIP.

Considering the cross-sections in Figure 4.4 (both interactions with AILs), the following observations can be made: (i) in all instances there was a local maximum in electron density fully explaining the presence of an AIL (ii) density at the geometrical critical point (placed in the middle between two interacting atoms) is comparable between the weak CH•••O and CH•••HC interactions, and (iii) qualitatively, there is no difference in the density distribution of the weak CH•••O and CH•••HC interactions. Similarly, there are no differences in the density distribution between (i) H•••O and CH•••HC interactions without AILs and a blue NCI-isosurface and (ii) O•••O and CH•••HC interactions without AILs and a red isosurface – all cross-sections are shown in Figure B3 in Appendix B.

Considering the plethora of intramolecular interactions analysed in this section, one would naturally assume that ZnNTPA is the preferentially formed complex as they all contribute to molecular stability. This clearly isn't the case and supports the conclusion that local indices in the final molecular product are insufficient to explain any global molecular changes.

We have analysed numerous interactions which have typically been associated with complex stability (coordination bond strength, lone pair donor atom repulsion, and weak intramolecular interactions) across various techniques (geometric, QTAIM, NCI, IQA) all provide contradictory and inconclusive results which fail to provide a conclusive solution.

Importantly, attempting to rationalize molecular stability on these grounds simply presents a cacophony of numbers which are more likely to confuse an inorganic chemist rather than rationalize the observed experimental trend. The only consistent trend which does emerge is that the coordination bonds of Zinc to the water molecules are stronger in ZnNTA given that (i) d(Zn–OH_2) is shorter in NTA, (ii) ρ_{BCP}(Zn–OH_2) is larger in ZnNTA, (iii) there is a large blue NCI isosurface and (iv) E_{int}^{Zn,OH_2} is more stabilizing in favour of ZnNTA. It is for these reasons that an alternative means of understanding relative complex stability was taken where focus has changed from understanding isolated interatomic interactions to understanding processes involved in complex formation.

Evaluating Processes involved in complex formation

Complex formation in an aqueous environment can be represented as a simplified sequence of imaginary events or decomposed individual processes shown in Scheme 4.1. The

Scheme 4.1. The decomposition of the complex formation process.

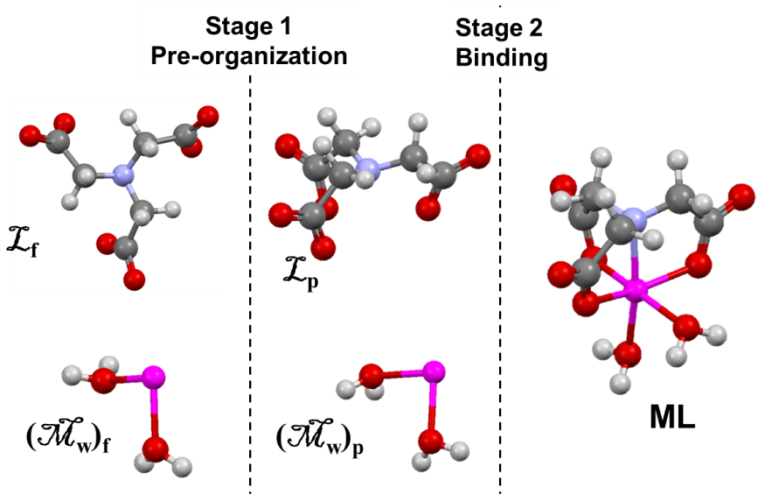

assumptions from the Be^{II} complexes (discussed in Chapter 3) hold for Zn^{II} complexes, that is: (i) the model is valid due to the excellent predictions of ΔE_{CRn}, (ii) hydration sphere around the different components may be ignored, (iii) the dissociation of water molecules from the hydrated metal ion is independent of the ligand present in solution, and (iv) metal fragment is dependent on the system under consideration *e.g.* for the Be^{II} complexes it was the bare Be^{2+} cation but for Zn^{II} complexes it is the $Zn(H_2O)_2^{2+}$ fragment. Note that the metal containing

fragment is represented as $\mathcal{M}_w$ for simplicity and generality. The complex formation process is divided into two major stages:

a) Stage 1 of Scheme 4.1, which represents the preorganization of a component (either the ligand $\mathcal{L}$, or the metal fragment $\mathcal{M}_w$), during which the fragment necessarily rearranges the structure from that as a "free" fragment ($\mathcal{L}_f$ or $(\mathcal{M}_w)_f$) to that as observed in the complex ($\mathcal{L}_p$ or $(\mathcal{M}_w)_p$) and an energetic penalty must be incurred, and is called the preorganization energy, $E^{\mathcal{L}}_{p\text{-org}}$ and $E^{\mathcal{M}}_{p\text{-org}}$, of a ligand and metal-containing fragment, respectively. These values will differ as: (i) the ligands have very different structures and numbers of atoms, so $E^{\mathcal{L}}_{p\text{-org}}(\text{NTA})$ and $E^{\mathcal{L}}_{p\text{-org}}(\text{NTPA})$, and (ii) the preorganized hydrated metal-containing fragments will have different structures, hence $E^{\mathcal{M}}_{p\text{-org}}(\text{NTA})$ and $E^{\mathcal{M}}_{p\text{-org}}(\text{NTPA})$. This should hopefully identify the sources of strain during the preorganization of all components under consideration.
b) Stage 2 in Scheme 4.1 represents the final step during complexation which leads to the binding of $\mathcal{L}_p$ to the metal centre in $(\mathcal{M}_w)_p$, and the energy released in this step is called the binding energy, E_{bind}. Alternatively, E_{bind} is a measure of the affinity of a ligand for the metal centre. Note that one can monitor the changes occurring in the fragment when $\mathcal{L}_p$ and $(\mathcal{M}_w)_p$ change to the complexed forms, $\mathcal{L}_c$ and $(\mathcal{M}_w)_c$, where each component is structurally identical but the atomic and interatomic properties are completely different due to the presence of additional interactions.

The preorganization energy, $E_{p\text{-org}}$, of a ligand related to the first stage in Scheme 4.1 can be written as

$$E^{\mathcal{L}}_{p\text{-org}} = E(\mathcal{L}_p) - E(\mathcal{L}_f) \qquad (4.2)$$

and the preorganization energy of a metal containing fragment can be written as

$$E^{\mathcal{M}}_{p\text{-org}} = E((\mathcal{M}_w)_p) - E((\mathcal{M}_w)_f). \qquad (4.3)$$

The binding energy between the preorganized fragments can be expressed as

$$E_{bind} = E(\text{ML}) - E(\mathcal{L}_p) - E((\mathcal{M}_w)_p) \qquad (4.4)$$

The sum of the processes $E^{\mathcal{L}}_{\text{p-org}}$ + $E^{\mathcal{M}}_{\text{p-org}}$ +E_{bind} should amount to the resultant complex formation energy $E_{\text{ML}} = E(\text{ML}) - E(\mathcal{L}_{\text{f}}) - E(\mathcal{M}_{\text{f}})$ related to the reaction of the free metal fragment with the free ligand $\mathcal{L}_{\text{f}}$. This approach is preferable to classical approaches as it fully recovers overall energetic effects that individually contribute to the formation of the complex, rather than focusing individual interactions (measured by interatomic distances, density etc) with juxtaposed energetic effects.

Table 4.6. Computed preorganization (strain) energies and binding energies (all in kcal/mol) using relevant energy terms obtained for $(\mathcal{M}_{\text{w}})_{\text{f}}$, $\mathcal{L}_{\text{f}}$ of NTA and NTPA, the complexes ZnNTA and ZnNTPA, and the respective $(\mathcal{M}_{\text{w}})_{\text{p}}$ and $\mathcal{L}_{\text{p}}$ at the X3LYP level of theory on the MP2 optimized structures.

$E^{\mathcal{M}}_{\text{p-org}}$			$E^{\mathcal{L}}_{\text{p-org}}$			E_{bind}			ΔE_{ML} [a]
NTA	NTPA	$\Delta E^{\mathcal{M}}_{\text{p-org}}$ [b]	NTA	NTPA	$\Delta E^{\mathcal{L}}_{\text{p-org}}$ [b]	ZnNTA	ZnNTPA	ΔE_{bind} [c]	
2.8	8.8	6.1	19.5	31.1	11.5	–104.5	–116.9	–12.4	5.2

[a] $\Delta E_{\text{ML}} = E_{\text{ZnNTPA}} - E_{\text{ZnNTA}}$; [b] $\Delta E_{\text{p-org}} = E_{\text{p-org}}(\text{NTPA}) - E_{\text{p-org}}(\text{NTA})$; [c] $\Delta E_{\text{bind}} = E_{\text{bind}}(\text{ZnNTPA}) - E_{\text{bind}}(\text{ZnNTA})$.

Table 4.6 shows the energy values associated with the various components of the decomposed complex formation. It is clear that both ligands became strained when the structure changed from $\mathcal{L}_{\text{f}}$ to $\mathcal{L}_{\text{p}}$ as a significant penalty is required to preorganize them. This process incurs a greater stain in NTPA, $E^{\mathcal{L}}_{\text{p-org}}(\text{NTPA}) > E^{\mathcal{L}}_{\text{p-org}}(\text{NTA})$ by about 11.5 kcal/mol at X3LYP, a trend also found for the Ni^{II} complexes.[39] This difference in strain energies is most likely a result of the additional atoms present in NTPA. A lesser penalty is incurred for the preorganization of the metal-containing fragments, and this inccures a greater strain in NTPA, $E^{\mathcal{M}}_{\text{p-org}}(\text{NTPA}) > E^{\mathcal{M}}_{\text{p-org}}(\text{NTA})$ by about 6.1 kcal/mol. For both complexes the binding between ligand and the metal-containing fragment necessarily overrides the strain incurred during the preorganization of both fragments and is more favourable in ZnNTPA (ΔE_{bind} ~– 12.4 kcal/mol). It is important to note that if one were to only sum up the preorganization of the ligand and affinity, the energy released would override the penalty incurred due to preorganization but would not suffice to make ZnNTA the preferential complex, $\Delta E^{\mathcal{L}}_{\text{p-org}}$ + ΔE_{bind} = – 0.9 kcal/mol at the X3LYP level of theory. Based on this result, it is clear that the preorganization of the metal-containing fragment plays a significant and determining role in the relative stability of these metal complexes.

The validity of this protocol comes from the ability to fully recover the experimental trend. The relative difference in the complex formation energy is given by

$$\Delta E_{ML} = (E^{\mathcal{I}}_{p\text{-}org}(NTPA) + E^{\mathcal{M}}_{p\text{-}org}(NTPA) + E_{bind}(ZnNTPA)) - (E^{\mathcal{I}}_{p\text{-}org}(NTA) + E^{\mathcal{M}}_{p\text{-}org}(NTA) + E_{bind}(ZnNTA)) \quad (4.5)$$

At the X3LYP level of theory, it shows that the formation of ZnNTPA is not preferential (*i.e.*, ΔE_{ML} of 5.2 kcal/mol not in favour of ZnNTPA), corresponding to the experimental trend. Moreover, this fully recovers E_{CRn}, as $\Delta E_{CRn} = -\Delta E_{ML}$, further reinforcing the validity of the protocol.

This is not the first attempt at understanding molecular stability using an *energetic* decomposition of the formation energy. The ETS-NOCV (Extended Transition State combined with the Natural Orbital for Chemical Valence) method[34-36] decomposes the formation process into preparation energy and interaction energy. In the previous study of Zn^{II} complexes of NTA and NTPA[40] the ETS-NOCV scheme was used to explore complex stability. Table 4.7 summarizes the results obtained.

Table 4.7. The ETS-NOCV decomposition[a] results describing the interaction between the preorganized ligands and the preorganized metal fragment.[40]

Energy term	ZnNTA	ZnNTPA	ΔE[b]
ETS-NOCV Energy components related to $E_{p\text{-}org}$			
$\Delta E_{dist\text{-}\mathcal{M}}$	21.1	37.3	16.2
$\Delta E_{dist\text{-}\mathcal{I}}$	20.5	31.8	11.3
ΔE_{dist}	41.6	69.1	27.6
ETS-NOCV Energy components related to E_{bind}			
ΔE_{int}	–148.7	–172.1	–23.4
ETS-NOCV Energy components related to E_{ML}			
$\Delta E_{total\ (solvent)}$	–107.1	–103.0	4.1

[a] The Becke-Perdew exchange correlation functional (BP86) was applied with the standard double double-ζ STO basis set on all atoms except Zn, where the TZP basis set was employed. This was done in the COSMO solvation model using water as solvent. [b] $\Delta E = E(NTPA) - E(NTA)$

The distortion energy of each fragment is the ETS-NOCV term for the preorganization of the fragment and the interaction energy corresponds to the binding energy. It is clear that trends are identical where: (i) $\Delta E_{dist\text{-}\mathcal{M}}$ is highly destabilizing and greater in NTPA than in NTA by

16.2 kcal/mol (ii) $\Delta E_{\text{dist-}\mathcal{I}}$ is highly destabilizing and greater in NTPA than in NTA by 11.3 kcal/mol (iii) ΔE_{int} is highly stabilizing in both complexes, but by far more stabilizing in ZnNTPA by 23.4 kcal/mol (iv) considering only the distortion (preorganization) of the ligand and the interaction between the two fragments, one obtains (ΔE_{int}(ZnNTPA) – ΔE_{int}(ZnNTA)) + ($\Delta E_{\text{dist-}\mathcal{I}}$(ZnNTPA) – $\Delta E_{\text{dist-}\mathcal{I}}$(ZnNTA)) = 12.1 kcal/mol, and (v) the total difference in the complexation energy is ΔE_{ML} = 4.1 kcal/mol and can only be obtained if the distortion of the metal fragment is considered. Evidently there is a strong destabilization of the metal fragment, which plays a crucial part in the relative stability of the complexes.

While these techniques – ETS-NOCV and the fragment decomposition used here – provide the necessary energetic information, they lack necessary resolution to identify the atoms and interactions with the greatest contribution to the formation of the molecular system. We want to encapsulate the energetic processes with the atomic partitioning available in QTAIM and IQA in order to identify the atoms and interactions that provide the greatest contribution to the overall energetic changes. Moreover, QTAIM gives one the capacity to analyse the topology of electron density hence track the movement of electron density within the molecule and map it to an associated energetic contribution. When combining the preorganization and binding energies with the QTAIM and IQA techniques it is possible to identify the following during preorganization: (i) atoms with the most significant changes in the desnity distribution (ii) atoms with the most significant change in the net atomic and total atomic energy and (iii) the interactions which contribute the most towards straining the molecule. Furthermore for the binding energy it is not only possible to look at the atomic changes but also analyse the interactions between the two fragments and determine which interactions contribute the most to the affinity of the ligand to the metal centre. With these findings and the fact that the results obtained here agreed qualitatively with the ETS-NOCV results obtained previously,[40] it is now possible to explore origins of strain and stability in both metal complexes, at the most suitable level of theory.

Exploring first stage of complex formation – toward understanding the pre-organization (strain) energy of a ligand

The previous section focused on the overall energy contributions, that of fragment preorganization and the binding between the $\mathcal{L}_{\text{p}}$ and $(\mathcal{M}_{\text{w}})_{\text{p}}$. To gain further insight into the

sources of strain during preorganization we will use QTAIM, NCI and IQA techniques. We begin by analysing the topological properties in the preorganized ligands. The molecular graphs of the $\mathcal{I}_p$-structures of NTPA and NTA are shown in Figure 4.5(a,b) and the corresponding NCI isosurfaces are shown in Figure 4.5(c,d).

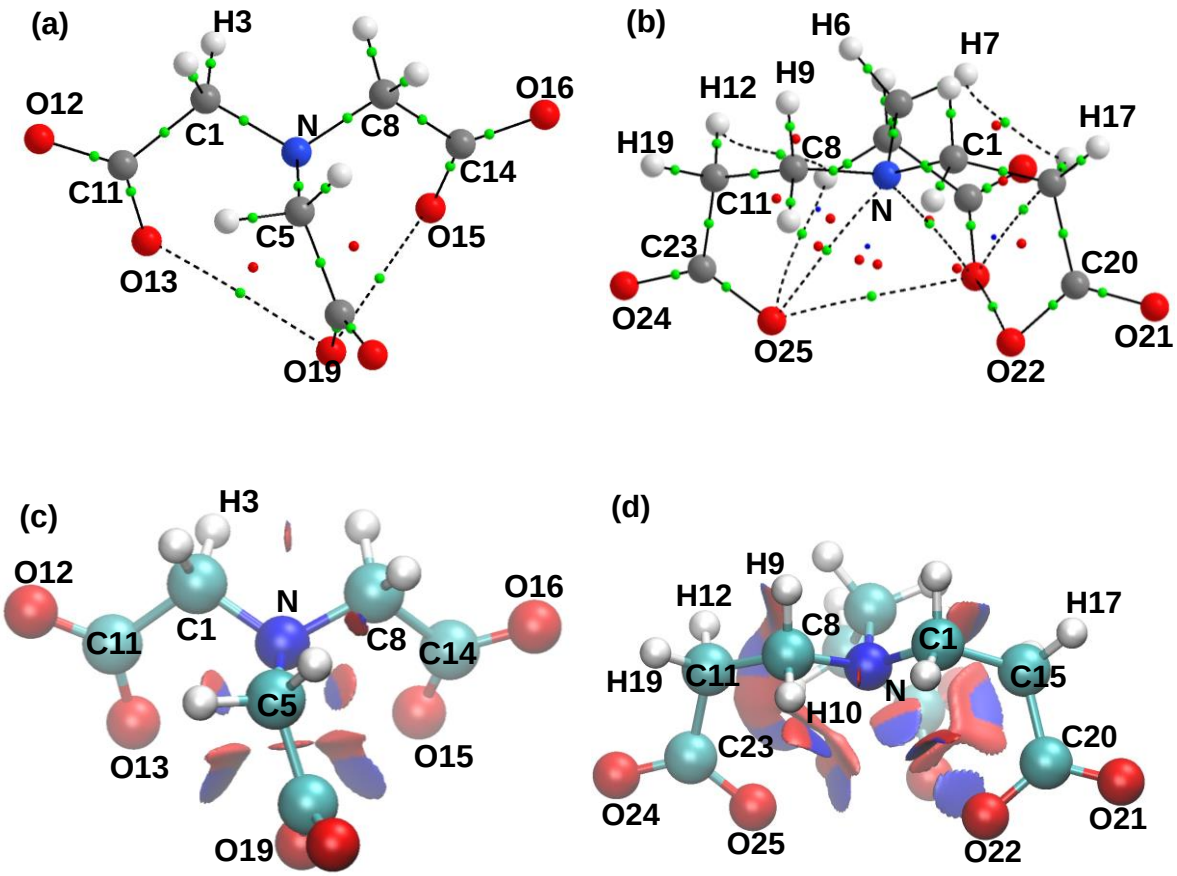

Figure 4.5. The QTAIM molecular graphs of ligands as found in (a) $\mathcal{I}_p$(NTA), and (b) $\mathcal{I}_p$(NTPA), as well as the NCI isosurfaces of (c) $\mathcal{I}_p$(NTA), and (d) $\mathcal{I}_p$(NTPA), with a RDG isovalue of 0.5 au and isosurfaces coloured from blue to red using –0.07 au ≤ sign(λ_2)×$\rho(r)$ ≤ +0.03 au.

The molecular graphs of the preorganized ligands reveal unexpected atomic interaction lines in the highly repulsive coordination sphere, *e.g.*, ρ_{BCP}(O19--O15) = 0.0091 and ρ_{BCP}(O28--O22) = 0.0080 au in NTA and NTPA, respectively. Interestingly, there are no AILs present between the coordinating O-atoms which are furthest apart in both complexes, *e.g.* O22 and O25 in NTPA, where the repulsion is likely to be at a minimum. This is counter intuitive and makes the classical interpretation of an AIL as a bonding interaction somewhat difficult. However, it is reasonable to postulate that in the region of the most significant repulsion (interatomic distances are shortest), the AIL minimizes repulsion between the

atoms. The AIL becomes a means of dissipating electron density, reducing electrostatic repulsion between the atoms, and simultaneously introducing an exchange correlation term (the presence of an AIL corresponds to the presence of an XC-term), which is always negative. Thus an increase in the XC-term and a decrease in electrostatic repulsion minimize the strain.

The molecular graph of NTPA reveals the presence of additional QTAIM-defined interactions: (i) there are AILs between N- and O-atoms (ρ_{BCP}(N--O25) = 0.0101 and ρ_{BCP}(N--O28) = 0.0093 au) with the shortest contacts, suggesting that this is a means of minimizing repulsive forces (ii) there are AILs between H- and O-atoms, indicative of a typical hydrogen bond (ρ_{BCP}(H18--O25) = 0.0092 and ρ_{BCP}(H17--O28) = 0.0046 au), and (iii) there are AILs representing CH•••HC interactions (ρ_{BCP}(H7--H17) = 0.013 and ρ_{BCP}(H12--H18) = 0.0091 au). Recall that the CH•••O and CH•••HC AILs are also present in the complex (except CH17•••O28). The NCI isosurfaces in Figure 4.5 correlate with the molecular graphs and all weak intramolecular interactions are fully recovered. There are blue regions of electron density accumulation that correspond to the AILs and red regions of density depletion coinciding with the ring critical and cage critical points. Note that there are no isosurfaces between the coordinating O-atoms which are furthest apart. There are additional red isosurfaces between αH-atoms where there were no AILs, and the interatomic distances are incredibly small. Traditionally, the NCI interpretation would be to suggest steric hindrance; however, as we have already shown we cannot infer an energetic contribution based on the local density distribution. The density distribution is likely due to the short CH---HC contact and small ring which forces the depletion of density from the local environment. There are additional bi-centric isosurfaces which correspond to the N--O interactions, without bond paths in both complexes, in which excess density was removed from the crowded environment and dissipated into the adjacent blue region.

Clearly, the interpretation of the molecular graphs and the NCI isosurfaces shown in Figure 4.5, particularly in the case of NTPA, is not simple and likely speculative as there is no measure of the energetic contributions. To gain an insight on the energetic origin of the strain in the molecule we used QTAIM and IQA atomic properties. As the energy of a molecule is the sum of the additive energies, E^{X}_{add}, of each atom in the molecule,

$$E = \sum_{X} E^{X}_{add} \qquad (4.6)$$

one can trace the changes in the additive energy of all atoms when the ligand changes from the $\mathcal{I}_f$ state to $\mathcal{I}_p$ state. Naturally, the atoms with the most significant change in the additive energy, ΔE^X_{add}, have the greatest impact on the energy of the molecule. Thus, if an atom experiences a significant increase in the additive energy, then the atom is highly destabilized and contributes significantly to the overall strain of the molecule. Additionally, the additive energy of an atom is defined in IQA as:

$$E^X_{add} = E^X_{self} + \sum_{Y \neq X} 0.5 E^{X,Y}_{int} \,. \qquad (4.7)$$

where the first term is the intra-atomic contribution (self-atomic energy) and the second term is the interatomic contribution (sum of half interaction energies with all other atoms) to the additive energy of an atom.

Table 4.8 shows the changes in selected QTAIM- and IQA-defined atomic properties as the ligand changes from the $\mathcal{I}_f$ state to $\mathcal{I}_p$ *i.e.* for each atomic property U, $\Delta U^X = U_{p\text{-}org} - U_{free}$, for a selected arm of each ligand (a more detailed explaintion is available in PART 2 of Appendix B). It is clear, based on ΔE^X_{add} and ΔE^X_{self}, which contains the chemical identity of an atom, that the most significant changes occurred in the carboxylate groups and on the N-atoms. Moreover, these changes are more pronounced in NTPA. Note that the additive energies of the H-atoms, regardless of the local environment, as well as the self-atomic energies, changed marginally when compared to N-atoms and the carboxylate groups (e.g. ΔE^{H12}_{self} = 3.6 and ΔE^{H17}_{self} = 0.6 kcal/mol). Thus, contrary to what is contemporary knowledge, H-atoms involved in a steric clash negligibly contribute to destabilizing of the molecule. Focussing on the groups of chemical significance, N-atoms and atoms in the carboxylate groups, the following pattern emerges: the highly negatively charged atoms, N, O(b) and O(nb) (except N-atom in NTA), experienced a large increase in atomic additive energies whereas the highly positively charged γC-atoms of the carboxylate groups became stabilized the most; this is exactly the same pattern as discovered for the preorganization of these ligands in the case of Be complexes.

Table 4.8. Relative from $\mathcal{L}_f$ structures to $\mathcal{L}_p$, changes in the selected QTAIM- and IQA-defined energy terms (in kcal/mol) and additional atomic properties of atoms in ZnNTPA and ZnNTA (at the X3LYP level of theory on the MP2 structure).[a]

Atom X	ΔE^X_{add}	$\Delta\sum_{Y\neq X}0.5E^{X,Y}_{int}$	ΔE^X_{self}	q^X_{free}	$q^X_{L_{p-org}}$	ΔN^X	ΔVol^X
ZnNTA							
αC8	–0.3	2.1	–2.4	0.314	0.319	–0.005	2.91
αH9	–0.5	–0.4	–0.1	–0.030	–0.028	–0.002	–0.99
αH10	0.1	1.7	–1.6	0.017	–0.002	0.019	2.63
βC14	–12.3	–10.7	–1.6	1.583	1.578	0.005	0.82
O15(b)	18.3	35.5	–17.2	–1.278	–1.248	–0.030	–0.83
O16(nb)	10.4	–12.2	22.6	–1.289	–1.321	0.032	0.45
N	–0.1	12.7	–12.8	–0.959	–0.900	–0.059	–9.28
ZnNTPA							
αC8	–3.8	–0.8	–3.0	0.339	0.335	0.005	0.10
αH9	0.1	–0.3	0.4	–0.030	–0.053	0.023	0.98
αH10	0.1	3.1	–3.1	0.004	–0.017	0.021	4.61
βC11	–1.0	0.2	–1.2	0.026	0.021	0.005	–0.45
βH12	1.4	–2.2	3.6	–0.010	–0.004	–0.006	–4.76
βH19	0.1	0.6	–0.5	–0.013	–0.012	–0.001	2.28
γC23	–28.9	–23.6	–5.2	1.573	1.565	0.008	0.57
O24(nb)	17.5	-6.4	24.0	–1.284	–1.322	0.038	–0.37
O25(b)	40.1	52.4	–12.2	–1.284	–1.236	–0.048	–7.57
N	19.2	49.4	–30.2	–0.969	–0.837	–0.131	–13.98

[a] N^X - average No of electrons in atom X (atomic electron population); Vol^X – atomic volume in bohr^3 (volume bounded by interatomic surfaces of atom X and by isosurface of the electron density distribution; 0.001 au isodensity surface was used).

The analysis of energy components, an intra-atomic contribution E^X_{self} and interatomic contributions $\sum_{Y\neq X}0.5E^{X,Y}_{int}$ which, when summed up, result in E^X_{add} as shown in Eq. (4.6), and other physical properties shown in Table 4.8, leads to the following conclusions:

(i) The preorganization of the ligand resulted in the outflow of electron density from O(b)- and N-atoms, $\Delta N^X < 0$ and the contraction of the atomic volume $\Delta Vol^X < 0$. The dissipated density is shared via AILs and accommodated on the carboxylate carbon and O(nb)-atom. The energetic destabilization is due to unfavourable increase in interactions with all remaining atoms in a ligand which is much greater in value than the change in self-atomic energies; $\Delta\sum_{Y\neq X}0.5E^{X,Y}_{int} >> \left|\Delta E^X_{self}\right|$.

(ii) The converse is noted for the O(nb)-atoms: the change in the additive energy is driven by the destabilization of the self-atomic energies, thus changes in the atomic basins, resulting in $\left|\Delta\sum_{Y\neq X}0.5E_{int}^{X,Y}\right| << \Delta E_{self}^{X}$. The N- and O(b)-atoms donate electron density to the O(nb)-atoms, $\Delta N^{X} > 0$, which increase the self-energies of these atoms significantly.

(iii) The positively charged carboxylate C-atoms gained stability, $\Delta E_{add}^{X} << 0$ as a result of far more stabilizing interactions, $\Delta\sum_{Y\neq X}0.5E_{int}^{X,Y} << 0$. These atoms also gained electron density, $\Delta N^{X} > 0$, dissipated from the local surrounding molecular environment which resulted in the stabilization of the self energies of these atoms, $\Delta E_{self}^{X} < 0$.

In general, the penalty due to preorganization of the ligand is due to the formation of destabilizing interactions between coordinating atoms (O(b) and N). Additionally, in order to compensate for this, electron density is dissipated into to the surrounding regions, resulting in the destabilization of the O(nb)-atoms and stabilization of the C-atoms in the carboxylate groups. It is interesting to note that we simultaneously confirm and contradict classical interpretations of interactions: we confirm that there is severe repulsion in the coordination sphere ($\Delta E_{add} > 0$ for O(b)- and N-atoms) and disagree with the repulsive nature and contribution of H-atoms. The difference in the preorganization strain energy is largely due to the formation of far more repulsive interactions in NTPA as measured by $\Delta\sum_{Y\neq X}0.5E_{int}^{X,Y}$. These trends are identical to those found for the Be^{II} complexes (in Chapter 3), suggesting that the changes in the ligand do not depend on the size of the metal ion coordinated.

Exploring first stage of complex formation – toward understanding the pre-organization (strain) energy of a metal-containing fragment

There is no immediate or obvious explanation for the preorganization of the metal fragment as there are no additional interactions revealed through QTAIM molecular graphs or NCI isosurfaces. As with the preorganization of the ligand, we decided to trace the origin of

preorganization energies from the IQA-perspectives. This reveals that the Zinc atom experiences a large increase in the additive atomic energy, E^{X}_{add}, and thus is highly destabilized. Table 4.9 shows that additional significant changes occur on two H-atoms. The variation in the additive atomic energies, ΔE^{X}_{add}, (when the metal containing fragment changed from the $(\mathcal{M}_w)_f$ to $(\mathcal{M}_w)_p$ structure) shows that by far more significant changes took place in NTPA. However, regardless of the magnitude of changes, there appears to be a consistent pattern in both systems: Zn, O, and two hydrogen atoms, experienced an increase in atomic additive energies whereas two hydrogen atoms, attached to the equatorial oxygen, became stabilized. The analysis of energy components shown in Table 4.9 and Table B9 in the Appendix B, leads to the following conclusions:

(i) The energy destabilization of the positively charged Zn centre, is a result of a destabilizing change in interactions with all other atoms and to a lesser extent the self-atomic energy; $\Delta\sum_{Y\neq X} 0.5E^{X,Y}_{int} >> \Delta E^{X}_{self}$. Preorganization of the fragment resulted in the dissipation of electron density into the surrounding environment, $\Delta N^{X} < 0$, with an expansion of the atomic volume $\Delta Vol^{X} > 0$. The result was less repulsive electron-electron interaction, $\Delta V^{XX}_{ee} < 0$, less attractive electron-neutron interaction, $\Delta V^{XX}_{ne} > 0$, and less repulsive electronic energy within the atomic basin. The combination of these changes explains the increase in the self-atomic energy, $\Delta E^{X}_{self} > 0$.

(ii) For the O-atoms on the water molecules, observed increase of these atoms additive atomic energies is due to the destabilizing interactions with all other atoms in the fragment and this overrides the decrease in self-energy of these atoms, $\Delta\sum_{Y\neq X} 0.5E^{X,Y}_{int} > |\Delta E^{X}_{self}|$. During preorganization electron density is dissipated from the negatively charged atoms, $\Delta N^{X} < 0$, and an expansion in the atomic volume was observed $\Delta Vol^{X} > 0$. Because of that, a reduction in the electron-electron repulsion, $\Delta V^{XX}_{ee} < 0$, and the electron-neutron attraction, $\Delta V^{XX}_{ne} > 0$, within atomic basins is observed. These two changes, in combination with $\Delta T^{X} < 0$, explain the observed decrease in the self-atomic energy, $\Delta E^{X}_{self} < 0$.

Interestingly, the same physical phenomenon (the outflow of electron density and the expansion of the atomic volume) resulted in the increase of the self energy of the zinc centre but the decrease in self-atomic energies of the O-atoms. This is because the self-atomic energy of an atom is lowest in the isolated neutral state. An outflow of electron density from a positively charged atom (such as Zinc) results in a further deviation in density from the neutral Zn atom. On the other hand, an outflow of electron density from a negatively charged atom (such as O-atoms) is a movement towards the neutral ground state and hence the self-atomic energy decreases.

Table 4.9. Relative from $(\mathcal{M}_w)_f$ structures to $(\mathcal{M}_w)_p$, changes in the selected QTAIM- and IQA-(at the RX3LYP level of theory on the MP2 structure) defined energy terms (in kcal/mol) and additional atomic properties.[a]

Atom X	ΔE^X_{add}	$\Delta\sum_{Y\neq X}0.5E^{X,Y}_{int}$	ΔE^X_{self}	q^X_{free}	$q^X_{M_{p-org}}$	ΔN^X	ΔVol^X
ZnNTA							
Zn20	10.8	9.6	1.2	1.753	1.761	–0.008	1.004
O21	0.6	9.7	–9.1	–1.152	–1.148	–0.004	3.788
H25	–5.3	–3.3	–2.0	0.639	–1.142	0.008	0.458
H26	–4.5	–1.8	–2.8	0.639	0.638	0.010	0.669
O22	1.6	5.7	–4.1	–1.153	0.631	–0.011	1.588
H23	3.8	3.8	0.0	0.638	0.631	0.000	–0.141
H24	3.7	5.2	–1.6	0.637	0.628	0.006	0.365
ZnNTPA							
Zn29	28.4	20.8	7.6	1.753	1.772	–0.019	4.785
O30	7.6	22.8	–15.3	–1.152	–1.151	0.000	7.868
H34	–10.0	–4.2	–5.8	0.639	0.617	0.022	1.315
H35	–11.8	–8.6	–3.3	0.639	0.626	0.013	0.847
O31	13.3	25.4	–12.0	–1.153	–1.110	–0.043	1.601
H32	0.6	4.4	–3.8	0.638	0.623	0.015	0.746
H33	0.5	3.8	–3.3	0.637	0.624	0.013	0.829

[a] details of each property are shown below Table 4.8

To gain deeper insight, the changes in all diatomic interaction energies were analysed in the metal-containing fragment – relevant data are included in Table B10 in the Appendix B. The origin of the greater penalty for preorganizing the metal-containing fragment in ZnNTPA can now be explained by the larger changes in the interaction energies. In both metal complexes, the coordination bonds to O(w1) show the greatest destabilization ($\Delta E^{Zn,O21}_{int}$ = 19.9 and $\Delta E^{Zn,O30}_{int}$ = 40.4 kcal/mol in ZnNTA and ZnNTPA, respectively) followed by the

coordination bond to O(w2) which is also longer in ZnNTPA, $\Delta E_{\text{int}}^{\text{Zn,O31}}$ = 18.7 kcal/mol. The increases are a result of changes in elongation of the coordination bonds as the metal-containing fragment changes from $(\mathcal{M}_{\text{w}})_{\text{f}}$ to $(\mathcal{M}_{\text{w}})_{\text{p}}$. The Zn–O(w1) bond increases by 0.116 and 0.250 Å in ZnNTA and ZnNTPA, respectively, and the Zn–O(w2) bond increases by 0.034 and 0.137 Å in ZnNTA and ZnNTPA, respectively. These changes can be explained as follows: the NTPA ligand is larger and hence occupies more space around the metal cation. In response, the water molecules move further away from the metal cation centre to accommodate the bulkier ligand. O(w2) shows smaller deviations because it is bonded in the axial position, away from the other coordinating atoms. Interestingly, these trends correspond to properties of the coordination bonds. The Zn–O(w) were stronger in ZnNTA across all techniques, and show the lesser deviations during preorganization, whereas those in ZnNTPA are consistently weaker and show the greatest deviation during preorganization.

To conclude, the observed penalty incurred during the preorganization of the metal-containing fragment is due to the formation of less stabilizing coordination bonds to the metal, and the observed outflow of electron density from the metal centre.

Exploring second stage of complex formation – towards understanding relative stability of complexes

Whilst the preorganization is clearly in favour of ZnNTA, NTPA clearly shows greater affinity for the Zn-containing fragment. Although, the preferential formation of ZnNTA is clearly a result of fragment preorganization, the investigation of the binding is still worthwhile to gain insight into the mechanism and energetic origin of the process. To achieve this goal, we decomposed E_{bind} utilizing the IQA and IQF methods. The protocol, ideally, needs to be of general purpose and applicable to any molecular system. In particular, when considering metal complexes decomposed into two fragments (bimolecular system), $\mathcal{L}$ the ligand fragment and $\mathcal{M}$ the metal containing fragment. The binding process takes into account the energy released when two preorganized fragments, $(\mathcal{M}_{\text{w}})_{\text{p}}$ and $\mathcal{L}_{\text{p}}$, form the metal complex. Furthermore, to represent the fragment properties in the complex (in the presence of the other fragment) $(\mathcal{M}_{\text{w}})_{\text{c}}$ and $\mathcal{L}_{\text{c}}$ will be used. The full derivation of terms used is explained in the Appendix B (PART 3), however, there are particular terms of interest which we would like to turn our attention to. Firstly, similar to the IQA framework, within the IQF

framework, the binding energy between fragments is the sum of the interaction energies between fragments and the sum of the deformation energies of the individual fragments. In the instances of metal complexes, E_{bind} is expressed as:

$$E_{\text{bind}} = E_{\text{def}}^{\mathscr{M}_{\text{w}}} + E_{\text{def}}^{\mathscr{L}} + E_{\text{int}}^{(\mathscr{M}_{\text{w}})_{\text{c}},\mathscr{L}_{\text{c}}} \tag{4.8}$$

The deformation energy of each fragment can be expressed as a sum of the contributions made due to change in the self-energies within the fragment ($\Delta E_{\text{self}}^{\mathscr{M}_{\text{w}}}$ and $\Delta E_{\text{self}}^{\mathscr{L}}$) and the change due to a change in the interaction energies within the fragment ($\Delta E_{\text{int}}^{\mathscr{M}_{\text{w}}}$ and $\Delta E_{\text{int}}^{\mathscr{L}}$). Thus the binding energy may be written as:

$$E_{\text{bind}} = \Delta E_{\text{self}}^{\mathscr{M}_{\text{w}}} + \Delta E_{\text{self}}^{\mathscr{L}} + \Delta E_{\text{int}}^{\mathscr{M}_{\text{w}}} + \Delta E_{\text{int}}^{\mathscr{L}} + E_{\text{int}}^{(\mathscr{M}_{\text{w}})_{\text{c}},\mathscr{L}_{\text{c}}}. \tag{4.9}$$

The interaction energy between two fragments is composed of the classical components and the exchange components and is obtained by summing all interactions between the fragments:

$$E_{\text{int}}^{(\mathscr{M}_{\text{w}})_{\text{c}},\mathscr{L}_{\text{c}}} = V_{\text{cl}}^{(\mathscr{M}_{\text{w}})_{\text{c}},\mathscr{L}_{\text{c}}} + V_{\text{XC}}^{(\mathscr{M}_{\text{w}})_{\text{c}},\mathscr{L}_{\text{c}}} = \sum_{\text{X}\in(\mathscr{M}_{\text{w}})_{\text{c}}} \sum_{\text{Y}\in\mathscr{L}_{\text{c}}} V_{\text{cl}}^{\text{X,Y}} + \sum_{\text{X}\in(\mathscr{M}_{\text{w}})_{\text{c}}} \sum_{\text{Y}\in\mathscr{L}_{\text{c}}} V_{\text{XC}}^{\text{X,Y}} \quad . \tag{4.10}$$

Table 4.10 shows the IQF and IQA-related energy terms used to evaluate the binding energy of the two complexes and it is clear that binding is highly stabilizing and in favour of ZnNTPA, ΔE_{bind} = –23.8 kcal/mol. Despite the restrictions of the AIMAll software, the trend in the binding energy as determined from electronic energies has been recovered (although the exact value is not obtained). The binding is favoured by the inter-fragment interaction energy term, $E_{\text{int}}^{(\mathscr{M}_{\text{w}})_{\text{c}},\mathscr{L}_{\text{c}}}$. This exemplifies the importance and significance of the protocol proposed in this work. The affinity to the metal ion is highly attractive for both ligands. Recall that the sum of the interaction energies of the coordination bonds to the ligand predicted the preferential formation of ZnNTPA by ~21kcal/mol and this result remarkably agrees with the trend in binding. Note however, that the opposite was true when the interaction energy of the coordination bonds to water molecules were considered, –518.5 and –485.1 kcal/mol for NTA and NTPA respectively (see Table 4.3). The value of the inter-fragment interaction energy term between $(\mathscr{M}_{\text{w}})_{\text{c}}$ and $\mathscr{L}_{\text{c}}$ is significantly smaller than the sum of the interactions of coordination bonds to the ligands, indicating that there are additional interactions other than the coordination bonds that are contributing to the binding of the metal of the complexes.

Whilst this result is consistent with results for Be^{II} complexes (discussed in Chapter 3), it is chemically counter-intuitive: the weaker complex has the stronger interaction energy between the incoming ligand and the metal-containing fragment. For both complexes, the binding process clearly results in the stabilization of metal-containing fragment, $E_{\text{def}}^{\mathcal{M}_{\text{w}}} < 0$, and the stabilization is marginally, by 2.0 kcal/mol, in favour of NTA. The deformation energy of the ligands, $E_{\text{def}}^{\mathcal{I}} > 0$, indicates that the binding energy results in a far greater energy penalty in the case of NTPA, by ~31 kcal/mol.

Table 4.10. The indicated energy components (in kcal/mol), computed within a IQA/IQF framework, which were used in the interpretation of relative stability of ZnNTA and ZnNTPA complexes.

Energy term	ZnNTA	ZnNTPA	ΔE[a]
Energy components of E_{bind}			
$E_{\text{def}}^{\mathcal{M}_{\text{w}}}$	–101.8	–99.8	2.0
$E_{\text{def}}^{\mathcal{I}}$	56.3	87.1	30.8
$E_{\text{int}}^{(\mathcal{M}_{\text{w}})_{\text{c}},\mathcal{I}_{\text{c}}}$	–672.1	–728.9	–56.7
E_{bind}	–717.6	–741.4	–23.8
Additional energy terms			
$\Delta E_{\text{self}}^{\text{ML}}$	30.2	72.7	42.5
$\Delta E_{\text{self}}^{\mathcal{M}_{\text{w}}}$	–108.5	–100.8	7.7
$\Delta E_{\text{int}}^{\mathcal{M}_{\text{w}}}$	6.7	1.0	–5.7
$\Delta V_{\text{cl}}^{\mathcal{M}_{\text{w}}}$	12.2	–2.2	–14.4
$\Delta V_{\text{XC}}^{\mathcal{M}_{\text{w}}}$	–5.6	3.2	8.8
$\Delta E_{\text{self}}^{\mathcal{I}}$	138.7	173.4	34.7
$\Delta E_{\text{int}}^{\mathcal{I}}$	–82.4	–86.3	–3.8
$\Delta V_{\text{cl}}^{\mathcal{I}}$	–137.9	–157.2	–19.3
$\Delta V_{\text{XC}}^{\mathcal{I}}$	55.5	70.9	15.4
$V_{\text{cl}}^{(\mathcal{M}_{\text{w}})_{\text{c}},\mathcal{I}_{\text{c}}}$	–443.4	–466.5	–23.1
$V_{\text{XC}}^{(\mathcal{M}_{\text{w}})_{\text{c}},\mathcal{I}_{\text{c}}}$	–228.7	–262.3	–33.6

[a]) $\Delta E = E(\text{NTPA}) - E(\text{NTA})$

In search for the origin of the above observation, we turn our attention to the additional terms, shown in Table 4.10. They reveal that the contribution of the self-energies to the overall deformation energy, $\Delta E_{\text{self}}^{\text{ML}}$, is highly destabilizing in both complexes and much larger in ZnNTPA by about 42.5 kcal/mol. The source of the destabilization can be traced to the

ligand fragment, where $\Delta E_{\text{self}}^{\mathcal{L}}$ is 138.7 and 173.4 kcal/mol in NTA and NTPA, respectively and the stabilization of the metal-containing fragment ($\Delta E_{\text{self}}^{\mathcal{M}_{\text{w}}}$ is –108.5 and –100.8 kcal/mol in NTA and NTPA, respectively) compensates the gain in energy of the ligand fragment. In both complexes, the intra-fragment interaction energy is stabilizing for the ligand fragments and in both complexes $\Delta V_{\text{cl}}^{\mathcal{L}} < 0$ and $\Delta V_{\text{XC}}^{\mathcal{L}} > 0$. The intra-fragment interaction energy term in the Zn-containing fragment is destabilizing, $\Delta E_{\text{int}}^{\mathcal{M}_{\text{w}}} > 0$ for both complexes. Focusing on the inter-fragment interaction energy, it is clear that this term is dominated the electrostatic attraction between the fragments, $V_{\text{cl}}^{(\mathcal{M}_{\text{w}})_{\text{c}},\mathcal{L}_{\text{c}}}$, and this electrostatic term is –23.1 kcal/mol more attractive in ZnNTPA. Additionally, there is a significant exchange-correlation term $V_{\text{XC}}^{(\mathcal{M}_{\text{w}})_{\text{c}},\mathcal{L}_{\text{c}}}$, that is the same order of magnitude as the classical term and by far more stabilizing in ZnNTPA by –33.6 kcal/mol.

The above decomposition identifies that the favourable binding of ZnNTPA is due to the more attractive interaction energy between $(\mathcal{M}_{\text{w}})_{\text{p}}$ and $\mathcal{L}_{\text{p}}$ but it is unclear which interactions are responsible. It is incredibly ineffective and time consuming to analyse every single interaction between the two fragments. To eliminate interactions that do not require analysis, the binding step was decomposed alternatively; rather than using two fragments, four fragments were used. The binding energy using a 4-component approach can be calculated as follows:

$$E_{\text{bind}} = E(\text{ML}) - E(\mathcal{L}_{\text{p}}) - E(\mathcal{M}_{\text{f}}) - E((\mathcal{W}_1)_{\text{p}}) - E((\mathcal{W}_2)_{\text{p}}). \qquad (4.11)$$

Using the electronic energy at the X3LYP level of theory, E_{bind} is –127.6 and –134.0 kcal/mol for ZnNTA and ZnNTPA, respectively. Hence it remains in favour of ZnNTPA by 6.4 kcal/mol. Note that the preorganization energy determined earlier cannot be used in this instance to determine the overall complexation energy. This is because preorganization is specific and requires that one looks at the preorganization of the individual fragments used in the binding. According to the IQA and IQF protocols the binding energy is given by:

$$E_{\text{bind}} = \sum_{\mathcal{G}} E_{\text{def}}^{\mathcal{G}} + 0.5 \sum_{\mathcal{G}} \sum_{\mathcal{H} \neq \mathcal{G}} E_{\text{int}}^{\mathcal{G},\mathcal{H}} \qquad (4.12)$$

Hence, one can determine the deformation energies of each fragment and the inter-fragment interaction energies between any pair of fragments in the molecular system. Remember that the deformation energy of a fragment, $\mathcal{G}$, is given by $E_{\text{def}}^{\mathcal{G}} = \Delta E_{\text{self}}^{\mathcal{G}} + \Delta E_{\text{int}}^{\mathcal{G}}$. Table 4.11

shows the different IQA/IQF components related to the binding energy. IQA maintains the trend in the binding energy, –847.2 and –851.6 kcal/mol in ZnNTA and ZnNTPA, respectively. The deformation energy of each fragment is largely destabilizing except in the instance of the bare metal ion, which is stabilized ($E_{\text{def}}^{\mathcal{M}} < 0$). $\Delta E_{\text{self}}^{\mathcal{G}}$ can be explained by the changes in the electron populations. For $\mathcal{L}_{\text{p}}$, $(\mathcal{W}_1^o)_{\text{p}}$ and $(\mathcal{W}_2^o)_{\text{p}}$, there is an outflow of electron density, $\Delta N < 0$, as they donate density to the bare metal ion during complex formation which results in the increase in the self energy contributions, $\Delta E_{\text{self}}^{\mathcal{G}}$. This overrides the stabilization

Table 4.11. The IQA/IQF partitioning of the ZnNTA and ZnNTPA complexes in relevant fragments using the RXL3YP wavefunction on the MP2 structures.

$\mathcal{G}$	$E_{\text{def}}^{\mathcal{G}}$	$\Delta E_{\text{self}}^{\mathcal{G}}$	$\Delta E_{\text{int}}^{\mathcal{G}}$	$\Delta N^{\mathcal{G}}$	$\mathcal{G}\bullet\bullet\bullet\mathcal{H}$	$V_{\text{clt}}^{\mathcal{G},\mathcal{H}}$	$V_{\text{XCt}}^{\mathcal{G},\mathcal{H}}$	$E_{\text{int}}^{\mathcal{G},\mathcal{H}}$
ZnNTA								
$\mathcal{L}_{\text{p}}$	56.3	138.7	–82.4	–0.517	$\mathcal{M}_{\text{f}}\bullet\bullet\bullet\mathcal{L}_{\text{p}}$	–441.9	–199.0	–640.9
$\mathcal{M}_{\text{f}}$	–205.3	–205.3	0.0	0.645	$\mathcal{M}_{\text{f}}\bullet\bullet\bullet(\mathcal{W}_1^o)_{\text{p}}$	–19.3	–30.3	–49.6
$(\mathcal{W}_1^o)_{\text{p}}$	39.0	52.3	–13.3	–0.056	$\mathcal{M}_{\text{f}}\bullet\bullet\bullet(\mathcal{W}_2^o)_{\text{p}}$	–17.1	–37.9	–55.0
$(\mathcal{W}_2^o)_{\text{p}}$	41.5	57.4	–15.9	–0.072	$\mathcal{L}\bullet\bullet\bullet(\mathcal{W}_1^o)_{\text{p}}$	1.3	–17.5	–16.2
					$\mathcal{L}\bullet\bullet\bullet(\mathcal{W}_2^o)_{\text{p}}$	–2.8	–12.2	–15.0
					$(\mathcal{W}_1^o)_{\text{p}}\bullet\bullet\bullet(\mathcal{W}_2^o)_{\text{p}}$	1.8	–3.9	–2.0
ZnNTPA								
$\mathcal{L}_{\text{p}}$	87.1	173.4	–86.3	–0.559	$\mathcal{M}_{\text{f}}\bullet\bullet\bullet\mathcal{L}_{\text{p}}$	–462.1	–213.8	–675.9
$\mathcal{M}_{\text{f}}$	–201.6	–201.6	0.0	0.638	$\mathcal{M}_{\text{f}}\bullet\bullet\bullet(\mathcal{W}_1^o)_{\text{p}}$	–20.4	–20.3	–40.7
$(\mathcal{W}_1^o)_{\text{p}}$	42.7	53.1	–10.4	–0.034	$\mathcal{M}_{\text{f}}\bullet\bullet\bullet(\mathcal{W}_2^o)_{\text{p}}$	–9.4	–29.1	–38.6
$(\mathcal{W}_2^o)_{\text{p}}$	30.6	44.4	–13.8	–0.051	$\mathcal{L}_{\text{p}}\bullet\bullet\bullet(\mathcal{W}_1^o)_{\text{p}}$	7.5	–24.7	–17.3
					$\mathcal{L}_{\text{p}}\bullet\bullet\bullet(\mathcal{W}_2^o)_{\text{p}}$	–12.0	–12.8	–35.7
					$(\mathcal{W}_1^o)_{\text{p}}\bullet\bullet\bullet(\mathcal{W}_2^o)_{\text{p}}$	1.4	–3.6	–2.2

of the interatomic contribution to the deformation energy destabilizing the fragments, $E_{\text{def}}^{\mathcal{G}} > 0$. On the other hand, for both complexes $\mathcal{M}_{\text{f}}$ gained electron density, $\Delta N > 0$, donated by all the other fragments, resulting in a stabilized self energy and hence highly stabilized deformation energy. Interestingly, the ligands consistently have attractive inter-fragment interaction energies with the water molecules and the inter-fragment interaction energy between water molecules in both complexes is also attractive. Similar to the Zn-O(w) coordination bonds interaction energies, the $\mathcal{M}_{\text{f}}\bullet\bullet\bullet(\mathcal{W}^o)_{\text{p}}$ interactions are more stabilizing in favour of ZnNTA, reaffirming our earlier conclusion that it can be used as an indicator of preferential complex formation between these two complexes. The stabilizing deformation of the Zinc metal and

the attractive interactions between the bare Zn^{2+} ion and the ligand have the most significant contribution to the binding energy in complexes. Note that the biggest contribution to the more favourable binding energy for ZnNTPA, is the highly stabilizing $E_{\text{int}}^{\mathcal{M},\mathcal{L}}$ which is 35 kcal/mol in favour of ZnNTPA. For these reasons, one can eliminate analysing most other interactions and focus on the interactions between the metal and the ligand of interest, significantly simplifying the analysis.

Table 4.12. IQA partitioning of two-bodied interaction energies of all interactions with the Zn atom in ZnNTPA and ZnNTA using the RXL3YP wavefunction on the MP2 structures.[a]

ZnNTPA					ZnNTA				
Atom Y	q^{Y}	$V_{\text{cl}}^{\text{X,Y}}$	$V_{\text{XC}}^{\text{X,Y}}$	$E_{\text{int}}^{\text{X,Y}}$	Atom Y	q^{Y}	$V_{\text{cl}}^{\text{X,Y}}$	$V_{\text{XC}}^{\text{X,Y}}$	$E_{\text{int}}^{\text{X,Y}}$
αC1	0.309	55.8	–0.9	54.9	αC1	0.304	57.2	–0.9	56.3
αH2	0.010	3.6	–0.2	3.4	αH2	0.030	6.0	–0.2	5.8
αH3	0.025	4.7	–0.1	4.6	αH3	0.045	7.8	–0.1	7.8
N4	–0.983	–221.1	–50.9	–272.0	N4	–1.020	–226.9	–46.3	–273.2
αC5	0.304	53.4	–0.7	52.8	αC5	0.288	54.7	–0.9	53.8
αH6	0.019	4.3	–0.1	4.2	αH6	0.035	6.6	–0.1	6.5
αH7	0.022	4.4	0.0	4.4	αH7	0.044	7.6	0.0	7.6
αC8	0.308	55.6	–1.0	54.6	αC8	0.300	56.2	–0.7	55.5
αH9	0.009	3.5	–0.2	3.3	αH9	0.033	6.3	–0.1	6.2
αH10	0.022	4.1	–0.3	3.8	αH10	0.045	7.7	0.0	7.7
C11	0.014	2.1	–0.2	2.0	γC11	1.590	249.0	–0.8	248.2
H12	0.024	4.0	0.0	4.0	O12(nb)	–1.239	–139.1	–0.5	–139.5
C13	0.017	2.5	–0.7	1.8	O13(b)	–1.212	–251.5	–48.8	–300.2
H14	0.021	4.4	0.0	4.4	γC14	1.593	249.7	–0.9	248.8
C15	0.013	1.9	–0.5	1.4	O15(b)	–1.216	–252.2	–48.6	–300.8
H16	0.027	5.0	0.0	5.0	O16(nb)	–1.241	–139.3	–0.5	–139.8
H17	0.025	4.1	–0.1	4.0	γC17	1.596	251.6	–0.9	250.7
H18	0.025	3.9	–0.4	3.6	O18(nb)	–1.240	–139.9	–0.5	–140.3
H19	0.032	5.1	0.0	5.1	O19(b)	–1.220	–253.6	–48.3	–301.9
γC20	1.579	245.0	–0.8	244.2					
O21(nb)	–1.244	–140.1	–0.6	–140.7					
O22(b)	–1.223	–258.6	–52.5	–311.1					
γC23	1.577	236.7	–0.7	236.1					
O24(nb)	–1.243	–135.8	–0.5	–136.3					
O25(b)	–1.229	–256.6	–50.2	–306.8					
γC26	1.567	240.1	–0.7	239.4					
O27(nb)	–1.241	–137.6	–0.5	–138.1					
O28(b)	–1.229	–257.0	–50.9	–307.9					
Sum (kcal/mol):		**–462.1**	**–213.8**	**–675.9**	Sum (kcal/mol):		**–441.9**	**–199.0**	**–640.9**

[a] Atom X is Zn. q^{Zn} in NTPA is +1.362 au and in NTA is +1.355 au. q^{Y} is measured in au and all interaction energies and components are measured in kcal/mol.

Table 4.12 shows all individual interactions between Zinc and the ligand fragment, as well as the charges on all atoms in the ligand fragment in both complexes (all other

interactions which contribute to $E_{\text{int}}^{(\vec{\mathcal{M}}_{\text{w}})_{\text{c}},\vec{\mathcal{I}}_{\text{c}}}$ are shown in Table B10 to B15 in the Appendix B). We note the following:

(a) Only the coordination bonds show significant exchange-correlation contributions to the interaction energy,
(b) Interestingly and importantly, the interactions of Zn with the N- and O-atoms are attractive whereas all other interactions are repulsive,
(c) The repulsive interactions of Zn with the C-atoms of the carboxylate groups are significantly more destabilizing than those with the α-carbon atoms. The interactions with β-carbon atoms in ZnNTPA are negligible.
(d) The coordination bonds of Zn to O(b)-atoms are more attractive in ZnNTPA, while all other interactions with negatively charged atoms, N- and O(nb)-atoms, are comparable in both complexes,
(e) The coordination bonds of Zn to the ligand are more attractive in ZnNTPA by ~20 kcal/mol. The sum of these interactions is –1197.8 and –1176.1 kcal/mol in ZnNTPA and ZnNTA, respectively,

Importantly, we also see the manifestation of the inductive effect in the binding step and how it influences the relative values of the binding energy. The presence of the additional fragment $–CH_2–$ in NTPA results in increased density of atoms in the neighbouring region, αH- and γC-atoms. These atoms have less positive charges than the analogous atoms in NTA, and O(b)-atoms have more negative charges in NTPA. This results in the electrostatic terms being less repulsive with the backbone of the NTPA ligand and having far more attractive coordination bonds. Thus, the inter-fragment interaction energy, and by extension the binding, is overly more attractive for NTPA.

Clearly the analysis of the binding step is incredibly complex and difficult. The strength of the coordination bonds does not sum up to the interaction energy or the binding energy but the trend is the same, all indicating that binding of NTPA to Zinc is stronger than that of NTA. This analysis shows that the results are puzzling and unexpected. The preferential formation of ZnNTA is clearly not due to preferential binding, but rather less destabilizing preorganization.

Conclusions

The understanding of the relative stability of molecular systems is at the core of all chemistry. In order to understand trends in the stability and behaviour of molecules chemists use thermodynamic constants that are able to reveal interesting chemical properties. Whilst this information is useful, chemical understanding of the behaviour of these molecular systems is still unclear and ambiguous. In this work, we have explored factors influencing the relative stability of the Zn^{II} complexes of NTA and NTPA, where ZnNTA is the preferentially formed complex. In this work we approach the understanding from two broad perspectives: (i) analysing individual interactions and inferring the energetic effect on relative molecular stability and (ii) understanding the complex formation as a sequence of simplified events.

Whilst the analysis of individual interactions yields interesting results and provides fascinating insight into properties of these metal complexes, it still fails to explain the preferential complex formation for two reasons. Quite often we would measure a property, such as geometrically-determined interatomic distances or local density distribution, using QTAIM and NCI, between two atoms and *infer* an energetic effect. However, as has already been shown, the energetic impact of the local properties, particularly in density distribution, is not clear and requires the actual determination of interaction energies. Moreover, even if the interaction energies are measured between two atoms, it is only the local measurement of the repulsive or attractive nature of the interactions without considering what is the energy penalty or gain when the interaction is formed in the molecular system. With this in mind, we turned out attention to an alternative means of understanding complex stability where the complex formation process was decomposed into a two-stage process. In Stage 1 the ligand as a molecular fragment, $\mathcal{L}$, and the metal-containing fragment, $\mathcal{M}_w$, were preorganized and the structure changed from that of lowest energy to that observed in the complex. Stage 2 of the complex formation process involved binding the two preorganized fragments to form the final complex. It was noted that the preorganization destabilized both fragments and for both fragments preorganization was far more energy demanding in NTPA ($E^{\mathcal{L}}_{\text{p-org}}(\text{NTPA}) > E^{\mathcal{L}}_{\text{p-org}}(\text{NTA})$ and $E^{\mathcal{M}}_{\text{p-org}}(\text{NTPA}) > E^{\mathcal{M}}_{\text{p-org}}(\text{NTA})$. The binding process however, was stabilizing and more so for ZnNTPA. Importantly, the overall relative complex formation energy, $\Delta E_{\text{ML}} = E^{\mathcal{L}}_{\text{p-org}}(\text{NTPA}) + E^{\mathcal{M}}_{\text{p-org}}(\text{NTPA}) + E_{\text{bind}}(\text{ZnNTPA}) - E^{\mathcal{L}}_{\text{p-org}}(\text{NTA}) + E^{\mathcal{M}}_{\text{p-org}}(\text{NTA}) + E_{\text{bind}}(\text{ZnNTA})$, was in favour of ZnNTA, as is known experimentally, if the preorganization

of the metal fragment was considered. These findings were supported by the results obtained from a similar decomposition using ETS-NOCV.[40]

Whilst, we had the overall energetic effect of the preorganization, we were still somewhat unsure of the cause (or the origin) of the large destabilization. Hence, we made use of the QTAIM and IQA molecular partitioning to reveal the source of the strain in the fragments. When the ligand preorganized and the O(b)- and N-atoms came into close contact, AILs were formed between the lone-pair donor atoms and the electron population increased in surrounding atoms, showing that density was dissipated from O(nb)- and N-atoms. This resulted in the large stabilization of the C-atoms in the carboxylate groups, however, the interactions of the coordinating atoms with all other atoms increased significantly, resulting in large destabilization. These results simultaneously (i) confirmed classical thinking, as the oxygen and nitrogen atoms were highly destabilized, and (ii) contradicted classical thinking as the changes in the energies of the H-atoms involved in "steric clashes" had an insignificant contribution to the energy penalty of the entire ligand. In order to accommodate the large ligand, the coordination bonds of the metal centre to the water molecules must elongate during preorganization. This makes the interactions of the metal to the oxygen atoms, O(w), significantly weaker and results in the outflow of density from the zinc atom. These are the sources of strain during the preorganization of the zinc metal fragment. The metal fragment for ZnNTPA incurs a greater penalty during preorganization because the NTPA is a larger ligand, thus arms of the ligand extend even further and occupy far more space around the central metal ion. Hence, the Zn–O(w) bonds must elongate further to accommodate the larger ligand and become even more destabilized that they are in ZnNTA.

In order to understand the binding of the ligand of the metal fragment, a combination of IQA- and IQF-related energy terms were used. The binding energy was decomposed into the sum of the deformation energies of the individual fragments and the interaction energy between them. The more favourable binding of the ligand and metal in ZnNTPA was largely driven by the more attractive coordination bonds with zinc, the attractive interactions of H-atoms on the water molecules with the N and O-atoms in the ligand and the minimization of repulsive interaction energy values between the two fragments. This is confirmed by the sum of all attractive interactions being –4411.9 and –4288.2 kcal/mol in ZnNTPA and ZnNTA respectively whilst the sum of the repulsive interactions is 3683.0 and 3616.0 kcal/mol in ZnNTPA and ZnNTA, respectively such that $E_{\mathrm{int}}^{\mathcal{M}_c,\mathcal{L}_c}$ was –56.7 kcal/mol in favour of

ZnNTPA. This highlights the need to not focus on individual interactions in the complex but consider all possible interactions between the two fragments and the resultant trend is a sum of all of them. This result is somewhat unexpected as one would naturally assume that the more favourable complex would also have the most favourable binding of the metal to the ligand. The deformation energy of each ligand fragment upon binding is destabilizing and by far more so in NTPA (by 30 kcal/mol). This is largely due to $\Delta E_{\text{self}}^{\mathcal{L}} >> \left|\Delta E_{\text{int}}^{\mathcal{L}}\right|$ and large density changes which occur within the atomic basins upon complex formation. The metal-containing fragment was stabilized, $E_{\text{def}}^{\mathcal{M}_{\text{w}}} < 0$, during binding and this is due to $\left|\Delta E_{\text{self}}^{\mathcal{M}}\right| >> \left|\Delta E_{\text{int}}^{\mathcal{M}}\right|$.

It was necessary to find a means of simplifying the analysis of the binding step by avoiding the analysis of hundreds of interactions. Additionally, in real environments there can be numerous fragments involved hence it is necessary for one to consider a polymolecular/fragment environment. In this instance we considered 4 fragments for each complex. We were able to recover the traditional notion of complex formation in which density is donated to the metal ion by the surrounding fragments (the ligand and the water molecules). The donation of density, as measured by the electron population for a fragment, resulted in an increase of the deformation energy of the density donor and a decrease in the self-energy of the density acceptor. From this approach we were able to reconfirm earlier suggestions that the larger ligand results in less attractive coordination bonds to the water molecules, as the interaction energy between Zn^{2+} and the water molecules was strongly in favour of ZnNTA. To our knowledge, this is the first application of IQF on a system containing more than four fragments. Most importantly, the primary driving force of the binding step is the interaction energy between the ligand fragment and the metal centre and was ~35 kcal/mol more stabilising for ZnNTPA.

The analysis of the individual interactions and charges reveals that the presence of the $-CH_2-$ group in the NTPA aliphatic chains results in increased density in the neighbouring atomic environment – as measured by the atomic charges. This results in less repulsive interactions with the backbone of NTPA and more attractive interactions with the O(b)-atoms and the aggregate effect is that the interaction energy is overall in favour of the NTPA, despite there being more atoms with which the Zn centre has repulsive interactions. This is the first

result that we can find which provides a combined IQA and QTAIM explanation of the inductive effect.

This was a highly successful use of a fragmented decomposition scheme of the metal complex system which encapsulated the atomic resolution of QTAIM and IQA and can be used as a general propose tool for understanding the relative stability of any molecular system. The valuable insight from this protocol suggests that contrary to our classical and intuitive chemical thinking, the preferential complexation is due to the presence or absence of water molecules. The protocol has allowed us not only to investigate the overall energy contributions of preorganization and binding, but also to investigate particular interactions and atoms that provide the largest contribution to the overall energy of the system. With the success in these systems, we are confident that similar protocols can now be utilized for other applications such as understanding reaction mechanisms.

References

[1] Martell, A. E.; Hancock, R. D. *Metal Complexes in Aqueous Solutions*, Plenum Press: New York, 1996.

[2] Hancock, R. D. *Acc. Chem. Res.***1990**, *23*, 253–257

[3] Thom, V. J.; Fox, C. C.; Boeyens, J. C. A.; Hancock, R. D. *J. Am. Chem. Soc.***1984**, *106*, 5947–5955.

[4] Hambley, T. W. *J. Chem. Soc., Dalton Trans.* **1986**, 565–569.

[5] Hancock, R.D.; Nikolayenko, I.V. *J. Phys. Chem. A.* **2012**, *116*, 8572−8583

[6] Hancock, R.D. *Chem. Soc. Rev.* **2013**, *42*, 1500–1524.

[7] R.W.F. Bader, Atoms in Molecules: A Quantum Theory, Oxford University Press: Oxford, U.K., 1990.

8] Bader, R. F. W. *J. Phys. Chem. A.* **2009**, *113*, 10391–10396.

[9] Cioslowski, J.; Mixon, S.T. *Can. J. Chem.* **1992**, *70*, 443-449.

[10] Cioslowski, J.; Mixon, S.T. *J. Am. Chem. Soc.* **1992**, *114*, 4382–4387.

[11] Jimenez-Vazquez, H.A.; Tamariz, J.; Cross, R.J. *J. Phys. Chem. A.* **2001**, *105*, 1315–1319.

[12] Kobayashi, K.; Nagase, S. *Chem. Phys. Lett*. **2002**, *362*, 373–379.

[13] Haaland, A.; Shorokhov, D.J.; Tverdova, N.V.*Chem.–Eur. J.* **2004**, *10*, 4416–4421.

[14] Jablonski, M.J. *J. Phys. Chem. A.* **2012**, *116*, 3753–3764.

[15] Cerpa, E.; Krapp, A.; Flores-Moreno, R.; Donald, K.J.; Merino, G. *Chem.–Eur. J.* **2009**, *15*, 1985–1990.

[16] Popov, A.A.; Dunsch, L. *Chem.–Eur. J.* **2009**, *15*, 9707–9729.

[17] Dem'yanov, P.; Polestshuk, P. *Chem.–Eur. J.* **2012**, *18*, 4982–4993.

[18] Poater, J.; Solà, M.; Bickelhaupt, F.M. Chem.–*Eur. J.* **2006**, *12*, 2889–2895.

[19] Poater, J.; Solà, M.; Bickelhaupt, F.M. *Chem.–Eur. J.* **2006**, *12*, 2902–2905.

[20] Poater, J.; Visser, R.; Solà, M.; Bickelhaupt, F.M. *J. Org. Chem.* **2007**, 72, 1134–1142.

[21] Krapp, A.; Frenking, G. *Chem. Eur. J.* **2007**, *13*, 8256–8270

[22] Grimme,S.; Mück-Lichtenfeld,C.; Erker,G.; Kehr,G. Wang,H.; Beckers,H.; Willner,H. *Angew. Chem. Int. Ed.* **2009**, *48*, 2592–2595.

[23] Bader, R.W.F. *J. Phys. Chem. A.* **2011**, *115*, 12432–12435.

[24] Matta, C.F.; Hernández-Trujillo,J.; Tang,T.H.; Bader,R.F.W.; *Chem.–Eur. J.* **2003**, *9*, 1940–1951.

[25] Bader, R.F.W. *Chem.–Eur. J.* **2006**, *12*, 2896–2901.

[26] Bader, R.F.W.; Fang, D.C. *J. Chem. Theory Comput.* **2005**, *1*, 403-414.

[27] von Hopffgarten, M.; Frenking, G. *Chem.–Eur. J.* **2008**, *14*, 10227–10231.

[28] Grabowski, S.J.; Ugalde, J.M. *J. Phys. Chem. A.* **2010**, *114*, 7223–7229.

[29] Frenking, G.; Hermann, M.;*Angew. Chem.***2 013**, 125, 6036–6039.

[30] Danovich, D.; Shaik, S.; Rzepa,H.S.;*Angew. Chem. Int. Ed.* **2013**, 52, 5926–5928.

[31] Weinhold, F.;*J. Comp. Chem.* **2012**, *33*, 2440–2449.

[32] Cukrowski, I.; de Lange,J.H.; Mitoraj,M.;*J. Phys. Chem. A.* **2014**, 118, 623–637

[33] Cukrowski, I.; Matta, C. *Chemical Physics Letters* **2010**, *499*, 66–69.

[34] Mitoraj, M. P.; Michalak, A.; Ziegler, T. *J. Chem. Theory Comput.* **2009**, *5*, 962-975.

[35] Mitoraj, M. P.; Michalak, A.; Ziegler, T. *Organometallics* **2009**, *28*, 3727–3733.

[36] Mitoraj, M. P. *J. Phys. Chem. A* **2011**, *115*, 14708-14716.

[37]Varadwaj, P. R.; Varadwaj, A.; Peslherbe, G. H.; Marques H. M. *J. Phys. Chem. A.* **2011**, *115*, 13180–13190

[38] NIST Standard Reference Database 46. NIST Critically Selected Stability Constants of Metal Complexes Database, version 8.0; Database collected and selected by Smith, R. M., A.E.; US Department of Commerce, National Institute of Standards and Technology: Gaithersburg, MD, 2004.

[39] Govender, K.K.; Cukrowski, I. *Inorg. Chem.* **2010**, *49*, 6931–6941.

[40] Cukrowski, I.; Govender, K.K.; Mitoraj, M.; Srebro, M. *J. Phys. Chem. A.* **2011**, *115*, 12746–12757.

[41] Johnson, E. R.; Keinan, S.; Mori-Sánchez, P.; Contreras-García, J.; Cohen, A. J.; Yang, W. *J. Am. Chem. Soc.* **2010**, *132*, 6498−6506.

[42] Contreras-García, J.; Johnson, E. R.; Keinan, S.; Chaudret, R.;Piquemal, J. P.; Beratan, D.; Yang, W. *J. Chem. Theory Comput.* **2011**, *7*, 625−632.

[43] Gillet, N.; Chaudret, R.; Contreras-García, J.; Yang, W.; Silvi, B.;Piquemal, J. P., *J. Chem. Theory Comput.* **2012**, *8*, 3993−3997.

[44] Contreras-García, J.; Yang, W.; Johnson, E. R. *J. Phys. Chem. A* **2011**, *115*, 12983−12990.

[45] Blanco, M. A.; Pendás, A. M.; Francisco, E. *J. Chem. Theory Comput.* **2005**, *1*, 1096−1109.

[46] Francisco, E.; Pendás, A. M.; Blanco, M. A. A. *J. Chem. Theory Comput.* **2006**, *2*, 90−102.

[47] Pendás, A. M.; Blanco, M. A.; Francisco, E. *J. Comput. Chem.* **2006**, *28*, 161−184.

[48] (2010) *Spartan 10, Wavefunction Inc.*.Irvine, CA 92612, USA.

[49] M. J. Frisch, G. W. Trucks, H. B. Schlegel, G. E. Scuseria, M. A. Robb, J. R. Cheeseman, G. Scalmani, V. Barone, B. Mennucci, G. A. Petersson, H. Nakatsuji, M. Caricato, X. Li, H. P. Hratchian, A. F. Izmaylov, J. Bloino, G. Zheng, J. L. Sonnenberg, M. Hada, M. Ehara, K. Toyota, R. Fukuda, J. Hasegawa, M. Ishida, T. Nakajima, Y. Honda, O. Kitao, H. Nakai, T. Vreven, J. A. Montgomery, Jr., J. E. Peralta, F. Ogliaro, M. Bearpark, J. J. Heyd, E. Brothers, K. N. Kudin, V. N. Staroverov, R. Kobayashi, J. Normand, K. Raghavachari, A. Rendell, J. C. Burant, S. S. Iyengar, J. Tomasi, M. Cossi, N. Rega, J. M. Millam, M. Klene, J. E. Knox, J. B. Cross, V. Bakken, C. Adamo, J. Jaramillo, R. Gomperts, R. E. Stratmann, O. Yazyev, A. J. Austin, R. Cammi, C. Pomelli, J. W. Ochterski, R. L. Martin, K. Morokuma, V. G. Zakrzewski, G. A. Voth, P. Salvador, J. J. Dannenberg, S. Dapprich, A. D. Daniels, Ö. Farkas, J. B. Foresman, J. V. Ortiz, J. Cioslowski, and D. J. Fox, Gaussian 09, Revision D.1, Gaussian, Inc., Wallingford CT, 2009.

[50] . A. Keith, AIMAll (Version 13.11.04), TK Gristmill Software, Overland Parks KS, USA, 2013 (aim.tkgristmill.com).

[51] Tognetti, V.; Joubert, L.; *J. Chem. Phys.* **2013**, *138*, 024102-024108.

[52] Cukrowski, I.; de Lange, J. H.; Adeyinka, A. S.; Mangondo, P. *Comput. Theoret. Chem.* **2015**, *1053*, 60–76

[53] Govender, K.K.; Cukrowski, I. *J. Phys. Chem. A.* **2010**, 114, 1868–1878.

[54] Govender, K.K.; Cukrowski, I. *J. Phys. Chem. A.* **2009,** *113*, 3639–3647.

[55] Bader, R. F. W.; Essen, H. *J. Chem. Phys.***1984**, *80*, 1943–1960

[56] Espinosa, E.; Alkorta, I.; Elguero, J.; Molins, E. *J. Chem. Phys.* **2002**, *117*, 5529−5542

[57] Flaig, R.; Koritsanszky, Dittrich, B.; Wagner, A.; Luger, P. *J. Am. Chem. Soc.* **2002**, *124*, 3407-3417

[58] Pendás, A.M.; Francisco, E.; Blanco, M.A.; Gatti, C. *Chem.–Eur. J.* **2007**, *13*, 9362–9371.

[59] Lane, J.R.; Contreras-Garcia, J.; Piquemal, J.; Miller, B.J.; Kjaergaard. *J. Chem. Theory Comput.* **2013**, *9*, 3263−3266

[60] Pendás, A. M.; Blanco, M. A.; Francisco, E.*J. Chem. Phys.* **2006**, *125*, 184112-19.

5. Conclusions

The understanding of the relative stability of molecular systems is complex and not fully understood. As chemists, we often find ourselves bound to interpretations which are excellent for explaining the behaviour of numerous simple systems, however it is challenging and near impossible to explain the behaviour of more complicated environments *e.g.*, the S_N2 reaction can easily be explained using inductive effects, the effect of solvation, and the leaving group for linear alkanes, however the substitution of benzyl chloride using adenine is not so simple to understand. As a result, in this work we attempted to explain the preferential complexation of ligands that form 5-membered chelate rings (5m-CR) over those which form 6-membered chelate rings (6m-CR) by investigating the Be^{II} and Zn^{II} complexes of NTA and NTPA All metal ions will preferentially complex with NTA to form a 5m-CR, except for Be^{II} which preferentially forms a 6m-CR with NTPA. To understand this chemical phenomenon the following theoretical techniques were used: the Quantum Theory of Atoms in Molecules (QTAIM), the Non-Covalent Interactions (NCI) isosurfaces, the Interacting Quantum Atoms (IQA) and the Interacting Quantum Fragments (IQF). It is important to note that there is a maximum difference of a mere 7.0 kcal/mol in the formation of the complexes, whilst the largest complex is ~1.75 million kcal/mol in energy; this task is effectively searching for a needle in a haystack.

We needed a protocol that could validate the quality of our structures and select an appropriate level of theory for subsequent analysis, hence competition reactions were used to predict the formation constants. We found that MP2-optimized structures provided the most suitable structures based on ΔG_{Crn} and ΔE_{Crn}, but failed to obtain thermodynamic data for very large structures (*e.g.* ZnNTPA). Moreover, techniques such as IQA and IQF are incredibly complex and the time required to complete such a computation increases exponentially when higher level of theories such as MP2 are used. To reach a suitable compromise, DFT wavefunctions on the MP2 optimized structures gave excellent predictions of the preferentially formed complexes (BeNTPA and ZnNTA).

Commonly, chemists have used local indices and interactions to explain molecular stability and compare relative stabilities *e.g.*, steric repulsion between H-atoms in complexes of biphenyl. The strength of the coordination bonds, repulsion between lone pair donor atoms, and weak CH•••HC, OH•••O and CH•••O were analysed thoroughly. The full battery of tools used (geometric, topological properties, NCI isosurfaces and IQA interaction energies) was useful in providing insight into the nature of the interactions. In the Be^{II} complexes, the coordination bonds between the ligand and the metal centre do not

conclusively point to either complex, where as the metal-ligand coordination bonds are consistently stronger in favour of ZnNTPA in the Zn^{II} complexes. The repulsion between lone pair donors is equally inconclusive. Additionally, there are numerous more weak attractive intramolecular interactions in the complexes, and more so in the complexes NTPA which would point at the complexes of NTPA being more stable, which is true for BeNTPA but not ZnNTPA. A number of important conclusions can be made based on this.

(i) As a chemist the first point of departure when investigating molecular systems is to measure interatomic distances and infer an energetic effect. This can be incredibly misleading as shown by the coordination bonds in ZnNTPA which are shorter but it is not the stronger complex.

(ii) Secondly, we are somewhat sceptical about the classical energetic effect of short contact H---H clashes present when the size of the chelating ring increases, as these interactions often show local accumulation of density, which manifests as an AIL, and almost always, in these systems have locally attractive interaction energies. Moreover, it is often overlooked that the short contacts are present in both the free ligand and the complexed forms of NTPA, and so there cannot be a significant energetic penalty that is incurred during complex formation as the environments are similar.

(iii) Finally, even when the IQA diatomic interaction energies are used as local indices, in general, the interaction energies cannot account for the observed change in preferential complex formation.

As chemists we should avoid juxtaposing a local index, such as the strength of an single interaction, to a global molecular change. Moreover, searching for an indicator, amongest numerous individual interactions, simply produces a cacophony of numbers which are more confusing than enlightening.

In order to gain deeper insight in this challenge, rather than searching for thousands individual interactions and hoping to extract an explanation for the trend, the complexes were decomposed into chemically meaningful fragments; $\mathcal{L}$ represents the ligand fragment in both complexes, $\mathcal{M}$ represents the bare metal fragment in Be^{II} complexes, and $\mathcal{M}_w$ represents the metal-containing fragment in Zn^{II} complexes. The complex formation was then divided into a simplified two stage process. In the first step, a fragment $\mathcal{G}$ under consideration must preorganise; preorganization is the structural rearrangement from the free form of the

fragment, $\mathcal{G}_{\text{free}}$, to the preorganised form, $\mathcal{G}_{\text{p-org}}$. Secondly, the preorganised fragments must bind together to form the final complex. The important nuance in this approach monitors the energetic changes in the system as it changes from one form to another rather than attempting to infer those energetic changes by analysing local properties. It was established that for all complexes of Be^{II} and Zn^{II} the preorganization of the ligand fragment is destabilizing ($E^{\mathcal{L}}_{\text{p-org}} > 0$) and the binding was stabilizing ($E_{\text{bind}} < 0$) overriding the preorganization. The preorganization of the metal-containing fragment for Zn^{II} complexes was also destabilizing, $E^{\mathcal{M}}_{\text{p-org}} > 0$. The preorganization of both $\mathcal{L}$ and $\mathcal{M}_{\text{w}}$ fragments was consistently more destabilizing for NTPA, however, the binding enery was always more stabilizing for the complexes of NTPA. The preferentially formed complex was correctly predicted by summing up both components. The preorganization and binding correlate with results previously found using ETS-NOCV.[1] Interestingly, there is no metal-containing fragment preorganization to consider for Be^{II} complexes and hence the overall complex formation is in favour of BeNTPA. On the contrary Zn^{II} ions (and most metal cations) will remain bonded to water molecules, even in the complexed form, and thus the destabilizing preorganization of the fragment must be considered and this preorganization results in the formation on ZnNTA being more favourable in conjunction with the preorganization of the ligand. Classically, the focus has been on the size of the metal cation; however, it is clear it is the presence of the water molecules that is responsible and not specifically the metal cation size.

It was important to interrogate these findings further and so both the preorganization step and the binding step were analysed using QTAIM, NCI and IQA. The QTAIM molecular graphs and NCI isosurfaces of the preorganized ligands revealed that the atoms that will eventually form bonds to the metal centre (N- and O(b)-atoms) will share density via an AIL or locally accumulated density (blue isosurface) as a means to minimise the repulsive interactions between them. We analysed the changes in the QTAIM- and IQA-defined properties of atoms as the ligands changed during preorganization. Consistently the C- and H-atoms in the alkyl backbone of all the ligands showed the least change in the additive energies thus contributing very little to the energetic change noted during preorganization. The total additive energies reveal that the most significant changes occur on the carboxylate atoms and the N-atoms. Preorganization forms strong repulsive between N- and O(b)-atoms. In response, density is removed from the coordinating atoms and dissipated into the neighbouring C-atoms of the carboxylate group and the O(nb)-atoms. For the N- and O(b)-

atoms the interactions are far more destabilizing and the density dissipation minimizes the damage as revealed by $\Delta\sum_{Y\neq X}0.5E_{int}^{X,Y} >> 0$ and $\Delta E_{self}^{X} < 0$. The accumulation of the dissipated density on the O(nb)-atoms results in a large increase self-atomic energy ($\Delta E_{self}^{X} >> 0$) which overrides the small stabilization of interactions ($\Delta\sum_{Y\neq X}0.5E_{int}^{X,Y} < 0$). The change in the molecular environment stabilizes the interactions of the carboxylate C-atoms with all other atoms and the accumulation of density stabilises the self-atomic energy, $\Delta E_{self}^{X} << 0$.

The preorganization of metal fragment, in the case of Zn^{II} of complexes, leads to an interesting and exciting discovery. Firstly, the change in QTAIM and IQA properties of atoms reveal that the most significant changes occur on the Zn atom according to the additive energy. Secondly, when the individual interactions are considered, the most significant change occurs in the Zn–O(w1) interaction and this interaction is destabilized. This interaction corresponds to the coordination bond in the equatorial position in the complex. The Zn–O(w2) interaction is also destabilized, albeit to a lesser extent, and both these changes to coordination bonds were far more significant in ZnNTPA. Thirdly, the observed changes corresponded to the properties of those bonds in the complex. The coordination bonds of Zn to water molecules are shorter and stronger in ZnNTA regardless of the property used in analysis, and in both complexes the Zn–O(w2) coordination bond is stronger than the Zn–O(w1) bond. These observations lead to the following suggestions: to accommodate these bulky ligands the coordination bonds of water to the zinc centre must elongate, and are elongated even further in ZnNTPA. NTPA, with the longer aliphatic chain, will occupy more space around the metal centre, hence the Zn–O(w) bonds are elongated even further and so these bonds are more destabilized (weaker) in ZnNTPA. The observed difference in properties of the Zn–O(w1) and Zn–O(w2) bonds can be explained by the fact that the Zn–O(w1) bond is in the equatorial position, and occupies the same plane as the Zn–O(b) bonds to the ligands, and thus water molecule must be further away from the Zn centre. The Zn–O(w2) bond is in the axial position, away from the ligand and hence is closer to the Zn atom, thus those bonds are shorter. In the Be^{II} complexes there are no water molecules that compete for space around the metal centre and hence and BeNTPA is the favoured complex. This is the first result that explains complex stability using the water molecules as an important factor.

The binding step was analysed using IQA and IQF. It was found that the binding step is largely driven by the stabilizing of deformation energy of the metal centre and the interaction

energy between the metal and the ligand framework. Closer examination shows that binding energy is more favourable for all NTPA complexes because of the interactions between the metal centre the backbone of ligand are less repulsive in NTPA than in NTA. The presence of the additional –CH_2– group in NTPA, results in increased electron density on neighbouring atoms, reducing the repulsion between the metal centre and backbone, and increased attraction between the metal centre and the O(b)-atoms. Here, we clearly indicate the presence of an inductive effective influencing the complex formation process, a first from the IQA perspective. This is an important result, as it shows that the greater stability of a molecular system may not lie in its strongest interactions (here coordination bonds) as chemists typically take for granted, but rather in a subtler energetic balance that considers the aggregate of numerous interactions.

Previously, the Ni^{II} complexes NTA and NTPA were investigated and similar results were found[2] – results from this work for Zn^{II} and previous Ni^{II} results are shown in Table 5.1. An energetic contribution, which corresponds to E_{bind} was strongly in favour of NiNTPA, and the preorganization of both fragments was destabilising and such that ΔE_{ML} was firmly in favour of NiNTA.

Table 5.1. Computed preorganization (strain) energies and binding energies (all in kcal/mol) using relevant energy terms obtained for $(\mathcal{M}_w)_f$, $\mathcal{I}_f$ of NTA and NTPA, the Ni^{II} [2] and Zn^{II} complexes, and the respective $(\mathcal{M}_w)_p$ and $\mathcal{I}_p$.

M	$E^{\mathcal{M}}_{p\text{-}org}$			$E^{\mathcal{I}}_{p\text{-}org}$			E_{bind}			ΔE_{ML} [a]
	NTA	NTPA	$\Delta E^{\mathcal{M}}_{p\text{-}org}$ [b]	NTA	NTPA	$\Delta E^{\mathcal{I}}_{p\text{-}org}$ [b]	MNTA	MNTPA	ΔE_{bind} [c]	
Zn^{II} [d]	2.6	8.6	5.9	19.5	31.6	12.0	–102.6	–114.6	–12.0	5.9
Ni^{II} [e]	3.0	33.8	30.8	24.5	40.2	15.7	–106.4	–146.5	–40.1	6.4

[a] $\Delta E_{ML} = E_{MNTPA} - E_{MNTA}$; [b] $\Delta E_{p\text{-}org} = E_{p\text{-}org}(NTPA) - E_{p\text{-}org}(NTA)$; [c] $\Delta E_{bind} = E_{bind}(MNTPA) - E_{bind}(MNTA)$; [d] electronic energy obtained by performing a single point calculation on the RMP2 structure at the B3LYP level of theory using 6-311++G(d,p) / PCM-UFF in this work; [e] electronic energy obtained from structures optimised at the B3LYP level of theory using 6-311++G(d,p)/PCM-UAO. [2]

Furthermore, QTAIM analysis was performed and the coordination bonds to water molecules were stronger in NiNTA than in NiNTPA, further reinforcing our findings that the larger ligand, occupies more space around the central metal cation, forcing the coordination bonds to water molecules to elongate and inducing strain that results in the preferential formation of NiNTA.

This work presents a novel interpretation and application of numerous computational techniques. It is the first and highly successful application of IQF in explaining the preferential formation of 5m-CRs over 6m-CRs. Secondly, IQF has typically been used for small bimolecular adducts, whereas in this work we use relatively larger fragments and for the first time apply it to a four fragment system. Using the meaningful insights from this work, it is easy to see how these computational protocols can be used to study other systems where relative stability of the molecular system is of importance such as the study of reaction pathways. Considering that this work was looking for the proverbial needle in a haystack, it has been highly and surprisingly successful. It has been able to provide an in-depth detailed understanding of the experimentally observed phenomenon.

Comparison of this work to classical notions of complex stability

It is important to compare the findings of this work to the classical explanations for complex stability. To do so we made use of the work by R. Hancock[3] which encapsulates most of the classical views on complex stability. We will now examine some of the main explanations, typically used by inorganic chemists, that are cited in the book:

(i) The influence of the steric hindrance on complex stability. This is mentioned numerously, however, the most important statements are "Where decreasing complex stability with increase in chelate ring size has not been interpreted in entropy terms, these enthalpy changes have been attributed to steric strain, or repulsion between lone pairs on donor atoms. The steric strain interpretation can be checked by molecular mechanics (MM) calculation…" and "The reason for the low stability of polyamine complexes having only six-membered chelate rings is generally that they cannot be joined together about a square or octahedral metal ion without causing a high level of steric strain." We find that this is not the case. Considering the fragment approach, we find that the destabilizing contributions of complex stability come from the preorganization of fragments and steric hindrance in the aliphatic carbon chains plays an insignificant role. It is the functional groups of significance, in this case N-atoms and COO^- that are of importance and the formation of repulsive interactions in the coordination sphere. Furthermore, it is difficult to sight steric repulsion as responsible because short H---H contacts exist in both the free ligand of NTPA and its complexes. Finally, we have repeatedly shown that all of the descriptors which apply to CH•••O interactions (classically attractive), also apply to CH•••HC interactions (classically

repulsive). If the CH•••O interactions can be considered locally attractive, then there is no reason to refute the attractive nature of CH•••HC interactions.

(ii) The influence of the metal cation size. This too is cited on numerous occasions and certain claims are made such as "an increase in chelate ring size leads to large drops in complex stability for large metal ions, and may even lead to an increase in complex stability for small metal ions…" and "Most metal ions are not small enough to satisfy the requirements of the six membered ring." This claim is difficult to dispute. There undoubtedly exists an important relationship between the size of the metal cation and formation constants, but the size of the metal is not the cause of the preferential complexation. Rather, it is the presence additional water molecules, in this case, which leads to greater destabilization of the metal-water coordination bonds when accommodating larger ligands such as NTPA.

(iii) The interplay between steric hindrance and the inductive effect. Hancock tells us that "it has been pointed out that the donor strength and the tendency to cause steric hindrance to complex formation increase along the series $NH_3 < NH_2R < NHR_2 < NR_3$ for R = CH_3. … The steric hindrance to complex formation so often outweighs the inductive effects that the latter tend to be overlooked, and when they do manifest themselves, are misinterpreted and ascribed to other effects. These inductive effects have been termed "hidden" inductive effects." This notion is premised on the existence and influence of steric hindrance of complex formation, which we have questioned in point (i). Secondly, we concede that inductive effects play an important role on the binding between the metal and the ligand framework and is in fact the reason binding is consistently more stabilizing for the larger ligand.

Given the above analysis it might be worth revising and combining our findings with classical concepts in inorganic chemistry to have a more holistic understanding of complexes.

Future Work

This work has been useful in understanding the Zn^{II} and Be^{II} complexes of NTA and NTPA, it has not exhausted the full scope and possibility of understanding metal complexes. With that in mind, here are suggestions for future studies.

(i) Extensive investigations have been conducted on the Ni^{II} complexes of NTA and NTPA previously[2,4] however these studies have not included IQA, NCI nor IQF.

Moreover, the body of knowledge on these complexes can be expanded by analysing the decomposed complex formation process using IQF and ETS-NOCV.

(ii) An in depth study of the Pb^{II} complexes of NTA and NTPA using QTAIM, NCI, IQA, IQF and the decomposed complex formation process. Pb^{II} would be important to study, because it has the largest ionic radius of ions that complex with NTA and NTPA that we know of. Furthermore, an in depth study of the Cu^{II} complexes of NTA and NTPA using QTAIM, NCI, IQA, IQF and the decomposed complex formation process.

(iii) Using alternative fragment decompositions of the binding step, such as removing one water molecule from the complex, to understand the influence of water molecules on the complex formation process.

(iv) Using alternative levels of theory to analyse the complex formation process, such as those that consider dispersion effects *e.g.*, ω-B97xD[5,6].

(v) Most importantly, this work opens up the possibilities of exploring other molecular systems, in which there is the preferential complexation of 5m-CRs over 6m-CRs. One can now look at the comparison between ethylene diamine and propylene diamine and compare if the findings still hold. Furthermore, there is scope to fully investigate numerous metal complexes in solution.

References

[1] Cukrowski, I.; Govender, K.K.; Mitoraj, M.; Srebro, M. *J. Phys. Chem. A.* **2011**, *115*, 12746–12757.

[2] Govender, K.K. *Theoretical studies of nitrilotriacetic acid and nitrilotripropionic acid geometries for estimation of stability constants of metal complexes by Density Functional Theory*. MSc Dissertation, University of Pretoria, 2009.

[3] Martell, A. E.; Hancock, R. D. *Metal Complexes in Aqueous Solutions*, Plenum Press: New York, 1996.

[4] Govender, K.K.; Cukrowski, I. *Inorg. Chem.* **2010**, *49*, 6931–6941.

[5] Minenkov, Y.; Singstad, Å.; Occhipinti, G.; Jensen, V. R. *Dalton Trans.* **2012**, *41*, 5526–5541.

[6] Kupka, T.; Nieradka, M.; Stachów, M.; Pluta, T.; Nowak, P.; Kjær, H.; Kongsted, J.; Kaminsky, J. *J. Phys. Chem. A.* **2012**, *116*, 3728–3738

A. Appendix for Chapter 3

Table A.1. Cartesian coordinates of the NTA ligand at the MP2 level of theory. Cartesian coordinates are identical for all SPFCs thus only molecular energies are provided).

Centre Number	Atomic Number	Atomic Type	Coordinates (Å)		
			X	Y	Z
1	6	0	0.8152	–1.1007	–0.5133
2	1	0	0.3029	–2.0394	–0.2714
3	1	0	0.9079	–1.0582	–1.6166
4	7	0	–0.0005	0.0000	–0.0165
5	6	0	–1.3636	–0.1543	–0.5080
6	1	0	–1.9190	0.7580	–0.2595
7	1	0	–1.3787	–0.2495	–1.6119
8	6	0	0.5462	1.2573	–0.5102
9	1	0	0.4644	1.3176	–1.6133
10	1	0	1.6153	1.2807	–0.2672
11	6	0	2.2406	–1.2170	0.0749
12	8	0	3.0428	–1.8938	–0.6357
13	8	0	2.4832	–0.6925	1.1940
14	6	0	–0.0637	2.5495	0.0805
15	8	0	–0.6303	2.4960	1.2039
16	8	0	0.1131	3.5827	–0.6324
17	6	0	–2.1763	–1.3325	0.0780
18	8	0	–3.1800	–1.6694	–0.6191
19	8	0	–1.8262	–1.8259	1.1823

Molecular Energy (MP2): –737.16095522 au

Molecular Energy (PBE1PBE): –738.22749526 au

Molecular Energy (B3LYP): –739.04403952 au

Molecular Energy (X3LYP): –738.75902221 au

Table A.2. Cartesian coordinates of the NTPA ligand at the MP2 level of theory. Cartesian coordinates are identical for all SPFCs thus only molecular energies are provided).

Centre Number	Atomic Number	Atomic Type	Coordinates (Å)		
			X	Y	Z
1	6	0	1.2809	0.5511	0.2217
2	1	0	1.2237	1.6420	0.1856
3	1	0	1.4409	0.2711	1.2818
4	7	0	0.0052	0.0006	–0.2574
5	6	0	–1.1100	0.8298	0.2208
6	1	0	–2.0257	0.2333	0.1828
7	1	0	–0.9487	1.1069	1.2813
8	6	0	–0.1577	–1.3796	0.2210
9	1	0	–0.4902	–1.3774	1.2778
10	1	0	0.8173	–1.8736	0.1947
11	6	0	–1.1332	–2.1932	–0.6318
12	1	0	–0.7008	–2.3058	–1.6319
13	6	0	–1.3215	2.0883	–0.6226
14	1	0	–1.6047	1.7770	–1.6338
15	6	0	2.4758	0.1052	–0.6226
16	1	0	2.3532	0.5164	–1.6308
17	1	0	2.5131	–0.9852	–0.6895
18	1	0	–0.3985	2.6714	–0.6770
19	1	0	–2.0906	–1.6723	–0.7169
20	6	0	3.7806	0.6332	–0.0036
21	8	0	3.9585	1.8852	–0.0642
22	8	0	4.5497	–0.2116	0.5409
23	6	0	–1.3475	–3.5762	0.0046
24	8	0	–2.4443	–3.7741	0.6049
25	8	0	–0.3840	–4.3916	–0.0937
26	6	0	–2.4410	2.9425	–0.0059
27	8	0	–2.0947	3.9834	0.6256
28	8	0	–3.6207	2.5068	–0.1526

Molecular Energy (MP2): –854.75183093 au

Molecular Energy (PBE1PBE): –856.05220453 au

Molecular Energy (B3LYP): –857.01889370 au

Molecular Energy (X3LYP): –856.66836563 au

Table A.3. Cartesian coordinates of the BeNTA ligand at the MP2 level of theory. Cartesian coordinates are identical for all SPFCs thus only molecular energies are provided).

Centre Number	Atomic Number	Atomic Type	Coordinates (Å)		
			X	Y	Z
1	6	0	0.1244	1.4342	1.1103
2	1	0	–0.8730	1.8534	1.2798
3	1	0	0.7274	1.6187	2.0039
4	7	0	–0.0022	–0.0007	0.7987
5	6	0	–1.3084	–0.6075	1.1109
6	1	0	–1.1732	–1.6803	1.2849
7	1	0	–1.7709	–0.1740	2.0022
8	6	0	1.1765	–0.8278	1.1123
9	1	0	1.0300	–1.4471	2.0019
10	1	0	2.0368	–0.1740	1.2908
11	6	0	0.7203	2.1518	–0.1170
12	8	0	1.1644	3.2924	–0.0128
13	8	0	0.6626	1.4487	–1.2136
14	6	0	1.5074	–1.6976	–0.1168
15	8	0	0.9256	–1.2988	–1.2135
16	8	0	2.2802	–2.6469	–0.0128
17	6	0	–2.2262	–0.4537	–0.1179
18	8	0	–3.4360	–0.6413	–0.0152
19	8	0	–1.5873	–0.1520	–1.2136
20	4	0	–0.0003	–0.0011	–0.9735

Molecular Energy (MP2): –751.80525159 au

Molecular Energy (PBE1PBE): –752.89579597 au

Molecular Energy (B3LYP): –753.73210727 au

Molecular Energy (X3LYP): –753.44050911 au

Table A.4. Cartesian coordinates of the BeNTPA ligand at the MP2 level of theory. Cartesian coordinates are identical for all SPFCs thus only molecular energies are provided).

Centre Number	Atomic Number	Atomic Type	Coordinates (Å)		
			X	Y	Z
1	6	0	1.3893	–0.1999	1.6210
2	1	0	1.8901	0.7725	1.6261
3	1	0	1.3388	–0.5534	2.6594
4	7	0	0.0003	–0.0002	1.1157
5	6	0	–0.5217	1.3021	1.6216
6	1	0	–1.6143	1.2487	1.6271
7	1	0	–0.1900	1.4348	2.6598
8	6	0	–0.8663	–1.1037	1.6214
9	1	0	–1.1470	–0.8832	2.6599
10	1	0	–0.2735	–2.0228	1.6264
11	6	0	–2.1008	–1.3054	0.7448
12	1	0	–2.6199	–0.3525	0.5841
13	6	0	–0.0791	2.4720	0.7446
14	1	0	1.0055	2.4441	0.5828
15	6	0	2.1800	–1.1685	0.7435
16	1	0	1.6123	–2.0930	0.5812
17	1	0	3.1137	–1.4385	1.2423
18	1	0	–0.3135	3.4150	1.2438
19	1	0	–2.7996	–1.9809	1.2438
20	6	0	2.4990	–0.5523	–0.6158
21	8	0	3.6194	–0.6801	–1.1179
22	8	0	1.5275	0.1145	–1.1717
23	6	0	–1.7282	–1.8875	–0.6157
24	8	0	–2.4007	–2.7922	–1.1187
25	8	0	–0.6648	–1.3800	–1.1715
26	6	0	–0.7711	2.4405	–0.6152
27	8	0	–1.2205	3.4750	–1.1168
28	8	0	–0.8623	1.2660	–1.1717
29	4	0	0.0001	0.0001	–0.6751

Molecular Energy (MP2): –869.41010958 au

Molecular Energy (PBE1PBE): –870.72792430 au

Molecular Energy (B3LYP): –871.71119060 au

Molecular Energy (X3LYP): –871.35521466 au

Table A.5. Computed ΔE_{CRn}, for the competition reaction for beryllium ion using the lowest energy conformers of the ligands and complexes of NTA and NTPA.

Method	*E*(aq)/au				ΔE_{CRn} [c]
	Be(NTA)	NTPA	Be(NTPA)	NTA	
MP2[a]	–751.8053	–854.7518	–869.4101	–737.1610	–8.8
PBE1PBE[b]	–752.8958	–856.0522	–870.7279	–738.2275	–4.7
B3LYP[b]	–753.7321	–857.0189	–871.7112	–739.0440	–2.7
X3LYP[b]	–753.4405	–856.6684	–871.3552	–738.7590	–3.4

[a] energies were obtained by optimizing the lowest energy conformer of each molecule. [b]electronic energy obtained by performing a single point calculation on the RMP2 structure at the level of theory of interest [c] value in kcal/mol.

Table A.6. Computed equilibrium constants, as logK_{CRn}, for competition reaction between ligands NTPA and NTA for Be^{II}; lowest energy conformers of the ligands and complexes were used.

Method	*G*/au				ΔG_{CRn} [b]	logK_{CRn}	Δlog$K$[c]
	BeNTA	NTPA	BeNTPA	NTA			
PBE1PBE[a]	–752.7960	–855.8834	–870.5444	–738.1393	–2.7	2.0	–0.4
B3LYP[a]	–753.6335	–856.8529	–871.5291	–738.9579	–0.3	0.3	–2.1
X3LYP[a]	–753.3416	–856.5015	–871.1726	–738.6723	–1.1	0.8	–1.6

[a]Gibbs free energy was obtained by performing a single point frequency calculation on the RMP2 structure. [c]Values in kcal/mol. [d] $\Delta\log K$ = (theoretical – experimental) value.

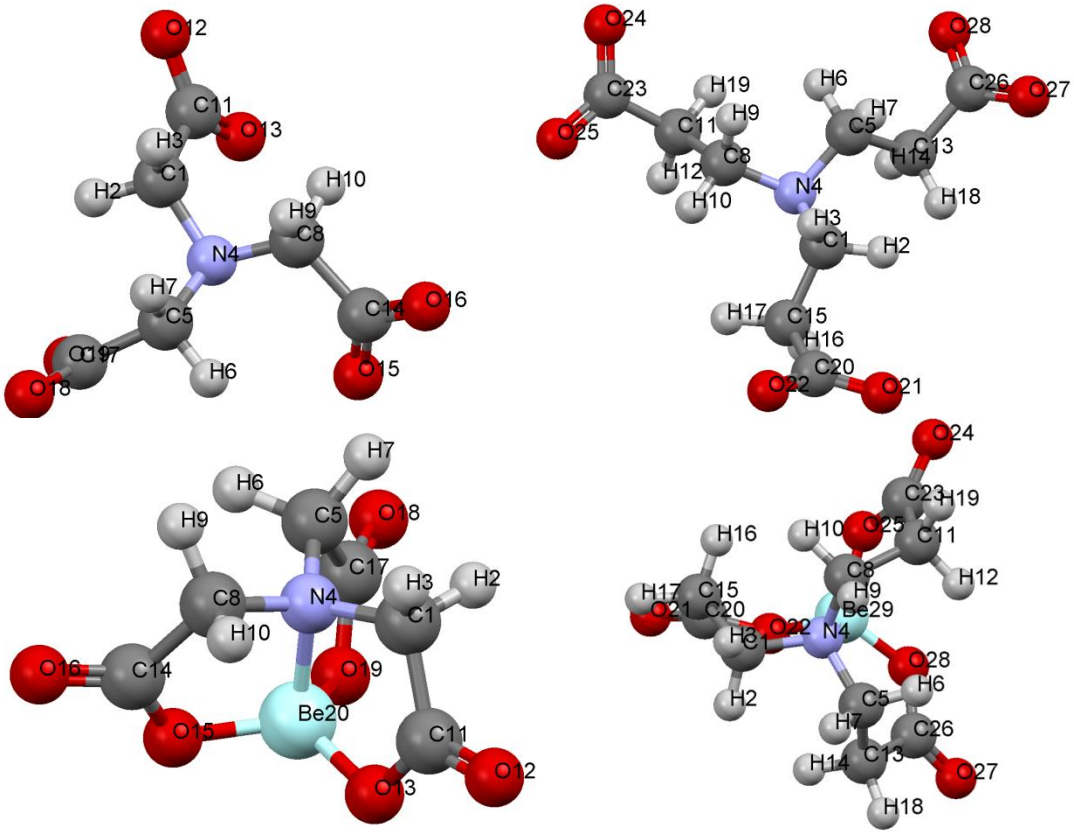

Figure A.1. The structures of L_{free} of NTA and NTPA and the complexes BeNTA and BeNTPA

Table A.7. Selected interatomic distances for steric contacts in both complexes at the MP2 level of theory.

BeNTA		BeNTPA	
Interaction	d / Å	Interaction	d / Å
N•••O13	2.568	N•••O22	2.753
N•••O15	2.568	N•••O25	2.753
N•••O19	2.566	N•••O28	2.753
O13•••O15	2.760	O25•••O28	2.653
O15•••O19	2.762	O25•••O22	2.653
O13•••O19	2.761	O22•••O28	2.653
H2•••H7	2.332	H2•••H14	2.160
H6•••H9	2.329	H6•••H12	2.159
H3•••H10	2.332	H10•••H16	2.157

Table A.8. Selected structural properties of the complexes for the comparison with minimum strain geometries (shown in brackets).

	BeNTA		BeNTPA	
Bond	d / Å	Δd	d / Å	Δd
Be–N	1.772 (2.5)	–0.728	1.791 (1.6)	0.191
Be–O	1.612 (>3.2)	–1.588	1.610 (1.9)	–0.290
Bond Angle	Angle / deg	Δ(angle)	Angle / deg	Δ(angle)
Be–N–C	102.24 (109.5)	–7.26	109.82 (109.5)	0.32
Be–O–C	112.21 (126)	–13.79	122.64 (126)	–3.36
O–Be–N (N–M–N)	102.24 (69)	33.24	107.96 (109.5)	–1.54
O–Be – N (O–M–O)	102.24 (58)	44.24	107.96 (95)	12.96

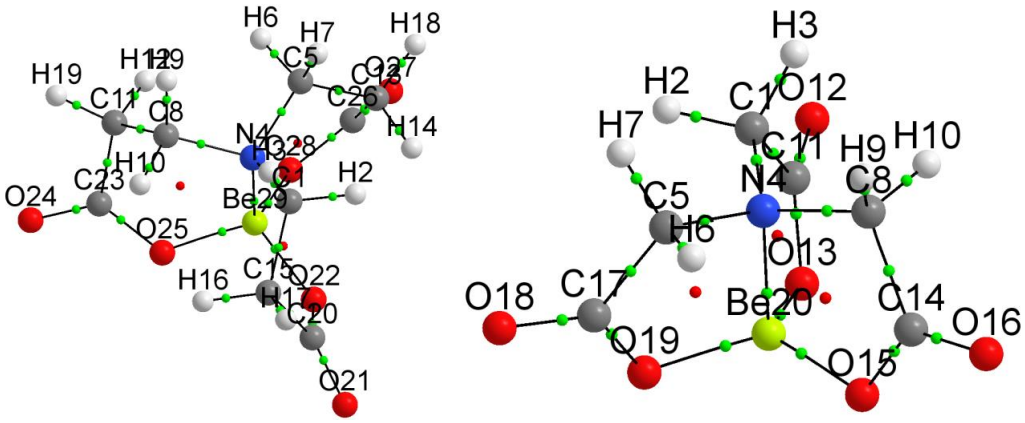

Figure A.2. The QTAIM molecular graphs of (a) the lowest energy conformer of Be(NTPA), and (b) the complex of Be(NTA).

Table A.9. QTAIM-defined topological data at RCPs of chelating rings in BeNTA and BeNTPA at the MP2[a] level of theory.

BeNTA			BeNTPA		
Atoms	$\rho(r)$	$\nabla^2\rho(r)$	Atoms	$\rho(r)$	$\nabla^2\rho(r)$
N4-C5-C17-O19-Be20	0.0336	0.1658	N4-C5-C13-C26-O28-Be29	0.0184	0.0886
C1-N4-Be20-O13-C11	0.0336	0.1654	N4-C8-C11-C23-O25-Be29	0.0184	0.0887
N4-C8-C14-O15-Be20	0.0336	0.1652	C1-N4-Be29-O22-C20-C15	0.0184	0.0887
av:	*0.0336*	*0.1655*	*av:*	*0.0184*	*0.0887*

[a] all values are in au.

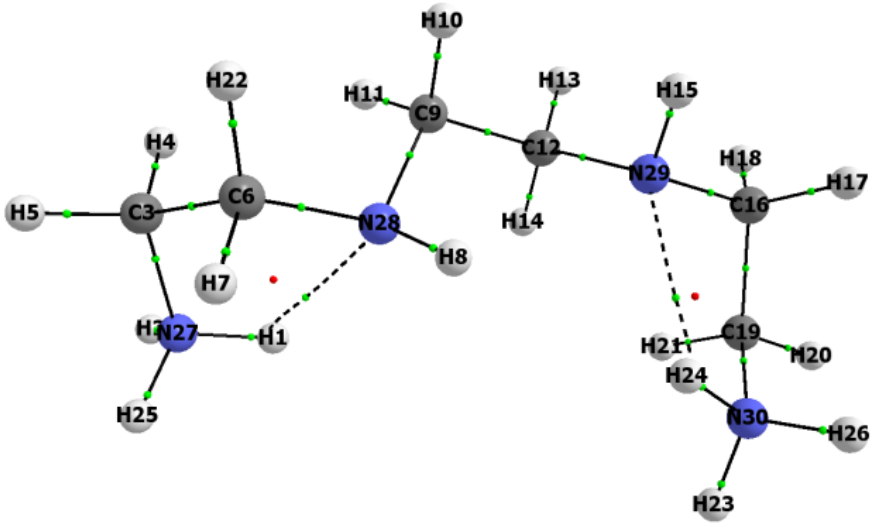

Figure A.3. An example of an AIL linking atoms N29 and H24 with d(N,H) = 2.566 Å even though in the same environment atoms N29 and H8 with d(N,H) = 2.511 Å are present and they are not linked by AIL.

Table A.10. Computed preorganization (strain) energies and affinity energies using L_{free} of NTA and NTPA, the complexes BeNTA and BeNTPA, and the respective $L_{p\text{-}org}$.

Level of Theory	$G_{p\text{-}org}$				G_{aff}				ΔG_{ML}
	NTA	NTPA	$\Delta G^{L}_{p\text{-}org}$	Ratio[c]	BeNTA	BeNTPA	$\Delta G^{Be,L^*}_{aff}$	Ratio[c]	
MP2[a]	53.8	65.0	11.2	1.2	–252.6	–270.3	–17.6	1.1	–6.4
PBE1PBE[b]	53.0	70.1	17.1	1.3	–256.4	–276.2	–19.8	1.1	–2.7
B3LYP[b]	55.3	73.2	17.8	1.3	–254.6	–272.7	–18.2	1.1	–0.3
X3LYP[b]	54.9	72.0	17.1	1.3	–256.2	–274.5	–18.2	1.1	–1.1

[a] energies were obtained by optimizing the lowest energy conformer of each molecule. [b] electronic energy obtained by performing a single point frequency calculation on the RMP2 structure at the level of theory of interest. [c] Ratio = (NTPA/NTA) value.

Table A.11. Computed affinity energies using the complexes BeNTA and BeNTPA, and the respective $L_{p\text{-}org}$.

Level of Theory	E^{a}					E_{aff}^{b}	
	Be	$NTA_{p\text{-}org}$	BeNTA	$NTPA_{p\text{-}org}$	BeNTPA	BeNTA	BeNTPA
MP2	–14.3024	–737.0781	–751.8053	–854.6543	–869.4101	–266.5	–284.5
PBE1PBE*	–14.3326	–738.1418	–752.8958	–855.9443	–870.7279	–264.4	–283.0
B3LYP*	–14.3450	–738.9588	–753.7321	–856.9082	–871.7112	–268.8	–287.4
X3LYP*	–14.3353	–738.6742	–753.4405	–856.5590	–871.3552	–270.5	–289.2

[a] values are in au; [b] values are in kcal/mol

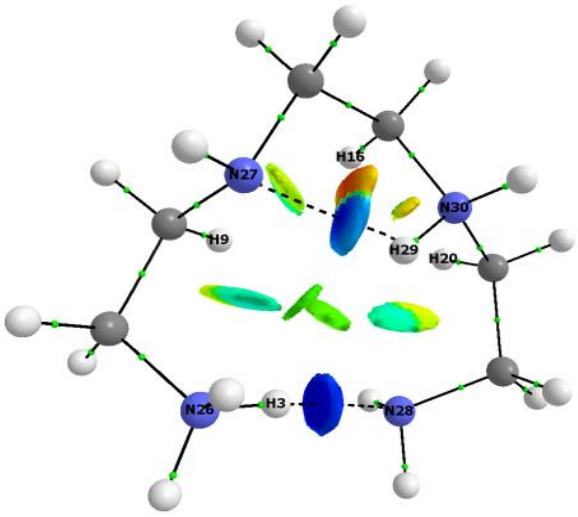

Figure A.4. Typical NCI blue-coloured isosurface between H3 and N28 which recovers a classical intramolecular NH•••N hydrogen bond.

B. Appendix for Chapter 4

Part 1:

Procedure for determining theoretical equilibrium constants for the competition reaction

The complex formation reactions between zinc and the ligands of interest are shown in equations (1) and (2) (charges have been omitted throughout for simplicity)

$$Zn(H_2O)_6 + NTA \leftrightarrow ZnNTA + 4H_2O \qquad K_1^{(a)} = \frac{[ZnNTA]}{[Zn][NTA]} \qquad (B1)$$

$$Zn\ (H_2O)_6 + NTPA \leftrightarrow ZnNTPA + 4H_2O \qquad K_1^{(b)} = \frac{[ZnNTPA]}{[Zn][NTPA]} \qquad (B2)$$

A competition reaction can be viewed as a combination of the two complexation reactions, (B1) – (B2), in which the ligands NTPA and NTA compete for Zn^{II} and the participation of water is cancelled

$$ZnNTPA + NTA \leftrightarrow ZnNTA + NTPA \qquad K_{CRn} = \frac{[ZnNTA][NTPA]}{[ZnNTPA][NTA]} \qquad (B3)$$

The equilibrium constant, $\log K_{CRn}$, for the competition reaction can be determined because the experimental formation constants are known ($\log K_1^{(a)} = 10.45$ $\log K_1^{(b)} = 5.3$) for both complexes. Hence

$$\log K_{CRn} = \log \frac{K_1^{(a)}}{K_1^{(b)}} = \log K_1^{(a)} - \log K_1^{(b)} = 5.15 \qquad (B4)$$

Considering the well-known relationship which correlates thermodynamic free energy and equilibrium constant, $\Delta G = -RT\ln K$, it is possible to determine the expected from experiment ΔG for the reaction using the conversion factor, 1 log unit = 1.36 kcal/mol. $\Delta G_{CRn}(aq) = -7.0$ kcal/mol experimentally. This information is particularly important as one can attempt to reproduce this value theoretically by computing the free energy of the competition reaction (B3) as

$$\Delta G_{CRn} = G(ZnNTA) + G(NTPA) - G(ZnNTPA) - G(NTA) \qquad (B5)$$

Part 2:

Preorganization of the ligand fragments

This section gives a full, in-depth analysis of the preorganization of the ligand fragments. Focussing on the groups of chemical significance, N-atoms and atoms in the carboxylate groups, the following pattern emerges: the highly negatively charged atoms, N, γO(b) and γO(nb), experienced a large increase in atomic additive energies whereas the highly positively charged γC-atoms of the carboxylate groups became stabilized the most. The analysis of energy components, an intra-atomic contribution E_{self}^{X} and interatomic contributions $\sum_{Y\neq X} 0.5E_{int}^{X,Y}$ and other physical properties shown in Table B1, leads to the following conclusions:

(i) For O(b)- and N-atoms, which will eventually coordinate to the metal atom, the energetic destabilization is due to unfavourable increase in interactions with all remaining atoms in a ligand which is much greater in value than the change in self-atomic energies; $\Delta\sum_{Y\neq X} 0.5E_{int}^{X,Y} >> |\Delta E_{self}^{X}|$. The preorganization of the ligand resulted in the outflow of density, $\Delta N^{X} < 0$, and the contraction of the atomic volume $\Delta Vol^{X} < 0$. This was accompanied by a resultant decrease in $\Delta T^{X} < 0$, reduced electron-electron repulsion, $\Delta V_{ee}^{XX} < 0$, and reduced electron-neutron attraction, $\Delta V_{ne}^{XX} > 0$, within the atomic basins. Note that for all N- and carboxylate atoms, if $\Delta N^{X} < 0$, then $\Delta T^{X} < 0$, $\Delta V_{ee}^{XX} < 0$ and $\Delta V_{ne}^{XX} > 0$ and if $\Delta N^{X} < 0$, then $\Delta T^{X} > 0$, $\Delta V_{ee}^{XX} > 0$ and $\Delta V_{ne}^{XX} < 0$. then explain the observed decrease in the self-atomic energy, $\Delta E_{self}^{X} < 0$; recall that $E_{self}^{X} = T^{X} + V_{ne}^{XX} + V_{ee}^{XX}$.

(ii) The converse is noted for the O(nb)-atoms: the change in the additive energy is driven by the destabilization of the self-atomic energies, thus changes in the atomic basins, resulting in $|\Delta\sum_{Y\neq X} 0.5E_{int}^{X,Y}| << \Delta E_{self}^{X}$. The dissipated density from the N- and O- atoms involved in contacts, is accommodated in the accumulation of density in the interatomic region (as shown with NCI isosurfaces and AILs) and the large inflow of density into the O(nb) atoms,$\Delta N^{X} > 0$. Consequently, the electron-electron repulsion became more repulsive, $\Delta V_{ee}^{XX} > 0$, and the electron-neutron attraction became more attractive, $\Delta V_{ne}^{XX} < 0$, in these atoms basins. Although $\left|\Delta V_{ne}^{XX}\right| > \left|\Delta V_{ee}^{XX}\right|$, we see that $\Delta T^{X} > \left|\Delta V_{ne}^{XX} + \Delta V_{ee}^{XX}\right|$ thus the combined effect lead to large increase in the self energies of the O(nb)-atoms.

(iii) Preorganization increased the stability of the highly, positively charged caboxylate C-atoms, $\Delta E_{\text{add}}^{\text{X}} << 0$. This is largely due to the more attractive molecular environment $\Delta \sum_{\text{Y}\neq\text{X}} 0.5 E_{\text{int}}^{\text{X,Y}} << 0$ for NTA and NTPA, stabilizing the interactions with all other atoms. These atoms assist with the dissipation electron density when the ligand goes from L_{free} to $\text{L}_{\text{p-org}}$ state, by accommodating more electron density, $\Delta N^{\text{X}} > 0$, albeit to a lesser extent. The charge re-arrangement in the atomic basin, resulted in similar, in sign (but not magnitude) changes to T^{X}, $V_{\text{ne}}^{\text{XX}}$ and $\Delta V_{\text{ee}}^{\text{XX}}$. However, the combined change is such that the self-energies are stabilized, $\Delta E_{\text{self}}^{\text{X}} < 0$.

Table B.1. Relative from L_{free} structures to $L_{p\text{-}org}$, changes in the selected QTAIM- and IQA-(at the RX3LYP level of theory on the MP2 structure) defined energy terms (in kcal/mol) and additional atomic properties of atoms in ZnNTA and ZnNTPA.[a]

Atom X	ΔE^X_{add}	$\Delta \sum_{Y \neq X} 0.5 E^{X,Y}_{int}$	ΔE^X_{self}	ΔT^X	ΔV^{XX}_{ne}	ΔV^{XX}_{ee}	q^X_{free}	$q^X_{L_{p-org}}$	ΔE^X	ΔN^X	ΔVol^X	Δd^X_e
ZnNTA												
αC8	–0.3	2.1	–2.4	–11.1	27.7	–19.1	0.314	0.319	12.0	–0.005	2.91	–0.0061
αH9	–0.5	–0.4	–0.1	3.1	–3.4	0.2	–0.030	–0.028	–3.1	–0.002	–0.99	0.0003
αH10	0.1	1.7	–1.6	3.8	–9.0	3.6	0.017	–0.002	–3.8	0.019	2.63	–0.0008
βC14	–12.3	–10.7	–1.6	7.6	–20.6	11.5	1.583	1.578	–6.7	0.005	0.82	–0.0023
O15(b)	18.3	35.5	–17.2	–43.2	156.8	–130.8	–1.278	–1.248	45.1	–0.030	–0.83	0.0002
O16(nb)	10.4	–12.2	22.6	49.2	–166.7	140.1	–1.289	–1.321	–47.5	0.032	0.45	0.0000
N4	–0.1	12.7	–12.8	–35.5	158.3	–135.5	–0.959	–0.900	37.0	–0.059	–9.28	0.0128
ZnNTPA												
αC8	–3.8	–0.8	–3.0	–2.7	–7.9	7.6	0.339	0.335	3.8	0.005	0.10	–0.0001
αH9	0.1	–0.3	0.4	7.3	–13.0	6.1	–0.030	–0.053	–7.3	0.023	0.98	0.0000
αH10	0.1	3.1	–3.1	2.8	–8.3	2.4	0.004	–0.017	–2.8	0.021	4.61	–0.0017
βC11	–1.0	0.2	–1.2	–4.6	–3.2	6.7	0.026	0.021	5.7	0.005	–0.45	0.0009
βH12	1.4	–2.2	3.6	0.6	1.5	1.5	–0.010	–0.004	–0.6	–0.006	–4.76	0.0020
βH19	0.1	0.6	–0.5	–2.0	3.5	–2.1	–0.013	–0.012	2.0	–0.001	2.28	–0.0011
γC23	–28.9	–23.6	–5.2	2.3	–19.6	12.0	1.573	1.565	–1.2	0.008	0.57	–0.0015
O24(nb)	17.5	–6.4	24.0	50.3	–183.7	157.4	–1.284	–1.322	–48.2	0.038	–0.37	0.0004
O25(b)	40.1	52.4	–12.2	–35.6	168.7	–145.3	–1.284	–1.236	38.0	–0.048	–7.57	0.0028
N4	19.2	49.4	–30.2	–57.4	346.5	–319.3	–0.969	–0.837	59.2	–0.131	–13.98	0.0173

[a] $E^X_{self} = T^X + V^{XX}_{ne} + V^{XX}_{ee}$, by definition; T^X - the electronic kinetic energy of an atom (a Hamiltonian form); V^{XX}_{ne} - attraction energy between electron density distribution of atom X and nucleus of Atom X; V^{XX}_{ee} - two-electron interaction energy of atom X with itself; E^X - approximation to a virial-based total energy of atom X; N^X - average No of electrons in atom X (atomic electron population); Vol^X – atomic volume in bohr^3 (volume bounded by interatomic surfaces of atom X and by isosurface of the electron density distribution (0.001au isodensity surface was used); $d^X_e = N(Vol^X)/Vol^X$ - average electron density in Vol^X where $N(Vol^X)$ is average number of electrons in Vol^X.

Part 3:

Derivation of the IQA/IQF-based protocol for molecular decomposition

Let us first express the components of the binding energy, as shown in Eq. (B6), in terms of additive atomic energies,

$$E_{\text{bind}} = \sum_{\text{X}\in\text{ML}} E_{\text{add}}^{\text{X}} - \sum_{\text{X}\in\mathcal{I}_{\text{p}}} E_{\text{add}}^{\text{X}} - \sum_{\text{X}\in(\mathcal{M}_{\text{w}})_{\text{p}}} E_{\text{add}}^{\text{X}} \qquad \text{(B6)}$$

Recall that the additive energy of an atom is the sum of the self-atomic contribution and the interatomic contributions, thus by substituting $E_{\text{add}}^{\text{X}} = E_{\text{self}}^{\text{X}} + \sum_{\text{Y}\neq\text{X}} 0.5E_{\text{int}}^{\text{X,Y}}$ into Eq. (B6) the binding energy is

$$E_{\text{bind}} = \sum_{\text{X}\in\text{ML}} E_{\text{self}}^{\text{X}} + 0.5\sum_{\text{X}\in\text{ML}}\sum_{\substack{\text{X}\neq\text{Y}\\ \text{Y}\in\text{ML}}} E_{\text{int}}^{\text{X,Y}} - \sum_{\text{X}\in\mathcal{I}_{\text{p}}} E_{\text{self}}^{\text{X}} - 0.5\sum_{\text{X}\in\mathcal{I}_{\text{p}}}\sum_{\substack{\text{Y}\neq\text{X}\\ \text{Y}\in\mathcal{I}_{\text{p}}}} E_{\text{int}}^{\text{X,Y}} - \sum_{\text{X}\in(\mathcal{M}_{\text{w}})_{\text{p}}} E_{\text{self}}^{\text{X}} - 0.5\sum_{\text{X}\in\mathcal{M}_{\text{p}}}\sum_{\substack{\text{Y}\neq\text{X}\\ \text{Y}\in(\mathcal{M}_{\text{w}})_{\text{p}}}} E_{\text{int}}^{\text{X,Y}} \qquad \text{(B7)}$$

The first two terms represent the energy of the complex in the primary IQA energy components; the third term represents the self-energies of all atoms in the preorganized ligand which can be written as $E_{\text{self}}^{\mathcal{I}_{\text{p}}}$, self-atomic energy contribution to the energy of the fragment $\mathcal{I}_{\text{p}}$; the fourth term sums up all unique diatomic interaction energies between atoms within the fragment, $\mathcal{I}_{\text{p}}$, and is the intra-fragment interaction energy, $E_{\text{int}}^{\mathcal{I}_{\text{p}}}$. Similarly, $E_{\text{self}}^{(\mathcal{M}_{\text{w}})_{\text{p}}}$ represents the contribution of the self-atomic energies and $E_{\text{int}}^{(\mathcal{M}_{\text{w}})_{\text{p}}}$ represents the intra-fragment energy contribution to the energy of the fragment $(\mathcal{M}_{\text{w}})_{\text{p}}$. The binding energy in Eq. B7 can be written in fragment notation as

$$E_{\text{bind}} = \sum_{\text{X}\in\text{ML}} E_{\text{self}}^{\text{X}} + 0.5\sum_{\text{X}\in\text{ML}}\sum_{\substack{\text{Y}\neq\text{X}\\ \text{Y}\in\text{ML}}} E_{\text{int}}^{\text{X,Y}} - E_{\text{self}}^{\mathcal{I}_{\text{p}}} - E_{\text{int}}^{\mathcal{I}_{\text{p}}} - E_{\text{self}}^{(\mathcal{M}_{\text{w}})_{\text{p}}} - E_{\text{int}}^{(\mathcal{M}_{\text{w}})_{\text{p}}}. \qquad \text{(B8)}$$

During the final formation, all diatomic interactions existing in the framework of the pre-organized fragments ($\mathcal{I}_{\text{p}}$ and $(\mathcal{M}_{\text{w}})_{\text{p}}$) must change to those present in the complex, $\mathcal{I}_{\text{c}}$ which interacts with $(\mathcal{M}_{\text{w}})_{\text{c}}$. As a matter of fact, because of a large density redistribution taking

place on complex formation, not only the diatomic interaction energies, but also the self-atomic and additive atomic energies in the each fragment must have changed too. To understand all the changes taking place in the ligand, it was necessary to further decompose the interaction energy term applicable to the ML complex (second term in Eq. (B8)) into separate contributions coming from (i) interactions between atoms within a ligand framework when in complex, (ii) interactions between atoms with in the metal-containing fragment when in complex, and (iii) all new diatomic interactions in the complex between all atoms in $\mathcal{M}_w$ and all atoms of $\mathcal{L}$, the first, second and third term in Eq. (B9), respectively

$$0.5\sum_{X\in ML}\sum_{\substack{X\neq Y\\ Y\in ML}}E_{int}^{X,Y} = 0.5\sum_{X\in \mathcal{L}_c}\sum_{\substack{Y\neq X\\ Y\in \mathcal{L}_c}}E_{int}^{X,Y} + 0.5\sum_{X\in(\mathcal{M}_w)_c}\sum_{\substack{Y\neq X\\ Y\in(\mathcal{M}_w)_c}}E_{int}^{X,Y} + \sum_{X\in(\mathcal{M}_w)_c}\sum_{Y\in \mathcal{L}_c}E_{int}^{X,Y} \qquad \text{(B9)}$$

The last term is effectively the interaction energy between two fragments (inter-fragment interaction energy) and in fragment notation we obtain

$$0.5\sum_{X\in ML}\sum_{\substack{X\neq Y\\ Y\in ML}}E_{int}^{X,Y} = E_{int}^{\mathcal{L}_c} + E_{int}^{(\mathcal{M}_w)_c} + E_{int}^{(\mathcal{M}_w)_c,\mathcal{L}_c} \qquad \text{(B10)}$$

Traditionally the focus has been on the coordination bonds, but an inter-fragment interaction energy term analyses all possible interactions between the two fragments. The expansion of the interatomic contributions to the energy of the complex also enables one to define a term that estimates the energy gain/lost as a result of the changes in the intra-fragment interaction energy,

$$\Delta E_{int}^{\mathcal{L}} = 0.5\sum_{X\in \mathcal{L}_c}\sum_{\substack{Y\neq X\\ Y\in \mathcal{L}_c}}E_{int}^{X,Y} - 0.5\sum_{X\in \mathcal{L}_p}\sum_{\substack{Y\neq X\\ Y\in \mathcal{L}_p}}E_{int}^{X,Y} \qquad \text{(B11)}$$

and

$$\Delta E_{int}^{\mathcal{M}_w} = 0.5\sum_{X\in(\mathcal{M}_w)_c}\sum_{\substack{Y\neq X\\ Y\in(\mathcal{M}_w)_c}}E_{int}^{X,Y} - 0.5\sum_{X\in(\mathcal{M}_w)_p}\sum_{\substack{Y\neq X\\ Y\in(\mathcal{M}_w)_p}}E_{int}^{X,Y} \qquad \text{(B12)}$$

These terms estimate the energy pertaining to the rearrangement of intra-fragment interactions within the fragment framework when it moves from the preorganized state ($\mathcal{L}_p$ and $(\mathcal{M}_w)_p$) to the final complexed state ($\mathcal{L}_c$ and $(\mathcal{M}_w)_c$). In the fragment notation we can express Eq. (B11) as

$$\Delta E_{\text{int}}^{\mathcal{I}} = E_{\text{int}}^{\mathcal{I}_c} - E_{\text{int}}^{\mathcal{I}_p} \tag{B13}$$

And Eq. (B12) as

$$\Delta E_{\text{int}}^{\mathcal{M}_w} = E_{\text{int}}^{(\mathcal{M}_w)_c} - E_{\text{int}}^{(\mathcal{M}_w)_p} \tag{B14}$$

By making use of expression (B10), (B13) and (B14) and combining contributions coming from self-atomic energies one can express Eq. (B8) in terms of primary energy terms used in the IQA partitioning scheme, self-atomic and diatomic interaction energies, as

$$E_{\text{bind}} = \sum_{X \in ML} \Delta E_{\text{self}}^{X} + \Delta E_{\text{int}}^{\mathcal{I}} + \Delta E_{\text{int}}^{\mathcal{M}_w} + E_{\text{int}}^{(\mathcal{M}_w)_c, \mathcal{I}_c} \tag{B15}$$

where

$$\sum_{X \in ML} \Delta E_{\text{self}}^{X} = \sum_{X \in ML} E_{\text{self}}^{X} - \sum_{X \in \mathcal{I}_p} E_{\text{self}}^{X} - \sum_{X \in (\mathcal{M}_w)_p} E_{\text{self}}^{X} \tag{B16}$$

which for brevity can be written as

$$\Delta E_{\text{self}}^{ML} = E_{\text{self}}^{ML} - E_{\text{self}}^{\mathcal{I}_p} - E_{\text{self}}^{(\mathcal{M}_w)_p} \tag{B17}$$

The term $\sum_{X \in ML} \Delta E_{\text{self}}^{X} = \Delta E_{\text{self}}^{ML}$ defined in Eq. (B16) accounts for the total energy contribution coming from the self-atomic energies of all atoms of the molecular system when the pre-organized ligand and metal fragment bind to form a final complex ML.

To learn about the nature of changes observed in diatomic interactions within each fragment, one can make use of a classical (electrostatic) contribution, $V_{\text{cl}}^{X,Y}$, and exchange-correlation, XC energy term, $V_{\text{XC}}^{X,Y}$ which are obtained from the decomposition of a diatomic energy term, $E_{\text{int}}^{X,Y} = V_{\text{cl}}^{X,Y} + V_{\text{XC}}^{X,Y}$. Thus we can isolate the interaction energy rearrangements in the fragment as being of the classical electrostatic and exchange-correlation origin,

$$\Delta E_{\text{int}}^{\mathcal{I}} = \Delta V_{\text{cl}}^{\mathcal{I}} + \Delta V_{\text{XC}}^{\mathcal{I}} \tag{B18}$$

where

$$\Delta V_{\text{cl}}^{\mathcal{I}} = 0.5 \sum_{X \in \mathcal{I}_c} \sum_{\substack{Y \neq X \\ Y \in \mathcal{I}_c}} V_{\text{cl}}^{X,Y} - 0.5 \sum_{X \in \mathcal{I}_p} \sum_{\substack{Y \neq X \\ Y \in \mathcal{I}_p}} V_{\text{cl}}^{X,Y} \tag{B19}$$

and

$$\Delta V_{\mathrm{XC}}^{\mathcal{I}} = 0.5 \sum_{\mathrm{X}\in\mathcal{I}_{\mathrm{c}}} \sum_{\substack{\mathrm{Y}\neq\mathrm{X} \\ \mathrm{Y}\in\mathcal{I}_{\mathrm{c}}}} V_{\mathrm{XC}}^{\mathrm{X,Y}} - 0.5 \sum_{\mathrm{X}\in\mathcal{I}_{\mathrm{p}}} \sum_{\substack{\mathrm{Y}\neq\mathrm{X} \\ \mathrm{Y}\in\mathcal{I}_{\mathrm{p}}}} V_{\mathrm{XC}}^{\mathrm{X,Y}} \tag{B20}$$

Similar definitions would apply to the metal containing fragment

$$\Delta E_{\mathrm{int}}^{\mathcal{M}_{\mathrm{w}}} = \Delta V_{\mathrm{cl}}^{\mathcal{M}_{\mathrm{w}}} + \Delta V_{\mathrm{XC}}^{\mathcal{M}_{\mathrm{w}}} \tag{B21}$$

where

$$\Delta V_{\mathrm{cl}}^{\mathcal{M}_{\mathrm{w}}} = 0.5 \sum_{\mathrm{X}\in(\mathcal{M}_{\mathrm{w}})_{\mathrm{c}}} \sum_{\substack{\mathrm{Y}\neq\mathrm{X} \\ \mathrm{Y}\in(\mathcal{M}_{\mathrm{w}})_{\mathrm{c}}}} V_{\mathrm{cl}}^{\mathrm{X,Y}} - 0.5 \sum_{\mathrm{X}\in(\mathcal{M}_{\mathrm{w}})_{\mathrm{p}}} \sum_{\substack{\mathrm{Y}\neq\mathrm{X} \\ \mathrm{Y}\in(\mathcal{M}_{\mathrm{w}})_{\mathrm{p}}}} V_{\mathrm{cl}}^{\mathrm{X,Y}} \tag{B22}$$

and

$$\Delta V_{\mathrm{XC}}^{\mathcal{M}_{\mathrm{w}}} = 0.5 \sum_{\mathrm{X}\in(\mathcal{M}_{\mathrm{w}})_{\mathrm{c}}} \sum_{\substack{\mathrm{Y}\neq\mathrm{X} \\ \mathrm{Y}\in(\mathcal{M}_{\mathrm{w}})_{\mathrm{c}}}} V_{\mathrm{XC}}^{\mathrm{X,Y}} - 0.5 \sum_{\mathrm{X}\in(\mathcal{M}_{\mathrm{w}})_{\mathrm{p}}} \sum_{\substack{\mathrm{Y}\neq\mathrm{X} \\ \mathrm{Y}\in(\mathcal{M}_{\mathrm{w}})_{\mathrm{p}}}} V_{\mathrm{XC}}^{\mathrm{X,Y}} \tag{B23}$$

Equally important is an insight one can gain from classical and XC contributions making up the $E_{\mathrm{int}}^{(\mathcal{M}_{\mathrm{w}})_{\mathrm{c}},\mathcal{I}_{\mathrm{c}}}$ term and this can be easily computed from

$$E_{\mathrm{int}}^{(\mathcal{M}_{\mathrm{w}})_{\mathrm{c}},\mathcal{I}_{\mathrm{c}}} = V_{\mathrm{cl}}^{(\mathcal{M}_{\mathrm{w}})_{\mathrm{c}},\mathcal{I}_{\mathrm{c}}} + V_{\mathrm{XC}}^{(\mathcal{M}_{\mathrm{w}})_{\mathrm{c}},\mathcal{I}_{\mathrm{c}}} = \sum_{\mathrm{X}\in(\mathcal{M}_{\mathrm{w}})_{\mathrm{c}}} \sum_{\mathrm{Y}\in\mathcal{I}_{\mathrm{c}}} V_{\mathrm{cl}}^{\mathrm{X,Y}} + \sum_{\mathrm{X}\in(\mathcal{M}_{\mathrm{w}})_{\mathrm{c}}} \sum_{\mathrm{Y}\in\mathcal{I}_{\mathrm{c}}} V_{\mathrm{XC}}^{\mathrm{X,Y}} \tag{B24}$$

All the above is of great importance as it allows us to trace changes in primary IQA energy terms and their components which we hope will be of great help in tracking the origin and nature of factors controlling preferential affinity between two fragments, $\mathcal{M}_{\mathrm{w}}$ and $\mathcal{I}$, in both complexes, hence also should explain relative stability of molecular systems.

Finally, it is also of interest and importance to recover the terms defined in the IQF approach. To achieve that, let us first recall that in the IQA framework, the deformation energy of an atom is defined as the change in the self-energy of an atom X, $E_{\mathrm{def}}^{\mathrm{X}} = \Delta E_{\mathrm{self}}^{\mathrm{X}} = E_{\mathrm{self}}^{\mathrm{X}} - E_{\mathrm{vac}}^{\mathrm{X}}$, where the last term typically represents the energy of an atom *in vacuo*. Because there are two fragments in the molecular system investigate here, the polyatomic $\mathcal{I}$ and $\mathcal{M}_{\mathrm{w}}$, the energy contribution due to the change in self-atomic energies ($\Delta E_{\mathrm{self}}^{\mathrm{ML}}$) can be conveniently divided into those for each atom of the ligand, $\Delta E_{\mathrm{self}}^{\mathcal{I}}$, when it changes from the $\mathcal{I}_{\mathrm{p}}$ to $\mathcal{I}_{\mathrm{c}}$ state and those of each atom of the metal fragment $\Delta E_{\mathrm{self}}^{\mathcal{M}}$ when it changes to its $(\mathcal{M}_{\mathrm{w}})_{\mathrm{p}}$ to $(\mathcal{M}_{\mathrm{w}})_{\mathrm{c}}$ state.

$$\Delta E_{\text{self}}^{\text{ML}} = \Delta E_{\text{self}}^{\mathscr{M}_{\text{w}}} + \Delta E_{\text{self}}^{\mathscr{I}} \tag{B25}$$

where

$$\Delta E_{\text{self}}^{\mathscr{M}_{\text{w}}} = \sum_{\text{X}\in(\mathscr{M}_{\text{w}})_{\text{c}}} E_{\text{self}}^{\text{X}} - \sum_{\text{X}\in(\mathscr{M}_{\text{w}})_{\text{p}}} E_{\text{self}}^{\text{X}} = E_{\text{self}}^{(\mathscr{M}_{\text{w}})_{\text{c}}} - E_{\text{self}}^{(\mathscr{M}_{\text{w}})_{\text{p}}} \tag{B26}$$

and

$$\Delta E_{\text{self}}^{\mathscr{I}} = \sum_{\text{X}\in\mathscr{I}_{\text{c}}} E_{\text{self}}^{\text{X}} - \sum_{\text{X}\in\mathscr{I}_{\text{p}}} E_{\text{self}}^{\text{X}} = E_{\text{self}}^{\mathscr{I}_{\text{c}}} - E_{\text{self}}^{\mathscr{I}_{\text{p}}} \tag{B27}$$

According to the IQF framework, the deformation energy of a fragment is defined as the sum of the atomic deformation energies within a fragment and the sum of all unique interaction energies within the fragment when separated atoms form a molecule. Because in our case free atoms are not used as a reference state to monitor changes in $\mathscr{I}$, we express the deformation energy of $\mathscr{I}$ as a difference in the net energies of fragments $\mathscr{I}_{\text{c}}$ and $\mathscr{I}_{\text{p}}$,

$$E_{\text{def}}^{\mathscr{I}} = E_{\text{net}}^{\mathscr{I}_{\text{c}}} - E_{\text{net}}^{\mathscr{I}_{\text{p}}} = \left(E_{\text{self}}^{\mathscr{I}_{\text{c}}} + E_{\text{int}}^{\mathscr{I}_{\text{c}}}\right) - \left(E_{\text{self}}^{\mathscr{I}_{\text{p}}} + E_{\text{int}}^{\mathscr{I}_{\text{p}}}\right) = \Delta E_{\text{self}}^{\mathscr{I}} + \Delta E_{\text{int}}^{\mathscr{I}}. \tag{B28}$$

$$E_{\text{def}}^{\mathscr{M}_{\text{w}}} = E_{\text{net}}^{(\mathscr{M}_{\text{w}})_{\text{c}}} - E_{\text{net}}^{(\mathscr{M}_{\text{w}})_{\text{p}}} = \left(E_{\text{self}}^{(\mathscr{M}_{\text{w}})_{\text{c}}} + E_{\text{int}}^{(\mathscr{M}_{\text{w}})_{\text{c}}}\right) - \left(E_{\text{self}}^{(\mathscr{M}_{\text{w}})_{\text{p}}} + E_{\text{int}}^{(\mathscr{M}_{\text{w}})_{\text{p}}}\right) = \Delta E_{\text{self}}^{\mathscr{M}_{\text{w}}} + \Delta E_{\text{int}}^{\mathscr{M}_{\text{w}}}. \tag{B29}$$

Thus, the binding energy for a metal complex can be expressed within the IQF framework as the sum of the deformation energies of the individual fragments and the interaction energy between the two fragments (intra-fragment interaction energy term) and by substituting Eq. (B25), (B28) and (B29) into Eq. (B15) we obtain

$$E_{\text{bind}} = \Delta E_{\text{self}}^{\mathscr{M}_{\text{w}}} + \Delta E_{\text{self}}^{\mathscr{I}} + \Delta E_{\text{int}}^{\mathscr{M}_{\text{w}}} + \Delta E_{\text{int}}^{\mathscr{I}} + E_{\text{int}}^{\mathscr{M}_{\text{c}},\mathscr{I}_{\text{c}}} = E_{\text{def}}^{\mathscr{M}_{\text{w}}} + E_{\text{def}}^{\mathscr{I}} + E_{\text{int}}^{\mathscr{M}_{\text{c}},\mathscr{I}_{\text{c}}} \tag{B30}$$

Comparing Eq. (B30) and (B15), the decomposition of the E_{bind} in Eq. (B30) refocuses the IQA-defined components into IQF related components; the contribution of intra-atomic energies, $\Delta E_{\text{self}}^{\text{ML}}$, and the contribution of diatomic interactions within a particular fragment, $\Delta E_{\text{int}}^{\mathscr{M}_{\text{w}}}$ and $\Delta E_{\text{int}}^{\mathscr{I}}$, are expressed in terms of relevant deformation energy terms, which, as will be seen from discussion that follows, makes the interpretation of relevant stability of molecular systems much easier and convincing.

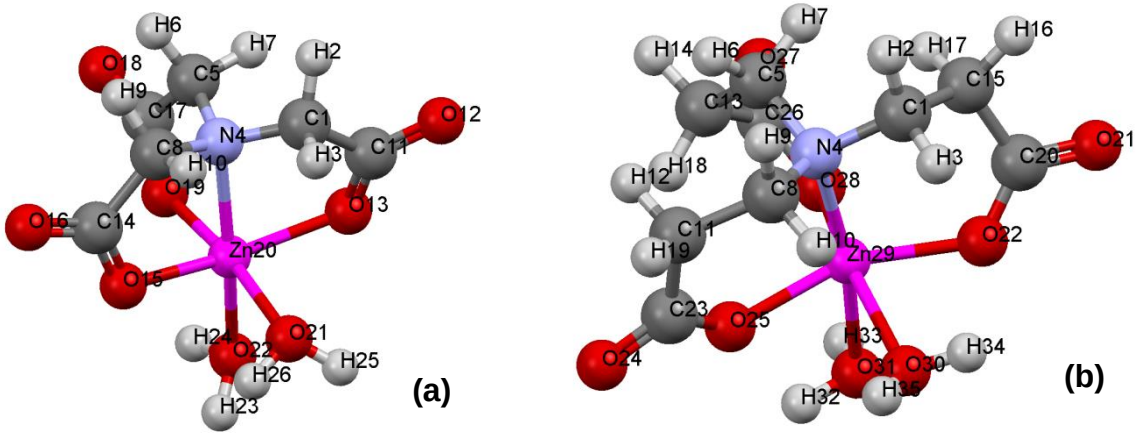

Figure B.1. Ball-and-stick representation of the MP2 structures LECs of (a) ZnNTPA, and (b) ZnNTA.

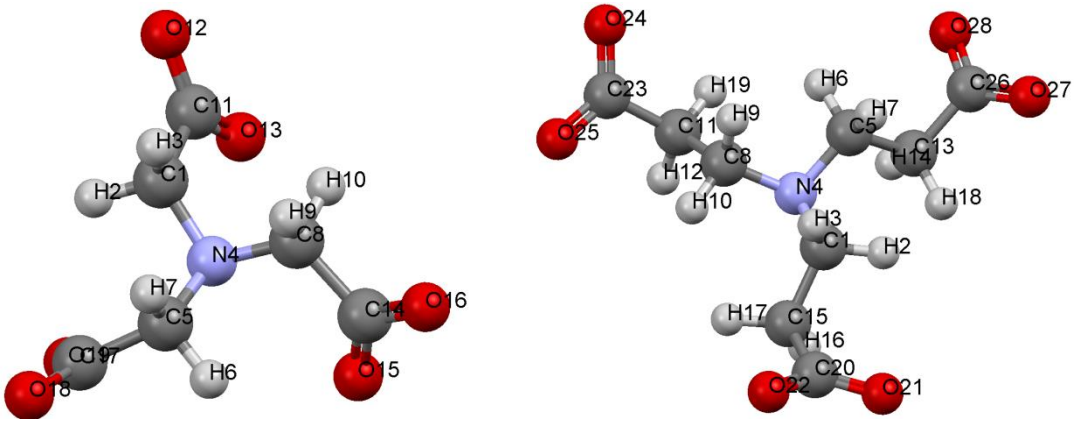

Figure B.2. Ball-and-stick representation of the MP2 structures LECs of (a) NTA, and (b) NTPA.

Table B.2. QTAIM-defined topological data at BCPs of the coordination bonds in ZnNTA and ZnNTPA at the X3LYP[a] level of theory on the MP2 optimized structure.

Bonds	$\rho(r)$	$\nabla^2\rho(r)$	$G(r)$	$V(r)$	$\lvert V(r)\rvert/G(r)$	DI(A|B)
			ZnNTA			
Zn–N	0.0688	0.2384	0.0757	–0.0918	1.21	0.31
Zn–O13	0.0676	0.3092	0.0864	–0.0955	1.11	0.33
Zn–O15	0.0677	0.3120	0.0870	–0.0961	1.10	0.33
Zn–O19	0.0679	0.3142	0.0876	–0.0967	1.10	0.33
Zn–O21	0.0446	0.1826	0.0517	–0.0577	1.12	0.21
Zn–O22	0.0537	0.2389	0.0665	–0.0733	1.10	0.26
			ZnNTPA			
Zn–N	0.0692	0.2425	0.0765	–0.0923	1.21	0.34
Zn–O22	0.0724	0.3567	0.0979	–0.1067	1.09	0.35
Zn–O25	0.0699	0.3445	0.0944	–0.1027	1.09	0.34
Zn–O28	0.0699	0.3374	0.0931	–0.1019	1.09	0.34
Zn–O30	0.0327	0.1238	0.0348	–0.0387	1.11	0.15
Zn–O31	0.0441	0.1682	0.0488	–0.0555	1.14	0.21

[a] all values are in au.

Table B.3. QTAIM-defined topological data at BCPs of the coordination bonds in ZnNTA and ZnNTPA at the MP2[a] level of theory.

Bonds	$\rho(r)$	$\nabla^2\rho(r)$	$G(r)$	$V(r)$	$\lvert V(r)\rvert/G(r)$	DI(A|B)
			ZnNTA			
Zn–N	0.0684	0.2452	0.0776	–0.0938	1.21	0.27
Zn–O13	0.0665	0.3141	0.0877	–0.0968	1.10	0.29
Zn–O15	0.0667	0.3169	0.0883	–0.0973	1.10	0.29
Zn–O19	0.0668	0.3191	0.0888	–0.0979	1.10	0.29
Zn–O21	0.0435	0.1860	0.0525	–0.0586	1.12	0.19
Zn–O22	0.0526	0.2441	0.0677	–0.0744	1.10	0.23
			ZnNTPA			
Zn–N	0.0685	0.2497	0.0783	–0.0941	1.20	0.30
Zn–O22	0.0713	0.3629	0.0994	–0.1080	1.09	0.31
Zn–O25	0.0687	0.3502	0.0958	–0.1040	1.09	0.30
Zn–O28	0.0688	0.3429	0.0944	–0.1030	1.09	0.30
Zn–O30	0.0318	0.1254	0.0354	–0.0395	1.12	0.13
Zn–O31	0.0433	0.1713	0.0498	–0.0567	1.14	0.18

[a] all values are in au.

Table B.4. QTAIM-defined topological data at BCPs of all atomic interaction lines in ZnNTA and ZnNTPA at the X3LYP[a] level of theory.

ZnNTA			ZnNTPA		
Atoms	$\rho(r)$	$\nabla^2\rho(r)$	Atoms	$\rho(r)$	$\nabla^2\rho(r)$
N4 - C5 - C17 - O19 - Zn20	0.0232	0.1119	C1-**N4–Zn29–O22**-C20-C15	0.0131	0.0578
C1 - N4 - Zn20 - O13 - C11	0.0215	0.1007	C8-**N4–Zn29–O25**-C23-C11	0.0125	0.0561
N4 - C8 – C14 - O15 - Zn20	0.0221	0.1041	C5-**N4–Zn29–O28**-C26-C13	0.0125	0.0570
av:	0.0223	0.1056	*av:*	0.0127	0.0570

[a] all values are in au.

Table B.5. QTAIM-defined topological data at BCPs of all atomic interaction lines in ZnNTA and ZnNTPA at the MP2[a] level of theory.

ZnNTA			ZnNTPA		
Atoms	$\rho(r)$	$\nabla^2\rho(r)$	Atoms	$\rho(r)$	$\nabla^2\rho(r)$
N4 - C5 - C17 - O19 - Zn20	0.0239	0.1110	C1-**N4–Zn29–O22**-C20-C15	0.0136	0.0581
C1 - N4 - Zn20 - O13 - C11	0.0221	0.0998	C8-**N4–Zn29–O25**-C23-C11	0.0131	0.0573
N4 - C8 – C14 - O15 - Zn20	0.0227	0.1033	C5-**N4–Zn29–O28**-C26-C13	0.0131	0.0566
av:	0.0229	0.1047	*av:*	0.0136	0.0576

[a] all values are in au.

Table B.6. IQA partitioning of two-bodied interaction energies in ZnNTA and ZnNTPA for selected interactions of interest using the XL3YP wavefunction on the MP2 structures.

ZnNTA				ZnNTPA			
Interaction	$V_{cl}^{X,Y}$	$V_{XC}^{X,Y}$	$E_{int}^{X,Y}$	Interaction	$V_{cl}^{X,Y}$	$V_{XC}^{X,Y}$	$E_{int}^{X,Y}$
Coordination bonds between Zn and NTA/NTPA							
Zn–N	–226.9	–46.3	–273.2	Zn–N	–221.1	–50.9	–272.0
Zn–O13$^-$	–251.5	–48.8	–300.2	Zn–O22$^-$	–258.6	–52.5	–311.1
Zn–O15$^-$	–252.2	–48.6	–300.8	Zn–O25$^-$	–256.6	–50.2	–306.8
Zn–O19$^-$	–253.6	–48.3	–301.9	Zn–O28$^-$	–257.0	–50.9	–307.9
Sum-1:	–984.2	–192	–1176.1	Sum-1:	–993.3	–204.5	–1197.8
Bonds with water molecules							
Zn–O21H$_2$	–220.3	–29.9	–250.2	Zn–O30H$_2$	–209.7	–20.0	–229.7
Zn–O22H$_2$	–231.0	–37.4	–268.3	Zn–O31H$_2$	–226.7	–28.7	–255.4
Sum-2:	–451.3	–67.3	–518.5	Sum-2:	–436.4	–48.7	–485.1
Total-1:	–1435.5	–259.1	–1694.7	Sum:	–1429.7	–253.2	–1682.9
Non-bonded interactions between donor atoms							
N•••O13$^-$	155.2	–6.2	148.9	N•••O22$^-$	133.0	–2.6	130.4
N•••O15$^-$	152.7	–5.2	147.5	N•••O25$^-$	137.0	–3.4	133.6
N•••O19$^-$	150.3	–4.2	146.1	N•••O28$^-$	136.1	–3.1	133.0
O13$^-$•••O15$^-$	116.9	–0.1	116.8	O22$^-$•••O25$^-$	118.8	–0.1	118.7
O13$^-$•••O19$^-$	149.6	–2.6	147.0	O22$^-$•••O28$^-$	158.0	–3.6	154.5
O15$^-$•••O19$^-$	159.8	–4.5	155.3	O25$^-$•••O28$^-$	149.9	–1.9	148.0
Sum-3:	884.5	–22.9	861.6	Sum-3:	832.8	–14.7	818.1
Between donor atoms in NTA/NTPA and O-atoms on water molecules							
N•••O21	114.4	–0.9	113.5	N•••O30	110.0	–0.7	109.3
N•••O22	91.7	–0.1	91.7	N•••O31	87.4	0.0	87.4
O13$^-$•••O21H$_2$	152.9	–5.6	147.3	O22$^-$•••O30H$_2$	163.4	–9.2	154.2
O13$^-$•••O22H$_2$	134.7	–2.1	132.6	O22$^-$•••O31H$_2$	140.9	–3.0	137.9
O15$^-$•••O21H$_2$	156.1	–6.7	149.5	O25$^-$•••O30H$_2$	154.7	–5.9	148.8
O15$^-$•••O22H$_2$	137.4	–2.1	135.3	O25$^-$•••O31H$_2$	161.4	–7.6	153.7
O19$^-$•••O21H$_2$	104.0	0.0	104.0	O28$^-$•••O30H$_2$	102.6	0.0	102.6
O19$^-$•••O22H$_2$	154.5	–6.1	148.4	O28$^-$•••O31H$_2$	158.9	–6.8	152.1
Sum-4:	1045.9	–23.5	1022.3	Sum-4:	1079.3	–33.3	1046.0
Between O-atoms on water molecules							
H$_2$O21•••O22H$_2$	138.9	–3.6	135.3	H$_2$O30•••O31H$_2$	134.2	–3.4	130.8
Total-2:	2069.3	–50.0	2019.3	Total-2:	2046.3	–51.4	1994.9
Total-3:	633.7	–309.1	324.6	Total-3:	616.6	–304.6	312.0

[a] Sum-1 stands for summed interaction energies and components of all coordination bonds with NTA/NTPA, Sum-2 stands for summed interaction energies and components of all coordination bonds with O-atoms of the water molecules, Sum-3 stands for summed interaction energies between O$^-$ and N atoms of the coordination spheres, Sum-4 stands for summed interaction energies and components between donor atoms in NTA/NTPA and O-atoms on water molecules, Total-1 stands for summed interaction energies and components of all coordination bonds, Total-2 stands for summed interaction energies and components of all repulsive interactions in the coordination sphere, and Total-3 stands for the summed interaction energies and components between all atoms in the coordination sphere.

Table B.7. QTAIM-defined topological data at BCPs of the weak intramolecular interactions in ZnNTPA at the X3LYP[a] level of theory on the MP2 optimized structure.

Bonds	$\rho(r)$	$\nabla^2\rho(r)$	$G(r)$	$V(r)$	$\lvert V(r)\rvert/G(r)$	DI(A|B)
H10•••O30	0.0078	0.0234	0.0053	–0.0047	0.8918	0.0310
H12•••H18	0.0092	0.0331	0.0068	–0.0053	0.7818	0.0126
H18•••O25	0.0096	0.0300	0.0067	–0.0058	0.8761	0.0317
H7•••H17	0.0134	0.0514	0.0105	–0.0081	0.7749	0.0241

[a] all values are in au except $|V(r)|/G(r)$ and DI(A|B)

Table B.8. QTAIM-defined topological data at BCPs of the weak intramolecular interactions in ZnNTPA at the MP2[a] level of theory.

Bonds	$\rho(r)$	$\nabla^2\rho(r)$	$G(r)$	$V(r)$	$\lvert V(r)\rvert/G(r)$	DI(A|B)
H10•••O30	0.0079	0.0242	0.0056	–0.0051	0.9134	0.0302
H12•••H18	0.0094	0.0342	0.0072	–0.0058	0.8095	0.0133
H18•••O25	0.0099	0.0306	0.0070	–0.0063	0.9078	0.0320
H7•••H17	0.0136	0.0533	0.0111	–0.0090	0.8036	0.0256

[a] all values are in au except $|V(r)|/G(r)$ and DI(A|B).

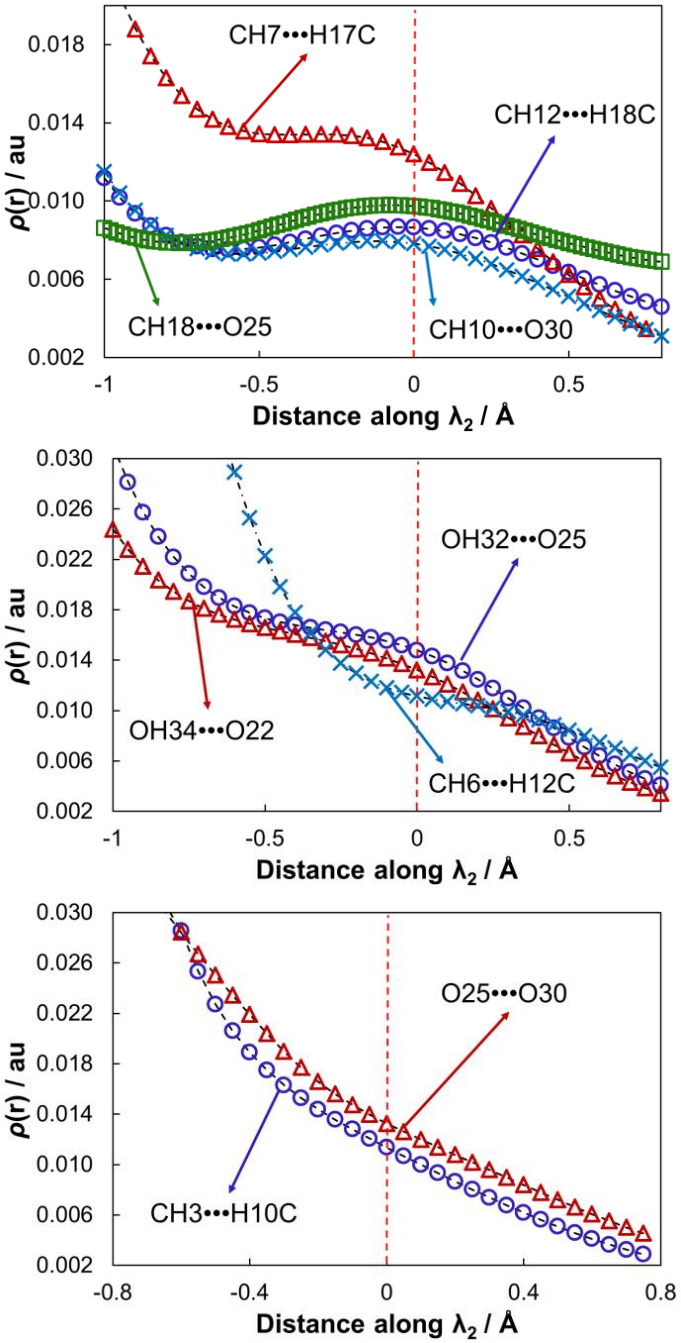

Figure B.3. The cross-sections, for selected interactions, of the electron density along the λ_2 eigenvector where the red line indicates the GIP (a) weak intramolecular interactions with bond paths, (b) weak intramolecular interactions without AILs, (c) intramolecular interactions with red spots.

Table B.9. Relative from $(\mathcal{M}_w)_f$ structures to $(\mathcal{M}_w)_f$, changes in the selected QTAIM- and IQA-(at the X3LYP level of theory on the MP2 structure) defined energy terms (in kcal/mol) and additional atomic properties of atoms in ZnNTA and ZnNTPA.

Atom X	ΔE^X_{add}	$\Delta \sum_{Y \neq X} 0.5 E^{X,Y}_{int}$	ΔE^X_{self}	ΔT^X	ΔV^{XX}_{ne}	ΔV^{XX}_{ee}	q^X_{free}	$q^X_{M_{p-org}}$	ΔE^X	ΔN^X	ΔVol^X	Δd^X_e
ZnNTA												
Zn20	10.8	9.6	1.2	–20.4	144.5	–122.9	1.753	1.761	–8.9	–0.008	1.004	–0.0031
O21	0.6	9.7	–9.1	–15.9	54.1	–47.2	–1.152	–1.148	14.7	–0.004	3.788	–0.0020
H25	–5.3	–3.3	–2.0	3.1	–6.1	1.0	0.639	–1.142	–3.2	0.008	0.458	–0.0001
H26	–4.5	–1.8	–2.8	4.2	–8.3	1.3	0.639	0.638	–4.3	0.010	0.669	–0.0001
O22	1.6	5.7	–4.1	–8.2	55.2	–51.1	–1.153	0.631	7.0	–0.011	1.588	–0.0010
H23	3.8	3.8	0.0	0.2	–0.1	–0.1	0.638	0.631	–0.2	0.000	–0.141	0.0001
H24	3.7	5.2	–1.6	2.4	–4.7	0.8	0.637	0.628	–2.4	0.006	0.365	0.0000
ZnNTPA												
Zn29	28.4	20.8	7.6	–44.2	339.5	–287.6	1.753	1.772	–10.7	–0.019	4.785	–0.0141
O30	7.6	22.8	–15.3	–23.8	78.0	–69.5	–1.152	–1.151	21.5	0.000	7.868	–0.0041
H34	–10.0	–4.2	–5.8	8.8	–17.3	2.8	0.639	0.617	–8.8	0.022	1.315	–0.0002
H35	–11.8	–8.6	–3.3	5.2	–10.1	1.6	0.639	0.626	–5.2	0.013	0.847	–0.0002
O31	13.3	25.4	–12.0	–25.5	184.7	–171.3	–1.153	–1.110	23.2	–0.043	1.601	–0.0012
H32	0.6	4.4	–3.8	5.9	–11.5	1.8	0.638	0.623	–5.9	0.015	0.746	0.0000
H33	0.5	3.8	–3.3	5.2	–10.1	1.6	0.637	0.624	–5.2	0.013	0.829	–0.0001

a

Table B.10. Relative from $(\mathscr{M}_w)_f$ structures to $(\mathscr{M}_w)_f$, $\Delta V_{cl}^{X,Y}$, $\Delta V_{XC}^{X,Y}$, and $\Delta E_{int}^{X,Y}$ (at the X3LYP level of theory on the MP2 structure) energy terms (in kcal/mol) for all diatomic interactions ZnNTA and ZnNTPA.

ZnNTA					ZnNTPA				
Atom X	Atom Y	$\Delta V_{cl}^{X,Y}$	$\Delta V_{XC}^{X,Y}$	$\Delta E_{int}^{X,Y}$	Atom X	Atom Y	$\Delta V_{cl}^{X,Y}$	$\Delta V_{XC}^{X,Y}$	$\Delta E_{int}^{X,Y}$
Zn20	O21	11.3	8.5	19.9	Zn29	O30	22.8	17.6	40.4
O21	H23	7.4	0.3	7.7	Zn29	O31	13.1	5.6	18.7
Zn20	H24	5.7	0.1	5.7	O30	H32	13.5	0.4	13.9
Zn20	O22	3.2	1.2	4.4	O31	H35	8.3	0.0	8.3
O21	H25	5.3	–1.9	3.4	O31	H32	12.1	–3.9	8.3
O21	H26	5.8	–2.6	3.2	O31	H33	11.0	–3.2	7.9
O22	H23	2.6	–0.3	2.3	O31	H34	6.9	0.0	6.9
O21	H24	2.0	0.0	2.1	O30	H35	9.3	–3.1	6.2
O22	H24	3.0	–1.5	1.4	O30	H34	10.8	–5.5	5.3
H23	H26	1.1	0.0	1.1	O30	H33	3.6	0.0	3.7
H24	H25	0.9	0.0	0.9	Zn29	H33	3.4	0.1	3.5
H24	H26	0.7	0.0	0.7	Zn29	H32	3.0	0.1	3.1
H23	H25	0.5	0.0	0.5	H33	H34	–1.6	0.0	–1.6
H23	H24	–0.3	0.0	–0.3	H32	H33	–2.6	0.0	–2.6
O22	H26	–2.1	0.0	–2.1	H33	H35	–3.2	0.0	–3.2
H25	H26	–2.2	0.0	–2.3	H34	H35	–4.4	–0.1	–4.5
O22	H25	–2.6	0.0	–2.5	H32	H35	–6.3	0.0	–6.3
Zn20	H23	–3.8	0.0	–3.8	Zn29	H34	–7.1	0.2	–6.9
Zn20	H26	–4.3	0.1	–4.2	H32	H34	–7.6	0.0	–7.6
O21	O22	–6.0	1.6	–4.4	O30	O31	–12.9	1.5	–11.5
Zn20	H25	–6.7	0.0	–6.7	Zn29	H35	–17.6	0.0	–17.6

Table B.11. IQA partitioning of two-bodied interaction energies of all interactions with the O-atom in ZnNTPA and ZnNTA using the XL3YP wavefunction on the MP2 structures.

ZnNTPA					ZnNTA				
Atoms		$V_{cl}^{X,Y}$	$V_{XC}^{X,Y}$	$E_{int}^{X,Y}$	Atoms		$V_{cl}^{X,Y}$	$V_{XC}^{X,Y}$	$E_{int}^{X,Y}$
X	Y				X	Y			
O30	C1	–32.9	–0.2	–33.1	O21	C1	–33.8	–0.7	-34.5
O30	H2	–2.1	0.0	–2.1	O21	H2	–4.1	0.0	-4.1
O30	H3	–1.9	–0.6	–2.5	O21	H3	–4.8	–1.1	-5.9
O30	N4	110.0	–0.7	109.3	O21	N4	114.4	–0.9	113.5
O30	C5	–27.3	0.0	–27.4	O21	C5	–27.0	0.0	-27.0
O30	H6	–2.0	0.0	–2.0	O21	H6	–3.3	0.0	-3.3
O30	H7	–2.2	0.0	–2.2	O21	H7	–3.8	0.0	-3.8
O30	C8	–35.0	–1.1	–36.0	O21	C8	–32.3	–0.2	-32.5
O30	H9	–2.3	–0.1	–2.4	O21	H9	–4.0	0.0	-4.0
O30	H10	–1.5	–3.3	–4.8	O21	H10	–4.6	–0.2	-4.8
O30	C11	–1.5	–0.1	–1.5	O21	C11	–171.5	–0.4	-171.8
O30	H12	–2.9	0.0	–3.0	O21	O12	108.4	–0.1	108.3
O30	C13	–1.4	0.0	–1.5	O21	O13	152.9	–5.6	147.3
O30	H14	–2.0	0.0	–2.0	O21	C14	–165.2	–0.2	-165.4
O30	C15	–1.6	0.0	–1.6	O21	O15	156.1	–6.7	149.5
O30	H16	–2.9	0.0	–3.0	O21	O16	102.1	–0.1	102.0
O30	H17	–2.7	0.0	–2.7	O21	C17	–117.7	0.0	-117.7
O30	H18	–1.8	0.0	–1.8	O21	O18	75.7	0.0	75.7
O30	H19	–3.5	0.0	–3.5	O21	O19	104.0	0.0	104.0
O30	C20	–159.4	–0.2	–159.6	Sum (kcal/mol):		241.8	–16.3	225.5
O30	O21	100.2	–0.1	100.1					
O30	O22	163.4	–9.2	154.2					
O30	C23	–164.5	–0.2	–164.7					
O30	O24	105.8	–0.1	105.7					
O30	O25	154.7	–5.9	148.8					
O30	C26	–110.1	0.0	–110.1					
O30	O27	72.8	0.0	72.8					
O30	O28	102.6	0.0	102.6					
Sum (kcal/mol):		247.8	–21.8	226.0					

Table B.12. IQA partitioning of two-bodied interaction energies of all interactions with the O-atom in ZnNTPA and ZnNTA using the XL3YP wavefunction on the MP2 structures.

ZnNTPA					ZnNTA				
Atoms		$V_{cl}^{X,Y}$	$V_{XC}^{X,Y}$	$E_{int}^{X,Y}$	Atoms		$V_{cl}^{X,Y}$	$V_{XC}^{X,Y}$	$E_{int}^{X,Y}$
X	Y				X	Y			
O31	C1	–24.7	0.0	–24.7	O22	C1	–25.4	0.0	–25.4
O31	H2	–1.4	0.0	–1.4	O22	H2	–2.8	0.0	–2.8
O31	H3	–2.0	0.0	–2.0	O22	H3	–3.7	0.0	–3.7
O31	N4	87.4	0.0	87.4	O22	N4	91.7	–0.1	91.7
O31	C5	–24.6	0.0	–24.6	O22	C5	–24.8	0.0	–24.8
O31	H6	–2.0	0.0	–2.0	O22	H6	–3.3	0.0	–3.3
O31	H7	–2.0	0.0	–2.0	O22	H7	–3.7	0.0	–3.7
O31	C8	–25.0	0.0	–25.0	O22	C8	–25.1	0.0	–25.1
O31	H9	–1.4	0.0	–1.4	O22	H9	–3.0	0.0	–3.0
O31	H10	–1.8	0.0	–1.8	O22	H10	–3.7	0.0	–3.7
O31	C11	–1.2	0.0	–1.3	O22	C11	–136.5	–0.1	–136.6
O31	H12	–2.1	0.0	–2.1	O22	O12	86.4	0.0	86.4
O31	C13	–1.5	0.0	–1.5	O22	O13	134.7	–2.1	132.6
O31	H14	–2.4	0.0	–2.4	O22	C14	–138.7	–0.1	–138.7
O31	C15	–1.1	0.0	–1.2	O22	O15	137.4	–2.1	135.3
O31	H16	–2.5	0.0	–2.5	O22	O16	87.6	0.0	87.6
O31	H17	–2.0	0.0	–2.0	O22	C17	–151.0	–0.1	–151.1
O31	H18	–2.0	0.0	–2.0	O22	O18	94.1	–0.1	94.0
O31	H19	–2.8	0.0	–2.8	O22	O19	154.5	–6.1	148.4
O31	C20	–142.5	–0.1	–142.6	Sum (kcal/mol):		265.0	–10.8	254.2
O31	O21	94.0	–0.1	93.9					
O31	O22	140.9	–3.0	137.9					
O31	C23	–154.2	–0.2	–154.3					
O31	O24	100.2	–0.1	100.1					
O31	O25	161.4	–7.6	153.7					
O31	C26	–152.5	–0.1	–152.6					
O31	O27	97.1	–0.1	97.0					
O31	O28	158.9	–6.8	152.1					
Sum (kcal/mol):		288.1	–18.3	269.9					

Table B.13. IQA partitioning of two-bodied interaction energies of all interactions with the H-atom in ZnNTPA and ZnNTA using the XL3YP wavefunction on the MP2 structures.

ZnNTPA					ZnNTA				
Atoms		$V_{cl}^{X,Y}$	$V_{XC}^{X,Y}$	$E_{int}^{X,Y}$	Atoms		$V_{cl}^{X,Y}$	$V_{XC}^{X,Y}$	$E_{int}^{X,Y}$
X	Y				X	Y			
H32	C1	12.5	0.0	12.5	H23	C1	12.3	0.0	12.3
H32	H2	0.7	0.0	0.7	H23	H2	1.4	0.0	1.4
H32	H3	1.0	0.0	1.0	H23	H3	1.8	0.0	1.8
H32	N4	–45.0	0.0	–45.0	H23	N4	–44.1	0.0	-44.1
H32	C5	12.7	0.0	12.7	H23	C5	11.7	0.0	11.7
H32	H6	1.0	0.0	1.0	H23	H6	1.5	0.0	1.5
H32	H7	1.1	0.0	1.1	H23	H7	1.8	0.0	1.8
H32	C8	13.2	0.0	13.2	H23	C8	12.4	0.0	12.4
H32	H9	0.8	0.0	0.8	H23	H9	1.5	0.0	1.5
H32	H10	0.9	0.0	0.9	H23	H10	1.8	0.0	1.8
H32	C11	0.7	0.0	0.6	H23	C11	65.2	0.0	65.2
H32	H12	1.2	0.0	1.2	H23	O12	–42.2	0.0	-42.2
H32	C13	0.8	0.0	0.8	H23	O13	–62.3	0.0	-62.3
H32	H14	1.2	0.0	1.2	H23	C14	71.4	0.0	71.4
H32	C15	0.6	0.0	0.6	H23	O15	–70.9	0.0	-70.9
H32	H16	1.2	0.0	1.2	H23	O16	–45.7	0.0	-45.7
H32	H17	1.0	0.0	1.0	H23	C17	69.1	0.0	69.1
H32	H18	1.0	0.0	1.0	H23	O18	–44.3	0.0	-44.3
H32	H19	1.6	0.0	1.6	H23	O19	–67.6	–0.1	-67.8
H32	C20	65.8	0.0	65.7	Sum (kcal/mol):		–125.3	–0.2	–125.5
H32	O21	–43.7	0.0	–43.7					
H32	O22	–63.6	0.0	–63.6					
H32	C23	93.7	0.0	93.6					
H32	O24	–60.8	0.0	–60.9					
H32	O25	–101.0	–3.2	–104.1					
H32	C26	74.9	0.0	74.9					
H32	O27	–48.2	0.0	–48.2					
H32	O28	–74.9	–0.1	–75.0					
Sum (kcal/mol):		–149.8	–3.4	–153.2					

Table B.14. IQA partitioning of two-bodied interaction energies of all interactions with the H-atom in ZnNTPA and ZnNTA using the XL3YP wavefunction on the MP2 structures.

ZnNTPA					ZnNTA				
Atoms		$V_{cl}^{X,Y}$	$V_{XC}^{X,Y}$	$E_{int}^{X,Y}$	Atoms		$V_{cl}^{X,Y}$	$V_{XC}^{X,Y}$	$E_{int}^{X,Y}$
X	Y				X	Y			
H33	C1	12.4	0.0	12.4	H24	C1	12.9	0.0	12.9
H33	H2	0.7	0.0	0.7	H24	H2	1.4	0.0	1.4
H33	H3	1.0	0.0	1.0	H24	H3	1.8	0.0	1.8
H33	N4	–43.8	0.0	–43.8	H24	N4	–47.1	0.0	–47.1
H33	C5	12.7	0.0	12.7	H24	C5	13.1	0.0	13.1
H33	H6	1.0	0.0	1.0	H24	H6	1.8	0.0	1.8
H33	H7	1.0	0.0	1.0	H24	H7	2.0	0.0	2.0
H33	C8	12.4	0.0	12.4	H24	C8	12.9	0.0	12.9
H33	H9	0.7	0.0	0.7	H24	H9	1.5	0.0	1.5
H33	H10	0.9	0.0	0.9	H24	H10	1.9	0.0	1.9
H33	C11	0.6	0.0	0.6	H24	C11	67.5	0.0	67.5
H33	H12	1.0	0.0	1.0	H24	O12	–43.3	0.0	–43.3
H33	C13	0.9	0.0	0.9	H24	O13	–65.3	0.0	–65.3
H33	H14	1.3	0.0	1.3	H24	C14	71.5	0.0	71.5
H33	C15	0.5	0.0	0.5	H24	O15	–69.3	0.0	–69.3
H33	H16	1.3	0.0	1.3	H24	O16	–45.9	0.0	–45.9
H33	H17	1.0	0.0	1.0	H24	C17	88.1	0.0	88.0
H33	H18	1.1	0.0	1.1	H24	O18	–54.9	0.0	–54.9
H33	H19	1.4	0.0	1.4	H24	O19	–93.1	–1.1	–94.2
H33	C20	73.2	0.0	73.2	Sum (kcal/mol):		–142.5	–1.2	–143.7
H33	O21	–49.1	0.0	–49.1					
H33	O22	–69.9	0.0	–69.9					
H33	C23	73.4	0.0	73.4					
H33	O24	–48.4	0.0	–48.4					
H33	O25	–74.7	–0.1	–74.7					
H33	C26	88.9	0.0	88.9					
H33	O27	–56.6	0.0	–56.6					
H33	O28	–95.2	–1.9	–97.1					
Sum (kcal/mol):		–150.3	–2.1	–152.4					

Table B.15. IQA partitioning of two-bodied interaction energies of all interactions with the H-atom in ZnNTPA and ZnNTA using the XL3YP wavefunction on the MP2 structures.

ZnNTPA					ZnNTA				
Atoms		$V_{cl}^{X,Y}$	$V_{XC}^{X,Y}$	$E_{int}^{X,Y}$	Atoms		$V_{cl}^{X,Y}$	$V_{XC}^{X,Y}$	$E_{int}^{X,Y}$
X	Y				X	Y			
H34	C1	17.1	0.0	17.1	H25	C1	15.9	0.0	15.9
H34	H2	1.2	0.0	1.2	H25	H2	1.9	0.0	1.9
H34	H3	0.9	–0.1	0.8	H25	H3	2.3	0.0	2.3
H34	N4	–54.5	0.0	–54.5	H25	N4	–52.3	0.0	-52.3
H34	C5	13.6	0.0	13.6	H25	C5	12.7	0.0	12.7
H34	H6	1.0	0.0	1.0	H25	H6	1.5	0.0	1.5
H34	H7	1.1	0.0	1.1	H25	H7	1.8	0.0	1.8
H34	C8	16.9	0.0	16.9	H25	C8	14.5	0.0	14.5
H34	H9	1.0	0.0	1.0	H25	H9	1.8	0.0	1.8
H34	H10	0.7	0.0	0.7	H25	H10	2.1	0.0	2.0
H34	C11	0.8	0.0	0.8	H25	C11	91.0	0.0	90.9
H34	H12	1.3	0.0	1.3	H25	O12	–58.5	0.0	-58.5
H34	C13	0.7	0.0	0.7	H25	O13	–82.1	–0.2	-82.3
H34	H14	1.0	0.0	1.0	H25	C14	72.0	0.0	72.0
H34	C15	0.9	0.0	0.9	H25	O15	–66.2	–0.2	-66.3
H34	H16	1.6	0.0	1.6	H25	O16	–46.1	0.0	-46.1
H34	H17	1.5	0.0	1.5	H25	C17	57.1	0.0	57.1
H34	H18	0.9	0.0	0.9	H25	O18	–37.1	0.0	-37.1
H34	H19	1.6	0.0	1.6	H25	O19	–50.4	0.0	-50.4
H34	C20	94.8	0.0	94.7	Sum (kcal/mol):		–118.2	–0.4	–118.6
H34	O21	–59.0	0.0	–59.0					
H34	O22	–98.9	–2.0	–100.8					
H34	C23	71.9	0.0	71.9					
H34	O24	–47.3	0.0	–47.3					
H34	O25	–66.1	–0.1	–66.3					
H34	C26	55.4	0.0	55.4					
H34	O27	–36.9	0.0	–36.9					
H34	O28	–51.6	0.0	–51.6					
Sum (kcal/mol):		–128.3	–2.3	–130.6					

Table B.16. IQA partitioning of two-bodied interaction energies of all interactions with the H-atom in ZnNTPA and ZnNTA using the XL3YP wavefunction on the MP2 structures.

ZnNTPA					ZnNTA				
Atoms		$V_{cl}^{X,Y}$	$V_{XC}^{X,Y}$	$E_{int}^{X,Y}$	Atoms		$V_{cl}^{X,Y}$	$V_{XC}^{X,Y}$	$E_{int}^{X,Y}$
X	Y				X	Y			
H35	C1	15.5	0.0	15.5	H26	C1	15.7	0.0	15.7
H35	H2	0.9	0.0	0.9	H26	H2	1.8	0.0	1.8
H35	H3	0.9	0.0	0.9	H26	H3	2.2	0.0	2.2
H35	N4	–51.9	0.0	–51.9	H26	N4	–54.3	0.0	-54.3
H35	C5	13.2	0.0	13.2	H26	C5	13.0	0.0	13.0
H35	H6	0.9	0.0	0.9	H26	H6	1.6	0.0	1.6
H35	H7	1.1	0.0	1.1	H26	H7	1.8	0.0	1.8
H35	C8	17.4	–0.1	17.3	H26	C8	16.0	0.0	16.0
H35	H9	1.2	0.0	1.2	H26	H9	2.1	0.0	2.1
H35	H10	0.7	–0.2	0.5	H26	H10	2.3	0.0	2.3
H35	C11	0.7	0.0	0.7	H26	C11	74.8	0.0	74.8
H35	H12	1.6	0.0	1.6	H26	O12	–48.7	0.0	-48.7
H35	C13	0.7	0.0	0.7	H26	O13	–65.2	-0.1	-65.3
H35	H14	1.0	0.0	1.0	H26	C14	92.4	0.0	92.4
H35	C15	0.7	0.0	0.7	H26	O15	–89.1	-0.6	-89.7
H35	H16	1.3	0.0	1.3	H26	O16	–57.4	0.0	-57.4
H35	H17	1.2	0.0	1.2	H26	C17	58.7	0.0	58.7
H35	H18	0.9	0.0	0.9	H26	O18	–38.2	0.0	-38.2
H35	H19	1.8	0.0	1.8	H26	O19	–51.7	0.0	-51.7
H35	C20	69.4	0.0	69.4	Sum (kcal/mol):		–122.3	–0.8	-123.1
H35	O21	–45.0	0.0	–45.1					
H35	O22	–67.6	–0.2	–67.8					
H35	C23	87.6	0.0	87.6					
H35	O24	–57.7	0.0	–57.7					
H35	O25	–78.5	–0.1	–78.6					
H35	C26	51.7	0.0	51.7					
H35	O27	–34.6	0.0	–34.6					
H35	O28	–47.1	0.0	–47.1					
Sum (kcal/mol):		–112.0	–0.6	–112.7					
Overall Sum (kcal/mol):		–466.5	–262.3	–728.9	Overall Sum (kcal/mol):		–443.4	–228.7	–672.1